Spring 2012

Evaluation of Ocean-Energy Conversion Based on Linear Generator Concepts

Michael Allen Stelzer
Old Dominion University

EVALUATION OF OCEAN-ENERGY CONVERSION BASED ON

LINEAR GENERATOR CONCEPTS

by

Michael Allen Stelzer
B.S. October 1990, DeVry Institute of Technology
M.S. August 2001, Old Dominion University

A Dissertation Submitted to the Faculty of Old Dominion University in Partial
Fulfillment of the Requirements for the Degree of

DOCTOR OF PHILOSOPHY

ELECTRICAL AND COMPUTER ENGINEERING

OLD DOMINION UNIVERSITY
May 2012

Approved by:

Ravindra P. Joshi (Director)

Helmut Baumgart (Member)

Frederic D. McKenzie (Member)

Adrian V. Gheorghe (Member)

ABSTRACT

EVALUATION OF OCEAN-ENERGY CONVERSION BASED ON LINEAR GENERATOR CONCEPTS

Michal Allen Stelzer
Old Dominion University, 2012
Director: Dr. R. P. Joshi

A turbine generator is a device that converts mechanical rotation into electrical energy. Unfortunately, the primary driving force that has been used to provide this rotation has, thus far, been fossil fuels. Although fossil fuels have proven to be a reliable resource to continually supply the growing demand for electrical power, they are not without their financial and environmental drawbacks. With the continuously increasing demand for energy, it is hypothesized that the world may, in time, exhaust this precious natural resource and/or inflict permanent environmental damage upon our planet.

However, motions that occur in nature, such as ocean waves, can play a significant role in generating environmentally safe and economically viable energy for human utilization.

As part of research at Old Dominion University, we propose to use a linear electrical generator (which uses a "back-and-forth" motion of a piston rather than a rotational movement) to probe the production of electrical energy simply from ocean waves. This would also be a less complex design compared to that of conventional rotational versions. Quantitative analysis for the voltage and power produced from the linear generator for a given set of ocean-wave characteristics will also be carried out, probed and discussed.

Previous research into this topic has primarily relied upon modeling an ideal buoy (i.e., one that matches the waves' height and motion at each instant in time) responding to

the surface ocean waves under the regular wave regime. This work, however, more closely analyzes the physical properties of the buoy and predicts the electrical power generation capabilities from a seabed mounted linear generator Wave Energy Convertor (WEC) tethered to the floating buoy operating under the influence of a non-ideal buoy and the more realistic irregular wave regime. Several buoy sizes will be modeled to exploit the buoys' natural heave frequency in an attempt to create a greater heave response for a given set of sea state conditions. It will be shown that a greater heave response from the buoy generally leads to an increase in the generated power from the linear generator.

ACKNOWLEDGEMENTS

I would like to thank Dr. Ravindra Joshi for his guidance and support as my academic and dissertation advisor. I would also like to take this opportunity to thank Dr. Helmut Baumgart, Dr. Adrian Gheorghe, and Dr. Federic McKenzie for their time and consideration in serving on my dissertation guidance committee.

TABLE OF CONTENTS

LIST OF TABLES

LIST OF FIGURES

CHAPTER I

INTRODUCTION

1.1 Introduction and background

World energy consumption has increased dramatically since 1950 and the extra demand to date has been provided primarily by fossil fuels [1]. Figure 1.1 shows one such projection for the world energy demand and the sources expected to supply that demand to the year 2050.
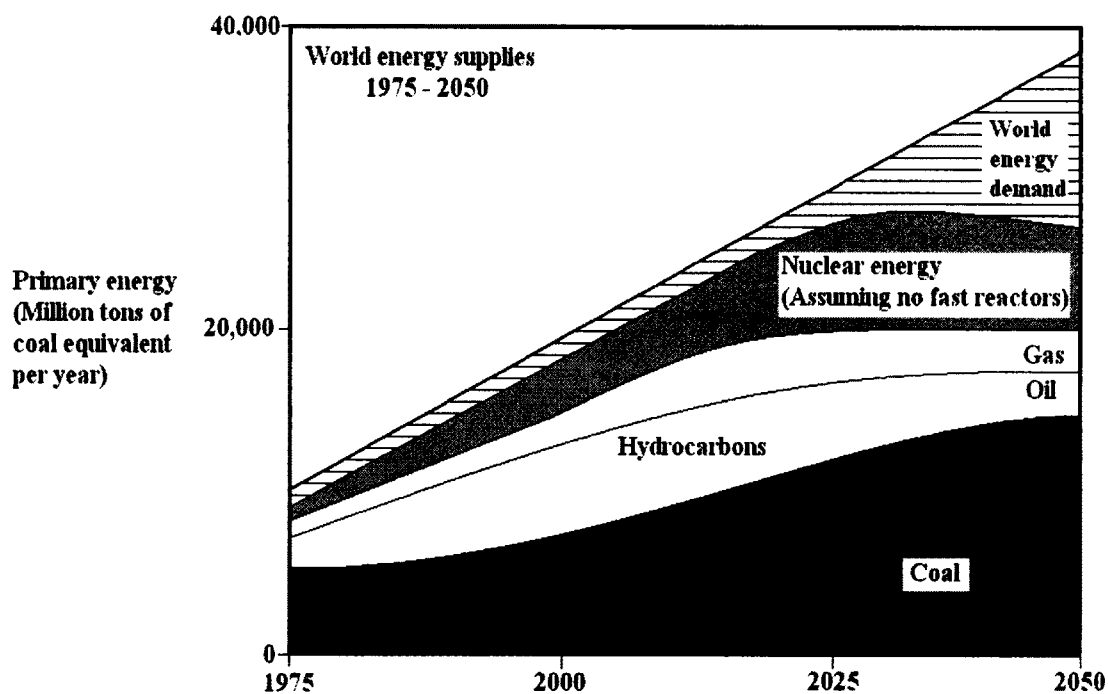
Figure 1.1. Future world energy supply and demand expectations [1].

Today, more than 80% of the world's electric power is generated from fossil fueled plants, which produce harmful CO_2 pollution as a by-product [2]. Since the demand for

electricity is forecast to increase in the future, the need for generating clean (non-harmful to the environment), economical, and renewable (also termed 'green') energy is ever-increasing.

Currently, the focus to create this energy has been in the areas of biomass, wind power and solar energy. However, direct electrical conversions of energy from these sources so that they possess a high degree of utilization (high number of full load hours per year) and high power density (concentrated power), have been considered to be both difficult and uneconomical [2]. Thus, alternate sources for creating 'green' energy must be investigated.

A few key points highlighting the projections and potential of harnessing wave energy for electrical generating purposes are listed below.

(a) It is estimated that more than 30% of the electricity consumption within the European Union alone can be supplied by wave energy [3].

(b) The total annual average wave energy off the U.S. coastlines, computed at a water depth of 60 meters, has been estimated to be 2,100 Tera-Watt-Hours (TWH) [4].

(c) Estimates suggest that wave motion may be harnessed to generate 1-10 trillion Watts (1-10 TW) of energy per year [5 - 6].

1.2   Sources of alternate energy

A few of the commonly considered sources of alternative 'Green' energy are briefly considered in this section for a general overview and completeness.

1.2.1 Tidal energy

Tidal energy (TE) is one option for extracting power from water. TE was harnessed hundreds of years ago when tide mills were erected along the coastlines of England, Wales, Brittany, the Lowlands, Spain, Russia, and the Atlantic coasts of Canada and the United States [7]. Figure 1.2 depicts a seaward view of the Rance River installation that is currently in operation.

Figure 1.2. The Rance tidal power station with the city and harbor of St. Malo [8].

In order to utilize the natural motion of a tide to generate electrical energy, a dam must be constructed across a tidal embayment, basin, or estuary. The water's rising and/or falling movements can then be harnessed to drive an electrical generator.

Unfortunately, the number of sites suitable for tidal power plants is limited by the following factors [7]:

1. The long dam needed to close off an embayment is expensive to build.

2. A head of greater than 5 meters is required to turn the turbines.

3. A site that is too distant from its potential market experiences high power losses.

Hence, tidal energy does not appear to be a reliable and efficient source of power.

1.2.2 Wind energy

The wind provides considerable energy offshore, and sea- or land-based electricity generating plants could utilize it to convert the rotational energy from a windmill or wind turbine into electrical energy [7]. Figure 1.3 depicts a typical offshore wind farm.

The disadvantages, however, associated with utilizing wind power to generate electricity include the following: (a) the high cost of manufacturing large windmills, (b) the inconsistency of the blowing wind, and (c) the navigational hazard that large, floating windmill systems pose to passing ships.

Furthermore, as the water depth in which the windmill is to be erected increases, the cost of offshore foundations will increase as well due to the added complexity and resources that are required for construction and maintenance below the waterline [9].

Figure 1.3. An offshore wind farm located in the North Sea off Belgium [10].

1.2.3 Current energy

Current energy uses the natural ocean current to mechanically turn a generator in order to produce electrical energy as shown in Figure 1.4. This type of energy conversion is highly inefficient since windmills and turbines immersed in a free stream only intercept a portion of the passing current [11].

Additionally, in an open free stream, such as an ocean current, the restriction to the flow through the energy conversion device cannot be too great or the flow will merely be displaced around the unit. Furthermore, the collection devices must not be spaced so close together that the overall flow of the current is restrained [7].
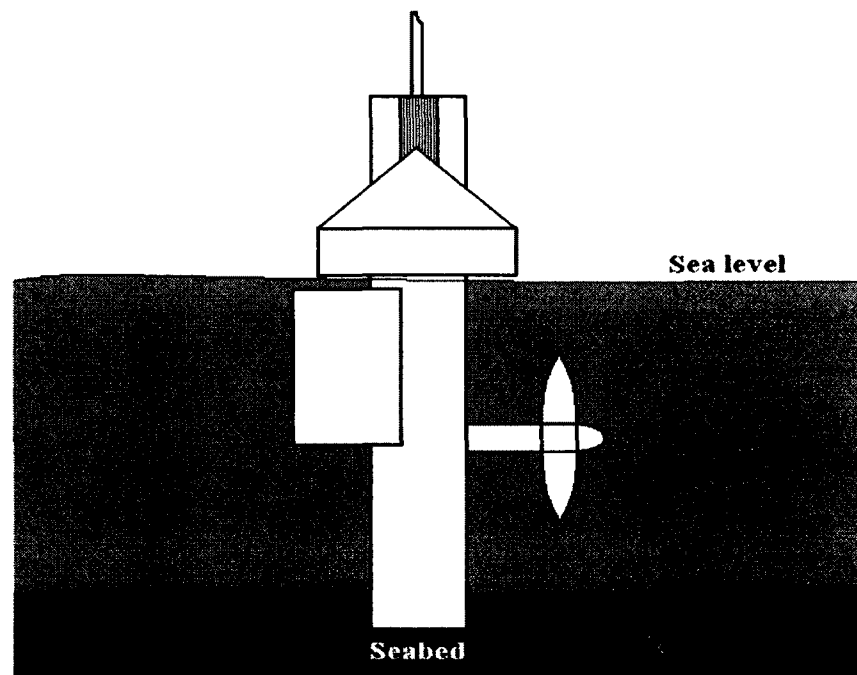
Figure 1.4. An example of a current turbine electrical generation plant [11].

Additional problems associated with current energy conversion include the following: corrosion, materials compatibility, marine bio-fouling of turbine blades, seasonal

variations to current flow, as well as engineering problems associated with hydrodynamic and structural design [7]. Finally, since water is about 800 times denser than air, current turbines would need to be constructed to be much sturdier than those for wind turbines, causing them to be heavier and more expensive to build [11].

1.2.4 Biomass energy

Marine plants can be used as a source of fuel in the form of methane or liquid hydrocarbons. The basic principle is to grow kelp, using nutrients brought up from the deep, harvest them, and then have them anaerobically digested into methane. Since kelp reproduces it weight every four to six months, researchers estimate that a 1-mile square kelp farm could feed 2,000 people and satisfy the natural gas need for 300 individuals [7].

Biomass conversion can occur on near-shore facilities or on marine facilities operating in the appropriate climate conditions. However, the level of productivity per hectare in the sea exceeds that of a land based facility. Although it is possible to grow giant kelp on offshore-submerged floats, these platforms are costly to manufacture and provide hazards to ocean navigation. Additionally, if they are of considerable size, they are more vulnerable to damage from adverse weather conditions [7].

1.2.5 Geothermal energy

Geothermal energy results from the heat of the Earth, it is present as natural radioactivity in small quantities in all rocks. This heat increases with depth into the earth and is transferred to the surface by steam or water.

Geothermal energy plants utilize the Earth's natural geothermal energy to turn turbines in order to generate electrical energy. Today, there are fourteen geothermal units generating electricity at The Geysers in Northern California, producing 500 MW of electricity, an amount sufficient to serve 150,000 people [7].

Geothermal plants can transfer thermal energy from the earth into electrical energy by either the direct or binary process. The direct process straightforwardly utilizes thermal energy from the earth to rotate a turbine in order to generate electrical energy. In the binary process, the earth's thermal energy (in the primary system) is used to heat a secondary fluid (in the secondary system) that expands through the turbine as a vapor and rotates the electrical generator. The vapor is then cooled by the condenser and is returned to the heat exchanger to be used for the next cycle. An example of a basic binary geothermal power plant is illustrated in Figure 1.5.
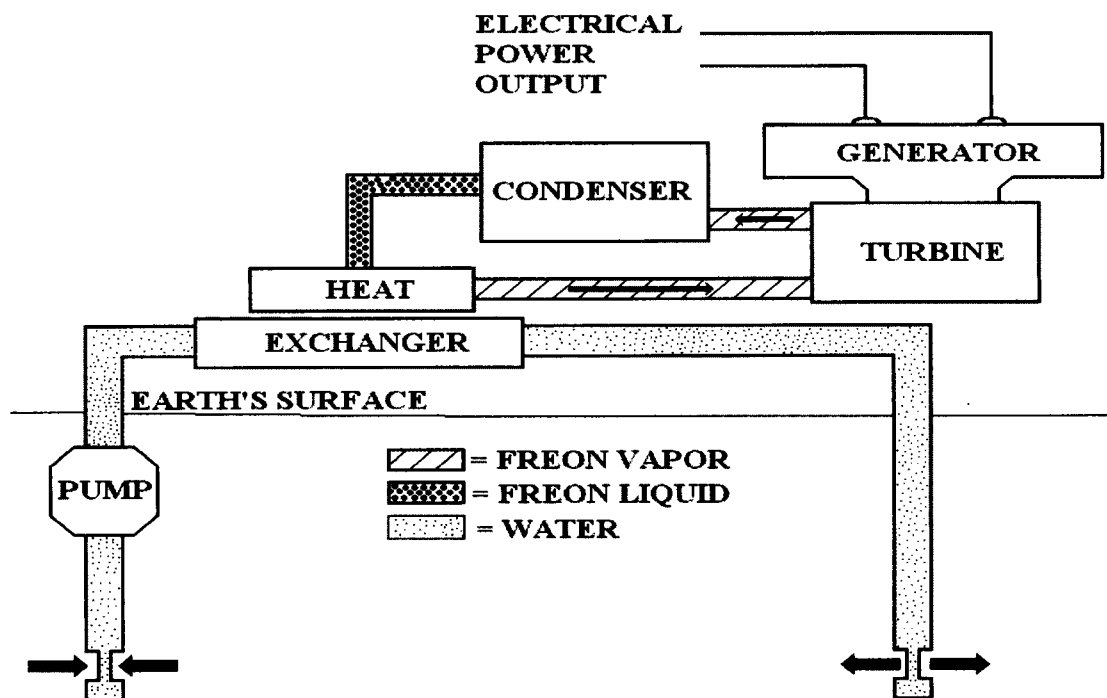
Figure 1.5. A basic binary geothermal electrical power plant [7].

The problems associated with geothermal energy utilization include environmental (disposal of salt water, toxic liquid wastes, release of hydrogen sulfide and methane), technical (melting of drilling equipment and corrosion) and economic (reducing the cost of drilling) problems.

Geothermal energy production is also suspected to produce a negative impact upon the environment by creating higher surface water temperatures, as well as noise, water, and air pollution. Therefore, the utilization of the oceans geothermal energy will have to be delayed until further technological refinements are discovered, a thorough assessment of the impact that the activity will have on the environment is determined, and international legal issues in dealing with tapping energy from the sea are clarified [7].

1.2.6 Ocean energy

Wave energy has the potential to make a major contribution toward supplying electrical energy free from the dependency of fossil fuels. Ocean waves form when a passing wind imparts force on to the open water. Thus, wind blowing over the surface of the ocean causes waves to be generated by the transfer of energy and momentum from the wind field [12]. The resulting wave can travel great distances across the surface before dissipating. Estimates suggest that a one-meter wave front carries approximately 100 kW of power [5]. This significant amount of renewable energy is dissipated wastefully as the surface waves clash upon the shoreline of any beach.

Waves have several advantages over other forms of renewable energy, such as wind and solar, in that the waves are more available (seasonal, but more constant) and more predictable with better demand matching. Wave energy also offers higher energy

densities, enabling devices to extract more power from a smaller volume at consequent lower costs and reduced visual impact [13].

Wave energy production devices can be stationed either by the shoreline or at an offshore location. An offshore device has the benefit of having a higher average unit capacity than that of a shoreline device making individual devices very effective, especially for remote or island communities. On the negative side, however, offshore devices are more difficult to access for maintenance purposes. Due to their larger capacity, offshore devices represent the most significant wave energy sector, contributing up to 58% of all forecast capacity [14]. On the other hand, higher installation costs and fewer potential sites limit shoreline facilities. These sites only accounted for 8% of the capacity forecasted from 2004-2008 [14].

With the aid of Wave Energy Converters (WECs), it is possible to convert the natural rhythm of the ocean into practical 'green' energy which is of great benefit for human utilization as well as non-detrimental to the environment. From the standpoint of Electrical Engineering, the main idea is to convert the periodic mechanical wave motion ever present in the oceans into electrical energy. *The most convenient approach for this would logically appear to be the use of electrical generators.* Such generator devices typically convert the movement of a "rotor" into electricity in the presence of a magnetic field environment.

Some North American energy data is available from publications by the Electric Power Research Institute (EPRI) [15]. The U.S. wave and current energy resource potential that could be credibly harnessed is about 400 TWh/yr or about 10% of national

energy demand. The EPRI studied the U.S. wave energy resource and estimates it to be about 2,100 TWh/yr.

Assuming an extraction efficiency of 15% wave to mechanical energy (which is limited by device spacing, device absorption, and sea space constraints), typical power train efficiencies of 90% and a plant availability of 90%, the electricity produced is about 260 TWh/yr. This is roughly equal to an average power of 30,000 MW at rated capacity of about 90,000 MW. This amount equals the total 2004 energy generation from conventional hydropower, which is about 6.5% of the total U.S. electricity supply. The Canadian wave energy resource was studied by Natural Resources Canada (NRC) and found to be about 1,600 TWh/yr.

1.3   Concepts in wave energy conversion

Modern ocean-wave energy research began during the oil crisis of the 1970s. Much of the early work was conducted by Salter [16] and Evans [17] in Great Britain and Falnes [18] in Norway, among others. Several promising concepts were developed by 1980 including point-absorber wave energy converters such as the infamous Salter duck [16] and oscillating water-column (OWC) devices utilizing a Well's turbine [19] for power take-off. With the decrease in oil prices in the early 1980s, much of the funding for ocean wave energy conversion was cut and no full-scale demonstrations of the technology were constructed. However, recent concerns about global warming and the increasing price of conventional energy has led to a resurgence in research on ocean wave energy conversion.

The main criteria for designing an ocean energy conversion system typically are survivability, reliability, and maintainability. So, systems often consist of a sea floor

mounted frame and housing, tethered to a buoy to couple with the waves. Putting the actual generation device on the floor is chosen for two reasons. First, housing the generator in a buoy would create the need for a specially designed buoy. Mounting on the ocean floor, on the other hand, allows the selection of a commercial off-the-shelf buoy rather than redesigning the generator housing for different buoy profiles. Second, the surface can be a violent and harsh environment. Although the ocean floor has its drawbacks as well, the rough and turbulent conditions at the surface can be avoided. Thus, maintainability is reduced by having the system submerged.

There are four general categories of ocean wave energy converters (WEC). These are the: oscillating water column (OWC), attenuator, overtopping, and point absorber. These four are discussed very briefly below.

a) *Oscillating water column (OWC)*: The OWC operates on the principle of air compression and decompression. An inverted chamber is placed in the water such that waves cause the "floor" of the chamber to rise and fall, therefore compressing and decompressing the air in the chamber. A turbine is placed at a small opening in the chamber to capture energy from the air as it rushes in and out.

b) *Attenuator*: Attenuators are usually devices with rectangular aspect ratios that can be oriented perpendicularly or collinearly with the wave front. For example, an energy absorbing structure on a jetty would be an attenuator. One of the largest commercial devices, the Pelamis, is an example of an attenuator design that is oriented perpendicular to the wave, spanning more than a wavelength.

c) *Overtopping*: Overtopping devices are effectively low head hydro systems. Large arms, either on the shore or on a floating structure, channel waves toward a

central collection basin. As the waves are focused on the basin, the volume of water rises up and spills over a retaining wall to fill the basin. This creates a small elevation differential with the surrounding water level that can be exploited via a standard low-head hydro turbine.

d) *Point absorber*: Point absorbers, often simply called a "buoy," are single, relatively small devices (compared individually to the other WEC types). They are typically (though not necessarily) cylindrical in shape and constrained to one major degree of motion, usually up-and-down (i.e., "heave"). They are generally significantly smaller in diameter than a wavelength.

1.3.1 Shoreline devices

Shoreline devices are devices fixed to or embedded in the shoreline. Examples include the oscillating water column (OWC), which is the most developed of the shoreline devices. An OWC system has a partially submerged hollow air chamber, which opens to the sea under the water line. A wave enters the air chamber and forces the air in the column to pass through a turbine; when the wave retreats, the air will be drawn back and passes through the turbine again [20] as shown in Figure 1.6. The turbine can be unidirectional or self-rectified. The unidirectional 'Wells turbine' is the best-known turbine for this kind of application. The world's first commercial wave power unit was the LIMPET 500, an OWC system mounted on the cliffs of the Islay island in Scotland by Wavegen. It generates a peak power of 500 kW, enough to provide service for about 400 island homes. This system has successfully fed electricity into the UK's national grid since November 2000.

Another representative of OWC technology is in development by Energetech in Australia [21]. Compared to the LIMPET, it uses a variable pitch turbine instead of the Wells to achieve higher system efficiency, and it has a relatively cheap parabolic wall behind the OWC to focus the wave energy on to the more expensive collector and associated plant.

The 'pendulum' was developed by the Japan Marine Science and Technology Center (JAMSTEC). It consists of a concrete box with one end open to the sea. A steel pendulum flap is hinged over this opening. Waves cause the pendulum flap to swing back and forth to power a hydraulic pump through a hydraulic system, which supplies a generator.
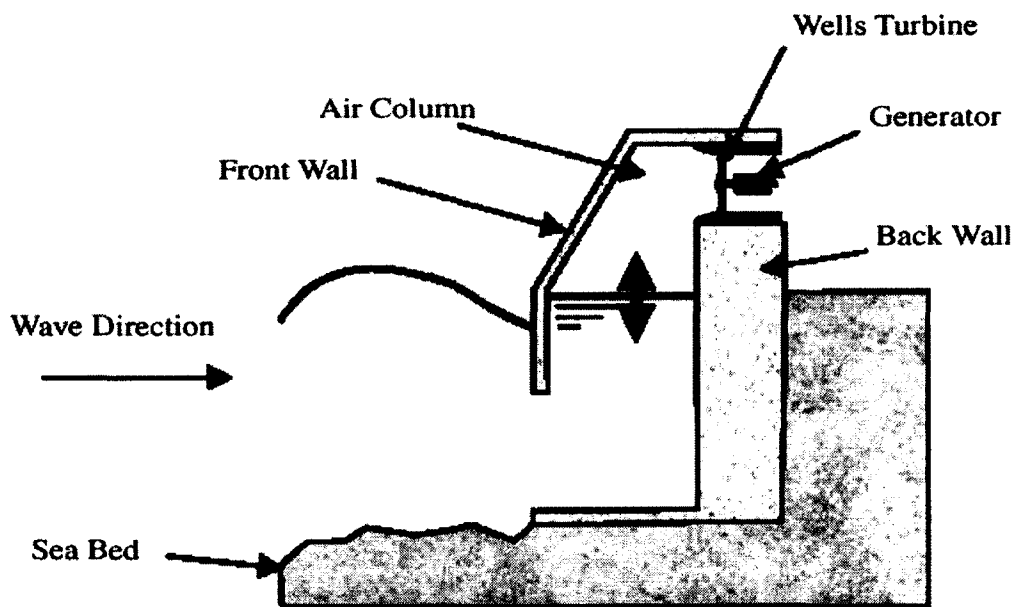
Figure 1.6. Working principle of an oscillating water column (OWC) [21].

The tapered channel system, or the TAPCHAN, was developed by Norwave AS of Norway. It applies the working principle of a traditional hydroelectric power plant. The

seawater is tapered into the reservoir constructed on a cliff and then flows back to the sea through a low-head hydroelectric generator to generate electricity [21].

1.3.2 Near-shore devices

Near-shore devices are in between the shoreline devices and offshore devices. Near-shore devices are used to extract the power directly from the breaker zone and the waters immediately beyond the breaker zone. Again, several approaches have been proposed.

The ocean swell powered renewable energy (OSPREY) is designed to operate in 15m of water within 1 km of the shore, generating up to 2 MW of power for coastal consumers [20]. The Mighty Whale is a floating OWC based device developed by JAMSTEC. A 120 kW prototype with three OWC's in a row has been operating since 1998 in water depths of 40 m, 1.5 km off Nansei-Town in Japan. The wind and ocean swell power (WOSP), is an integrated near shore wave and wind-powered station. It is designed to operate in much the same way as the OSPREY device, generating 3.5 MW of power, and offers major advances in accessing multiple offshore renewable energy resources [20]. Another example of a near-shore device is the Pelamis developed by Ocean Power Delivery in Edinburgh, Scotland [22]. This device is a semi-submerged, articulated structure composed of cylindrical sections linked together by hinged joints. As the waves peak and trough, the sections of the Pelamis act as a pump to move hydraulic fluid through hydro-turbine generators. The power generated from each segment runs to an underwater substation and then to land via a submersible electric cable. A 750 kW prototype of the OPD Pelamis was tested in August 2004 off the coast of Orkney, Scotland.

The Pelamis, as mentioned above, uses a rotational generator for ocean energy conversion and is shown in Figure 1.7. This device functions on the principle that wave

motion can be converted into reciprocal motion using vertical floating plates to create a liquid pumping action [7]. The pumping liquid is then routed through a pneumatic motor to turn an electrical generator. The central aim of this device is to ensure that it can survive virtually maintenance free while operating in very adverse marine weather conditions as opposed to other systems which have been optimized in favor of maximum energy conversion. Thus ruggedness and durability, rather than efficiency, are the central objective of the Pelamis.

Figure 1.7. The Pelamis Wave Energy Converter on site at the European Marine Energy Test Centre (EMEC) [23].

1.3.3 Offshore devices

Offshore devices, such as the proposed buoy generator, are the farthest out to sea; they extend beyond the breaker lines and utilize the high energy densities and higher power wave profiles available in deep-water (>40 m) waves and surges. In order to extract the maximum amount of energy from the waves, the devices need to be at or near the surface. This makes it a requirement to have flexible moorings. In addition, for utility grid support applications, submersible electrical cables are needed to transmit the generated power onto land where they can be interconnected to the grid. These devices

can be placed in such a way that they have little visible impact (e.g., >2 miles offshore) and can actually provide homes for many aquatic creatures, similar to an artificial reef.

The AquaBuoy is one such offshore buoy system. The technology was originally patented in Sweden, and is now being promoted by the AquaEnergy Group of Mercer Island, Washington [24].

Each AquaBuoy is simple in design, operates without polluting the planet, and is capable of producing up to 250 kW of electricity [25 – 26].

1.3.4 Comparison of different technologies

Shoreline devices have the advantages of being easier to access for installation and maintenance and they do not need deep-water moorings or long underwater electrical cables. However, when a wave travels towards the shoreline, its power is greatly reduced by the friction caused by the rough seabed. This can be partially compensated by placing the devices at locations of natural energy concentration.

Off-shore devices can take advantage of the more powerful wave profiles available in deeper water (>40 m in depth). In order to extract the maximum amount of energy from the waves, these devices need to be at or near the surface, causing them to usually require flexible moorings and submarine electrical cables for power transmission. These features cause critical cost issues in construction and maintenance.

Near-shore devices exhibit compromises between shoreline and offshore devices, e.g., when there are environmental objections to shoreline devices, near shore devices can provide an alternative solution.

1.4   Applications for wave power stations

The potential applications for utilizing wave energy for constructive purposes are numerous. A partial listing of applications for this natural resource is presented below.

1.4.1   Large scale power stations

Wave power stations which supply electricity to mainland national grid distribution systems would consist of several hundred individual WEC devices. Since most large scale grid systems are capable of accepting up to 15% of their power from fluctuating sources, WEC devices could effectively provide for this tolerable condition. Control of the individual devices is necessary in order to optimize output and each device must be capable of being shutting down should the grid lose its load [27].

1.4.2   Isolated communities and offshore islands

For isolated communities and offshore islands there is usually an existing diesel generation system to provide for the local electrical power demand. However, medium scale (100 kW – 2MW) wave energy converters could be integrated into the system to function as a fuel saving mode with the diesel generators providing security for the supply [27].

1.4.3   Sea-water pumping using wave energy

There are several applications which involve the pumping of sea-water. One such application involves artificially inducing the upwelling of nutrient rich water from the deep ocean to be used in lagoons for fish or shellfish cultures.

Ocean Thermal Energy Conversion (O.T.E.C.) requires seawater to be pumped through the system in order to generate electricity. These pumps typically require an

input of 250 kW/MW to operate. Fortunately, favorable O.T.E.C. locations are situated in equatorial trade wind zones where swell waves are consistent, providing an ideal opportunity for WECs to provide power to the O.T.E.C. pumps [27].

1.4.4 Wave energy desalination system

This application uses a sea-water pumping system to bring up seawater which is then desalinated into freshwater for practical purposes.

1.4.5 Hydrogen production

Hydrogen produced through electrolysis can be used in most modern appliances without reforming and could be competitive for bottled low pressure gas (L.P.G.). This application is particularly useful for island communities where the end product is used in heating and cooking. It is assumed that an integrated wave-diesel system could integrate an electrolyser to provide for the storage of wave energy (Harris et al. 1978) [27].

1.4.6 Maritime applications

Commercial wave energy converter systems have been in use for a number of years in sizes up to 5 kW for use in navigational buoys and lighthouse power.

A novel idea for a ship propulsion system using wave actuated aerofoils was developed in Norway (Jacobsen 1978). This vessel was able to travel up to 4 knots against the wind and waves when powered by it's fins [27].

1.5   Environmental and social implications of wave energy converters

Although wave energy utilization is not a completely benign activity, its environmental impact is expected to be low. The environmental and social implications

to be considered when planning to erect a wave energy conversion plant include the following:

1.5.1 Direct impact on ecosystems

Although the impact of WECs on the ecosystem is suspected to be minimal, site specific problems may still arise. Natural water circulations within the near-shore regions may be altered due to their interactions with large numbers of WECs moored to the sea-bed. This disturbance could affect migratory marine species such as salmon and also the growth of algal species such as Laminaria. Additionally, marine life may get trapped within the system creating a reduction in energy generation efficiency. Finally, many areas suitable for wave energy development have unique natural habitats onshore and conflicts of interest can arise. For example, the best site for the Norwegian demonstration scheme was located within a nature reserve [27].

1.5.2 Coastal morphological changes

Morphological alterations occur on sandy coastlines due to wave actions. Short steep waves, normally generated by storms near the coast, tend to remove (by a process known as erosion) beach material from the coast, whereas long waves (swells) tend to deposit (a process known as accretion) material from the deep waters onto the beach. The offshore (erosion) process generally occurs more frequently in winter storms, while the onshore (accretion) process occurs during the summer [28].

The effect of near-shore WECs can be used to reduce the wave steepness at the shoreline. Although this activity would result in a reduced rate of erosion of the

shoreline, its effect will only become significant when a large number of WEC devices are installed [27].

1.5.3 Maritime activities

Wave energy devices are considered hazardous to shipping because they generally possess a low freeboard. Adequate navigational aids, such as beacons and lighting, must be installed on these devices to prevent collisions with passing ships. If large arrays of WECs are installed, navigational gaps must be incorporated into the array to allow for the passage of ships. The WEC array presents an additional problem for small boats due to the presence of wave reflections from the converters which cause standing waves to form of increased amplitude, thereby increasing the difficulty for controlling the boat [28]. Fortunately, most areas with suitable wave climates for WECs also have low marine traffic densities [27].

The existence of a WEC acts as an artificial reef; which generally cause fish to shoal around the devices; thereby creating a beneficial effect on fisheries. Care must be taken, however, to avoid erecting a WEC plant in spawning or feeding regions [27].

Additional concerns that must be investigated prior to the establishment of a WEC facility include the effects on the local marine life due to the influence of electrical transmission cables and corona discharges. Transmission cables which transfer electrical power from the WEC to the shore processing station induce electromagnetic fields and heat that emit outside of the cable into the surrounding environment. It is suspected that the radiated electromagnetic field may produce an effect on marine life that may be sensitive to electric and/or magnetic fields [29-30]. These species include electro sensitive fish, notably elasmobranches (sharks, skates and rays) as well as eels and other

fish and mammal species. For example, elasmobranches have been found to be attracted to electrical fields in the range 0.5-100 μV/m and potentially repelled by electric fields above 100 μV/m [30]. Finally, it is suspected that the audible hum due to corona discharge may deter certain animals from crossing power line corridors.

1.5.4 Visual impact

It is suspected that the visual impact of wave energy converters will be minimal. Typically, the devices will be located several kilometers from shore and, due to their low freeboard, they will not intrude far above the horizon. However, the on-shore transmission systems are believed to produce a negative impact upon the scenic beauty of the land [27].

1.5.5 Socio-economic activity

Regions suitable for large scale wave energy development are generally locations where the indigenous industrial base is low resulting in a declining population of the local area. However, the construction of wave energy converters and the availability of energy can reverse this trend.

Large wave power stations require a great number of WEC devices, which can be constructed locally to reduce expenses. The establishment of large construction facilities has proven to significantly impact the local employment figures. In order to erect a power station rated at 2GW, over 500 WEC devices would need to be fabricated. Estimates suggest that several thousand people would need to be employed in order to produce 4 devices per month. At this pace, it would require 10 - 15 years to complete the project while simultaneously maintaining a healthy local employment rate.

Additionally, maintenance of these devices must be conducted on a routine basis in order to sustain satisfactory performance. Large stations will require about one thousand specialists in order to perform these tasks. Finally, due to the growing demand for employment in the area, it is suspected that the local population will rise and additional businesses will migrate to the region.

Unfortunately, the socio-economic impact of small- to medium- scale wave energy plants is assumed to be minimal. Existing construction yards could be used to fabricate the limited number of WEC devices required and the servicing requirements would likewise be low [27].

1.6 Wave energy economics

The Electric Power Research Institute (EPRI) has estimated that the first utility-scale wave power plants (which could provide up to 100 MW total installed capacity) would have a cost of energy (COE) of approximately 10 cents per kWh. This estimated cost is currently two to three times more expensive than that which can be currently produced through modern hydroelectric, coal, or wind plants. However, through large-scale utilization, the COE for wave energy is predicted to become quite competitive, and may approach 3 to 4 cents per kWh as the installed world-wide capacity exceeds 10,000 MW. This low COE estimate is based upon the natural high power density of wave energy, but the overall COE will also be highly dependent on the reliability, efficiency, and maintainability of mature wave energy conversion technology. The issues of reliability, maintainability, and survivability will hold greater significance for ocean wave energy as compared to wind and solar devices due to the energetic and corrosive nature of the

ocean. Additionally, the extra safety and financial obligations necessary to perform field maintenance on these devices must be considered in a cost-to-benefit ratio [31].

Since a number of wave energy technologies are in their pre-commercial stage, in the absence of experience gained through large-scale deployment, the actual cost scenarios pertaining to the electrical network design are difficult to predict. However, the information on plant cost development can be estimated, to some extent, from the wind energy sector. As indicated by recent studies (see Figure 1.8), the collection system (electrical power delivery) for offshore wind farms has encountered higher costs (approximately 25- 30% more) compared to onshore turbines. This condition arises due to the added complexity of offshore installations, grid connections and the requirement for specialized logistics. However, the higher annual wind energy extraction typical for offshore sites has been proven to be the dominant factor in determining offshore wind's economic success.
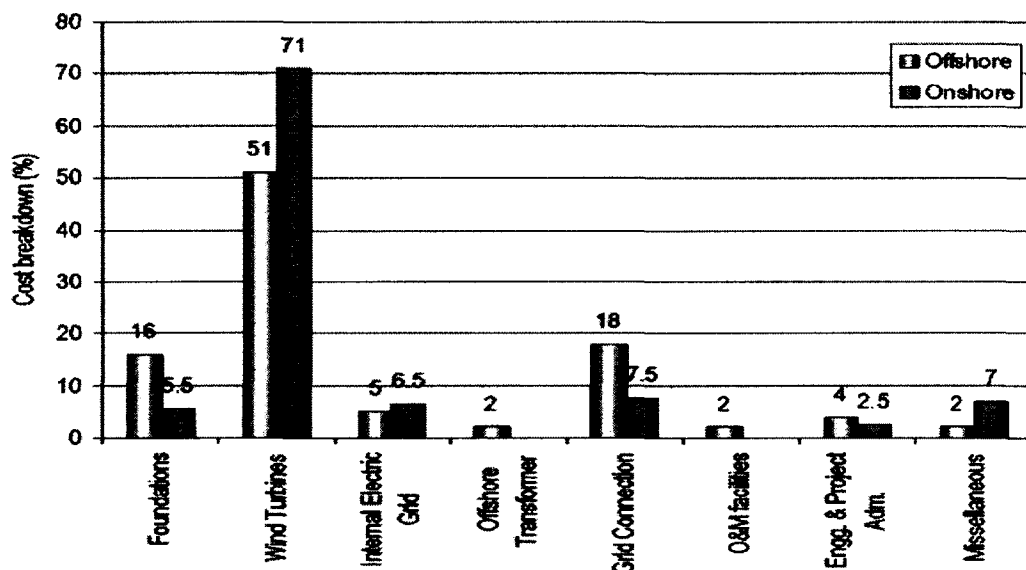
Figure 1.8. Capital cost breakdown comparisons for onshore and offshore wind farms [32-34].

Since many of the technologies and concepts being used in the wind industry (i.e. underwater cable, DC transmission with power electronic interfaces, etc.) are potentially applicable for ocean wave energy plants, it is believed that the cost for collection systems would remain similar.

1.7 Dissertation outline

Chapter I introduced the requirement to find alternate sources of electrical energy that are not harmful to the environment in order to meet the public's growing demand for electrical power. Then, the basic concepts of alternate energy generation techniques currently in operation along with a description of their advantages and disadvantages were discussed. Finally, the analysis of this chapter focused on the wave energy conversion sector, describing the applications, environmental and social impact, and costs for installing and maintaining a wave energy plant.

Chapter II provides a literature review of the following topics: the basic characteristics of surface ocean waves and techniques for measuring and modeling them; general properties of floating buoys and their wave induced motion, as well as their role in generating electrical power; and the basic concepts, construction materials, configuration, and power losses that occur for linear electric generators.

In Chapter III, the mathematical models for the floating buoy and linear electric generators are constructed. The models are constructed mathematically using formulas and equations provided from previously published papers. From these models, various physical and electrical parameters will be derived and plotted, the analysis of which will be discussed in the following chapter.

Simulation results are given and an analysis of the data generated is discussed in Chapter IV. Here specifically, the results for the mathematical models of the floating buoy and a permanent magnet linear generator are discussed. First, the wave height as a function of time is computed and plotted for several different sea conditions. Next, the parameters for a specific buoy are assigned and its motion is simulated under each of the different sea conditions. Then, a basic linear generator model is introduced and its generated voltage is compared with those from previously published findings to verify and validate the model. Finally, the electrical output parameters for the linear generator operating under various buoy sizes and sea conditions are simulated, analyzed and compared in an attempt to define the optimal operating conditions.

Finally, conclusions for the models and suggestions for further work in this field are presented in Chapter V.

CHAPTER II

BACKGROUND AND LITERATURE REVIEW

2.1 Introduction

This chapter is subdivided into the following four main topics: (a) basic characteristics of ocean waves, (b) modeling the ocean surface waves, (c) harnessing the oceans energy through the use of floating buoys, and (d) electrical energy generation principals using linear generators.

The chapter begins with a discussion of the origin and basic characteristics of surface ocean waves. Wave properties such as sea state, wave celerity and energy and power density will be defined both physically and analytically.

A basic introduction to modeling ocean surface waves begins with a discussion of the characteristics for the regular and irregular wave regimes. Since all models are dependent upon real data to be accurate, techniques for measuring wave properties in both the real ocean and in the laboratory environments are briefly presented. Then, concepts such as the ocean spectra and a fully developed sea are introduced along with effective tools, such as the Pierson-Moskowitz and Bretschneider Spectrums, which can be used to accurately simulate the ocean's surface characteristics under specified conditions.

The discussion then branches into how the ocean's energy can be used for practical purposes, such as in the production of electrical energy through the surface wave's interaction with floating buoys. A short description of floating buoys, including their physical properties, classes, and the environmental, static and dynamic forces which

affect them, are presented. Then, the Response Amplitude Operator for the buoy in heave is briefly described, along with an analysis of how it is affected by the various buoy parameters.

Principals of electrical energy generation through the mechanical linkage of a linear generator to a heaving buoy are the topic of the final section. Basic principles of the magnetic properties of materials, electrical energy generation through the use of a linear generator, and the power losses that naturally occur during energy production are discussed.

2.2   Basic characteristics of surface ocean waves   .

Ocean surface waves are produced through the absorption of wind energy, seismic activity, and influences by the moon and sun [35]. Wind-generated waves typically have periods from 1 to 25 seconds, wave lengths from 1 to 1000 meters, speeds from 1 to 40 m/s, and heights less than 3 meters. Seismic waves, or tsunamis (which are not analyzed in this work), have periods typically from 10 minutes to one hour, wave lengths of several hundreds of kilometers, and mid-ocean heights usually less than half a meter [36]. Influences from the moon and sun produce tides on the ocean surface and possess extremely long wave periods. Figure 2.1 illustrates the principal causes of ocean waves, the resulting wave type produced, and the probability for the wave having a specified period.
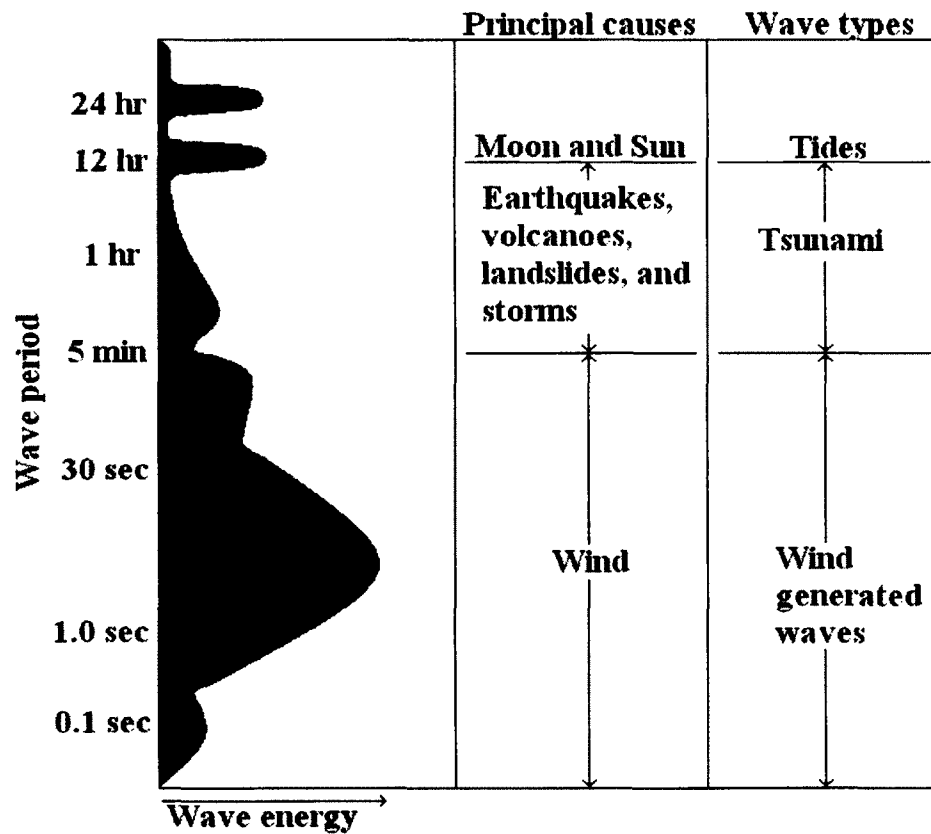
Figure 2.1. Sources of ocean waves [35].

Figure 2.2 illustrates the characteristics of a simple wave upon an ocean's surface. From this image, it can be observed that the wave height (H) is the vertical distance between a wave's crest and an adjacent trough; the wave's amplitude (a) is defined by the height of the wave above the still water line and represents ½ of the magnitude of the height (i.e., a = H/2) [36]; the waves' period (T) is the time required for two successive crests or troughs to pass a fixed point; the mean water depth (h, not shown) defines the distance below the still water line to the sea bed [36-37]; and the wavelength (λ) is the horizontal distance between two crests or troughs. The wavelength for a deep-water condition (where the depth of the body of water (h) is greater than half of the wavelength) can be derived from the following formula [38]:

$$\lambda = (g/2\pi) T^2 \ , \tag{2.1}$$

where
λ is the wave's wavelength,
g is the acceleration due to gravity, and
T is the wave's period.
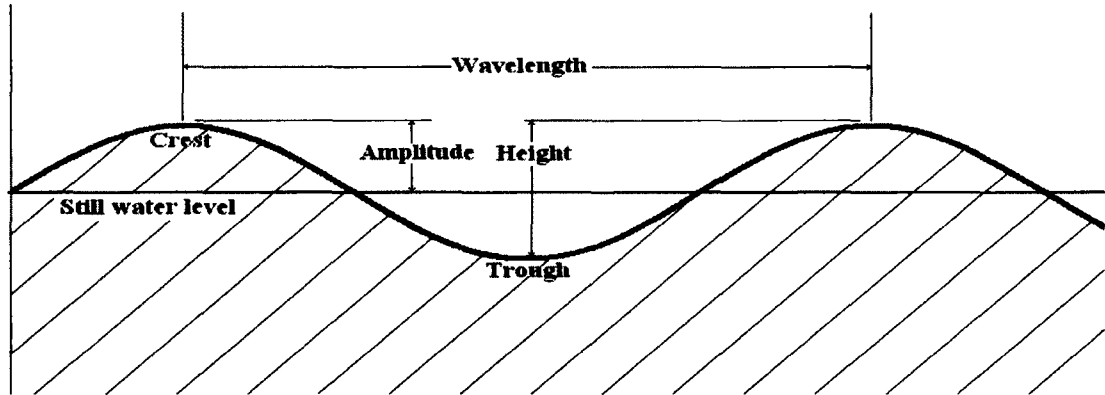
Figure 2.2. Characteristics of a simple wave [39].

The area over the ocean in which a particular set of waves is developed depends on the size of the pressure fronts involved. This area is called a "fetch." Waves developed in a fetch can travel great distances with little attenuation. For example, the waves at any given time on the West Coast of the U.S. are a combination of large swells produced over the open ocean that have traveled for hours or days to reach the shore, and smaller "chop" waves from the local wind [13].

Ocean wave conditions are stochastic in nature and are generally described using statistical parameters such as the significant wave height H_s and period, T_s. The significant wave height is defined as the average wave height of one third of the highest waves, and the wave's period is defined as the reciprocal of the frequency at which the peak of power spectral density occurs [37].

The formation of ocean waves, however, is not constant and is subject to continuous variations as well as seasonal influences. Table 2.1 describes how the wave characteristics vary for the winter and summer seasons for that region off of the coast of Oregon.

Table 2.1. Seasonal wave characteristics off of the Oregon coast [37].

Wave Parameter	Condition		
	Winter	Summer	Units
Significant height (H_s)	3.5	1.5	(m)
Significant period (T_s)	8	6	(s)
Wavelength (λ)	99.84	56.26	(m)

The World Meteorological Organization (WMO) sea state code is used to classify the condition of the sea with respect to the average wave height and is presented in Table 2.2 below.

Table 2.2. WMO sea state code [40].

WMO Sea State Code	Wave Height (meters)	Characteristic
0	0	Calm (glassy)
1	0 to 0.1	Calm (rippled)
2	0.1 to 0.5	Smooth (wavelets)
3	0.5 to 1.25	Slight
4	1.25 to 2.5	Moderate
5	2.5 to 4	Rough
6	4 to 6	Very rough
7	6 to 9	High
8	9 to 14	Very High
9	Over 14	Phenomenal

2.2.1 Wave celerity

A wave whose crest travels in a direction parallel to the still water line is called a traveling or progressive wave. The phase velocity of this wave is called celerity (C) and describes the distance travelled by a crest per unit time, i.e., it is given as [36]:

$$C = \lambda/T \ . \tag{2.2}$$

Waves transmit energy through the cyclic motion of particles in the ocean. Ocean waves dissipate this energy within several strata of circular oscillations. These particles move in circular orbital paths when acted upon by the force of gravity which only occurs at the surface. The diameter of these wave motions decrease with an increasing water depth. At a water-depth defined by half of the wavelength, the motion is non-existent. In deep water conditions (where the depth is greater than half of the wave length) there is no interaction with the seabed and the wave celerity is proportional to the wavelength (λ) of the waves.

In shallow water regions, where the depth is smaller than the wave length, these circular oscillations are squashed by their own pressure and the seabed into ellipses which approximates a back-and-forth motion. For shallow sea waves, the celerity is proportional to the water depth (h) [41].

Figure 2.3 illustrates the differences for wave motions occurring in deep and shallow water depths.

(a) Deep-water wave: Depth ≥ 1/2 wavelength	(b) Shallow-water wave: Depth < 1/20 wavelength
Wave motion	Wave motion
Wave length	
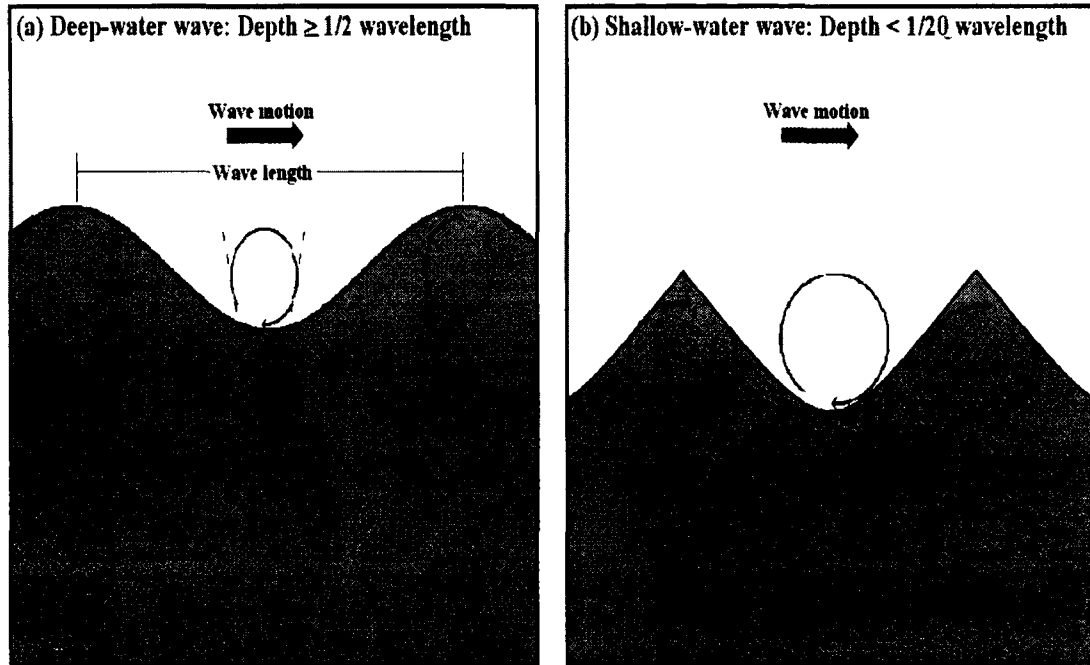
Figure 2.3. Celerity of waves for different water depths [41].

The small amplitude theory requires that both a/λ and a/h be small. Following this assumption and solving the equation of motion for small amplitude waves yields the following expression for the wave celerity [36]:

$$C = \left\{ \frac{g\lambda}{2\pi} \tanh \left[\frac{2\pi h}{\lambda} \right] \right\}^{0.5} , \qquad (2.3)$$

where g is the gravitational acceleration (9.81 m/s^2).

For deep water conditions ($h/\lambda > 0.5$) the $\tanh(2\pi h/\lambda)$ term approaches unity and the celerity is simplified to $(g\lambda/2\pi)^{0.5}$. In shallow water conditions ($h/\lambda < 0.05$) the $\tanh(2\pi h/\lambda)$ term approaches ($2\pi h/\lambda$) simplifying the celerity to $(g h)^{0.5}$.

Table 2.3 lists the three wave types along with their applicable equations for celerity and wavelength. This table reveals that in deep water the celerity is independent of the water depth (h). This is not surprising due to the fact that deep water waves do not

interact with the bottom surface. Shallow water surface waves, on the other hand, do interact with the seabed and slow down as the square root of the depth.

Table 2.3. Wave types [36].

Relative Depth h/λ	Wave type	Wave celerity	Wave length
h/λ < 0.05	Shallow water wave	$(g \cdot h)^{0.5}$	$(g \cdot h)^{0.5} \cdot T$
0.05 < h/λ < 0.50	Intermediate depth wave	$\left\{ \dfrac{g\lambda}{2\pi} \tanh\left(\dfrac{2\pi h}{\lambda} \right) \right\}^{0.5}$	$\dfrac{g \cdot T^2}{2 \cdot \pi} \tanh\left(\dfrac{2 \cdot \pi \cdot h}{\lambda} \right)^{0.5}$
h/λ > 0.50	Deep water wave	$\left(\dfrac{g\lambda}{2 \cdot \pi} \right)^{0.5}$	$\dfrac{g \cdot T^2}{2 \cdot \pi}$

A further inspection of Table 2.3 also indicates that as surface waves travel across various water depths their period (T) does not change. In deep water, therefore, the wave lengths are constant, but as the waves approach a beach, the wave length decreases as the square root of the depth.

2.2.2 Energy and power density

The total energy of a surface ocean wave represents the sum of its kinetic and potential energies. The kinetic energy represents water particle velocities associated with the wave motion. Potential energy results from that part of the fluid mass being above the trough of the wave crest. Thus, the total energy is given by [42]:

$$E_{WAVE} = E_{KINETIC} + E_{POTENTIAL} = \int_{x}^{x+\lambda} \int_{-h}^{\eta} \rho \cdot \frac{u^2 + w^2}{2} \, dz \, dx + \int_{x}^{x+\lambda} \rho \cdot g \left[\frac{(\eta+h)^2}{2} - \frac{h^2}{2} \right] \cdot dx \,, \qquad (2.4)$$

where
λ is the wavelength,
η is the elevation of the water surface,
ρ is the seawater density,
u, and w are the fluid velocities in the x- and z- directions respectfully, and
h is the water depth.

According to the Airy theory, if the potential energy is determined relative to the still water level and all waves are propagated in the same direction, the potential and kinetic energy components are equal. Thus, the total wave energy in one wavelength per unit crest width is given by [42]:

$$E_{WAVE} = \frac{\rho \cdot g \cdot H_s^2 \cdot \lambda}{16} + \frac{\rho \cdot g \cdot H_s^2 \cdot \lambda}{16} = \frac{\rho \cdot g \cdot H_s^2 \cdot \lambda}{8} \,. \qquad (2.5)$$

The total average wave energy per unit surface area is called the specific energy or energy density, and is computed by [42]

$$E_{density} = \frac{E_{WAVE}}{\lambda} = \frac{\rho \cdot g \cdot H_s^2}{8} \,. \qquad (2.6)$$

The energy density of a wave, as defined by Equation (2.6), represents the mean energy flux crossing a vertical plane parallel to a wave's crest. The energy per wave period represents the power density for the wave. Equation (2.7) reveals that the wave power density can be derived merely by dividing the energy density by the wave period [42], i.e.

$$P_{density} = \frac{E_{density}}{T} = \frac{\rho \cdot g \cdot H_s^2}{8 \cdot T} \,, \qquad (2.7)$$

where
$P_{density}$ is the wave's power density,
$E_{density}$ is the wave energy density,
T is the wave's period,
ρ is the seawater density,

g is the gravitational acceleration, and
H is the wave height.

The rate at which the wave energy propagates is directly dependent on the group velocity of the wave. The group velocity is given by [42]:

$$C_g = n \cdot C , \tag{2.8}$$

where n is a constant evaluated as:

$$n = \frac{1}{2} \left(\frac{1 + 4 \pi h/\lambda}{\sinh (4 \pi h/\lambda)} \right) . \tag{2.9}$$

A wave resource for energy generation purposes is typically described in terms of power per square meter of wave front (or wave crest). This power can be calculated by multiplying the wave celerity by the power density as equation (2.10) demonstrates [42].

$$P_{WAVEFRONT} = n \cdot C \cdot P_{density} = C_g \cdot P_{density} = \frac{\rho g H_s^2}{16T} \left(\frac{1 + 4 \pi h/\lambda}{\sinh (4 \pi h/\lambda)} \right) \tag{2.10}$$

2.3 Modeling the ocean surface

The ocean surface can be modeled using two different approaches; the regular and the irregular wave regimes. Both models will be incorporated in this work to test the functionality of a modeled wave energy converter (WEC). First, the WEC shall be tested under the regular wave regime to validate the basic function of a modeled linear generator WEC. Then, the modeled generator is tested under the irregular wave regime to test its operability under the more realistic ocean surface conditions.

2.3.1 The regular wave regime

The regular wave regime is simplistic in nature and assumes that ocean surface waves maintain a constant maximum amplitude and steady period [25]. The amplitude of a

surface wave as functions of its maximum height, cyclic frequency, phase angle between

wave and force, and time is expressed by:

$$A_W (Z_{WAVE}, \omega, \varphi \ t) = Z_{WAVE} \ \cos(\omega t + \varphi), \tag{2.11}$$

where

A_W is the wave's amplitude,

Zwave is the wave's maximum amplitude (Zwave = $H_s/2$),

ω is the cyclic frequency of the wave ($\omega = 2\pi/T$), and

φ is the phase difference between the wave and the force (we set $\varphi = 0$).

2.3.2 The irregular wave regime

The irregular wave regime is much more complex in nature. In the irregular wave

regime, the wave is super-imposed by many regular waves of different heights, periods,

and phase angles which combine to create irregular wave patterns in a random or

irregular sea. Figure 2.4 illustrates how four surface waves having different

characteristics combine to create an irregular wave pattern.
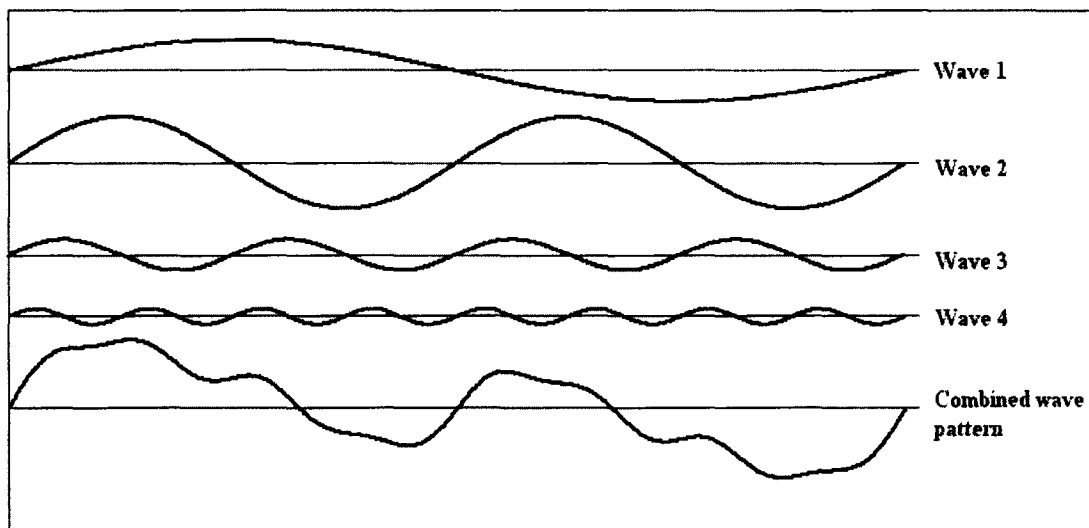
Figure 2.4. Wave pattern combining four regular waves.

In computing the energy density for the irregular wave regime, the exciting wave height is computed as the sum of each of the individual wave heights [43]. Thus, to compute the energy density for the combined wave appearing in Figure 2.4, the computation would be

$$E_{density} = \frac{\rho g}{8}(H_{Wave\,1}^2 + H_{Wave\,2}^2 + H_{Wave\,3}^2 + H_{Wave\,4}^2) . \qquad (2.12)$$

Clearly, equation (2.12) reveals that the intensity of the sea is characterized by its total energy. Through the use of practical mathematical tools (e.g., Fourier analysis), it is possible to determine the contribution that is made by each of its component waves [43]. The height of each wave component is governed by the Wave Energy Density Spectrum (also known as the wave spectrum). This spectrum defines how much energy is contained in each frequency of the wave. Using actual periodic sea measurements (for example, every 20 minutes) the average wave period and significant wave height parameters can be obtained. Then, using this data, it is possible to reproduce an irregular wave having the same significant wave height and average period through the use of the Bretschneider Spectrum which will be discussed later [25].

2.4 Instrumentation for measuring the ocean parameters

In order to accurately represent an oceans' surface, important parameters must first be measured to ensure a valid model is created. Due to the fact that waves influence so many processes and operations at sea, many techniques have been invented for measuring waves. A partial listing is summarized below:

2.4.1 Real ocean data acquisition techniques

2.4.1.1 Satellite altimeters

Satellite altimeters are now the most widely used source for wave measurements. Altimeter data is used to produce monthly mean maps of wave-heights and the variability of wave energy density in time and space. This data is also assimilated into wave forecasting models in order to increase the accuracy of wave forecasts [44].

The satellite altimeter functions by reflecting a radio pulse first from the wave crests and later from the trough. The reflection stretches the altimeters' pulse in time, and the stretching is measured and used to calculate wave height. This technique operates with an accuracy of ±10%. Figure 2.5 illustrates the shape of the radio pulse received by the altimeter due to the influence of ocean waves.
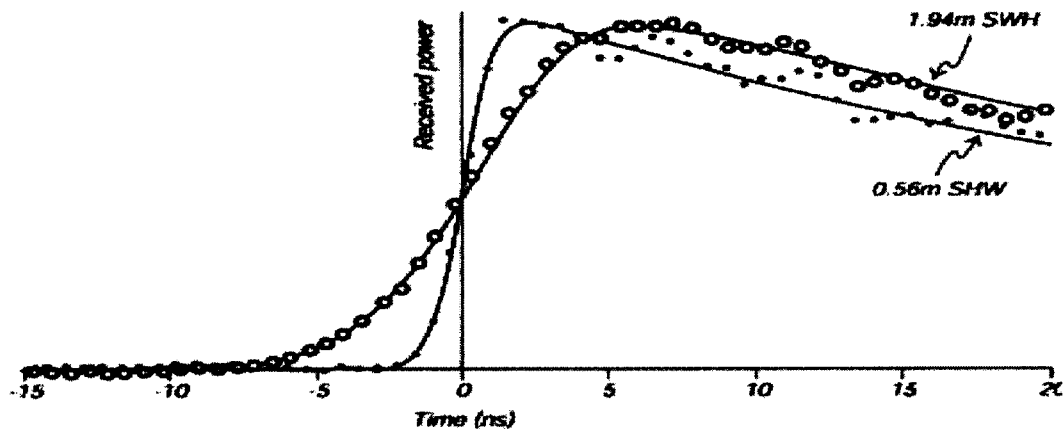
Figure 2.5. Shape of the radio pulse received by the Seasat altimeter is used to calculate significant wave-heights [44].

2.4.1.2 Synthetic aperture radars on satellites

These radars map the reflectivity of the sea surface with a spatial resolution of 6-25 meters. Maps of reflectivity show wave-like features related to the real waves on the sea surface.

2.4.1.3 High frequency radar

Although satellite-based radar systems are useful for mapping surface currents in the remotest parts of the ocean, they have limited capabilities close to the shore and in bays and estuaries. Winds, tides, the outflow of rivers, and the shape of the seafloor and land all contribute their influence in shaping the coastal currents. Additionally, shifting sandbars, random storms, and the influx of eddies spinning off of larger currents further complicate the task of measuring the coastal behavior [45].

Then, starting in the late 90s, high frequency (HF) radar systems emerged. These land mounted instruments can map surface currents in wide swaths of coastal waters up to 200 km off shore, 24 hours a day, and in all weather conditions. A practical example of a high frequency radar system is the CODAR Ocean Sensors SeaSonde HF Radar System. This system uses high-frequency (HF) radar pulse backscatter to map surface currents over wide swaths of the coastal ocean. Currently, the Bodega Marine Laboratory operates five HF radar stations located in Bodega Bay, Point Reyes, Salt Point, and Point Arena, CA [45].

The physics behind high frequency radar is fairly simple. A transmitter broadcasts electromagnetic waves generally between 5 and 25 megahertz toward the coast. If the signal strikes an ocean wave that is exactly half of the broadcast signal's wavelength, and if the ocean wave is traveling towards or away from the transmitter, the signal reflects back. This phenomenon is identified as Bragg scattering [45]. Since there are an abundance of waves of various wavelengths present in the ocean, there are always plenty of waves that meet this criterion.

The direction of movement of the ocean waves shifts the frequency of the returning signal due to the Doppler effect. The frequency increases when the current pulls the waves towards the transmitter and decreases when it pushes them away. By measuring this Doppler shift, it can be determined if the speed of the currents pull the waves towards or pushes them away from the transmitter [45].

In order to calculate the directions of the currents, a second HF radar installation needs to measure the same currents from a different angle. The direction of the current can then be derived through their vectors [45].

2.4.1.4 Accelerometer mounted on meteorological or other buoy

This is a less common measurement technique, although it is often used for measuring waves during short experiments at sea. The Pierson-Moskowitz spectrum (discussed later) was experimentally derived by analyzing the data recorded from accelerometers mounted on weather ships. The measurements recorded from these accelerometers are accurate to ±10% or better [44].

2.4.1.5 Wave gauges

Gauges may be mounted either on platforms or on the seafloor in shallow water. Many different types of sensors are available to measure the height of the wave or subsurface pressure which is related to the wave-height.

Sound, infrared beams and radio waves can be used to determine the distance from the sensor to the sea surface provided the sensor can be mounted on a stable platform which does not interfere with the waves. Pressure gauges can be used to measure the depth from the sea surface to the gauge. Arrays of bottom-mounted pressure gauges may

be used to determine wave directions. The accuracy of gauges is also rated at ±10% or better.

2.4.2 Laboratory techniques

Wave velocity measurements can also be obtained in the laboratory through the use of the Acoustic Doppler Velocimeter (ADV) or Laser Doppler Velocimeter (LDV). Both of these devices are discussed below.

2.4.2.1 The Acoustic Doppler Velocimeter (ADV)

The Acoustic Doppler velocimeter, as illustrated in Figure 2.6, is designed to record instantaneous velocity components at a single-point at a relatively high frequency. Measurements are acquired by measuring the velocity of water particles in a remote sampling volume based upon the Doppler shift effect. The sampling volume is typically a cylinder of water with a diameter of 6 mm and a height of 9 mm and is located 5 or 10 cm from the tip of the transmitter. The velocity component is measured along the line connecting the sampling volume to the receiver in the probe head [46].

http://www.sontek.com/apps/flume/adv-swf/adv-swf.htm

Figure 2.6. Acoustic Doppler Velocimeter (ADV) [37].

Although acoustic Doppler velocimetry (ADV) has become a popular technique in laboratory and field applications, several researchers accurately claim that the ADV signal outputs include the combined effects of turbulent velocity fluctuations, Doppler noise, signal aliasing, turbulent shear and other disturbances. Additionally, the signal may be further adversely affected by velocity shear across the sampling volume and boundary proximity. Due to these proven deficiencies, "raw" ADV velocity data are not to be considered as "true" turbulent velocities and should never be used without adequate post-processing [46].

2.4.2.2 The Laser Doppler Velocimeter (LDV)

A Laser Doppler Velocimeter (LDV), as depicted in Figure 2.7, can be used to measure the velocity of a heaving buoy [37]. LDV measures the direction and speed of fluids by crossing two beams of a collimated, monochromatic, and coherent laser light in

the flow of the fluid being measured. The two beams are made to intersect at their focal points, where they interfere and generate a set of straight fringes.

The sensor is aligned to the current flow such that the fringes are perpendicular to the flow direction. As the water particles pass through the fringes, they reflect light (only from the regions of constructive interference) into a photo-detector. By measuring the Doppler equivalent frequency-shift of the scattered light, it is possible to calculate the velocity of the tracer particle and thus the velocity flow of the liquid [47].

Figure 2.7. Laser Doppler Velocimeter (LDV) [47].

2.5   Ocean wave spectra

As the wind begins to blow (between 0.5 - 2 knots) over a calm ocean surface, small (less than 2 cm in wavelength) ripples, capillary waves or "cat-paws", tend to form. As

the wind becomes stronger, the wave amplitude increases and the waves become longer in order to satisfy the dispersion relationship [48]. The deep water dispersion relation and phase velocity equations are represented by [49-50] as:

$$\omega = \sqrt{(gk)} \quad , \qquad (2.13)$$

$$V_p = \omega/k = \sqrt{(g/k)} = g/\omega , \qquad (2.14)$$

where
g is the acceleration due to gravity,
k is the wave number ($k = 2\pi/\lambda$),
V_p is phase velocity, and
ω is the cyclic frequency of the wave.

This wave growth is driven by Bernoulli effects, frictional drag, and the separation drag on the wave crests.

Winds must blow for long periods of time and over large distances to reach a fully developed sea state. When the phase speed of the wave crest matches the wind speed all non-linear interactions stop (except friction) and the phase speed is maximized. The limiting frequency of the waves can be determined by the equation for deep water phase velocity and the dispersion relationship [48]:

$$V_p \approx U_w = \omega/k = g/\omega \quad , \qquad (2.15)$$

$$\omega_c \approx g/U_w \qquad , \qquad (2.16)$$

where
V_p is the phase speed of the wave,
U_w is the wind speed, and
ω_c is the limiting frequency.

Once the wind stops blowing, viscosity erodes the waves slowly. Those waves having the smallest wavelengths decay the fastest followed by those having longer wavelengths. A sample ocean wave spectrum is illustrated in Figure 2.8.
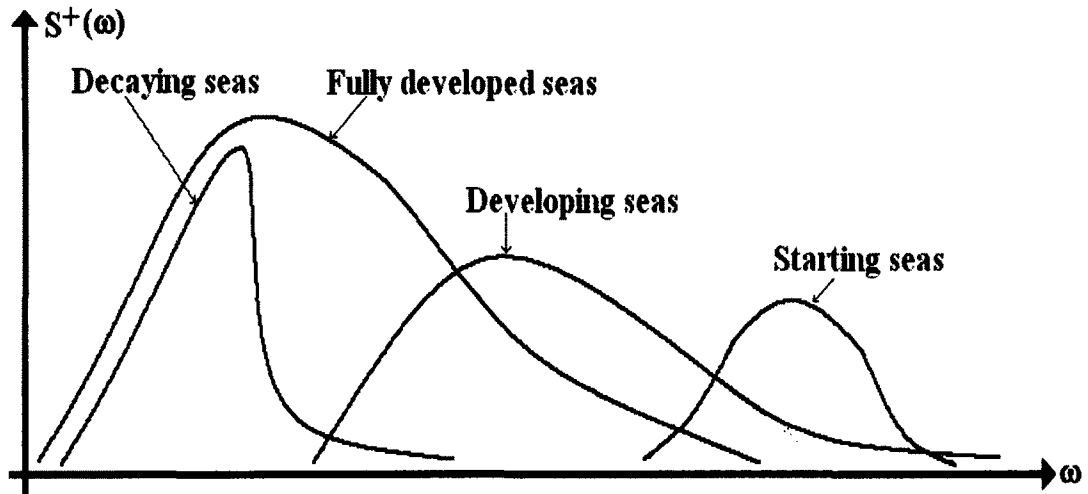
Figure 2.8. Sample of an ocean wave spectrum [48].

2.5.1 The fully developed sea

The concept for a fully developed sea assumes that winds blow steadily for a long time over a large ocean surface area, causing the waves to come into equilibrium with the wind. Generally, a long time is considered as roughly ten-thousand wave periods, and a "large area" is approximately five-thousand wave-lengths on a side [51].

In order to readily simplify the conditions to justify a fully developed sea, the development of storms can be tabulated. Table 2.4 lists the storm conditions according to the Beaufort scale. In this table, fetch is the length of water, given in standard miles, over which the wind must blow to create fully developed seas and the storm duration, given in hours, lists the duration that the storm must last to result in a fully developed sea.

Table 2.4. Beaufort scale for storms [48].

Wind Warnings	Beaufort Scale	Wind Speed (mph)	Fetch (miles)	Storm Duration (hours)
	3 - 4	12	15	3
small craft	5 -6	25	100	12
	7	35	400	28
gale	9	50	1,050	50
hurricane		70+		

2.5.2 Developing the ocean wave spectra

Most ocean wave spectra take a standard form following the mathematical formulation [48]:

$$S^{+}(\omega) = \frac{A_s}{\omega^5} \exp(-B_s/\omega^4) \qquad (2.17)$$

For this spectrum, the peak frequency is called the modal frequency. The area under the spectrum is the zeroth moment, M_o, which may be defined in terms of the significant wave height (H_s), and A_s and B_s are spectral constants. In some instances, a certain spectra can have more than one peak, it is assumed that a single storm produces a single-peaked spectrum and any secondary peak is created from a distant storm that sends waves to the considered location.

Some parameters that may influence this spectrum and associated issues and questions include the following [48]:

- Fetch limitations – Does the area under consideration have some physical boundaries which do not permit the waves to fully develop?

- Observed behavior - Is the condition of the sea developing or decaying?

- Seafloor topography – is the proper spectrum being constructed for the water depth?

- Local currents – are local currents significant enough to affect the wave spectrum?

- Presence of swells – Are waves from distant storms arriving at the location from an angle which differs from the observed wind direction?

2.5.3 The Pierson-Moskowitz spectrum

The Pierson-Moskowitz spectrum (see Figure 2.9) was developed for fully developed

seas in the Northern Atlantic Ocean generated by local winds [48].
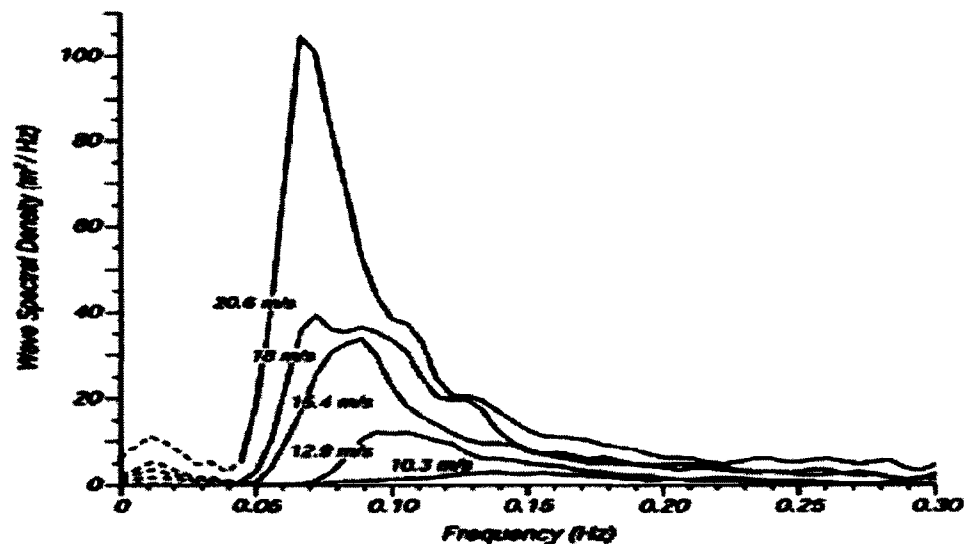
Figure 2.9. The Pierson-Moskowitz spectrum for a fully developed sea using different wind speeds [51].

To obtain this spectrum, measurements were taken by accelerometers on British

weather ships in the North Atlantic. First, they selected the wave data for times when the

wind had blown steadily for long durations over large areas of the North Atlantic. Then,

they calculated the wave spectra for various wind speeds, and they found that the spectra

were of the form [51]

$$S^+(\omega) = \frac{\alpha \cdot g^2}{\omega^5} \exp\left(-\beta\left[\frac{\omega_0}{\omega}\right]\right)^4 , \tag{2.18}$$

where
$\omega = 2 \cdot \pi \cdot f$, with f being the wave frequency in Hertz,
$\alpha = 8.1 \times 10^{-3}$,
$\beta = 0.74$, and
$\omega_0 = g/U_{19.5}$, with g being the gravitational constant and $U_{19.5}$ is the wind speed at a height of 19.5m above the sea surface (the height of the anemometers on the weather ships used by Pierson and Moskowitz in 1964).

For most air flow over the sea, the atmospheric boundary layer has nearly neutral

stability [51], and

$$U_{19.5} \approx 1.026 \cdot U_{10} , \tag{2.19}$$

assuming a drag coefficient of 1.3×10^{-3}.

The frequency for the peak of the Pierson-Moskowitz spectrum is calculated by

solving $dS/d\omega = 0$ for ω_p, to obtain [51]

$$\omega_p = 0.877 \cdot g/ U_{19.5} . \tag{2.20}$$

The wave speed at the peak is calculated as:

$$V_p = g/\omega_p = 1.14 \cdot U_{19.5} \approx 1.17 \cdot U_{10} . \tag{2.21}$$

The significant wave-height is calculated from the integral of $S(\omega)$ to obtain:

$$<\zeta^2> = \int_0^\infty S(\omega) \cdot d\omega = 2.74 \times 10^{-3} \cdot \frac{(U_{10})^4}{g^2} . \tag{2.22}$$

Since $H_{1/3} = 4 < \zeta^2 >^{1/2}$, the significant wave-height can be calculated as:

$$H_{1/3} = 0.21 \cdot \frac{(U_{19.5})^2}{g} \approx \frac{0.22 \cdot (U_{10})^2}{g} . \tag{2.23}$$

Figure 2.10 plots the significant wave height and period at the peak of the spectrum for a fully developed sea calculated using the Pierson-Moskowitz spectrum.
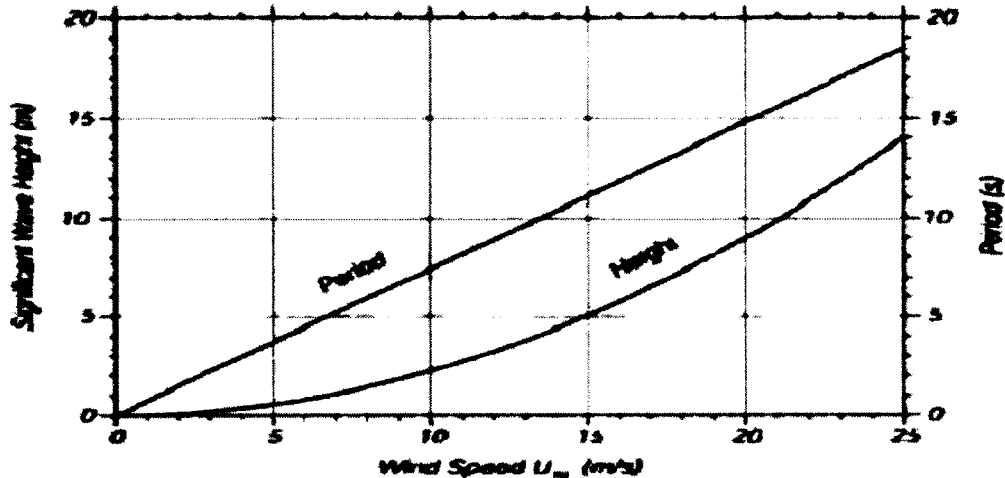
Figure 2.10. Significant wave-height and period as a function of wind speed derived using the Pierson-Moskowitz spectrum [51].

2.5.4 The Bretschneider spectrum

In order to overcome the limitations of a fully developed sea, the two-parameter Bretschneider spectrum was developed [52]. The Bretchneider spectrum replaced the Pierson-Moskowitz spectrum as the ITTC standard [48].

To evaluate the validity of the Bretschneider spectrum, a case study was carried out in the Caspian Sea. This area was chosen as the study area, since sufficient data on wave characteristics was not previously available in some regions of the Caspian Sea. Thus, the testing would be used to determine if sensitive operations such as the installation of offshore petroleum platforms would be feasible [53].

The simulation of wave characteristics was conducted based on available wind data recorded by the Khazar Oceanography Buoy (KEPCO 2001). This buoy is located in the south eastern part of the Caspian Sea, 30 km from Neka Harbour at a water depth of 35 m

and operated by KEPCO (an Iranian Company for the exploration of oil in the Caspian Sea) [53].

Wave characteristics were simulated in deep water parts of the Caspian Sea based on recorded wind data using the Bretschneider spectrum (Bhattacharyya 1972, Cold Bay Study [CBS] 1999) and various modeling equations (U.S. Army Coastal Engineering Research Center 1980, Sadeghi 1989, 2001). Wind duration and velocity, fetch length, and water/air temperature differences were considered in the simulation. Some constrains for the wave velocity and periods, as well as the wind velocity, were used as limitation criteria for offshore installation operations.

The resulting formula for the Bretschneider ocean wave spectrum is [52, 54]

$$S^+(\omega) = (5/16) \cdot (\omega_m^4/\omega^5) \cdot H^2_{1/3} \cdot \exp(-5 \cdot \omega_m^4/4\omega^4) , \qquad (2.24)$$

where
ω_m is the modal or peak frequency of any given wave,
ω is the frequency of the wave in radians per second, and
$H_{1/3}$ is the significant wave height.

Figure 2.11 plots the Bretschneider spectrum for the summer conditions off the Oregon coast. The parameters for this plot (as obtained from Table 2.1) were $H_{1/3}$ = 1.5m, and T_s = 6s. An additional example of the Bretschneider spectrum appears in Figure 2.12 which compares the plots of the several different sea states as given in Table 2.5.
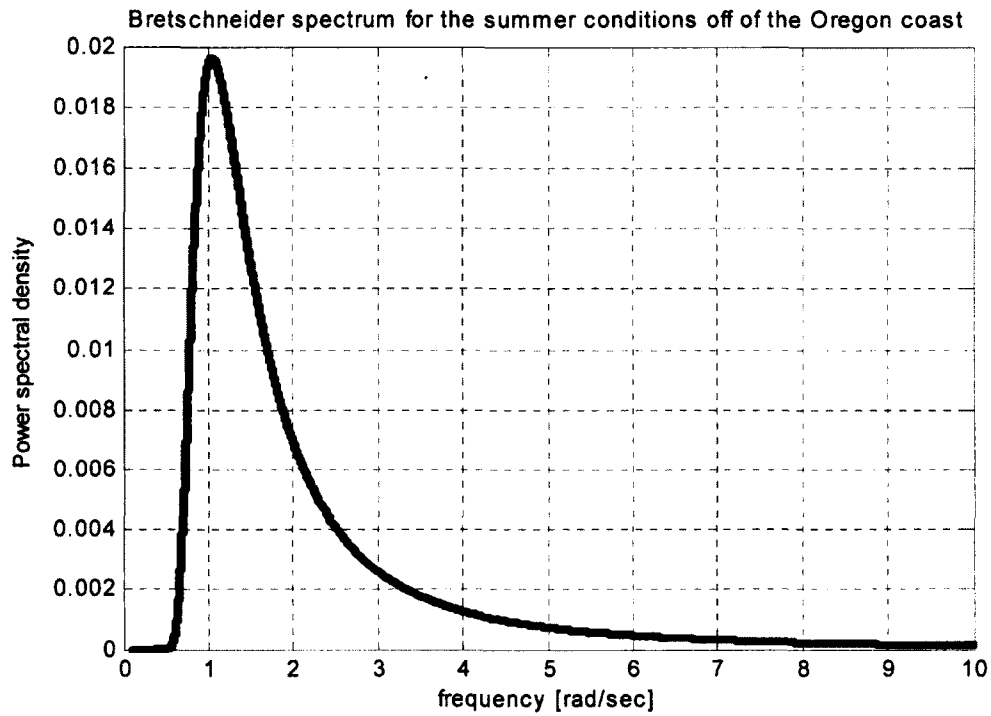
Figure 2.11. Bretschneider spectrum for the summer conditions off of the Oregon coast.
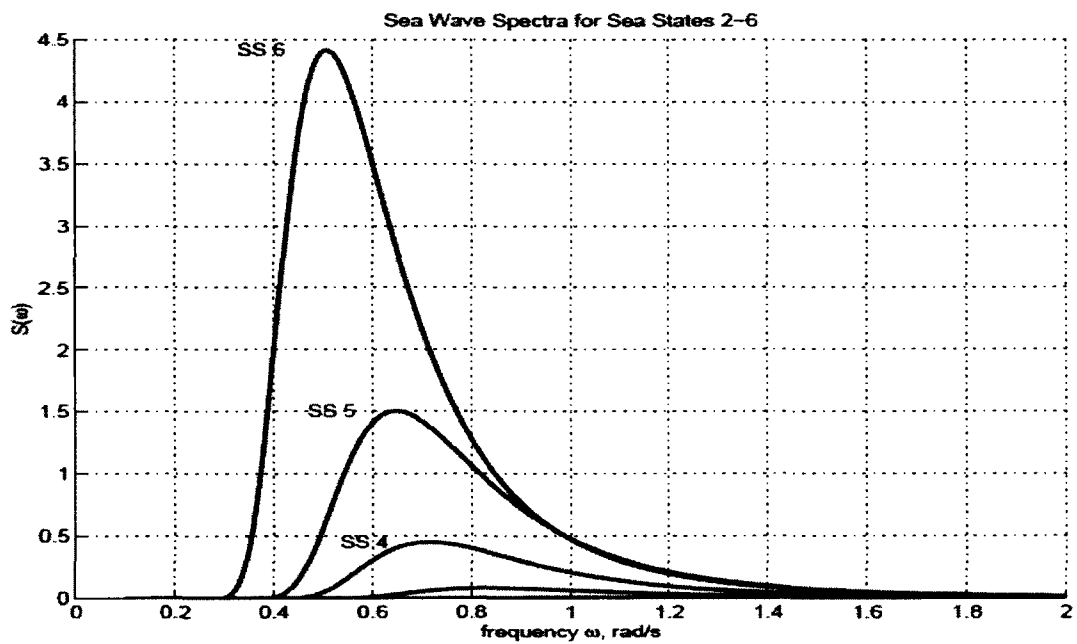
Figure 2.12. Bretschneider spectrum for the sea states defined by Table 2.5 [54].

Table 2.5. Various sea states conditions [54].

Sea State	$2\pi/\omega_m$ (sec)	$H_{1/3}$ (m)
2	6.3	0.3
3	7.5	0.9
4	8.8	1.9
5	9.7	3.3
6	12.4	5.0

The amplitude for each wave component can be obtained from the Bretschneider spectrum by [25, 55]

$$A_i = (2\,S^+(\omega)\,\Delta\omega)^{0.5} \quad , \tag{2.25}$$

with a corresponding random phase angle defined by [25]

$$\theta_i = 2\pi\,\text{rand}(1). \tag{2.26}$$

The time series for the wave spectrum, defined as the wave height as a function of time, is then calculated at any time t by the summation of the individual products of each amplitude component and the wave exciting force at each frequency (calculated at unit wave amplitude) [25, 55]. Thus,

$$H(t) = \sum_i A_i\,\cos(\omega_i\,t + \theta_i). \tag{2.27}$$

where
H(t) is the wave height at time t,
A_i is the amplitude component at cyclic frequency ω_i,
ω_i is an individual waves' cyclic frequency, and
θ_i is the phase angle for an individual wave.

Figure 2.13 plots an example time series of a wave spectrum having a significant wave height of 2 meters and a mean period of 5.3 seconds.
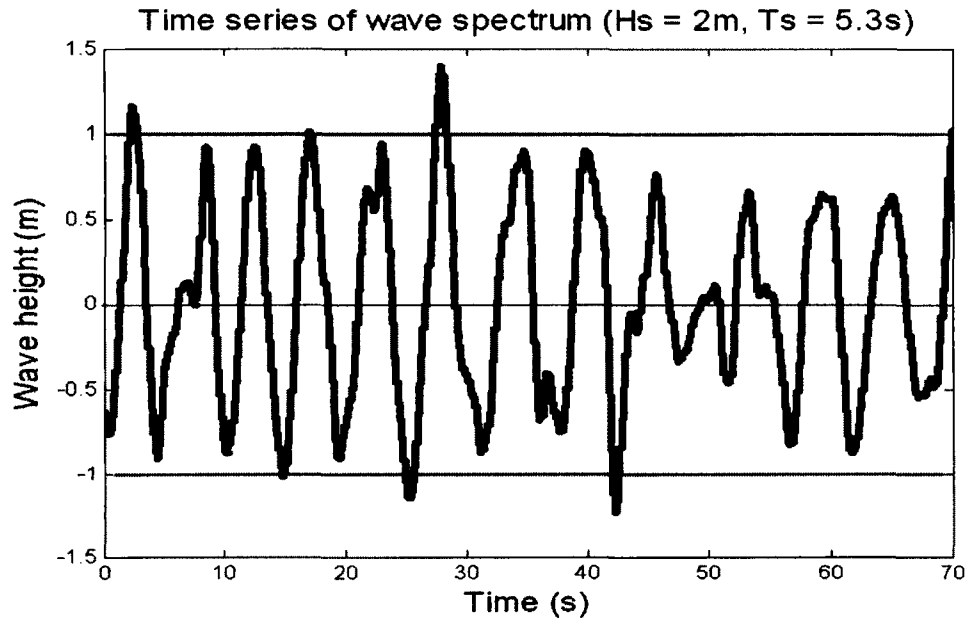
Figure 2.13. Time series of waves derived from the wave spectrum where $H_s = 2m$, and $T_s = 5.3s$. The light gray lines mark significant wave heights [55].

Using physical wave data obtained from the National Buoy Data Center (NBDC), typical wave parameter values for a specific sampled period may be used to plot the Bretschneider spectrum for that period [56]. Then, equations (2.25) through (2.27) may be used to re-create the sea state for that same period.

2.6 Harnessing the ocean's energy

Now that the ocean has been identified as an ever-changing turbulent environment, it would prove ideal to harness a portion of this energy constructively in order to generate 'green' electricity. This procedure can be accomplished through the use of floating or submerged buoys. These devices can effectively generate electricity either by floating upon the surface of the water and responding to the up and down heaving of the passing surface waves, or submerged below the surface reacting to pressure differentials. Since these devices merely absorb energy at the affected point, they are termed point absorbers.

A rigid floating body has six motional degrees of freedom; three translational, i.e., in the x- y- and z-directions, and three rotational around each of the axes. The names for each degree of freedom are given in Figure 2.14.
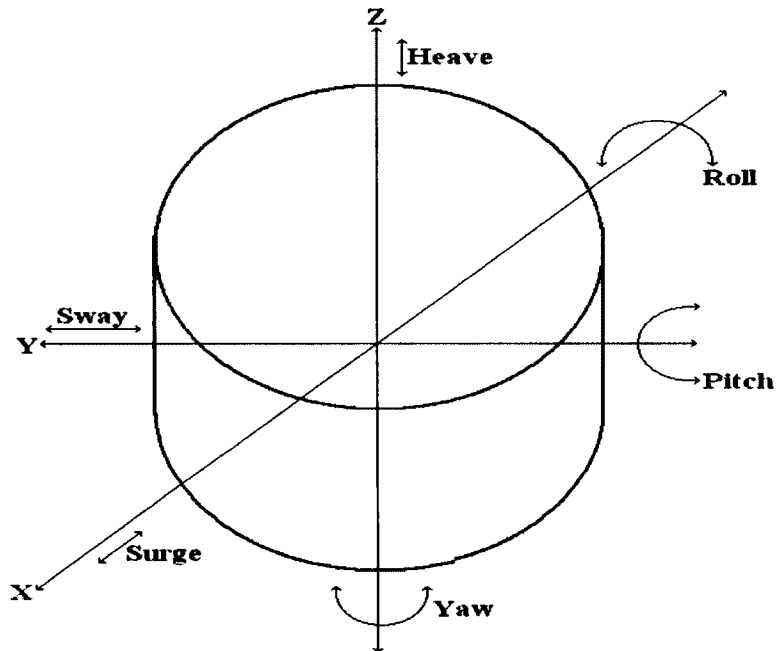
Figure 2.14. Motional degrees of freedom of a floating body [55].

2.6.1 Classes of buoys

There are many types of surface and subsurface buoys that have been built to suit a large variety of oceanic applications. These buoys can be classified into one of the following three classes:

2.6.1.1 Surface following buoys

Surface following buoys (which are the focus of this work) have the tendency to closely follow the waves. They are generally disc (Figure 2.15a), toroid (Figure 2.15b),

and boat hull shaped. These buoys are subject to strong heave and roll motion, and

unless they are of large dimensions, may capsize in breaking seas. These buoys do,

however, have the following advantages [57]:

- They can provide ample reserve buoyancy when strong currents increase the mooring line tension.
- Their contribution to the total system drag is relatively small, and
- Being of simple shape, their fabrication difficulty and construction costs are minimized.
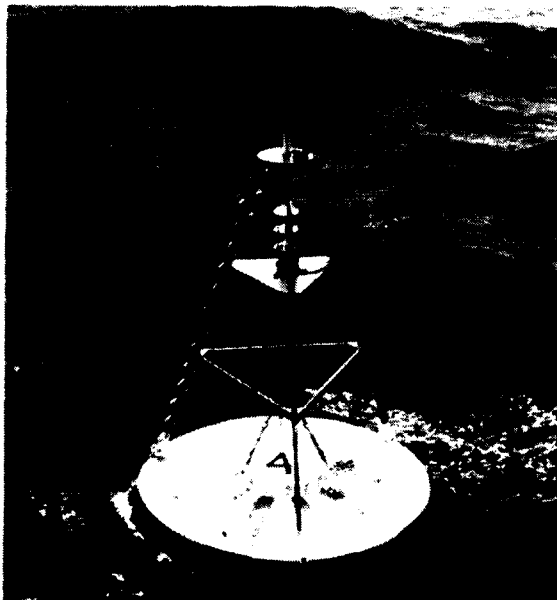
(a)   (b)

Figure 2.15. Buoy geometries. (a) Disc-shaped buoy, and (b) toroid-shaped buoy [57].

2.6.1.2 Surface decoupled buoys

Surface decoupled buoys are preferred for instances where reduced heave and roll

motions of the surface buoy are desirable. A buoy having a large mass and small cross

section at the water level will experience a small heave (vertical acceleration) as the

water level changes with the passing waves. Roll motion can be minimized by

distributing the buoys' mass to provide a strong righting moment. A typical example of a surface decoupled buoy is a floating slender cylinder with a counterweight at its lower end. However, the length of a spar having a constant cross-section must be quite large to still be effective for large wave periods [57].

Improved versions of the elementary spar are often constructed of a series of watertight and water-filled tanks supporting a mast or a tower at the top end and a damping plate at the lower end. A typical spar buoy is depicted in Figure 2.16.

To be efficient, spar buoys cannot have much reserve buoyancy. Furthermore, since their draft is typically large, their hydrodynamic resistance is fairly high. These two limiting efficiency factors must be accurately assessed when the spar buoy is to be moored in deep water.
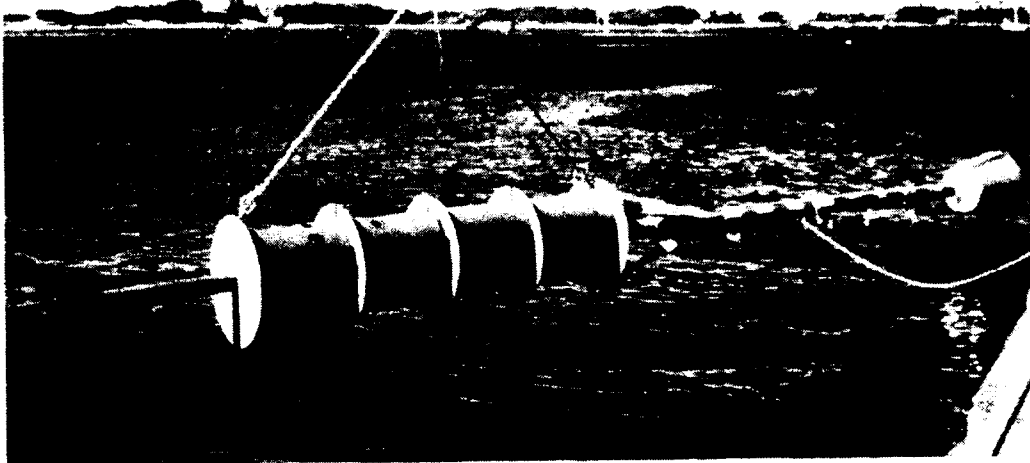
Figure 2.16. A 53-foot long spar buoy [57].

2.6.1.3   Subsurface buoys

Subsurface buoys are moored below the water's surface. The size, shape, and construction materials for subsurface buoys vary with the intended implantation depth.

57

In the upper region of the water column, large amounts of buoyancy can be achieved through the use of conventional pressure resistant shells or through the selection of pressure resistant construction materials of relatively low density. As the depth increases, the shell thickness must increase as well to resist hydrostatic pressure, thereby causing the weight of the buoy to increase. As the buoys' weight increases, its efficiency decreases rapidly [57].

2.7   Forces on floating buoys

There are many factors that affect a buoy's service life and operation. Those factors which affect its service life (i.e., material construction, geometry, etc.) are generally considered for its proposed operating location during the fabrication stage of the buoy. The factors acting upon the operational buoy include environmental, static, and dynamic forces.

2.7.1   Environmental forces

When moored in the oceanic environment, surface buoys are subjected to wind action, wave action, oceanic currents, and sometimes icing. Additionally, buoys are subjected to severe loads during deployment and retrieval. These external forces are considered in both the construction and operational stages of the buoy. A brief overview of these environmental and operational constraints and their consequences are described below [57].

Wind action – Wind creates additional drag on the buoy. The winds' resistance force results in stresses on the buoys' superstructure and introduces a capsizing moment.

Wave action – Wave action causes the buoy to heave and roll. The allowable heave and roll that a buoy may experience for a given sea spectrum is considered as a design criterion in the construction of the buoy.

Oceanic currents – This force includes the hydrodynamic resistance force due to oceanic currents passing by the buoy and its resulting moment.

Icing – Ice covering the deck and superstructure of a surface buoy will cause an upward shift on the buoys' center of gravity, diminishing the buoys' righting moment and altering its response in roll and heave. Additionally, icing creates an increase in the structures' area resulting in an increase in the wind drag force and capsizing moment.

Hydrostatic pressure – Structural stresses due to hydrostatic pressure must be evaluated during the design phase of the buoy.

Launching and retrieval loads – During deployment, the buoys' attachment point may need to sustain the weight of the anchor and entire mooring line prior to anchor bottoming. In retrieval operations, the load at the point of lift may be equal to the sum of the buoys' weight in the air, the weight of the mooring line (and perhaps the anchor), and the dynamic loading due to the ships motion.

2.7.2 Static force

A body immersed in a fluid of density ρ_{water} experiences an upward force known as the buoyancy force. Consider the buoy of Figure 2.17 having an elementary area of dA and height $h = h_2 - h_1$.
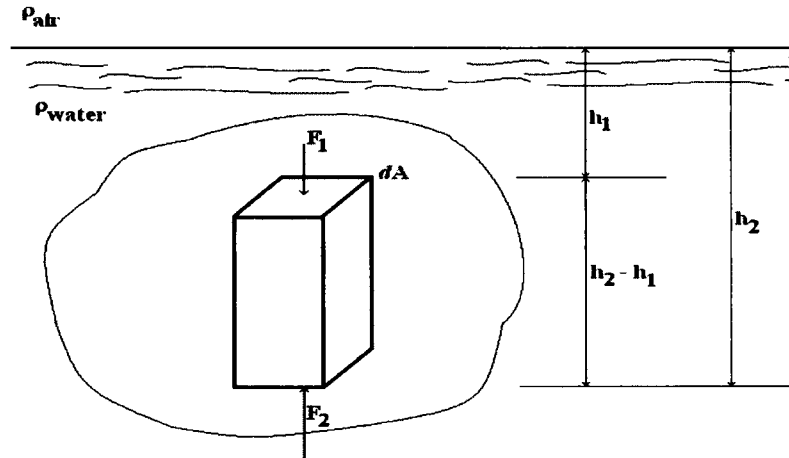
Figure 2.17. Buoyancy force on a submerged buoy [58].

This buoy is subjected to lateral and longitudinal pressure forces. Since the buoy is symmetrical about the lateral axis, the lateral forces cancel out. However, the longitudinal forces present upon the elementary unit of area results in [58] a force dF:

$$dF = F_2 - F_1 = (p_2 - p_1) \, dA \, , \tag{2.28}$$

where p_2 is the pressure at the bottom surface of the buoy and is equal to $g \, \rho_{water} \, h_2$, and p_1 is the pressure at the top surface of the buoy and is equal to $g \, \rho_{water} \, h_1$, and g is the acceleration due to gravity. Thus, for a fully submerged buoy, dF is given as:

$$dF = g \, \rho_{water} \, (h_2 - h_1) \, dA = g \, \rho_{water} \, dV \, , \tag{2.29}$$

where dV is the volume of an elemental unit. For a floating buoy:

$$dF = g \, (\rho_{water} \, h_2 - \rho_{air} \, h_1) \, dA \, , \tag{2.30}$$

where h_1 represents the height of the buoy above the waterline, h_2 the height of the buoy below the waterline (known as the draft), and ρ_{air} is the density of air.

This result, known as the principle of Archimedes, shows that the buoyancy force experienced on a buoy is equal to the weight of the fluid displaced by the body [58].

2.7.3 Dynamic forces

The dynamic forces on a floating buoy relate to the varying forces acting upon the buoy in motion and include added mass, and the damping, restoring, and wave exciting forces. A brief introduction describing the basic principles of these forces will be discussed in this chapter followed by the governing equations that define them in Chapter 3. Finally, Chapter 4 quantifies these forces for a sample buoy for modeling and simulation purposes.

2.7.3.1 Added mass

In fluid mechanics, the added mass, m', is the inertia added to a system because an accelerating or decelerating body within a fluid must move some volume of the surrounding fluid as it moves through it, since the object and fluid cannot simultaneously occupy the same physical space. This principal is generally modeled as some volume of fluid moving with the object, although in reality the velocity of "all" of the fluid is affected to various degrees [59].

The added mass is generally added to the hydrodynamic mass of the body (i.e. the mass of the buoy in water) to create the virtual mass (m_v) which considers the body and its surrounding fluid as an object having a single mass.

2.7.3.2 The restoring force

A restoring force tends to restore a perturbed system back toward equilibrium [60]. For a floating buoy, the restoring force restores the buoy to the water's surface after it is removed from equilibrium by the presence of a passing wave. The restoring force for a vertically floating cylindrical buoy of constant cross-sectional area is proportional to its

cross-sectional area defined by the undisturbed water free-surface, the restoring spring constant (which anchors the buoy to the seabed), and the buoy's vertical (heave) displacement.

2.7.3.3 The damping force

In the field of physics, damping is defined as any effect that tends to reduce the amplitude of oscillations in an oscillatory system [61]. For a floating buoy heaving in an oscillatory fashion due to the influence of passing waves, these effects include the friction (D_f), radiation (D_r), and energy extraction (D_e) components.

The frictional loss of the buoy (D_f) is represented by the drag coefficient, C_D, which is derived based upon the geometry and degree of roughness on the external surfaces of the buoy.

The radiation damping coefficient (D_r) corresponds to the surface waves that are produced when a body oscillates at the surface of a liquid. These waves are produced by the alternating displacement volume of the body and by friction and surface tension. Its magnitude is estimated based upon the geometry of the body, the angular frequency of oscillation, and, in the case of an array of devices, from the spacing and alignment of the array to the wave crests [62].

The energy extraction coefficient (D_e) resists the upward motion of the buoy in proportion to the size of the load requiring the extracted energy and a suitable optimum performance condition.

Each of the individual damping coefficients are summed together to comprise the overall damping coefficient. This coefficient is then multiplied by the velocity of the heaving action of the buoy to create the damping force.

Generally, all of these forces are considered together and are expressed by a linearized damping coefficient.

2.7.3.4 The wave exciting force

The wave exciting force represents the force that a wave imparts upon a floating buoy and is proportional to the heave response (vertical displacement) for that buoy. This complex force is a function of the following variables: the waves' amplitude and number, the draft of the buoy (how deeply it is submerged), the restoring force coefficient, the added mass of the floating buoy, the angular frequency of the waves, the damping coefficient, and the phase angle between the force and the wave.

2.8 The Response Amplitude Operator

The Response Amplitude Operator (RAO) is effectively the transfer function used to determine the effect that a sea state will have upon the motion of a ship through the water. It is traditionally used to determine if the addition of cargo to a vessel will require measures to be taken to improve its stability and prevent the cargo from shifting within the vessel. Generation of extensive RAOs during the design phase allow shipbuilders to determine if modifications to a design may be required for safety reasons (i.e., to make the design more robust and resistant to capsizing or sinking in highly adverse sea conditions) or to improve performance (e.g., to improve top speed, fuel consumption, or stability in rough seas) [63].

The ratio of the buoy's heave to wave amplitude (RAO_{HEAVE}) is primarily governed by the distance that the cyclic frequency of the waves are displaced from the resonant frequency of the floating buoy (discussed in Chapter 3) and its magnitude of damping.

This ratio can be maximized by constructing the buoy using the optimal values for each of the following parameters:

1. Weight – The wave exciting force exponentially decreases as a function of the wave number, k, and the draft of the buoy. This exponential loss can be minimized by operating the buoy in ocean regions having longer wavelengths (decreasing the k parameter) and/or by minimizing the buoys' draft by reducing its weight in air, or by increasing its surface area.

2. Restoring Force – The restoring force is directly proportional to the buoy's hydrostatic force (which is proportional to the buoy's surface area) and restoring spring constant. Thus, the larger the surface area of the buoy and/or the stronger the spring constant, the greater the restoring force. This force is dominant at wave frequencies below the resonant frequency and can be properly "tuned" to provide for a better heave response within this frequency region.

3. Damping force - The linearized damping force present on the buoy is directly proportional to the ocean parameters of significant wave height (H_s) and its cyclic wave frequency (ω) and the buoy's drag coefficient. The damping force limits the buoy's heave response and should ideally be minimized. This force may be minimized by operating the buoy in an ocean region having smaller significant wave heights and cyclic frequencies or by decreasing the buoy's drag coefficient (by constructing the buoy of the proper shape and dimensions and by ensuring the surfaces are very smooth).

4. Buoy shape & dimensions – The buoy's shape and dimensions affect the hydrodynamic coefficient (C_m), which affects the added (m') and virtual (m_v) mass of the buoy as well as the drag coefficient (C_D) which plays a factor on the buoy's damping force. At cyclic wave frequencies above resonance, the mass of the buoy limits the heave RAO and should be minimized to ensure an adequate heave response within this frequency range.

Once the RAO_{HEAVE} parameter for the buoy is derived using the above mentioned parameters, the buoy's heave response can readily be derived for either wave regime operating in any sea state by using the additional functions of time and the waves' height and cyclic frequency.

2.9 Electrical energy production

From the standpoint of Electrical Engineering, the main idea is to convert the periodic mechanical motion of a heaving buoy into electrical energy. *The most convenient approach for this would logically appear to be the use of electrical generators.* Such generator devices typically convert the rotation or up-and-down action of a "rotor" into electricity in the presence of a magnetic environment. By constructing a spatially appropriate magnetic field, through which the piston moves, it becomes possible to generate a voltage associated with Faraday's law of induction.

2.9.1 The generator concept

The fundamental principal behind AC electrical generation lies in an application of Faraday's Law. This law, which is expressed mathematically as

$$V = - N \, d\phi/dt, \qquad (2.31)$$

states that the induced voltage V in a conductor is proportional to the time rate of change of the magnetic flux ϕ linked with it [64]. The minus sign is mandated by Lenz's law, while N denotes the number of turns of the wire through which the time-varying magnetic flux passes. The negative sign, arising from Lenz's Law simply denotes that the current flow in a conductor due to an induced voltage is in a direction that would create a magnetic flux opposing the one inducing the voltage.

Since the magnetic flux linkage is given by $\Lambda = N\phi$, and the induced voltage is the time rate of change of these linkages, the induced voltage can be derived in terms of the velocity of the conductors by [64]:

$$V = - N \, d\phi/dt = - N \cdot B \cdot l \cdot ds/dt = - N \cdot B \cdot l \cdot v ,$$ (2.32)

where
N is the number of conductors,
B is the magnetic flux density,
l is the length of the conductor in the magnetic field,
ds is the differential distance traveled by the conductor through the field, and
v is the velocity of the conductor traveling in the magnetic field

2.9.2 Magnetic properties of materials

Magnetization (M) is the magnet moment associated with the orbital and spinning movement of electrons per unit volume at a given point in a medium [65]. This quantity is measured in amperes per meter (A/m). The magnetization (M) and magnetic field intensity (H) contribute to the magnetic induction by the field equation, expressed as [65]

$$B = \mu_0 (H + M) ,$$ (2.33)

where
B is the magnetic flux density,
μ_0 is the permeability of a vacuum,
H is the magnetic field intensity, and
M is the magnetization.

Ferromagnetic materials are magnetic dipoles that can reach very high levels of magnetization. The relative permeability (μ_r) of a material compares how a material leads its magnetic flux to that of a vacuum. The permeability (μ) of the material is a function of its magnetization and is expressed by [65]:

$$\mu = \frac{B}{H} = \mu_o \left(1 + \frac{M}{H} \right) \qquad . \qquad (2.34)$$

Since ferromagnetic materials have high levels of permeability, they are generally used in electric generators to lead the magnetic flux. The M/H quotient is material dependant and is termed the susceptibility X_m of the material. The magnetization quantity for various materials is plotted on a B vs. H graph and is depicted in Figure 2.18.
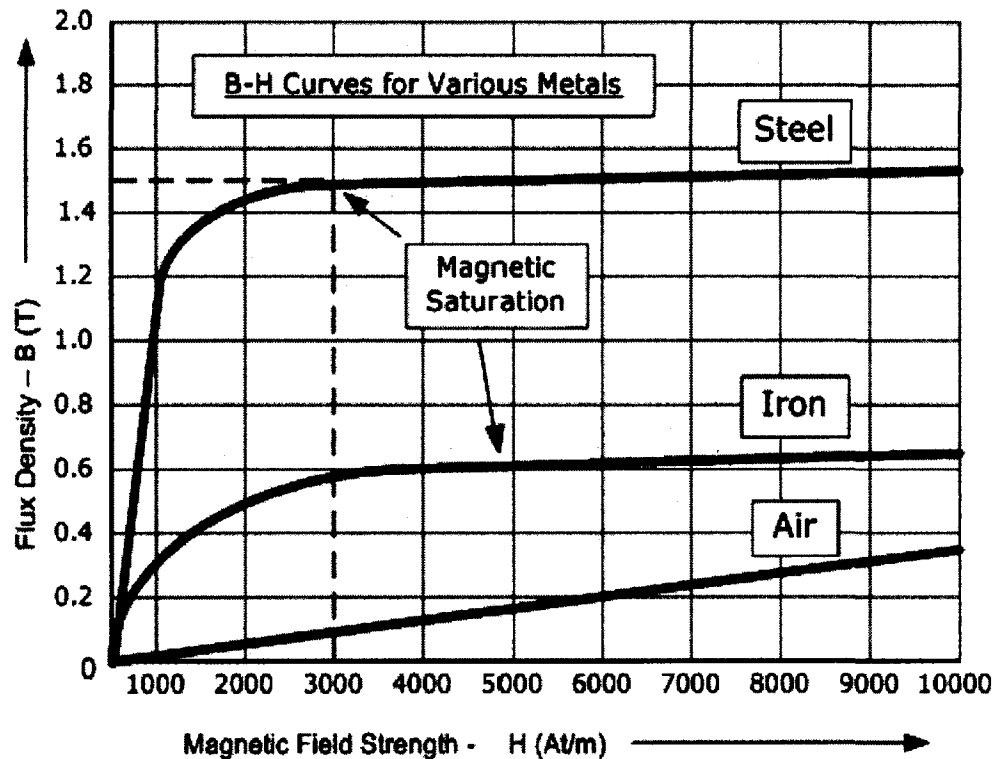
Figure 2.18. Typical magnetization curve for various materials [66].

Figure 2.18 reveals that the flux density increases in proportion to the field strength until it reaches a certain value it can no longer increase and becomes almost level and constant as the field strength continues to increase. This 'leveling-off' effect occurs because there is a limit to the amount of flux density that can be generated by the core once all of the domains within the material have become perfectly aligned. Any further increase will have no effect on the value of magnetization, and the point on the graph where the flux density reaches its limit is called its *Magnetic Saturation* or *Saturation of the Core* [66].

Saturation occurs once the normally random haphazard arrangement of the molecular structure within the core material changes as the tiny molecular magnets within the material become "lined-up". As the magnetic field strength (H) increases, these molecular magnets become more and more aligned until they reach a perfect alignment pattern. Once this perfect alignment occurs, the maximum flux density is achieved and any additional increase in the magnetic field strength will have little or no effect [66].

Steel is a ferromagnetic material that possesses a saturation induction limit of approximately 1.5 Teslas (depending upon the material), making it a good conductor for magnetic flux in linear electric generators. On the other hand, the saturation induction limit for iron is only about 0.6 Teslas. Hence, iron can effectively be used (i.e. in the case of pole pieces) to concentrate and direct magnetic flux to a desired location.

2.9.3 Types of electrical generators

Electrical generators are generally constructed using two basic configurations, rotational and linear. The difference between the two lies in the manner in which the rotor (which is referred to as the piston in linear generators) moves with respect to the

stator in order to generate electricity. In a rotational generator, the rotor turns within the stator, and for a linear generator, the piston (which could be alluded to as the "rotor" part) travels in and out of the stator.

A linear generator (LG) is a device that converts the mechanical inward- and outward- motion of a piston into practical electrical energy. Linear generators may be classified according to one of the following categories [67]:

1. Moving coil type,
2. Moving iron type, and
3. Moving magnet (or electromagnet) type.

The moving coil LG requires flexible leads, which tend to wear out due to cyclic stress and are not suitable for high-power applications [67].

Moving iron LGs are rugged in construction, but they tend to be relatively heavier and more expensive than the moving magnet type [67].

For the moving magnet LG the piston is generally constructed using multiple stacked magnets or with a single moving magnet (permanent or electromagnetic). The moving magnet linear generator does not suffer from the above mentioned limitations and is well suited for operation in the marine environment, making it the ideal choice as a wave energy converter.

A practical example of an ocean WEC that uses a linear generator is the floating buoy type of device. Figure 2.19 illustrates the basic components for this particular category of WEC.

In this arrangement, the buoy is connected to a linear electric generator by a rope, which is connected to the permanent magnet (PM) generator's piston (rotor). As the waves pass by the floating buoy, the attached rope causes the piston to ascend and

descend with the momentum of the passing wave [38]. This relative motion between the

rotor and stator generates a voltage at the linear generator's output terminals which is sent

through the transmission lines lying on the seabed to a shore based processing facility

where it is conditioned for practical human usage.
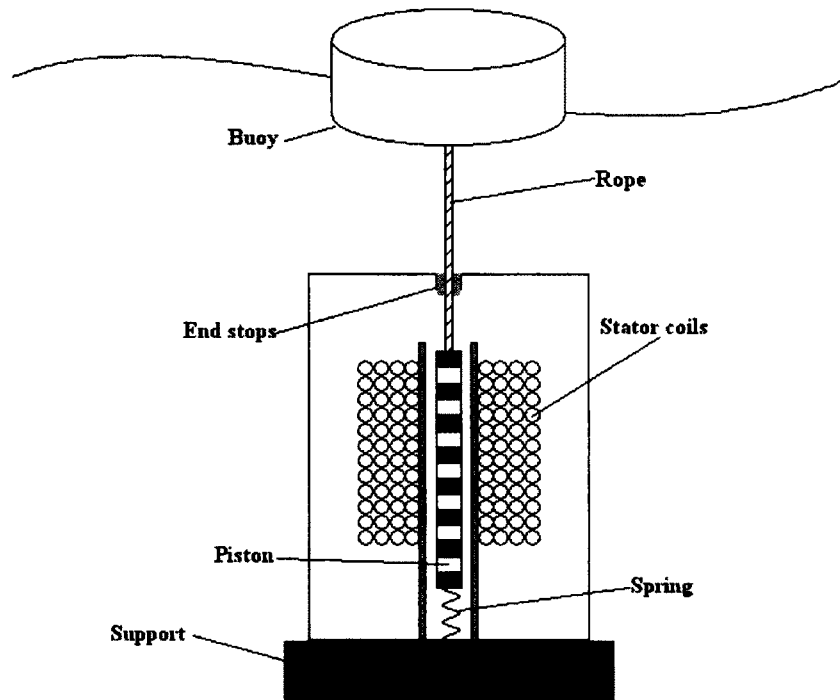
Figure 2.19. Basic components of a buoy-type WEC using a linear generator.

As the piston moves relative to the stator coils, an induced electromotive force (EMF)

is generated within the windings.

The buoy's dimensions, mass and shape should be optimized for effective wave

energy extraction. For efficient operation, the buoy should be large enough to absorb the

maximum energy from the passing waves, and yet be small enough that it does not get

destroyed in stormy weather [38].

Attached to the bottom of the piston is a spring that serves to increase the downward speed of the piston. Without the assistance of the spring, the downward motion of the piston would only be influenced by gravity, resulting in a slower response [38].

Finally, the end stops serve to protect the generator at high waves and prevents the piston from being removed from the stator.

2.9.4 Power losses

The power losses in a linear generator are due to:

A. Losses due to the varying magnetic field (a.k.a. steel losses).
B. Resistive losses which occur in the coil windings, and
C. Mechanical losses (i.e. friction and deformation). – not considered here.

2.9.4.1 Steel losses

Steel losses consist of Hysteresis and Eddy Current losses.

Hysteresis losses describe the energy required to reverse the magnetization of a material and only applies to materials that are magnetic dipoles. Since copper is not a magnetic dipole, hysteresis losses will not occur within the copper magnet wires of the stator and are not considered in this work [65].

Eddy current power losses arise due to the circular electric currents produced in a material that are induced by a changing magnetic field [64-65]. The eddy current loss is proportional to the material constant representing the conductivity of the stator coils, the magnetic flux density, the geometric volume of the stator coil, and the frequency of the magnetic field. Generally, due to the increased number of frequencies which influence the movement of the rotor in the irregular wave regime, the eddy current power loss is much greater than that which occurs under the regular wave regime.

2.9.4.2 Resistive losses and efficiency

The electrical resistance of the stator coil windings creates a power loss in the form of heat dissipation. This loss, however, can be minimized by using a load resistance which is much larger than the internal coil's resistance. As the ratio of load to internal resistance increases in magnitude, a greater portion of the generated voltage drops across the output terminals of the linear generator than across the stator coils giving a desirable high output voltage. This increase in output voltage, however, comes at the price of a reduction in the output current of the device which results in the condition that less than ideal power is sent to the load. On the other hand, if the load resistance were selected to be much smaller than the coils' resistance, although the output current will increase in value, its voltage delivered to the load will be reduced, thereby again delivering less than ideal power to the load.

Efficiency for a linear generator is a measure of the ratio of input power (generated) to output (delivered to the load) power. Thus, when the load to coil resistance ratio is at a large value, a large total resistance is presented to the generated voltage causing the current to be minimized in the stator coils, resulting in a low power loss across the coils and a high power condition to be sent to the load, giving the linear generator a high efficiency. Should the load to coil resistance ratio be very small in value, the stator current is maximized leading to a high power loss across the stator coils, a small proportion of the generated power to be delivered to the load, and a low efficiency condition to dominate.

Chapter 3 will introduce the basic linear generator model and define all of the governing equations which characterize it. Then, Chapter 4 determines the optimal

'trade-off' between maximizing either the power delivered to the load or the linear generators' efficiency by comparing the output parameters of voltage, current, and power under various load resistances. Finally, Chapter 5 validates the model and simulates the electrical output parameters for the linear generator operating in both wave regimes and under varying buoy dimensions.

CHAPTER III

MATHEMATICAL MODEL AND DETAILS FOR ANALYSIS

3.1 Simulating the ocean surface

This work shall simulate the three different sea states presented in Table 3.1 below.

Table 3.1. Simulated sea states.

Sea State	H_s (m)	T_s (s)
TEST	0.4	4.5
WINTER	3.5	8
SUMMER	1.5	6

First, the regular wave regimes for the selected sea states will be plotted using Equation (2.11). Next, the Pierson-Moskowitz spectrum will be derived (via the plot of Equation (2.18)) for each of the desired sea states. Since this spectrum is primarily derived as a function of wind speed for a fully developed sea, the wind speeds as a function of significant wave heights must first be computed through an algebraic manipulation of Equation (2.23). Thus, the wind speed at a height of 19.5m above the sea surface ($U_{19.5}$), and the significant (ω_o) and peak (ω_p) frequencies can be computed by

$$U_{19.5} = ((g \cdot H_{1/3})/0.21)^{0.5}, \qquad (3.1)$$
$$\omega_o = g/U_{19.5}, \text{ and} \qquad (3.2)$$
$$\omega_p = 0.877 \cdot g/U_{19.5}. \qquad (3.3)$$

Then, the Bretschneider spectrum shall be derived (via the plot of Equation (2.24)) using the given parameters for significant wave height and period. Finally, the time series for both wave spectrums will be plotted (using Equations (2.25) through (2.27)) and their results compared.

3.2 Modeling the buoy

3.2.1 Basic construction

The specially designed buoy in this work is assumed to be of the vertical floating cylinder variety. The actual physical properties for the buoy will be selected to have a diameter of 6m, depth of 2m, and draft of approximately 1m with these dimensions being chosen from a similar research paper [38]. Additionally, this buoy is modeled as having a body weight in air of 1,719 kilograms and a ballast weight of 27,200 kilograms.

Other buoy properties, such as its material construction, response to winds, oceanic currents, icing, hydrostatic pressures, launching and retrieving loads, and other factors not mentioned in this work are not considered in this simulation.

3.2.2 Simulating the buoy's motion

The buoy, as described above, is simulated as floating upon the ocean surface in an infinite body of water and is only affected by the heave motion, which is the up and down movement along the z-axis taken to be normal to the ocean surface. The pitch, roll, sway, yaw, and surge motions of the buoy are not considered in this simulation. This chapter introduces the basic concepts and equations necessary for modeling the buoy's motion about the z-axis in response to incident ocean surface waves. Chapter 4 will quantify the required parameters and describe the results obtained.

3.2.2.1 Buoy's response in heave

3.2.2.1.1 Added mass

In order to accelerate a buoy immersed in water, not only must the buoy itself be accelerated but additionally, the mass of a certain amount of water close to, or ahead of,

that of the buoy has to be moved as well. As a result, the force needed to accelerate the

buoy in water is greater than that required to accelerate the same buoy in a vacuum. This

force can be expressed by [68]

$$F = (m + m')a = m_v a \quad , \tag{3.4}$$

where
F is the applied force,
a is the acceleration, and
m_v is the virtual mass, representing the sum of the mass of the buoy in water (m) and the added mass (m') of the surrounding water. The values for mass and added mass are computed as [37]

$$m = \rho(\text{Volume}), \text{ and} \tag{3.5}$$
$$m' = C_m \rho(\text{Volume}) \; , \tag{3.6}$$

where
C_m is the added mass coefficient,
ρ is the seawater density, and
(Volume) is the volume displaced by the immersed body.

Coefficients for the added mass are dependent upon the geometry of the floating body

and can easily be obtained for a variety of shapes from hydrodynamic mass tables [69].

Although, the added mass is also dependent on the frequency of the exciting wave

motion [70], the frequency dependence is weak and is not considered in this work. In the

case of cylindrical buoys, there are two different added volumes to consider, one for the

sides and one for the top and bottom parts of the cylinder. This situation is described by

Figure 3.1 below.
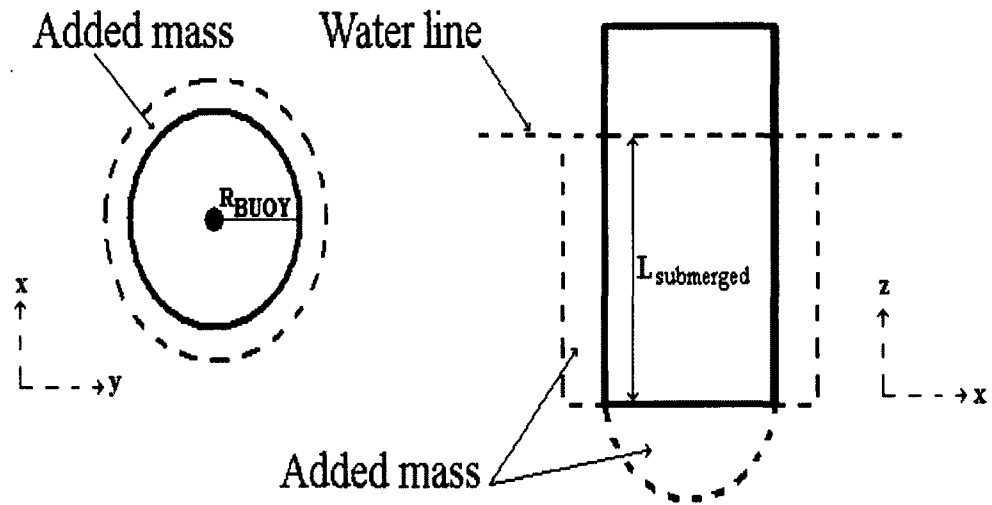
Figure 3.1. The added mass area for a cylindrical buoy semi-submerged in water.

Mathematically, the outer cylinder (water) at the sides has the same volume as the inner cylinder (buoy), and the added volume at the bottom is approximately 60% of the volume of a half-sphere of the same radius as the buoy (R_{BUOY}), so that [70]

$$m_{ax} = m_{ay} = \rho \cdot L_{submerged} \cdot \pi \cdot R_{BUOY}^2 \text{ , and} \tag{3.7}$$

$$m_{az} = 0.64 \cdot \rho \cdot 4/3 \cdot \pi \cdot R_{BUOY}^3 \text{ .} \tag{3.8}$$

In heave, (the vertical motion of the buoy) the term m_{az} is used to define the added mass, and in surge or sway, (the horizontal motion of the buoy), m_{ax} and m_{ay} are used instead [70]. In order to simplify the model, only the heaving motions of the buoy will be considered in this work.

3.2.2.1.2 The restoring force coefficient

The restoring force coefficient (S) is composed of the hydrostatic (f_{hs}) and spring restoring force (k_s) and is given by:

$$S = f_{hs} + k_s . \tag{3.9}$$

The hydrostatic force is defined as the change in buoyancy force per unit vertical movement and is defined by [62, 71]:

$$f_{hs} = \rho \, g \, A_{BUOY} \quad , \tag{3.10}$$

where:
f_{hs} is the hydrostatic force coefficient,
ρ is the seawater density,
g is the acceleration due to gravity, and
A_{BUOY} is the buoy cross-sectional area defined by the undisturbed water free-surface.

A spring restoring force is provided by a rope attached to the bottom of the buoy and connected to the seabed. Generally, the rotor of a linear generator (or other WEC devices) is connected between the rope and spring in order to utilize the waves' energy to generate electricity. This force assists the buoy in returning to the water's surface after a wave passes and is represented by [71]:

$$f_s = -k_s \, z , \tag{3.11}$$

where
f_s is the restoring force due to the spring,
k_s is the spring constant, and
z is the vertical displacement of the floating buoy.

3.2.2.1.3 The damping force coefficient

The damping force coefficient (D_f) consists of friction (D_F), radiation (D_R), and energy extraction (D_E) components. Generally, all of these forces are considered together and are expressed in linear form as [68]:

$$D_f = (4/3\pi) \, \rho \, C_D \, A_{BUOY} \, v_1 , \tag{3.12}$$

where
D_f is the damping force coefficient,
ρ is the density of seawater,
C_D is a measured drag coefficient,

A_{BUOY} is the buoy's water plane area ($A_{BUOY} = (\pi/4) \cdot Diameter_{BUOY}^2$), and
$v_1 =$ is the velocity of the heaving buoy ($v_1 = z^* = H_s \omega$).

3.2.2.1.4   The natural frequency in heave and the linear damping coefficient

With the previous parameters derived, the natural or resonant frequency (p^2) and the

linear damping coefficient (n) for the buoy in heave can now be defined by:

$$p^2 = (S/m_v) \text{ , and} \tag{3.13}$$

$$2 n = (D_f / m_v) . \tag{3.14}$$

3.2.2.1.5   The wave exciting force

The wave exciting force for bodies oscillating in heave in deep water is given by [68]

$$F_e = A_w e^{-kD} \sqrt{\{(S - m'\omega^2)^2 + D_f^2 \cdot \omega^2\}} e^{j\sigma} , \tag{3.15}$$

where
F_e is the wave exciting force,
A_w is the significant wave's amplitude,
k is the wave number ($k = \omega^2/g$),
S is the restoring force coefficient,
m' is the added mass of the floating buoy,
ω is the angular frequency of the waves,
D_f is the damping force coefficient,
σ is the phase angle between the force and the wave given by

$$\sigma = \tan^{-1}\{-D_f \omega/(S - m'\omega^2)\} \text{ , and} \tag{3.16}$$

D is the draft of the buoy defined by

$$D = \text{Weight of the buoy in air}/(A_{BUOY} \cdot \rho_{seawater}) . \tag{3.17}$$

3.2.2.1.6   The Response Amplitude Operator for heave

In order to realize the Response Amplitude Operator for the buoy in heave, it is first

necessary to define the forces acting upon it with the aid of a free body diagram. The

free body diagram for a floating buoy upon the surface of a turbulent body of water is

presented in Figure 3.2. An incident wave upon the buoy produces a periodic disturbing

force of the form $F\cos(\omega t)$. There also exists upon the buoy a restoring force $(S z)$, which is produced by the changing buoyancy and an anchoring spring force, and a damping force $(D_f z^*)$ caused by friction, energy extraction, and radiation [62].
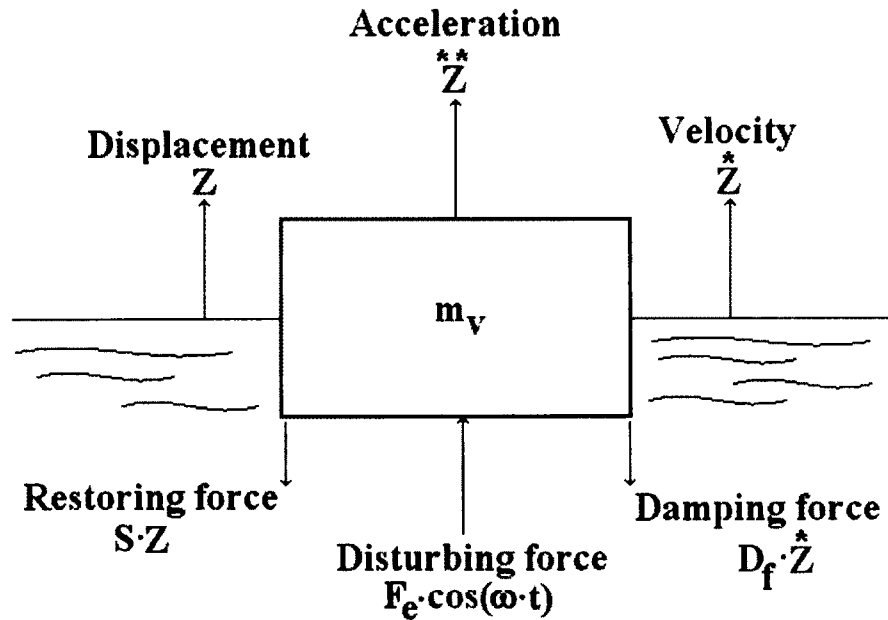
Figure 3.2. Free body diagram for a floating buoy.

The resulting change in acceleration of the buoy can be determined using the classical equation for forced, damped oscillations [62]:

$$m_v z^{**} + D_f z^* + S z = F_e \ . \tag{3.18}$$

Dividing both sides of the equation by m_v and applying Equations (3.13) and (3.14) yields

$$z^{**} + 2 n z^* + p^2 y = (F_e/m_v) \ , \tag{3.19}$$

Assigning the value of $z = B e^{j\omega t}$ to Equation (3.19), and then dividing by the exponential term produces [62]

$$-\omega^2 B + j\omega 2 n B + p^2 B = (F_e/m_v) \quad . \tag{3.20}$$

Equation (3.20) can now be factored as

$$B(p^2 - \omega^2 + j\omega 2n) = (F_e/m_v) .$$ (3.21)

The value of the coefficient, B, can then be solved by

$$B = (F_e/m_v)/\{ p^2 - \omega^2 + j\omega 2n \}.$$ (3.22)

The magnitude of the denominator can be expressed in polar form as

$$\sqrt{\{ (p^2 - \omega^2)^2 + 4n^2 \omega^2 \}} e^{j\phi_{heave}} ,$$ (3.23)

where ϕ_{heave} represents the phase angle between the force and heave motion and is computed by

$$\phi_{heave} = \tan^{-1} \{ -2n\omega/(p^2 - \omega^2) \} .$$ (3.24)

Since $z = B \cdot e^{j\omega t}$,

$$z = \frac{| F_e/m_v | e^{-j\phi_{heave}}}{\sqrt{\{ (p^2 - \omega^2)^2 + 4n^2 \omega^2 \}}} e^{j\omega t} = \frac{F_e e^{j[(\omega t - \phi heave)]}}{m_v \sqrt{\{ (p^2 - \omega^2)^2 + 4n^2 \omega^2 \}}}$$ (3.25)

The final equation for the heaving buoy can now be expressed by

$$z = \frac{A_w e^{-kD} \sqrt{\{ (S - m' \omega^2)^2 + D_f^2 \omega^2 \}}}{m_v \sqrt{\{ (p^2 - \omega^2)^2 + 4n^2 \omega^2 \}}} \cos(\omega t + \sigma + \phi_{heave}) .$$ (3.26)

Equation (3.26) reveals that the phase difference which occurs between the wave and the heaving buoy is the sum of the phase angle σ between the wave and exciting force and of the phase angle ϕ_{heave} between the exciting force and the heave response. Furthermore, the heave amplitude is primarily a function of the wave frequency, ω, and of the damping coefficient n. Thus, for small levels of damping and at excitation frequencies, ω, close to the natural frequency, p, of the buoy, the heave response can be very large [68].

A simple modification of Equation (3.26) yields an expression for the Response Amplitude Operator for the heaving buoy which is the ratio of heave height to wave height. Thus, [68, 37]

$$RAO_{HEAVE} = |H_{BUOY}(\omega)| = \frac{z}{A_w} = \frac{e^{-kD} \sqrt{\{(S - m'\omega^2)^2 + D_f^2 \omega^2\}}}{m_v \sqrt{\{(p^2 - \omega^2)^2 + 4 \cdot n^2 \omega^2\}}} \quad . \qquad (3.27)$$

3.2.2.1.7 Time series for heave

Once the RAO for heave is constructed, it is then a simple matter to plot the time series for the surface waves and the resulting buoys' height displacement using equation 3.26.

For the regular wave regime (defined by Equation 2.11)), where the wave's cyclic frequency maintains a constant value, the corresponding ratio between heave height to wave height (as obtained from the RAO$_{HEAVE}$ function) also maintains a constant value. Thus, a time series for the wave height and the buoys' height displacement (heave) can be obtained by plotting equations 2.11 and 3.26 simultaneously using time as the input variable.

The time series for the ocean waves height and the buoys' heave for the irregular wave regime, however, is more complex in nature. In this instance, first the Bretschneider spectrum must be defined (using Equation 2.24)). Next, Equations 2.25 and 2.26 must be used to respectively derive the amplitude component and phase angle as a function of the wave's cyclic frequency. Then, the magnitude of each amplitude component (as a function of its frequency) must be multiplied by the buoys' response amplitude operator (RAO) for heave (defined by Equation (3.27)) computed at the same frequency as the amplitude component to derive the buoys' height displacement as a

function of the cyclic frequency. Finally, the buoy's height displacement as a function of time is obtained through the summation of each of its component height displacements, plus its respective phase angle for each frequency component. Thus, a time series for the wave's and buoy's height for the irregular wave regime can be obtained by plotting Equation (2.27) for the wave height, and the summation of each amplitude component (A_i) at its associated frequency (ω_i) multiplied by its corresponding heave displacement (by assigning $A_i = A_w$ and $\omega_i = \omega$ in Equation (3.26)) for the buoy height.

3.3 Practical utilization of the buoy's motion

Historically, the heaving motion of floating buoys has been successfully harnessed to generate clean electrical energy. This process was usually performed by pumping a fluid through a pneumatic system in order to turn the rotor of an electric generator (such as in the case of the AquaBuOy WEC). Other WECs utilize the buoy's heave motion directly through the use of linear generators in the design. Since linear generators operate using a up-and-down motion of the rotor (instead of a rotating movement which occurs in conventional rotational generators), a much less complicated and more dependable design can be achieved.

This section begins by modeling the magnetic and electrical properties of the basic linear electric generator which will be used in this work. Then, the focus will shift to the analysis of power losses that occur within the modeled linear generator will be analyzed. Next, the typical arrangement for the components which comprise a buoy-type linear generator WEC will be described along with a basic discussion of how electrical energy is generated in this configuration. Finally, a speculation will be conducted on the ability

to selectively design a buoy to have a RAO$_{HEAVE}$ function greater than unity in order to generate additional electrical energy under the same sea state conditions.

3.4 Modeling the linear generator

3.4.1 Magnetic circuit design

A moving magnet type linear generator WEC is to be simulated in this work. For this model, the translator (also known as the rotor or piston) is simulated as being constructed of an alternating assembly of 1.0 cm thick Neodymium–Iron–Boron (Nd–Fe–B) permanent magnets, interspersed with soft iron pole pieces mounted on a threaded aluminum shaft as illustrated in Figure 3.3.

Neodymium magnets are made from an alloy of neodymium, iron, and boron to form the $Nd_2Fe_{14}B$ tetragonal crystalline structure. They are considered to be the strongest type of permanent magnet ever made. Due to their strong magnetic fields, they have replaced other types of magnets in the many applications which require strong permanent magnets in modern products, such as motors in cordless tools, hard disk drives, and magnetic fasteners [72].

The magnets would be stacked in pairs to force the opposing fluxes of the magneto motive forces (MMFs) through the pole pieces and across the air gap (0.006m) to the stator coils [21, 65]. Figure 3.4 illustrates the configuration of the magnet/pole piece positions and the resulting flow of magnetic flux.

In this construction, the thickness of each magnet pair and the iron poles pieces are both 0.020m, resulting in a pole pitch of 0.040m [21]. The total length of the translator for the seabed mounted linear generator is modeled as 5m (125 magnet/pole piece

assemblies) in order to respond to a higher than average significant wave height for the WINTER sea state.

As this translator system moves up- and down within the stator assembly, the magnetic flux on the central shaft causes a change in flux linkage with the coils mounted on the stator, which in turn generates an electro-motive force (EMF) on the stator's output terminals.
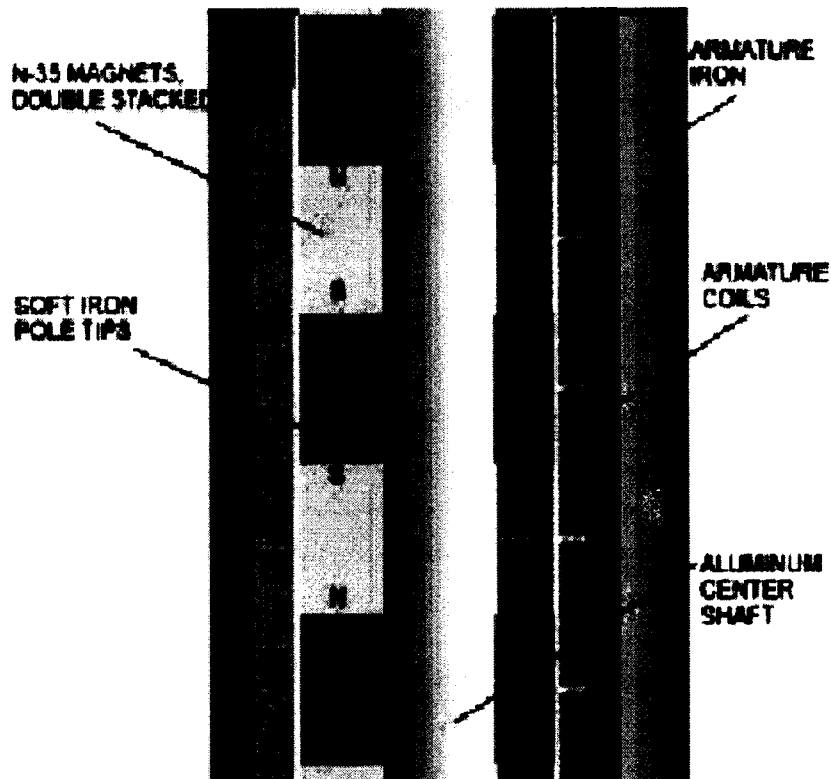
Figure 3.3. Partial cross section of the generator magnetic circuit [21].
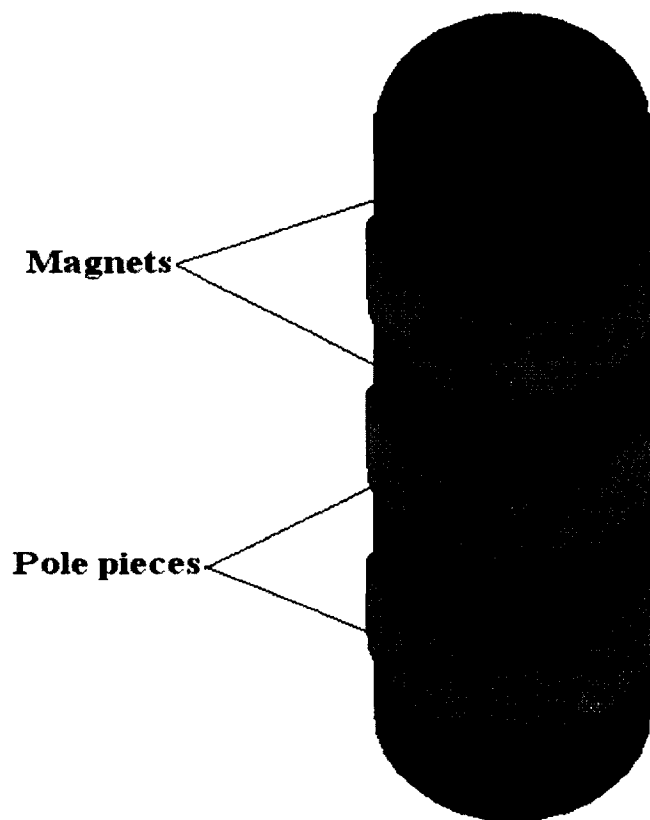
Figure 3.4. Basic rotor construction and resulting magnetic flux flow [65].

For the stator, a single-phase armature system is modeled as a thin walled tube wrapped with 48 turns of copper magnet wire to form four individual coil sections. Each section is assumed to be insulated from its neighbors by means of mica spacers placed between each coil section. These mica spacers introduce a distance of 0.020m between adjacent coil sections, combined with a pole spacing of 0.040m results in a 90-degree phase shift between adjacent coil sections. In order to provide a return path for the flux to the rotor, the armature coils are modeled as being wrapped with thin lamination steel. Finally, the steel core is simulated as being encased in a cylindrical aluminum shell for mechanical support [21].

The parametric dimensions for this specific generator are presented in Figure 3.5.
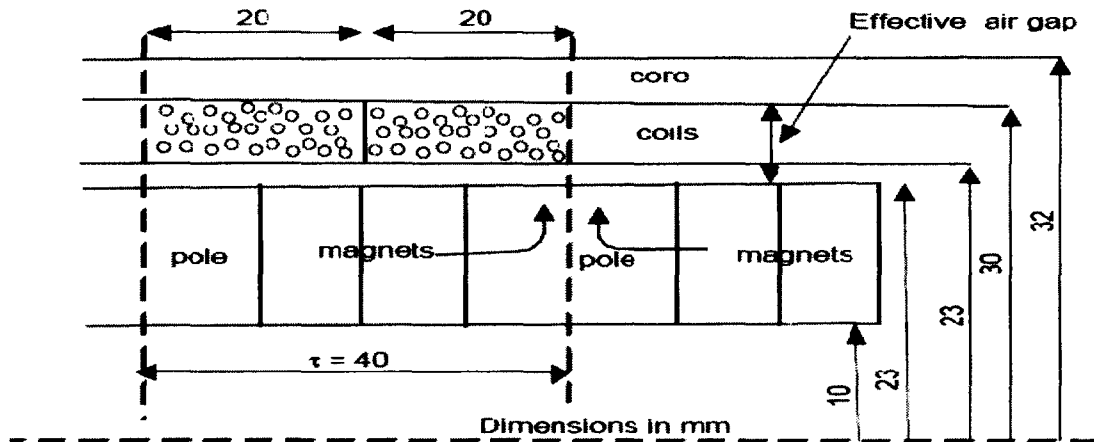
Figure 3.5. Parametric dimensions (in mm) for the magnetic circuit of the proposed linear generator [21].

Figure 3.6 plots the magnitude of the magnetic flux density along an axial line drawn in the air-gap of the machine (from the pistons surface) at a given time. From this plot, it is possible to derive the strength of the magnetic flux density for the desired airgap distance.
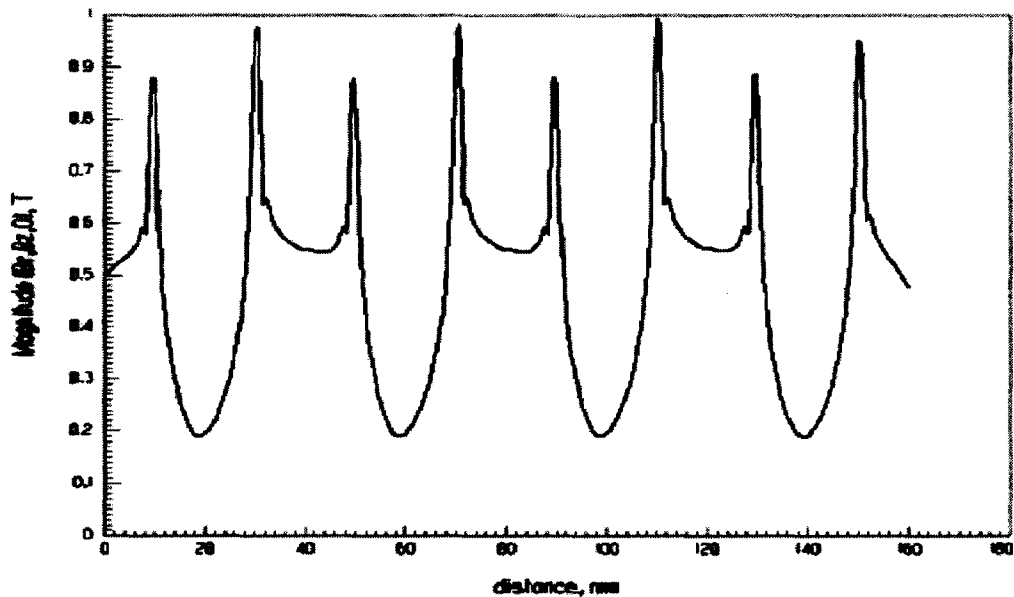
Figure 3.6. Magnetic flux density [21].

3.4.2 Electric circuit design

The electrical and magnetic circuits for this proposed generator are illustrated in Figure 3.7.
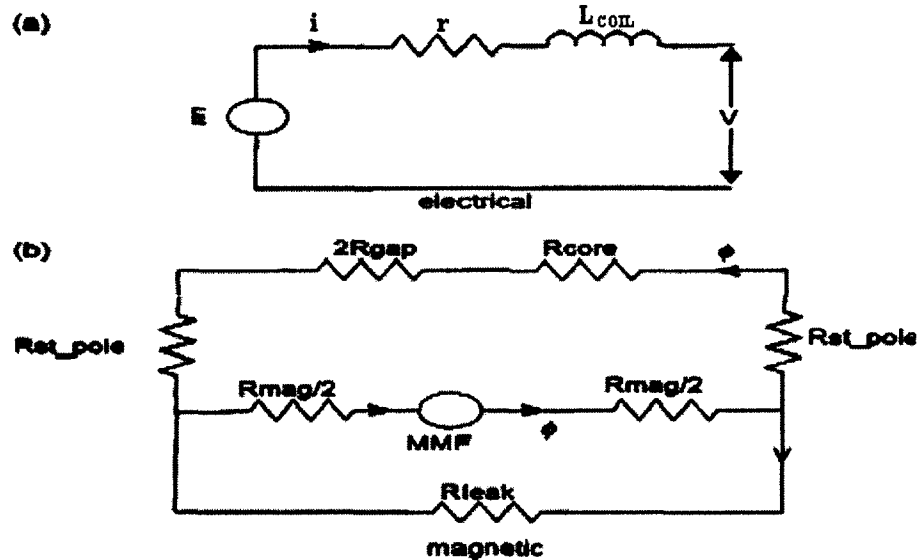
Figure 3.7. Electrical and magnetic circuits for the proposed generator model [21].

An analysis of Figure 3.7(a) reveals that the output voltage (V) from the generator is diminished from the induced voltage (E) due to the result of the copper losses for the stator coils (in terms of a resistance "r") and the self and mutual inductance for adjacent coils (L_{COIL}). This voltage can be expressed mathematically as [21]:

$$V = -r \cdot i + d/dt \, \lambda, \tag{3.28}$$

with

$$\lambda = -L_{COIL} \cdot i + \lambda_f, \tag{3.29}$$

where
r is the stator coil's resistance,
i is the current of the stator,
L_{COIL} represents the self and mutual inductances for the stator coils, and
λ_f is the flux linkage between the rotor and stator coils.

The individual values for the self and mutual inductances are generally determined through a control systems analysis approach during the design process or through a Bode diagram analysis of the model [73]. In this work, however, I shall use the modeled component values for inductance and resistance from a similar model and represent these values as 12.7 mH and 4.75 ohms, respectively [37].

The degree of flux linkage between the rotor magnets and stator coils depends upon the pole pitch and the displacement. The maximum flux linkage occurs when the axis of the coil is aligned with that of the soft iron pole piece. Under these conditions, maximum electromotive force (emf) occurs at peak linear speed. Since the pole pitch is fixed at 40mm, the flux linking to a coil is dependent on the relative motion between the translator shaft and stator [21]. Thus, the induced emf created by the relative motion between the permanent magnets of the piston and the stator coils is expressed by

$$E = d/dt \ (\lambda_f) = d/dz \ (\lambda_f) \ dz/dt \ , \tag{3.30}$$

where

$$\lambda_f = N\phi = N\phi' \cos((\pi/\tau)z) \tag{3.31}$$

where
λ_f is the magnetic flux linkage between the rotor and stator,
z is the displacement of the rotor relative to the stator,
τ is the pole pitch of the generator,
N is the number of stator turns, and
ϕ' is the peak flux.

Upon expanding Equation (3.28) and solving Equation (3.30), we derive:

$$V = -ri - L_{COIL} \, d/dt \ (i) + d/dt \ (\lambda_f), \text{ and} \tag{3.32}$$

$$E = d/dt \ (\lambda_f) = -N\phi'(\pi/\tau)\sin((\pi/\tau)z) \ dz/dt \ . \tag{3.33}$$

Thus, upon algebraically solving Equations (3.32) and (3.33), we have

$$d/dt \, (i) = (1/ \, L_{COIL}) \cdot (E - V - ri) \quad . \tag{3.34}$$

Under the condition of a load resistance, Equation (3.34) changes to:

$$d/dt \, (i) = (1/ \, L_{COIL}) \cdot (E - (i \, (R_{LOAD} + r))) , \tag{3.35}$$

which can be further algebraically modified to yield the current as a function of time. Thus,

$$i \, (t) = \frac{E - L_{COIL} \cdot d/dt \, (i)}{R_{LOAD} + r} . \tag{3.36}$$

The voltage drops across the stator coils (which represent a voltage/power loss) and the load can be computed, respectively, by:

$$V_{STATOR \, COILS} = i(t) \, r, \text{ and} \tag{3.37}$$
$$V_{LOAD} = i(t) \, R_{LOAD} . \tag{3.38}$$

Finally, the output power as a function of time may be defined by

$$P_{LOAD} = i(t)^2 \, R_{LOAD} \quad . \tag{3.39}$$

3.5 Power losses

The only power losses that are analyzed in this linear generator model are eddy current losses and resistive losses. This chapter will briefly introduce the basic concepts and governing equations. Actual values for the analyzed power losses will be derived in the next chapter.

3.5.1 Eddy current power losses

Eddy current losses arise due to circular electric currents in a material that are induced by a changing magnetic field [64, 65]. The total eddy current power loss which occurs within the stator coils is expressed by [65]

$$P_E = C_E \, B^2 \cdot (\text{Volume of cable}) \, f_{rotor}^2 \quad , \tag{3.40}$$

where
P_E is the total eddy current power loss in the stator coils,
C_E is a material constant representing the conductivity of the coils,
B is the magnetic flux density emanating from the rotor,
(Volume of cable) is the geometric volume of the stator coil, and
$f_{rotor} = \omega_{WAVE}/2\pi$ is the periodic frequency of the rotor (magnetic field).

Since the regular wave regime consists of only a single cyclic frequency, the resulting eddy current power loss can easily be computed via Equation (3.40) using the known cyclic frequency of the wave and the non-changing material properties integrated in the design of the linear generator.

The eddy current power loss for the irregular wave regime, however, is more complicated to compute. In the irregular wave regime, the rotor's motion is governed by the summation of all of the waves' frequencies at each moment in time. In order to realize the effect that the irregular wave regime has on a heaving buoy, the amplitude component at each of the wave's cyclic frequencies (as derived by Bretschneider's spectrum) is multiplied by the RAO for the heaving buoy to define a new spectrum. Since not every cyclic wave frequency for the new spectrum holds a significant amplitude component, it is possible to simplify the analysis by only accepting a bandwidth of frequencies whose amplitude components are within a certain threshold. This threshold level has been chosen at a magnitude of the peak -5%, thereby representing the cyclic frequencies responsible for 90% of the total rotor's motion. Thus, the resulting eddy current power loss for the irregular wave regime may be expressed by

$$P_{E\text{-}IRREGULAR} = C_E \cdot B^2 \cdot (\text{Volume of cable}) (f_{MIN\omega}^2 + f_{MIN\omega+\Delta\omega}^2 + \dots + f_{MAX\omega}^2), \quad (3.41)$$

where
$P_{E\text{-}IRREGULAR}$ is the total eddy current power loss in the stator coils for the irregular wave regime,
C_E is a material constant representing the conductivity of the coils,

B is the magnetic flux density emanating from the rotor,

$f_{MIN\omega} = \omega_{MIN}/2\pi$ is the minimum periodic frequency (occurring at peak amplitude –5%),

$f_{MAX\omega} = \omega_{MAX}/2\pi$ is the maximum periodic frequency (occurring at peak amplitude –5%), and

$\Delta\omega$ is the increment between cyclic frequencies.

For an AC conductor, the alternating current generates an alternating magnetic field resulting in eddy currents arising in the conductor. This phenomenon is called skin effects. The skin depth is a measure of how deeply the current penetrates the leader. When the radius of the leader is smaller than the skin depth, the skin effects are considered negligible. The skin effect is calculated by [65]:

$$\delta = \frac{1}{(\pi \cdot \mu_r \cdot \mu_o \cdot \sigma_s \cdot f)^{0.5}} \quad , \tag{3.42}$$

where the material properties,
$\mu_r = 1$, and
$\sigma_s = 6 \cdot 10^7$.

3.5.2 Resistive power losses

Resistive losses in the coil windings are referred to as copper losses. The resistive losses that occur within the coils are defined by [65]:

$$P_c = i^2 \cdot r = i^2 \cdot \left(\frac{l_{coil}}{\sigma_c \cdot A_{coil}} \right) \quad , \tag{3.43}$$

where
P_c is the power due to copper losses,
i is the current of the coil,
r is the resistance of the coil,
l_{coil} is the length of a stator coil,
σ_c is the conductivity of the coils' material, and
A_{coil} is the cross sectional area of the coil.

All losses occur as heat dissipation within the material. It is assumed that this heat dissipation will not result in any adverse reactions, since the linear generator is assumed to be surrounded by water and thus readily cooled.

3.5.3 Efficiency

The efficiency of the linear generator is expressed as the ratio of output power to input power and is computed by [65]:

$$\eta_{LG} = \frac{P_{out}}{P_{in}} = \frac{P_{out}}{P_{out} + P_{losses}} \quad , \tag{3.44}$$

where
η_{LG} is the efficiency of the linear generator,
P_{out} is the power output of the linear generator,
P_{in} is the power input to the linear generator, and
P_{losses} is the power losses due to hysteresis, eddy currents, and resistive losses.

3.6 Modeling the energy generated for the buoy in heave

The configuration shown in Figure 3.8 illustrates the basic buoy-type WEC system typically used to convert the heaving motions of a floating buoy into electrical energy. As the surface waves impact upon the buoy, it heaves (rises) in the water which in turn causes the attached rope to rise and fall accordingly. The ensuing undulation of the rope causes the rotor of the seabed mounted linear generator to rise and fall, creating relative motion between the rotor and stator thereby generating electricity.
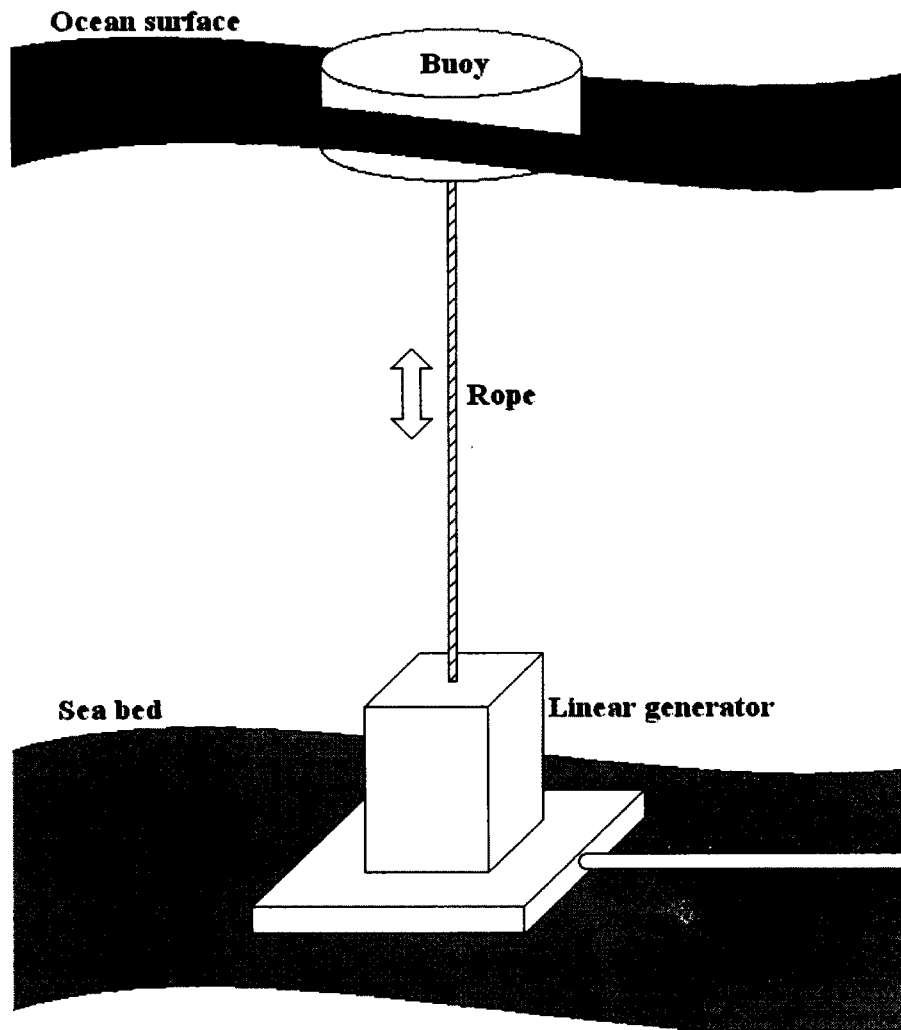
Figure 3.8. Buoy configuration in heave.

The generated voltage and current, and the output voltage and power can be calculated as functions of time for both wave regimes and all sea states using Equations (3.33), (3.36), (3.38), and (3.39), respectively.

3.7   Optimizing the buoy

It is suspected that the buoy can be manufactured to permit a large heave response for the significant cyclic frequency of waves occurring in a particular area.   This feat can

theoretically be accomplished by selecting the proper dimensions for the buoy so that its natural frequency of heave lies in close proximity to that of the waves occurring in the immediate area. Four different buoy sizes will be modeled for each of the SUMMER and WINTER sea states to have heave ratios of approximately 1.0, 1.25, 1.5, and 1.9 when reacting to the significant wave period within both of these sea states. Then, a statistical analysis will be performed for each sea state under both wave regimes to determine the buoy size which will provide the maximum average output power. This information can then be used to practical advantage when evaluating the feasibility for establishing a buoy-type WEC off of the Oregon coast.

CHAPTER IV

RESULTS AND DISCUSSION

4.1   Simulating ocean surface waves

4.1.1   The regular wave regime

Table 4.1 lists the significant wave height (H_s) and period (T_s) for the three selected

sea states. It also lists the calculated Pierson-Moskowitz parameters for wind speed

($U_{19.5}$), and significant (ω_o) and peak frequencies (ω_p) based on Equations (3.1) - (3.3).

For the sea state identified as TEST, the waves are characterized by smooth, small waves

(known as wavelets) and represent the activity in a relatively calm body of water. The

WINTER and SUMMER sea states represent the conditions of the sea off the Oregon

coast during the different seasons.

Table 4.1. Selected sea state conditions and the associated Pierson-Moskowitz
parameters.

Selected sea state parameters			Pierson-Moskowitz Parameters		
			Wind speed	Frequencies	
Name	H_s (m)	T_s (s)	$U_{19.5}$ (m/s)	ω_o (s^{-1})	ω_p (s^{-1})
TEST	0.4	4.5	4.32	2.27	1.99
WINTER	3.5	8	12.78	0.77	0.67
SUMMER	1.5	6	8.37	1.17	1.03

Upon assigning the appropriate substitutions for wave amplitude (Z_{wave}), cyclic

frequency (ω), and phase angle between the wave and force ($\varphi = 0$) into Equation (2.11),

the wave height as a function of the listed parameters and time for each sea state may be

calculated by

$$A_W (H_s, T_s, t) = (H_s/2)*\cos((2\pi/T_s)t). \qquad (4.1)$$

Figure 4.1 plots the wave amplitude as a function of time for each selected sea state.

In each of these plots, the ocean surface waves maintain a constant maximum amplitude

(which is equal to ½ of the significant wave height) and steady period which defines the
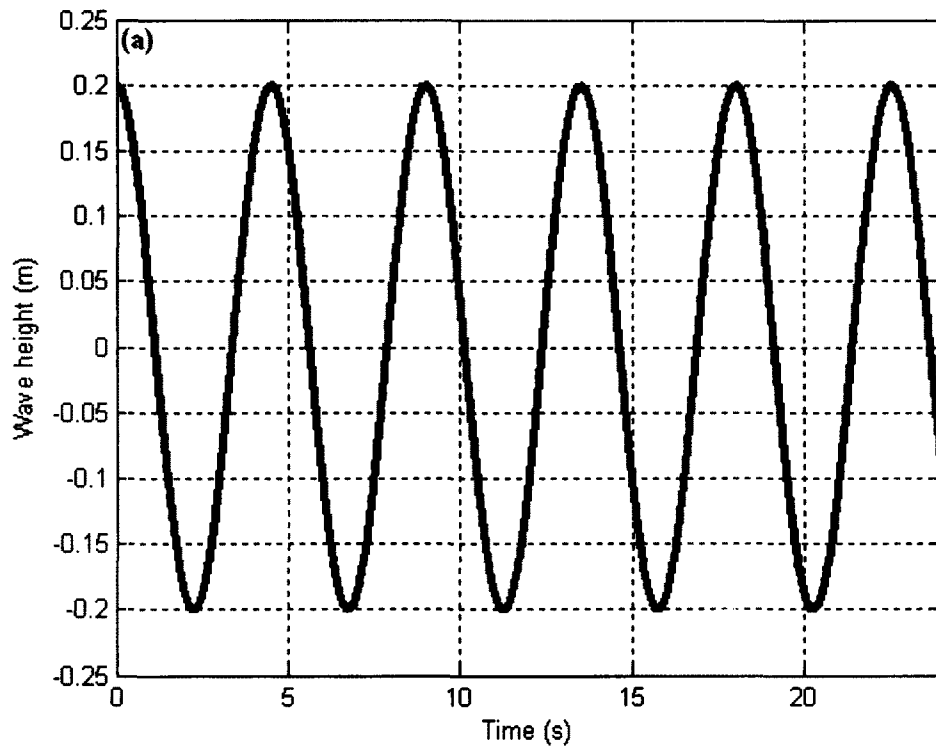
regular wave regime.

Figure 4.1. Time series for the regular wave regime for selected sea states. (a)The TEST, (b) WINTER, and (c) SUMMER sea-states.
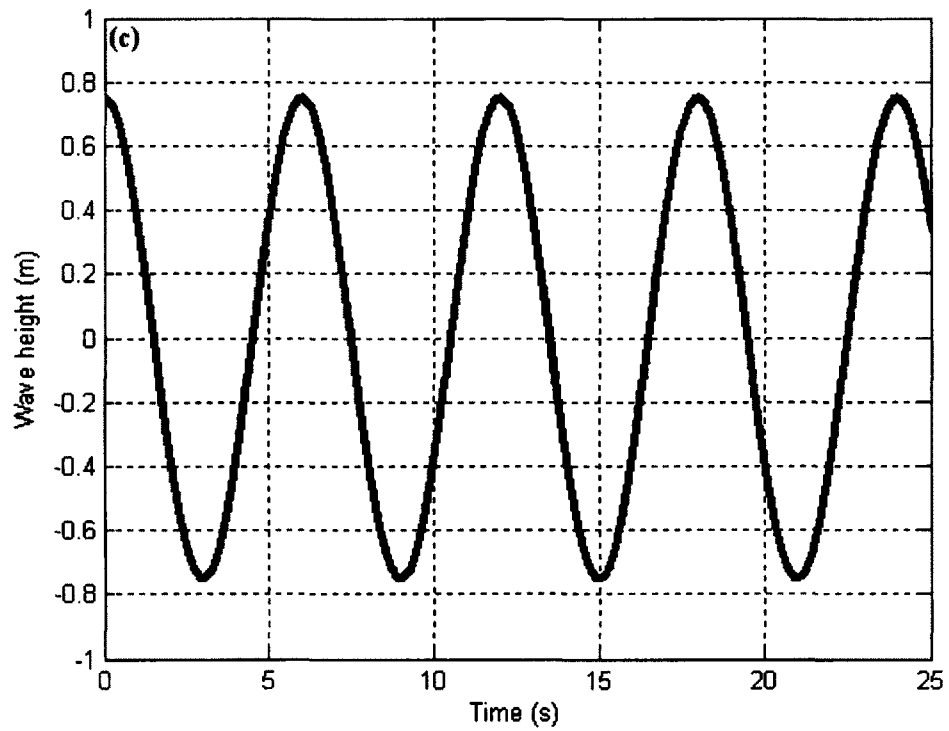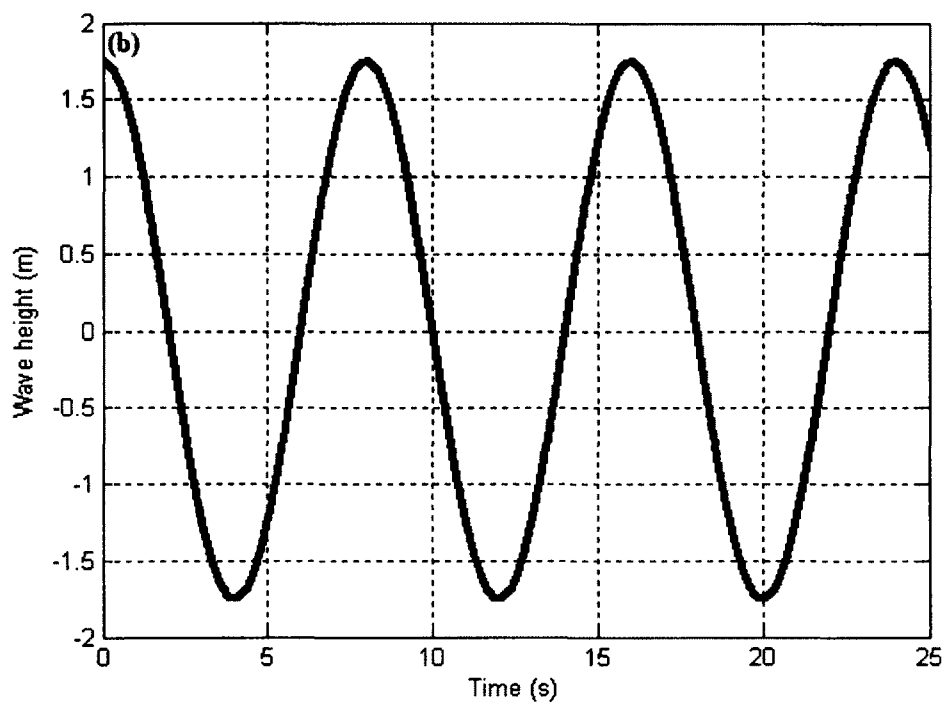
Figure 4.1. Continued.

4.1.2 The irregular wave regime

The irregular wave regime for each sea state is derived from the Pierson-Moskowitz (Equation (2.18)) and Bretschneider spectrums (Equation (2.24)) using the parameters listed in Table 4.1. Figure 4.2 plots the amplitude components as a function of the cyclic frequency of the waves for each spectrum on the same graph for comparison. Generally, there is little deviation between the two spectra in regards to shape, magnitude and peak frequency for each sea state condition, which indicates that either spectrum would produce a 'fair' representation of ocean surface activity.

Figure 4.2 Pierson-Moskowitz and Bretschneider spectrums for selected sea states. (a) The TEST, (b) WINTER, and (c) SUMMER sea-states.
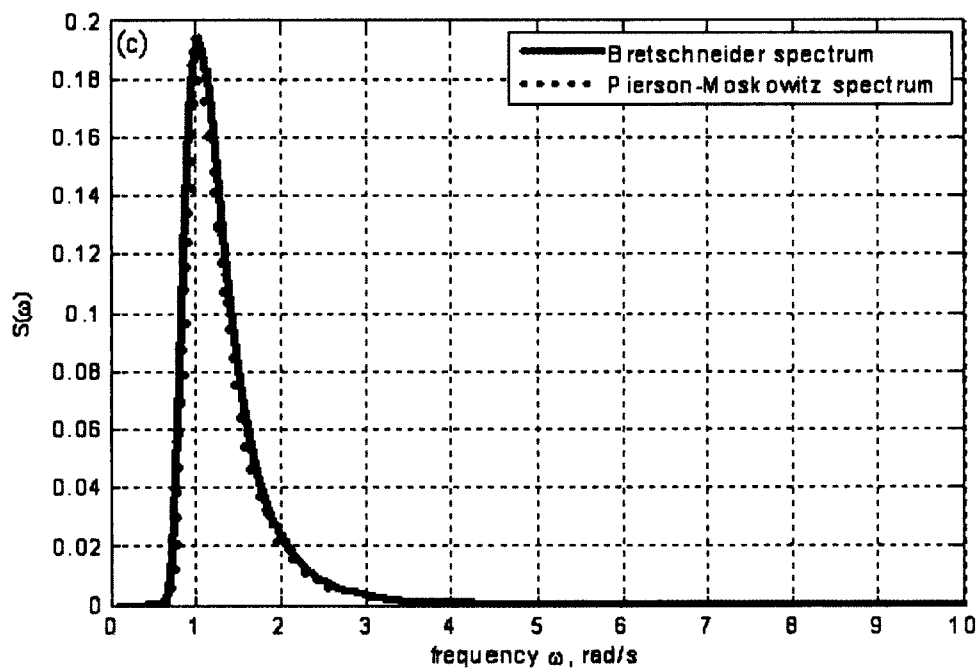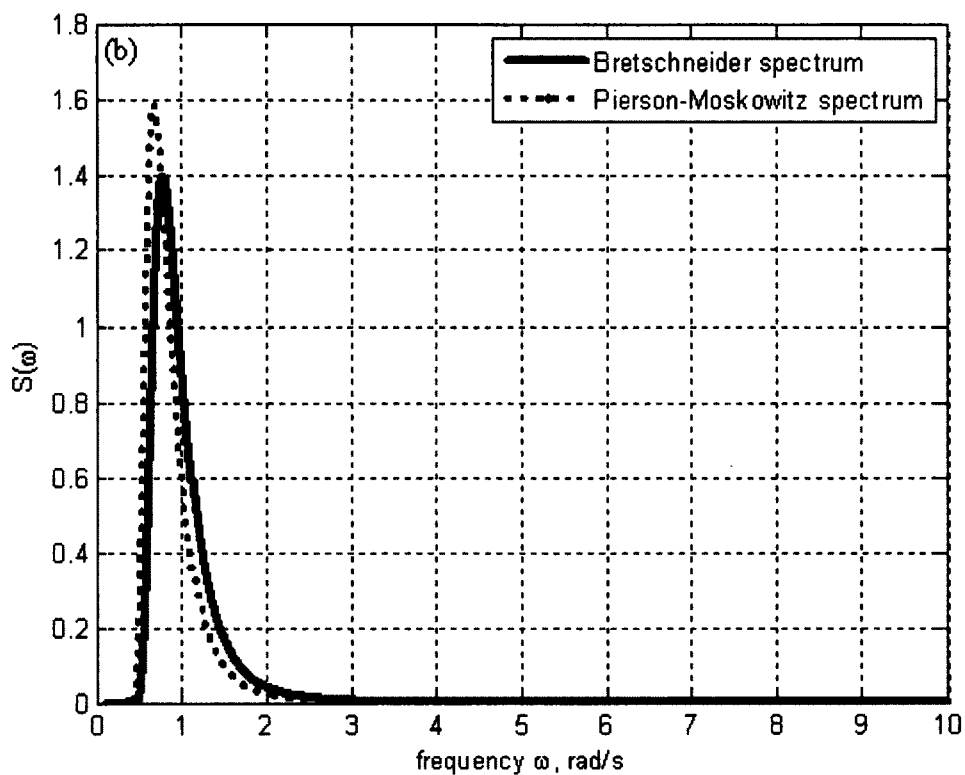
Figure 4.2. Continued.

With both spectrums derived, Equations (2.25) through (2.27) can now be used to generate the time series for the surface waves from both spectra, the results of which are presented in Figure 4.3. As might be expected, since both wave spectrums are similar in appearance and magnitude, the time series for the waves generated from both spectra would likewise be similar in appearance and magnitude. However, due to the limitation that the Pierson-Moskowitz spectrum depends upon the requirement of a fully developed sea to be accurate, and since the Bretchneider spectrum has been accepted as the ITTC standard [48], only the Bretschneider spectrum will be further considered in this work.
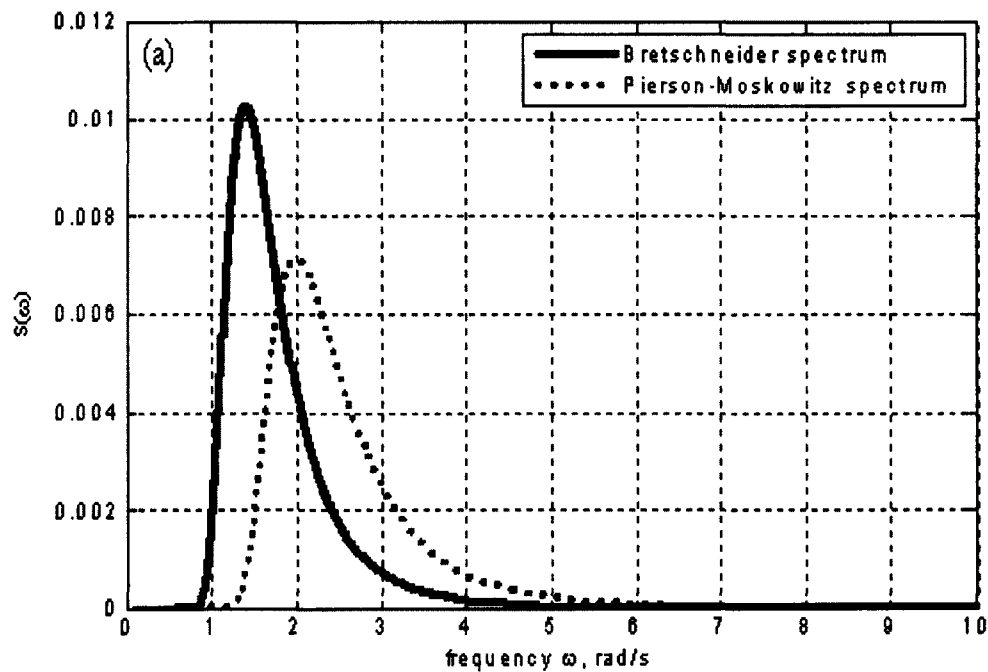

Figure 4.3. Comparison of the time series of surface waves generated from the Pierson-Moskowitz and Bretschneider spectrums. (a) The TEST, (b) WINTER, and (c) SUMMER sea-states.
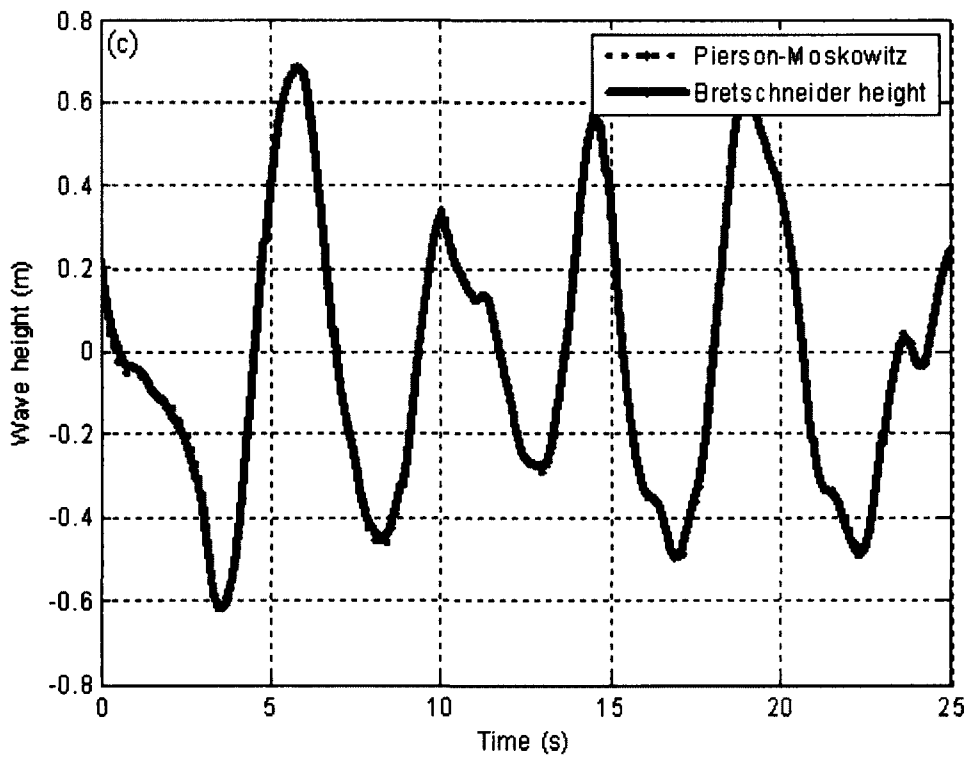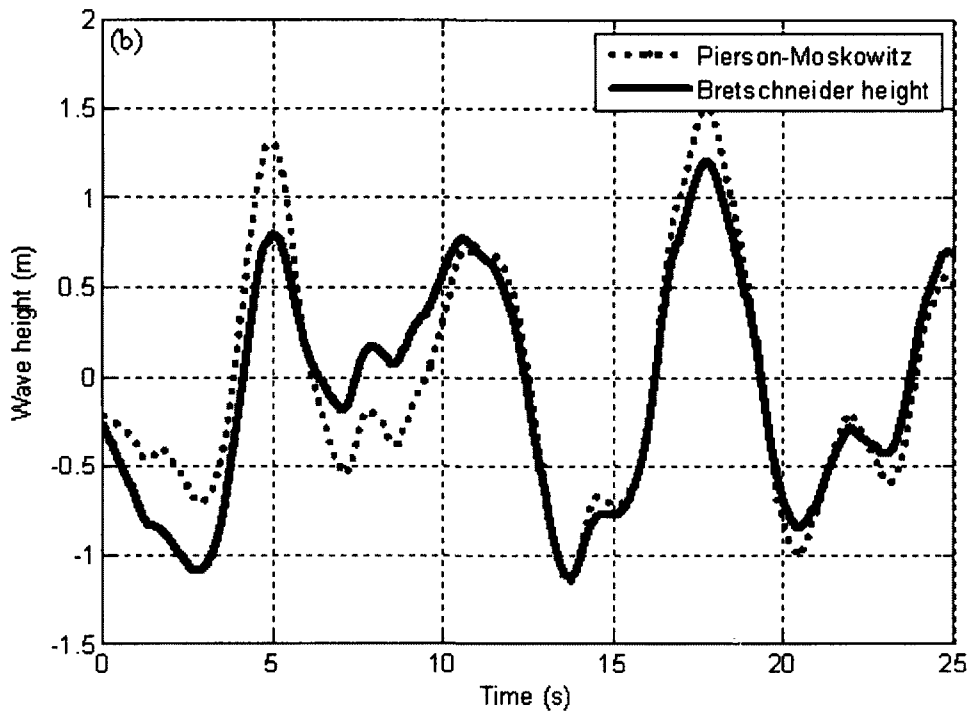
Figure 4.3. Continued.

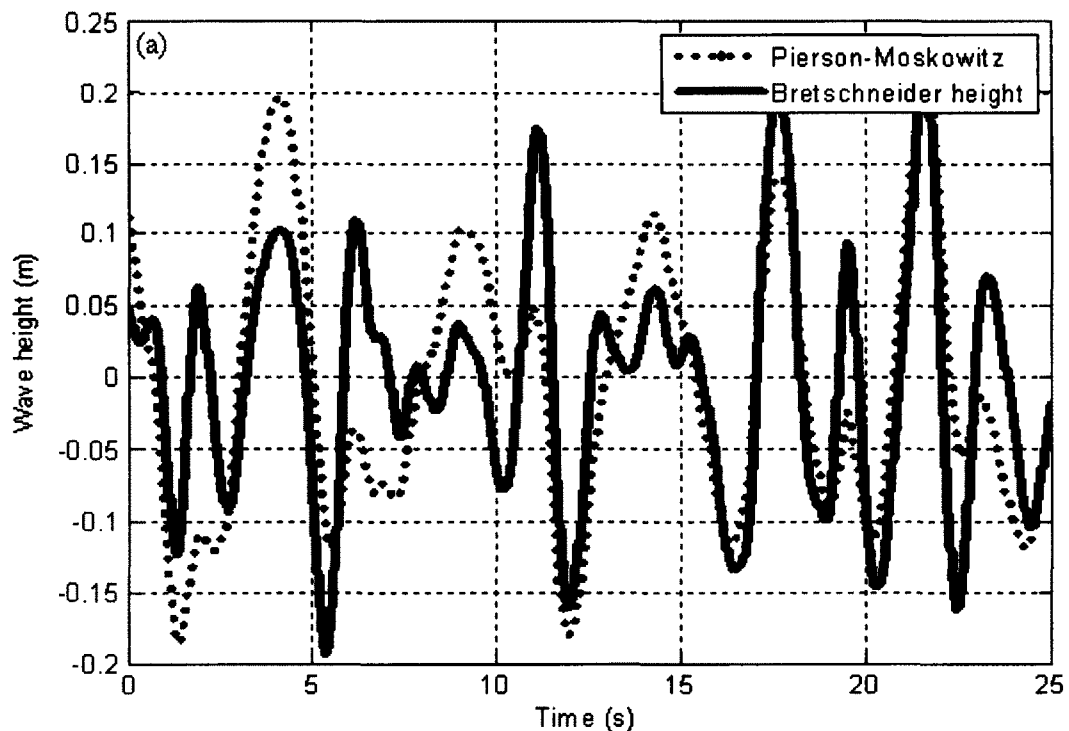## 4.2 Buoy's response in heave

4.2.1 Added mass

The masses for the buoy (as represented by the weight of the displaced water), the entrained water surrounding the buoy, and the combined system are calculated respectively as:

$$M_{BUOY} = \rho \cdot Area \cdot Draft = (1,025 \text{ Kg/m}^3)(\pi \cdot 3m^2)(0.9979m) = 28,920 \text{ Kg}, \tag{4.2}$$

$$M_{ADDED} = C_m \cdot \rho \cdot (4/3)(\pi \cdot r^3) = (0.64)(1,025 \text{ Kg/m}^3)(4/3)(\pi)(3m)^3 = 74,192 \text{ Kg, and} \tag{4.3}$$

$$M_V = M_{BUOY} + M_{ADDED} = 103,112 \text{ Kg}. \tag{4.4}$$

4.2.2 The restoring force coefficient

The restoring force coefficient (S) is composed of the hydrostatic and spring restoring force (k_s) and is computed in this model as:

$$S = \rho \cdot g \cdot A + k_s = (1,025 \text{ Kg/m}^3)(9.8 \text{ m/s}^2)(\pi)(3m)^2 + 40 \text{ Kg/s}^2 = 324,016 \text{ Kg/s}^2 \tag{4.5}$$

4.2.3 The damping force coefficient

The damping force coefficient (D_f) expressed as functions of the wave height and cyclic frequency is calculated as:

$$D_f (H_s,\omega) = (4/3\pi) \cdot \rho \cdot C_D \cdot A_{BUOY} \cdot v_1 = (0.4244)(1,025 \text{ Kg/m}^3)(0.63)(\pi)(3m)^2(H_s)(\omega) \tag{4.6}$$
$$= (7,749 \text{ Kg/m})(H_s \cdot \omega)$$

Figure 4.4 simultaneously plots the damping force coefficient for each of the chosen sea states. Since the damping force is linear and proportional to the significant wave height, the greater the significant wave height for a specific sea state, the larger the damping coefficient at each cyclic frequency. The damping force coefficient plots in Figure 4.4 validate this principle.
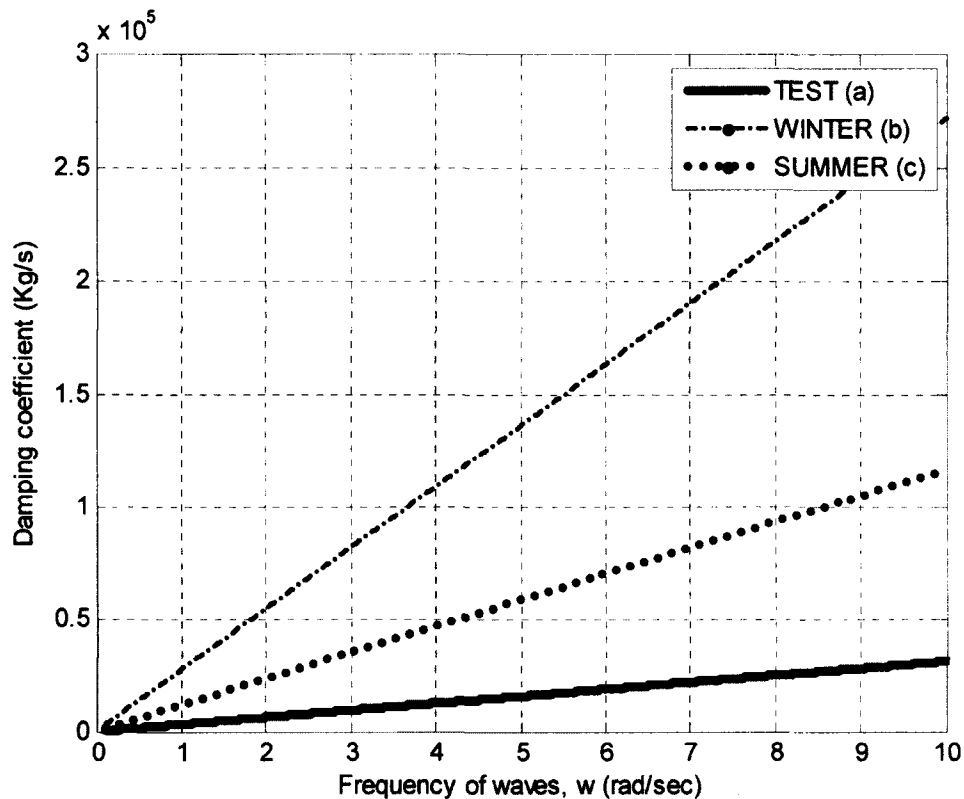
Figure 4.4. Damping coefficient as a function of the cyclic frequency of the waves for each sea state. (a) The TEST, (b) WINTER, and (c) SUMMER sea-states.

4.2.4 The natural frequency for heave of the buoy and its linear damping coefficient

The resonant frequency for heave of the buoy is computed as

$$p = (S/m_v)^{0.5} = (324,016 \ Kg/s^2 / 103,112 \ Kg)^{0.5} = 1.77 \ rad/sec. \qquad (4.7)$$

It will later be seen that the buoy heaves dramatically at cyclic frequencies near this resonant (natural) cyclic frequency.

Since the linear damping coefficient, n, is defined as the ratio between the damping force coefficient and twice the virtual mass of the buoy/water system, a plot of this function (Figure 4.5) appears similar to the plot of the damping force coefficient (Figure 4.4), but reduced in slope and magnitude.
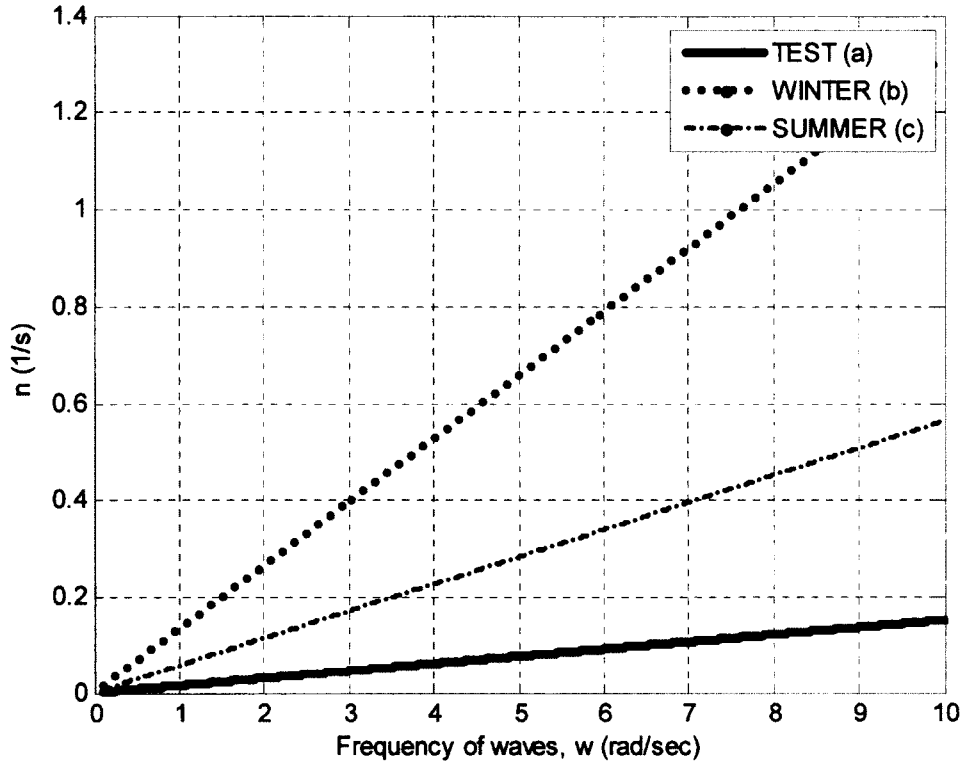
Figure 4.5. Linear damping coefficient as a function of cyclic wave frequency. (a) The TEST, (b) WINTER, and (c) SUMMER sea-states.

4.2.5 The wave exciting force

The wave exciting force defined in the previous chapter for bodies oscillating in heave in deep water is relisted here as

$$F_e = A_w \cdot e^{-kD} \sqrt{\{(S - m' \cdot \omega^2)^2 + D_f^2 \cdot \omega^2\}} e^{j\sigma}, \tag{4.8}$$

where
F_e is the exciting force,
A_w is the significant wave's amplitude,
k is the wave number,
D is the draft of the buoy,
S is the restoring force coefficient,
m' is the added mass of the floating buoy,
ω is the angular frequency of the waves,
D_f is the damping force coefficient, and
σ is the phase angle between the force and the wave.

Figure 4.6 simultaneously plots the wave exciting force for each of the selected sea states. As the figure clearly demonstrates, the magnitude of the wave exciting force maintains proportional to the significant wave height throughout the cyclic frequency bandwidth, in compliance with Equation (4.8). Further inspection of the figure reveals that the total response can be divided into three different regions of activity.
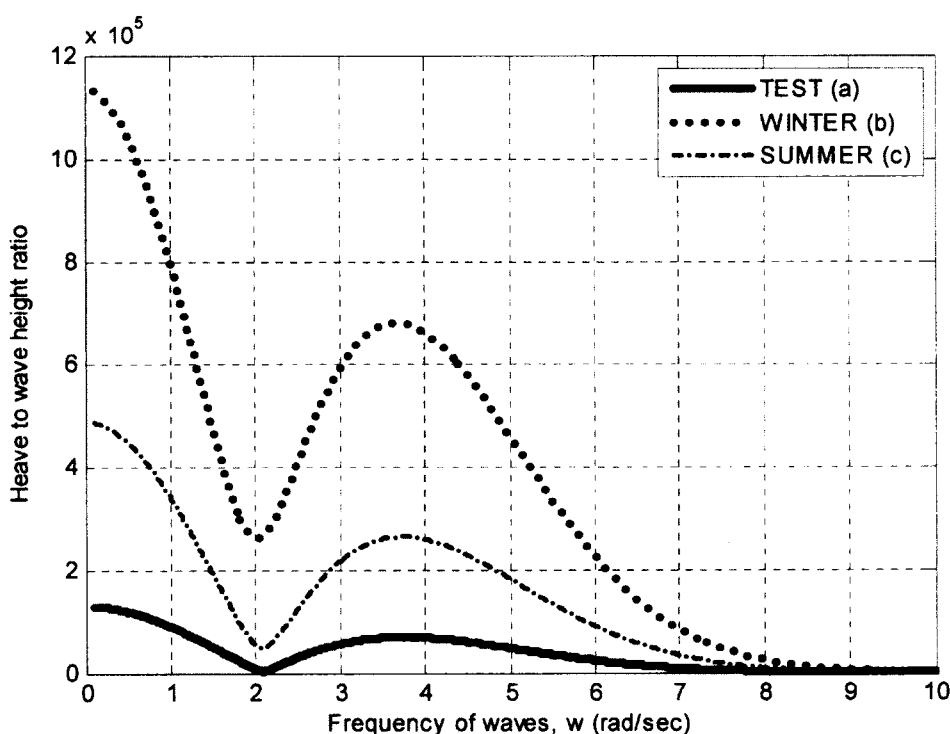
Figure 4.6. Wave exciting force as a function of cyclic wave frequency for various sea states. (a) The TEST, (b) WINTER, and (c) SUMMER sea states.

In the first region, defined by a cyclic wave frequency between approximately 0 to 2 radians per second, the magnitude of the wave exciting force is dominated by the restoring term. As the cyclic frequency of the waves increase, the $-m'\omega^2$ term also increases in magnitude causing the influence of the restoring force to diminish. Although

the damping force also increases in magnitude during this region, it only imparts a minor influence on the rate of descent of the wave exciting force in this region. At a cyclic frequency of approximately 2 radians per second, the restoring force is cancelled out by the activity of the added mass and the net result is reduced to only the damping force.

The second region occurs within a cyclic wave frequency of approximately 2 to 3.5 radians per second. In this region, although the $(S- m'\omega^2)$ term continues to decrease in the negative direction, its squared value increases with the wave's cyclic frequency. Additionally, the damping force rises with the wave's cyclic frequency in this region, which further increases the wave exciting force up to approximately 3.5 radians per second.

In the final region, defined by the cyclic wave frequencies above 3.5 radians per second, the wave exciting force diminishes toward zero. This activity occurs because at high frequency rates the influence of the exponential term rises in dominance due to the increasing wave number $(K = \omega^2/g)$ which results in a rapidly diminishing exciting force.

4.2.6 The RAO for heave

The RAO for heave for a vertically floating cylindrical buoy having the previously stated properties is displayed in Figure 4.7 for the various sea states. A comparison of these figures reveal that, although each heave response is similar in shape, they vary in peak magnitude near the buoy's natural frequency region and beyond. An explanation for this behavior is discussed in the next section.
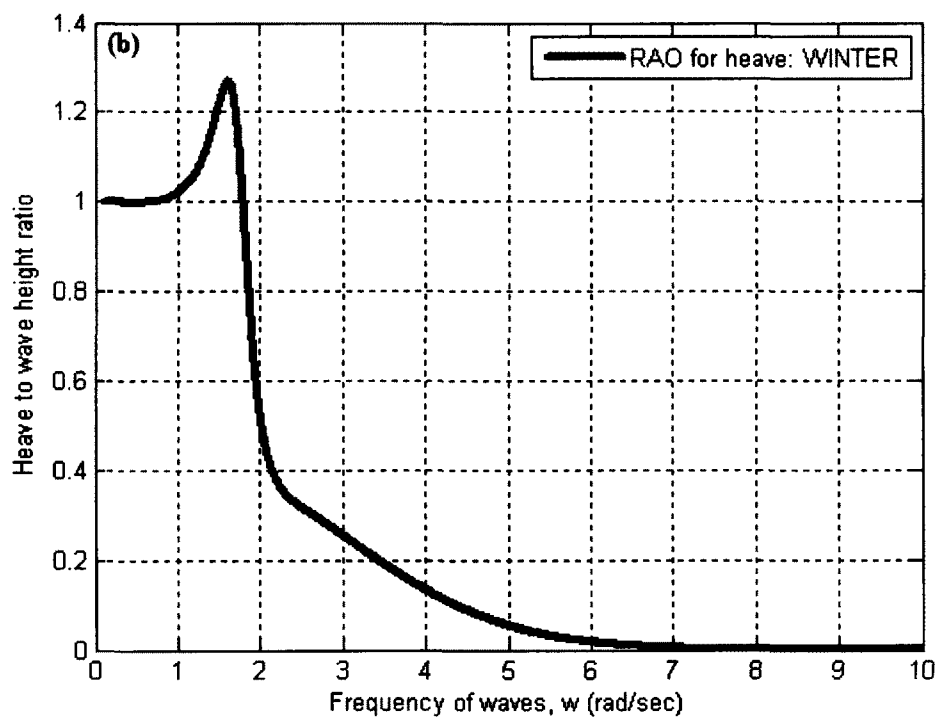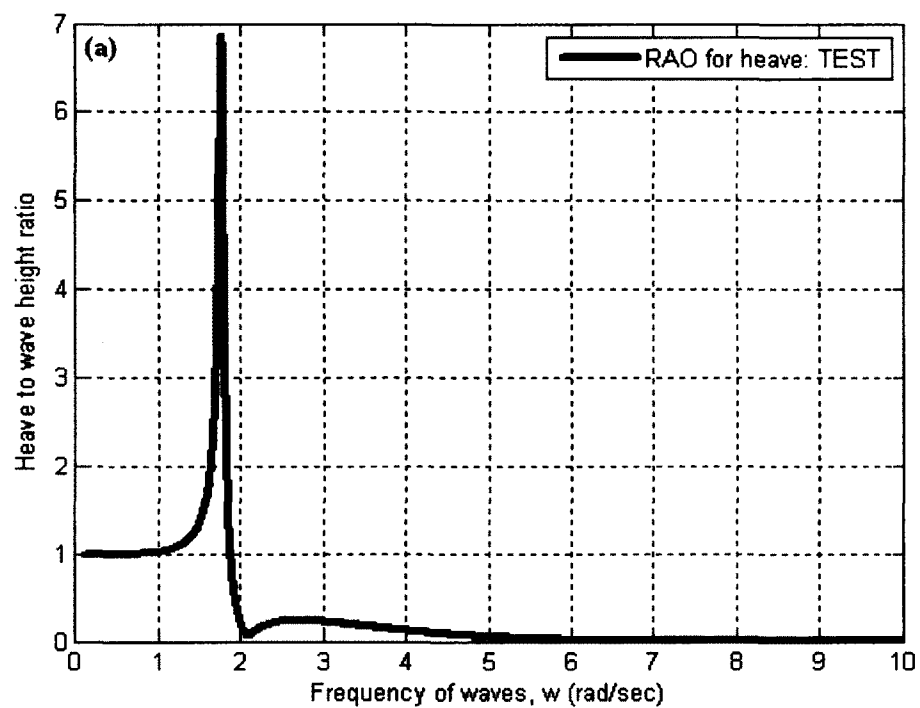
Figure 4.7. RAO for heave for a vertical floating cylindrical buoy under various sea states. (a) The TEST, (b) WINTER, and (c) SUMMER sea states.
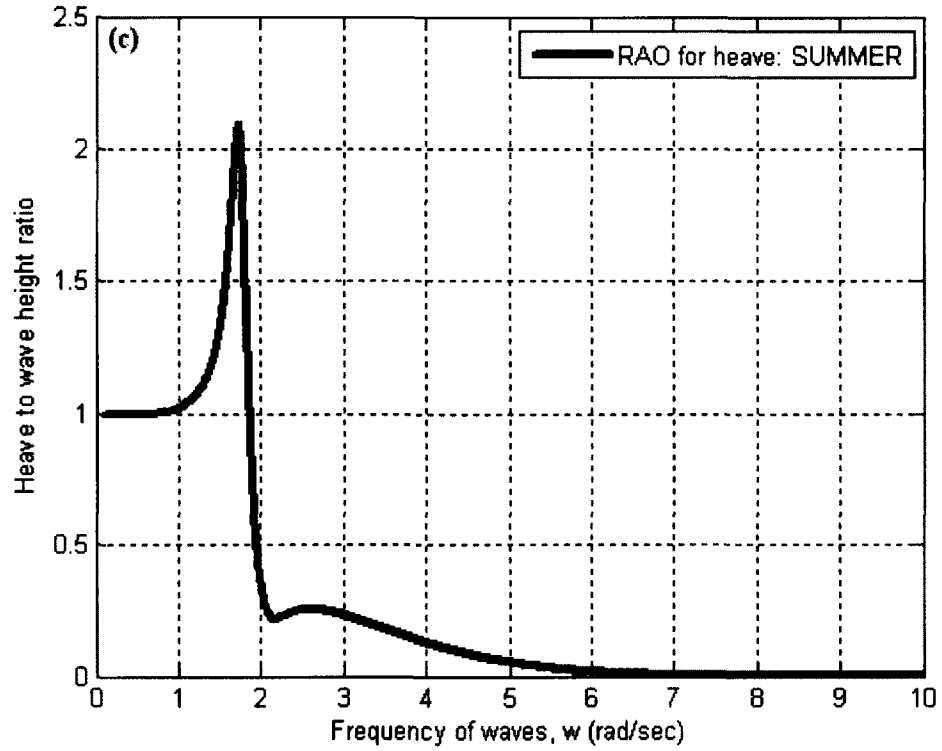
Figure 4.7. Continued.

Generally, the RAO is not determined for each individual sea state but averaged over all of the waves that are expected to be encountered. Figure 4.8 depicts the RAO for heave for the average of the SUMMER & WINTER sea states.
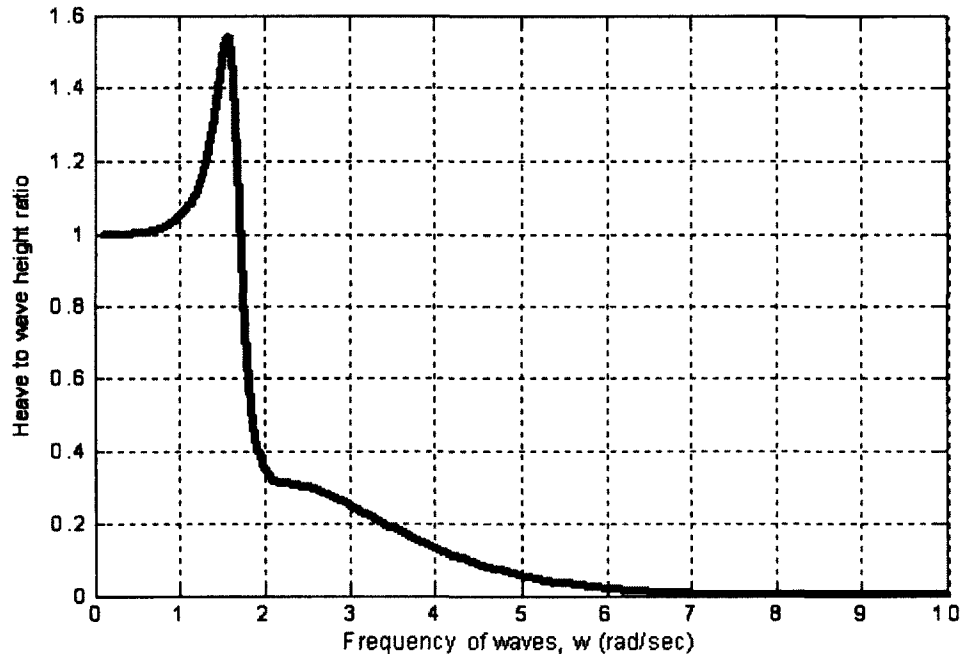
Figure 4.8. RAO for average heave for the SUMMER & WINTER sea states.

4.2.6.1   Heave response behavior

An analysis of Figures 4.7 and 4.8 reveal that the heave response for the floating buoy

can be divided into the three frequency regions as shown in Figure 4.9.
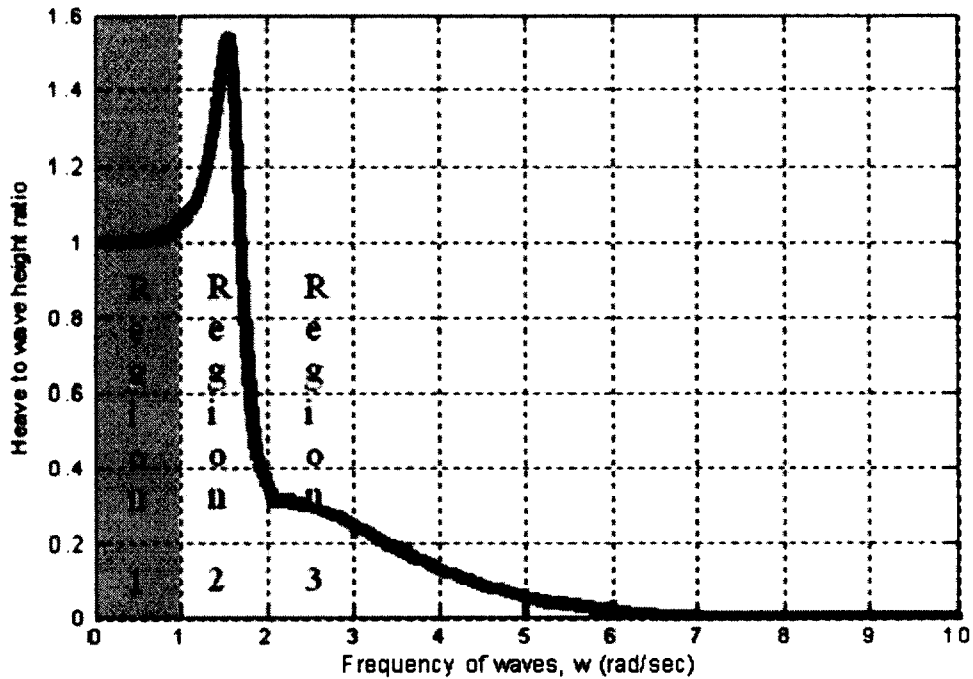
Figure 4.9. Frequency areas with respect to heave behavior.

Each of these regions describes the response of the buoy as determined by the dominant force acting upon it. These regions are defined by:

Region 1. The low frequency area, defined by $\omega^2 \ll S/(m+m')$, has the vertical motions dominated by the restoring spring term. In this region, the buoy tends to follow the waves as the frequency decreases, the RAO tends toward 1.0 and the phase lag tends to zero. At very low frequencies, the wave length is very large compared to the horizontal length (diameter) of the buoy and it will bounce upon the waves [74].

Region 2. At the natural frequency area, $\omega^2 \approx S/(m+m') \approx p^2$, the vertical motions are dominated by the damping term. In this region, a high resonance can be expected for low levels of damping. A phase shift of $-\pi$ occurs approximately at the natural frequency (see the equation for ϕ_{heave} in Equation 3.24). This phase shift is very abrupt here, due to the small damping on the buoy. Since the magnitude of damping is proportional to the

product of the wave's significant height and cyclic frequency (see Equation (3.12)), as this product increases in magnitude, so does the damping loss that occurs for the buoy, resulting in a lower heave response. This effect can be verified by noticing that the peak heave response in Figures 4.7 and 4.8 is *inversely* proportional to the product of the significant wave height and cyclic frequency for each sea state [74].

Region 3. For the high frequency area, $\omega^2 \gg S/(m+m')$, the vertical motions are dominated by the mass term. Here, the waves are losing their influence on the behavior of the buoy. A second phase shift appears at $\omega^2 \approx S/m'$ caused by a phase shift in the wave load (see the equation for Sigma (σ) in Equation 3.16) [74].

It is important to realize that the region in which a buoy would be operating is determined by the response of the RAO, and not by the frequency bands identified in Figure 4.9. By selectively altering the parameters of the buoy, the frequency regions can be shifted to the left or right to better suit a design criteria. For example, Figure 4.10 shows that the frequency regions affecting the buoy can be shifted toward the right by increasing the value of the restoring spring constant. This figure also reveals that as the spring becomes tighter in magnitude, the heave response of the buoy diminishes at each cyclic frequency. This behavior makes logical sense, since the restoring force is proportional to the spring constant (see Equation 3.9).
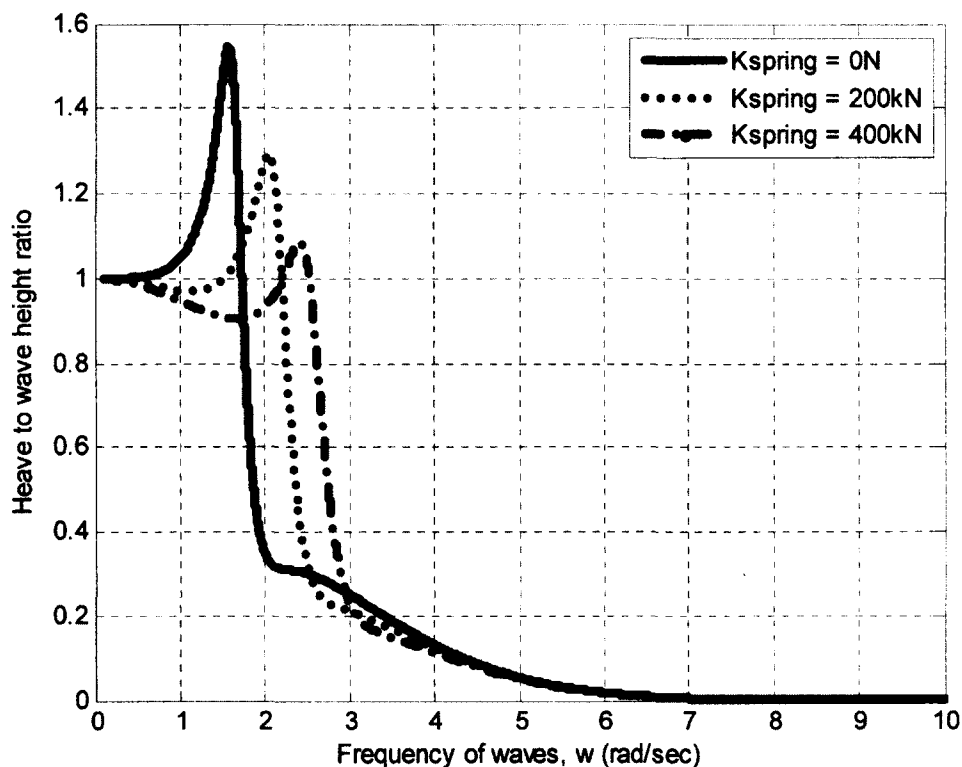
Figure 4.10. Altering the RAO for heave through the use of various restoring spring constants.

4.2.6.2 Time series for heave

The time series for the wave height and buoy displacement for each sea state under the regular wave regime is given in Figure 4.11. An inspection of these results reveals that the buoy closely follows the surface waves for each sea state both in direction and also approximately in magnitude.

For the TEST sea state, illustrated by Figure 4.11(a), the buoy bounces upon the surface of the ocean waves. This activity indicates that the heave transfer function is greater than unity. Upon examining Figure 4.7(a), it can be seen that the response of the buoy for this particular cyclic frequency is measured at 1.2 and lies within frequency

region 2, where the buoy response is close to resonance. Thus, an RAO> 1 is acceptable for this particular sea state and the response of Fig. 4.11(a) is as expected.

The WINTER and SUMMER sea states, illustrated respectively by Figures 4.11(b) and 4.11(c), show that the buoy's height is approximately equal to the wave's height, signifying that the RAO for both sea states is approximately equal to unity. Upon examining the respective RAOs for heave (Figures 4.7(b) and (c)), it is found that the value at each cyclic frequency (0.785 & 1.047 radians per second, respectively) is slightly greater than unity indicating that the buoy is operating near frequency region 1 for both sea states.
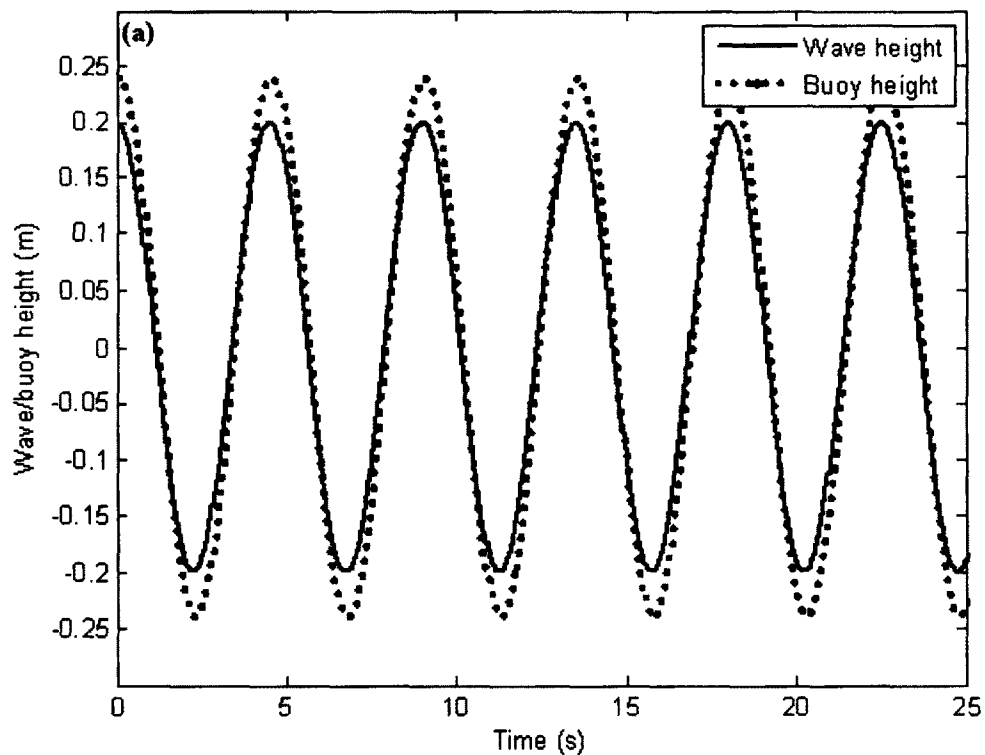
Figure 4.11. Wave height and buoy displacement under the regular wave regime for various sea states. (a) The TEST, (b) WINTER, and (c) SUMMER sea states.
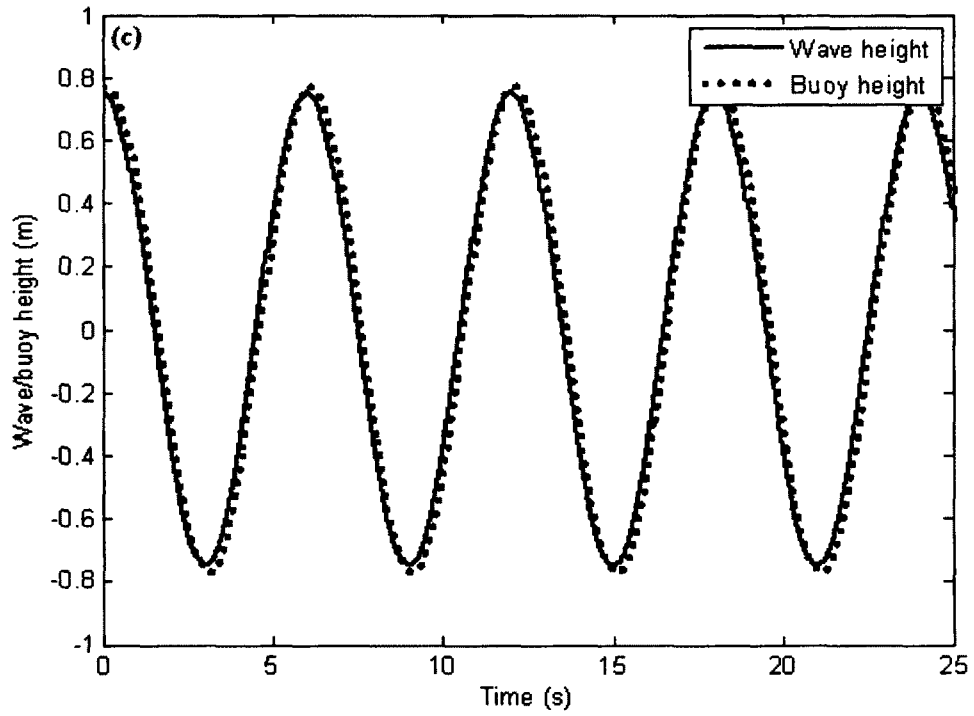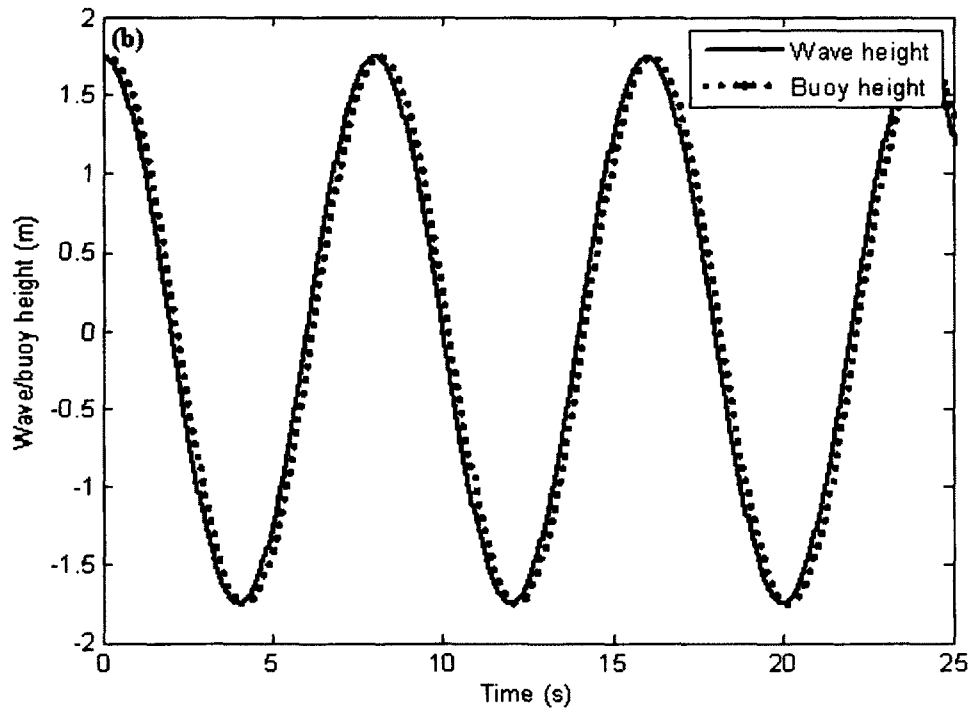
Figure 4.11. Continued.

The time series for each sea state under the irregular wave regime is depicted in Figure 4.12 below. Here, the buoy approximately follows the irregular surface waves for each sea state. The buoy, however, has a tendency to overshoot the wave height (likely due to its momentum) and then lose synchronicity with the waves. It is thus very likely that in this scenario the motion of the buoy is the net result of the forces of inertia, gravitational weight, and the heaving action from the waves.
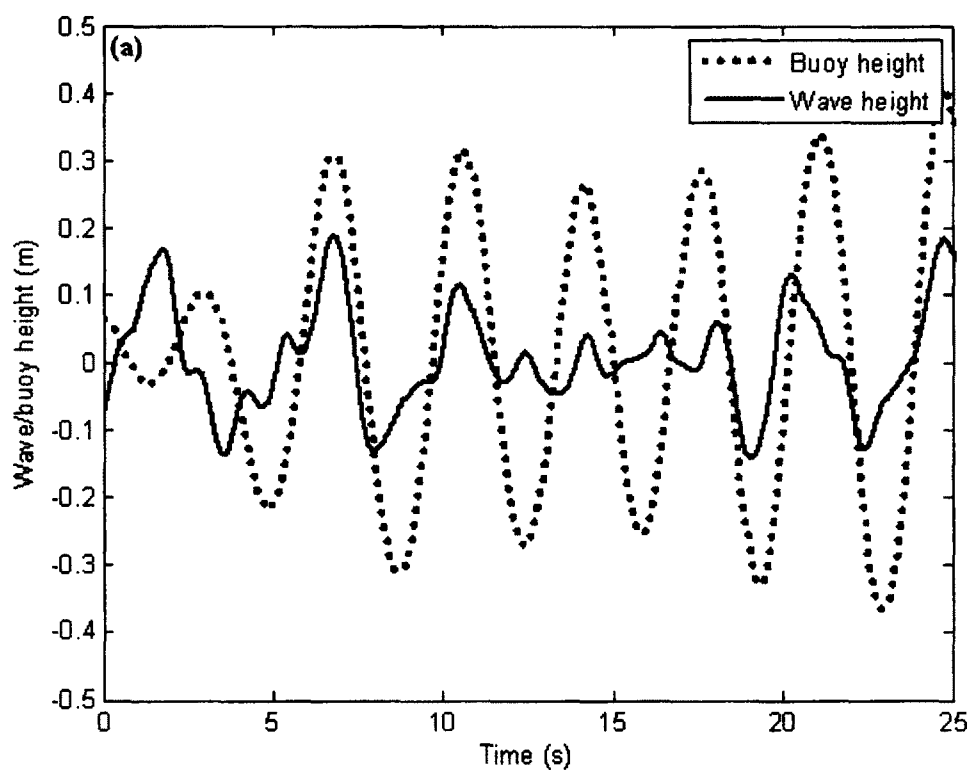
Figure 4.12. Time series for the wave and buoy heights under the irregular wave regime. (a) The TEST, (b) WINTER, and (c) SUMMER sea states.
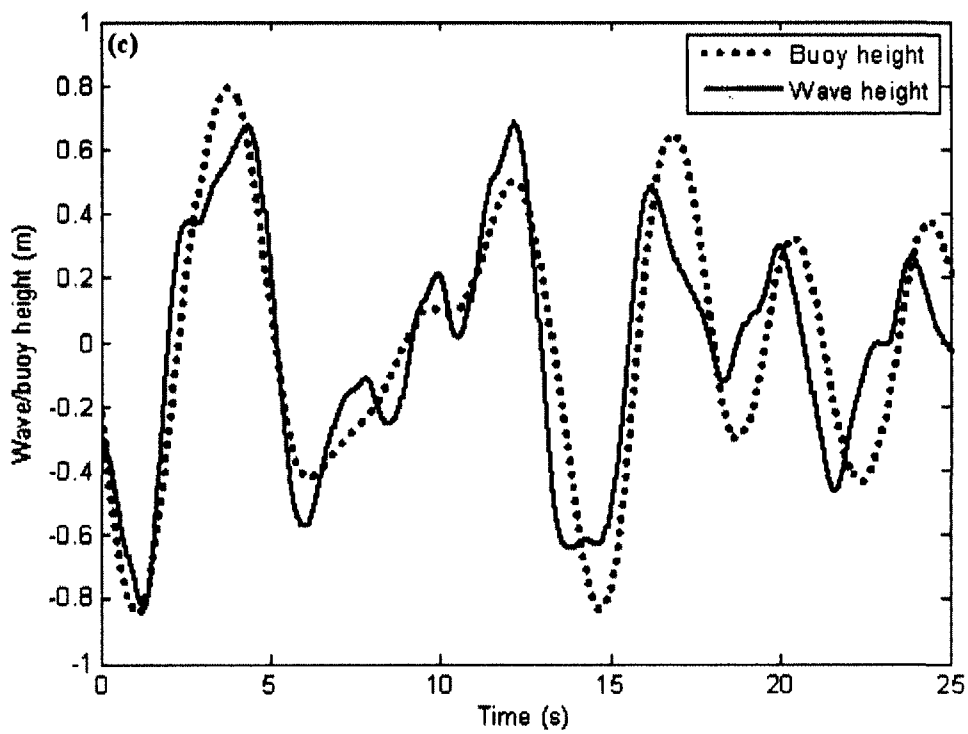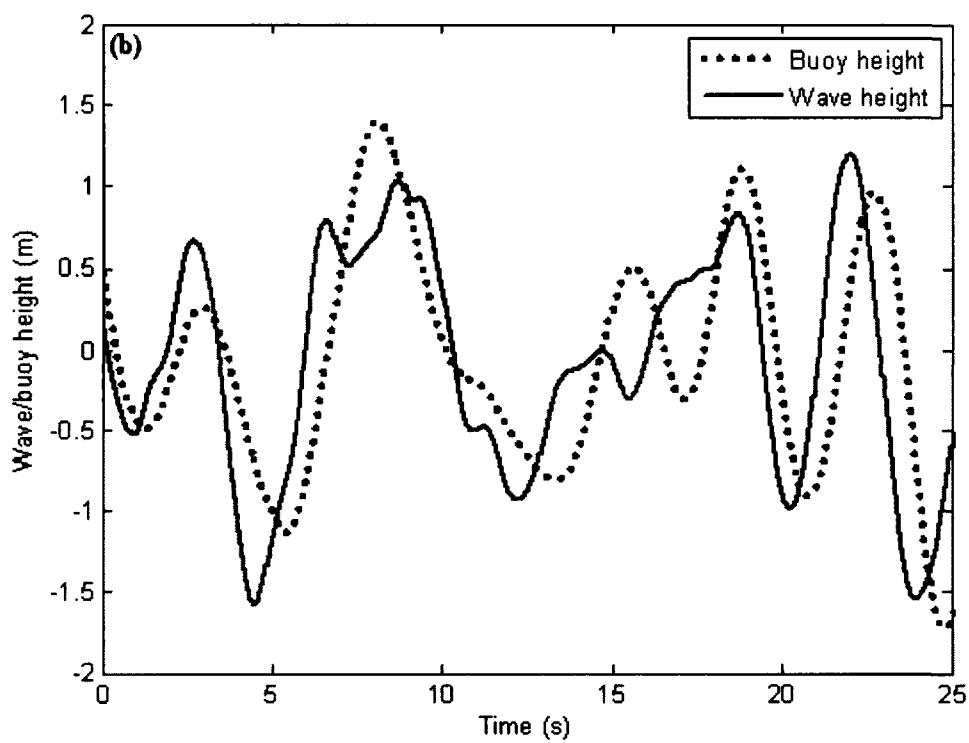
Figure 4.12. Continued.

4.3   Modeling the linear generator

An electrical circuit representing the stator coils used in this analysis is presented in

Figure 4.13 below.   The electrical generation will be driven by the motion of the piston

from the heaving ocean waves.
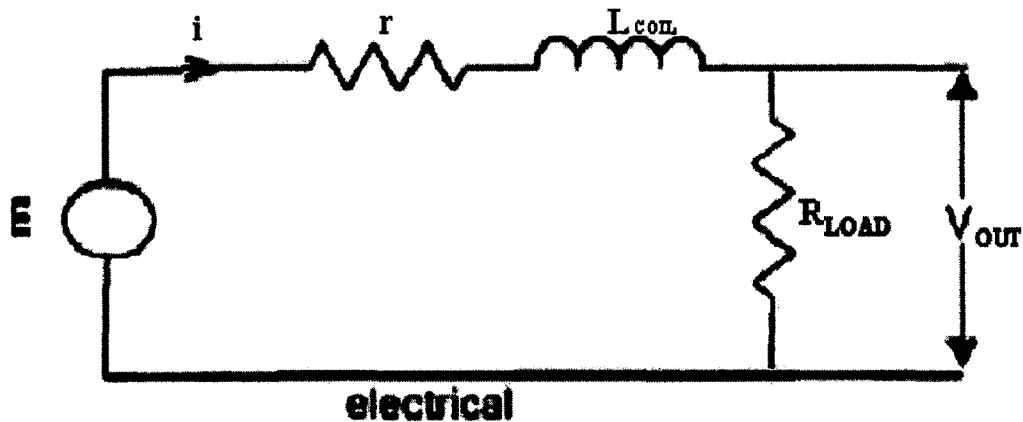
Figure 4.13. Electrical schematic of stator coil assembly [21].

where
E is the generated voltage,
i is the current of the stator,
r is the stator coil's resistance (r = 4.75 Ω),
L represents the self and mutual inductances for the stator coils (L_{COIL} = 12.7mH),
R_{LOAD} is the load resistance (R_{LOAD} = 5 Ω), and
V_{out} is the output voltage of the linear generator.

The generated voltage is computed as a function of time according to Equation (3.33),

which is relisted as

$$E = -N\phi'(\pi/\tau)\sin(\pi/\tau \cdot z)dz/dt \quad , \tag{4.9}$$

where
E is the generated voltage,
N is the number of stator turns (N = 48),
τ is the pole pitch of the generator (τ = 0.040m),
z is the displacement of the rotor relative to the stator,
dz/dt is the velocity of the rotor's motion, defined by [75]

$$dz/dt = \lim_{\Delta t \to 0} \frac{z(t) - z(t-\Delta t)}{\Delta t} \text{ ,and} \tag{4.10}$$

$\phi' = \iint_s B \cdot dS$ is defined as the peak magnetic flux over the area of the surface [76]

where
ϕ' is the peak magnetic flux,
B is the magnetic field,
S is the surface (area), and
dS is an infinitesimal vector, whose magnitude is the area of a differential element of S, and whose direction is the surface normal.

For an air gap of 6mm, the magnetic field intensity (as depicted in Figure 3.6) is 0.55T. Given that the rotor's magnets have an external radius of 0.0225m, and an air gap clearance (between the outer edge of the magnet to the stator coils) of 0.006 m, the resulting radius would calculate to 0.0285m. Thus, the resulting area for the magnetic flux would be Area $= \pi \cdot r^2 = 0.0026m^2$, giving a peak flux of

$$\phi' = 0.55 \text{ V} \cdot \text{s/m}^2 * 0.0026 \text{ m}^2 = 0.0014 \text{ V} \cdot \text{s}, \tag{4.11}$$

and by inserting the derived parameters into Equation (4.9), the generated voltage simplifies to

$$E = -N \cdot \phi' \cdot (\pi/\tau) \cdot \sin(\pi/\tau \cdot z) \cdot dz/dt$$
$$E = (-48)(0.0014 \text{ V} \cdot \text{s})(78.6m^{-1}) \cdot \sin(78.6m^{-1} z) \cdot dz/dt$$
$$E = (-5.278 \text{ V} \cdot \text{s} \cdot \text{m}^{-1})(dz/dt) \cdot \sin(78.6 \text{ m}^{-1} * z). \tag{4.12}$$

Under the specified circuit parameters, Equation (3.35) changes to

$$d/dt(i) = 78.74 \cdot (E - (i \cdot (5 + 4.75))), \tag{4.13}$$

Thus, the current as a function of time can be expressed by

$$i(t) = 0.103 \cdot \{E - 0.0127 \cdot d/dt(i)\}. \tag{4.14}$$

With the stator current defined, the voltage drops across the stator coils and load can be computed, respectively, by:

$$V_{STATOR \, COILS}(t) = 4.75 \cdot i(t), \text{ and} \tag{4.15}$$
$$V_{LOAD}(t) = 5 \cdot i(t). \tag{4.16}$$

Finally, the output power generated as a function of time may be calculated directly from the current and load resistance by

$$P_{LOAD}(t) = 5 \cdot i(t)^2 . \tag{4.17}$$

4.3.1   Power losses in the linear generator

Table 4.2 gives a partial listing of a wire properties chart. This table will be referenced to obtain the electrical and physical properties of an actual copper cable which will be modeled to simulate the stator coils in this work.

Under normal operating conditions, the maximum generated current (plus safety margin) for the selected sea states is estimated to be 1.4 Amps. It is found that 28AWG wire meets this current requirement for chassis wiring. Additionally, it has a skin depth level well below that expected to be encountered by traveling surface waves, making it an ideal choice for the stator coils. By multiplying the number of turns (N = 48) by the circumference (2π*0.0285m = 0.179m) of the interior of the stator, an estimated cable length of approximately 9 meters is obtained. Then, the product of the length and the cross-sectional area (80.45 nm^2) yields a total cable volume of 724 nm^3.

Table 4.2. Basic copper cable parameters [77].

AWG gauge	Conductor Diameter (mm)	Ohms per km.	Maximum amps for		Maximum power transmission for 100% skin depth for solid conductor copper
			Chassis wiring	Power transmission	
11	2.30378	4.1328	47	12.000	3200 Hz
27	0.36068	168.8216	1.7	0.280	130 kHz
28	0.32004	212.872	1.4	0.226	170 kHz
29	0.28702	268.4024	1.2	0.182	210 kHz

4.3.2 Eddy current power losses

Again, by referring to Table 4.2, the conductance (1/R) for this gauge wire can be computed by dividing 1000m by its intrinsic resistance of 212.872Ω/km to obtain the C_E constant of 4.698 m/Ω. The magnetic flux density is obtained graphically via Figure 3.6, which reveals that the magnetic flux density for an air gap of 6mm is 0.55T (0.55 V·s·m^{-2}). Finally, the tethering rope between the buoy to the seabed mounted linear generator is considered to be non-elastic and remains taut throughout its movements. By replacing the known values for the variables in Equation (3.40), the eddy current power loss as a function of frequency for the regular wave regime can be represented by

$$P_{E\text{-REGULAR}}(f) = (4.698\ m/\Omega)(0.3025\ V^2 \cdot s^2 \cdot m^{-4})(724\ nm^3) f^2 = 1.03\mu V^2 \cdot s^2 \cdot \Omega^{-1}) f^2. \quad (4.18)$$

The periodic magnetic field frequency (1/T$_s$) for the TEST, WINTER, and SUMMER regular wave regime sea states are 0.222s, 0.125s, and 0.167s, respectively, which produces eddy current power losses of 50.86nW, 16.09nW, and 28.61nW, also respectively. Since the wave frequency remains constant for all time in the regular wave regime, the power loss would also remain constant with respect to time. These are extremely low power loss values.

The amplitude components derived through the Bretschneider spectrum as well as their response in heave are plotted in Figure 4.14 for each selected sea state under the irregular wave regime. Although the peak amplitude under heave is greater than that obtained through the Bretschneider spectrum, of particular importance is the narrowing of the cyclic frequency bandwidth which occurs under the heave response. As this bandwidth decreases in magnitude, the number of cyclic frequencies which generate eddy

currents decrease accordingly, thereby lowering the eddy current power loss. Similar to the regular wave regime, since the eddy current power loss for the irregular wave regime is the result of the same cyclic frequencies at each instant in time, its result does not vary with time either.
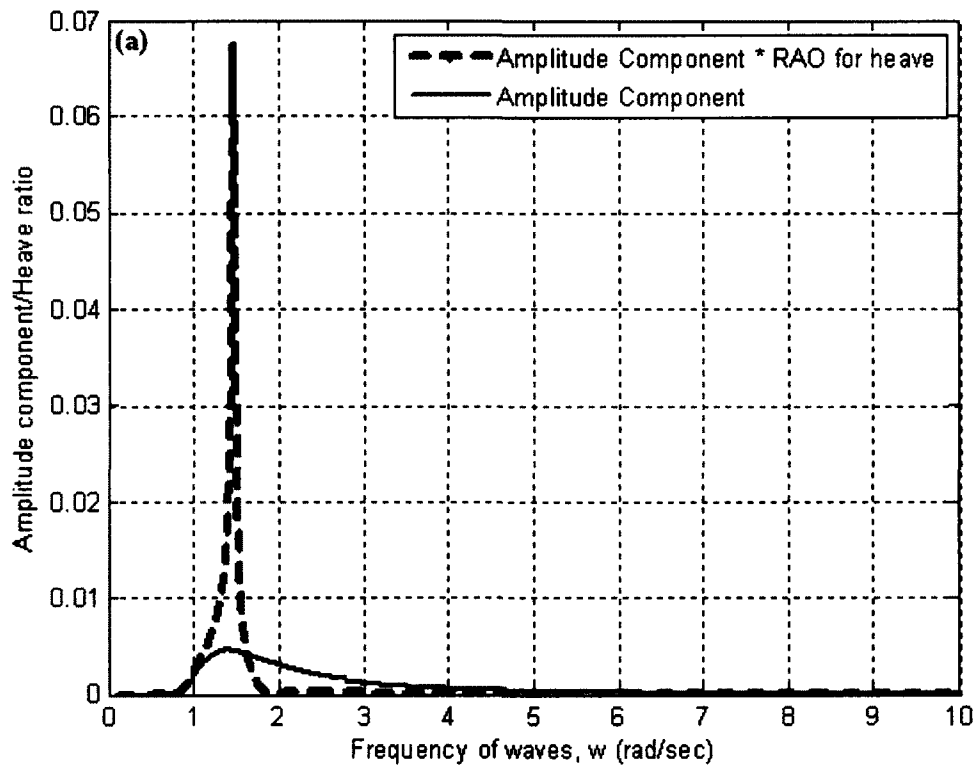
Figure 4.14. Amplitude components and their response in heave for select sea states under the irregular wave regime. (a) The TEST, (b) WINTER, and (c) SUMMER sea states.
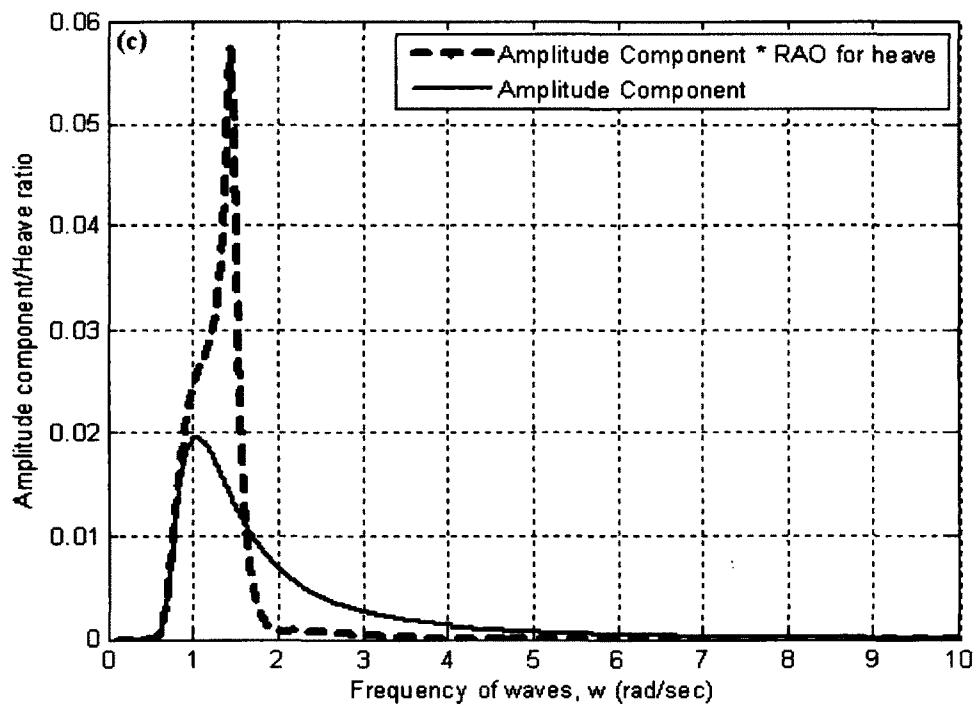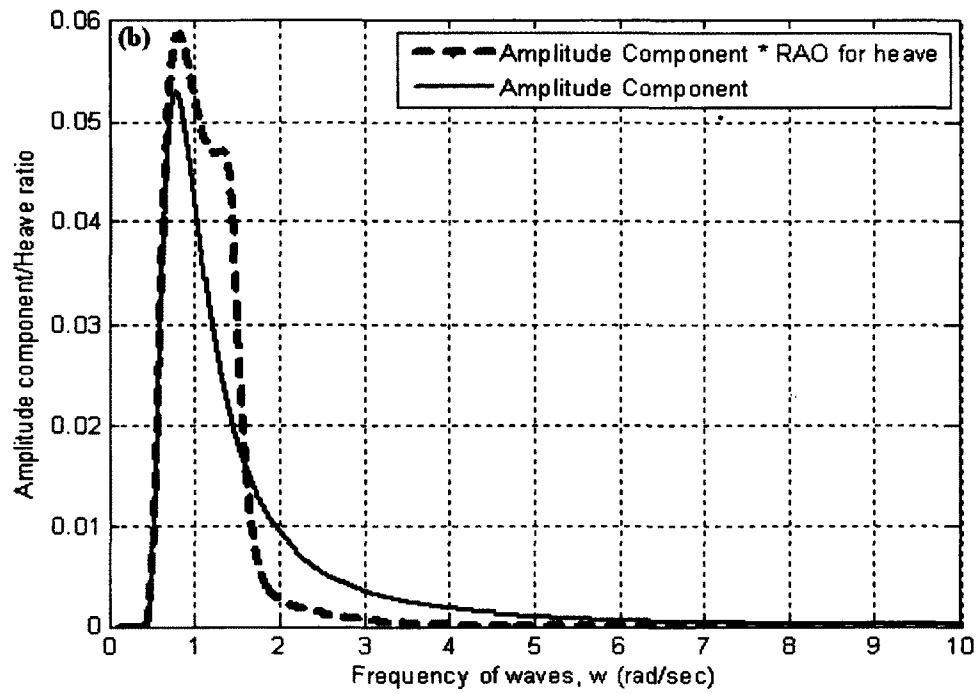
Figure 4.14. Continued.

Table 4.3 lists the peak amplitude encountered under heave, the minimum and maximum cyclic frequencies at which 5% of the peak amplitude occurs, and the computed (via Equation (3.41)) eddy current power losses for each selected sea state under the irregular wave regime. Although the eddy current power losses are much greater for the irregular wave regime (due to the effect of multiple cyclic frequency components), a maximum power loss of 10% occurs only within 0.1% and 7% of the sampled output power waveform (sampled at a rate of 0.01 seconds for 100 wave cycles) for the regular and irregular wave regimes, respectively. Simultaneously run simulations on Matlab, which compared output voltage and power with and without eddy current power losses, produced no visible difference in the magnitude or shape of the selected waveforms. Thus, due to the relatively low ratio of power loss to power generated, and the low frequency of occurrence, eddy current power losses can be considered negligible and left out of the modeling equations.

Table 4.3. Derived parameters for calculating the eddy current power losses in the irregular wave regime for each sea state.

Sea State	Peak amplitude	Frequency range for 95% of peak amplitude component		Eddy current power loss (μW)
		Minimum	Maximum	
TEST	0.08	1.04	1.66	2.97
WINTER	0.06	0.47	1.94	6.21
SUMMER	0.06	0.67	1.78	4.61

4.3.3 Resistive power losses

Resistive losses in the coil windings are identified as copper losses. The total resistive (R_t) load as seen by the generated voltage is equal to the sum of the coil (r) and

load resistance (R_{LOAD}). Thus, the output voltage and current can easily be computed through fundamental circuit theorems, such as the voltage divider rule and Ohms' Law.

Figure 4.15 shows that as the load resistance increases for each sea state, the maximum output voltage increases and the generated current decreases. This behavior agrees with the aforementioned circuit laws. Additionally, the figure also plots the power responses for each sea state as a function of load resistance. This plot reveals that maximum output power is attained when the load resistance is approximately equal to the coil's resistance ($4.75\Omega \approx 5\Omega$). This condition satisfies the resistive condition for the law of maximum power transfer for AC circuits [78].
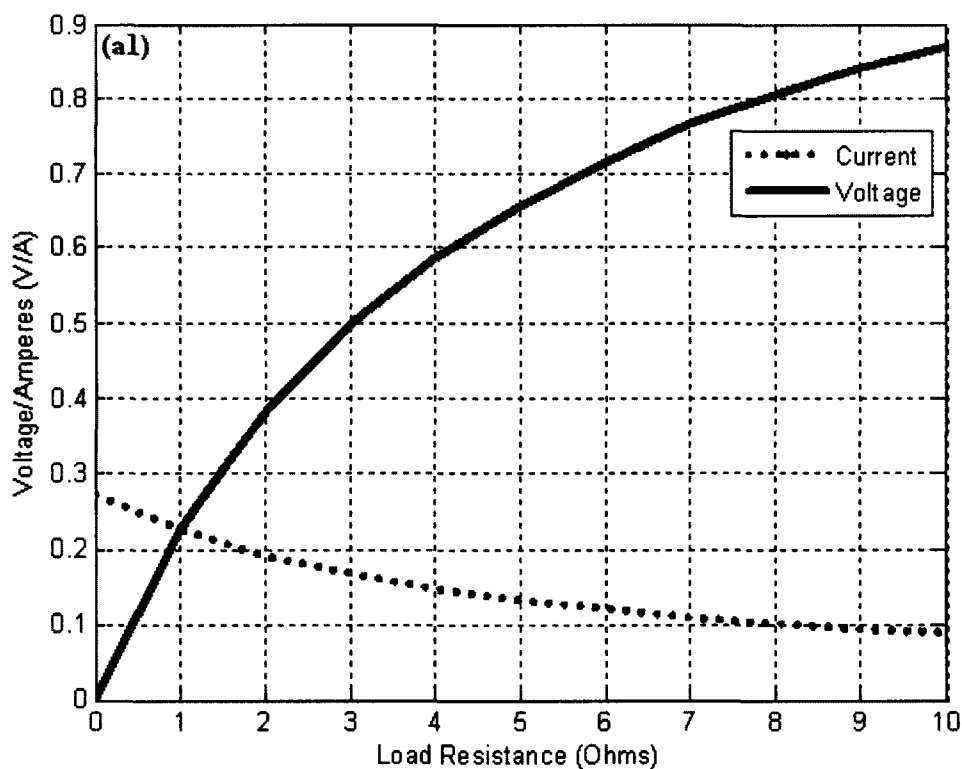
Figure 4.15. Output voltage and current (1), and power response (2) for each sea state under various load resistance values. (a) The TEST, (b) WINTER, and (c) SUMMER sea states.
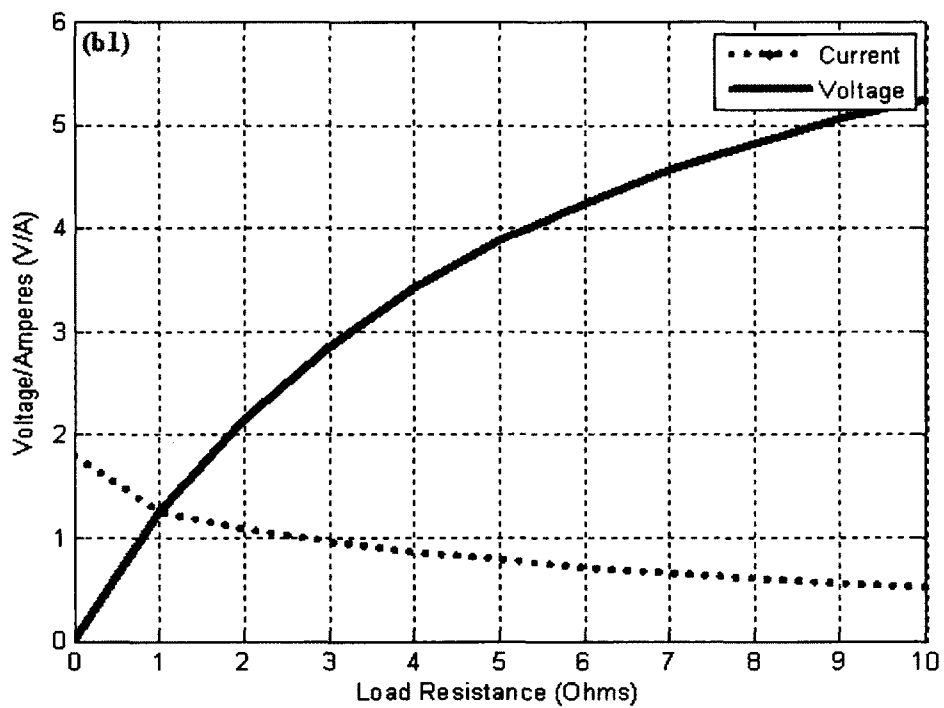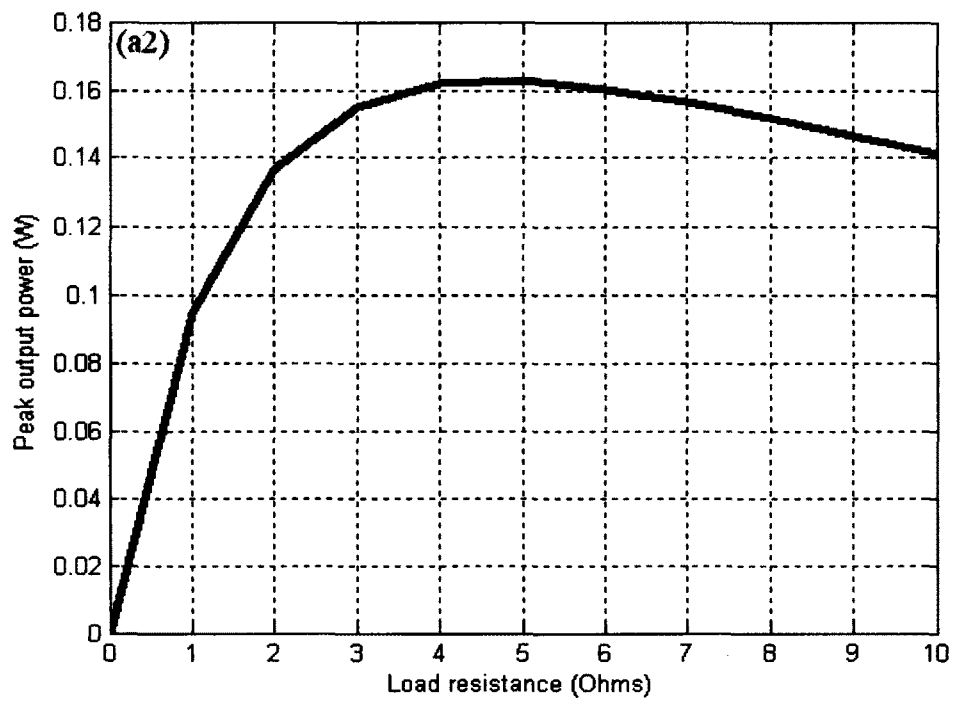
Figure 4.15. Continued.
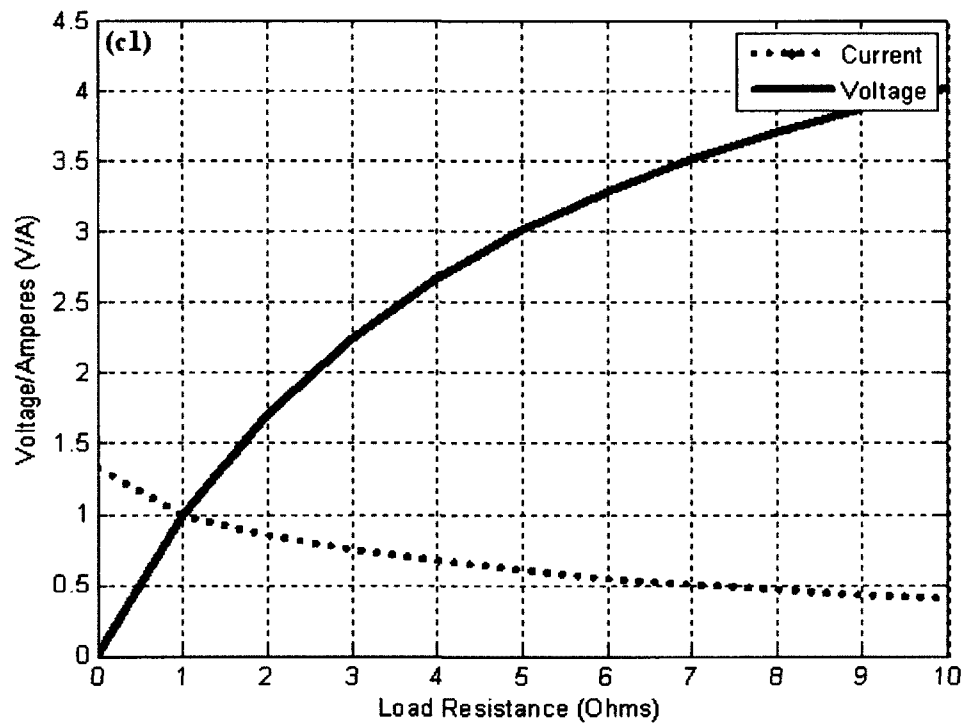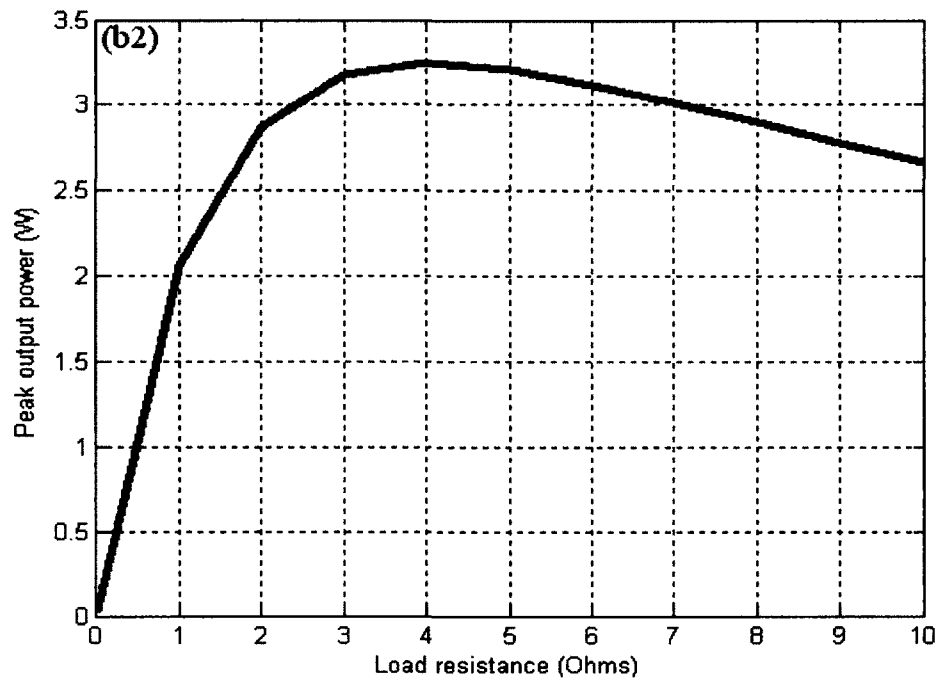
Figure 4.15. Continued.
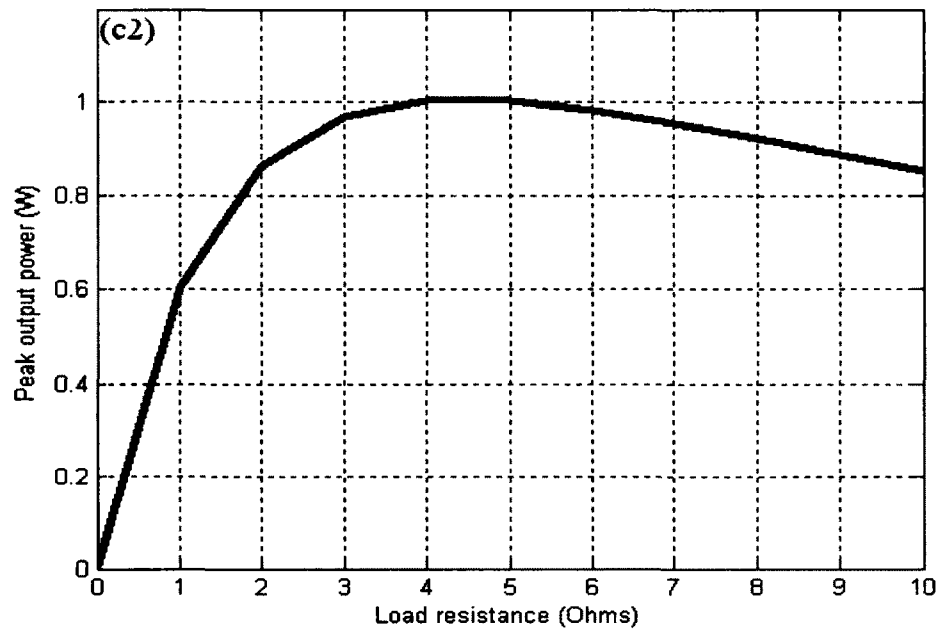
Figure 4.15. Continued.

In order to fully satisfy the law of maximum power transfer, the reactive losses must also cancel out. This condition is fulfilled when a capacitive element is connected to the output terminals such that

$$X_{LOAD} = X_{COIL} \ . \tag{4.19}$$

Thus,

$$\omega L_{COIL} = (\omega C_{OUT})^{-1} \tag{4.20}$$

or,

$$C_{OUT} = (\omega^2 \ 0.0127 \ H)^{-1} \ . \tag{4.21}$$

The computed capacitances necessary to cancel out the reactive losses due to the inductance of the stator coils for the TEST, WINTER, and SUMMER sea states are 40.4F, 127.6F, and 71.8F, respectively. If these capacitors were to be constructed using a dielectric having a very high permittivity (water), then according to the equation for calculating capacitance [79],

$$C_{OUT} = (\varepsilon_o \ \varepsilon_r \ A_{cap})/d \ , \tag{4.22}$$

where
C_{OUT} is the capacitance value,
ε_o is the permittivity of free space ($\varepsilon_o = 8.854 \cdot 10^{-12} \ C^2/N \cdot m^2$),
ε_r is the relative permittivity of water ($\varepsilon_r = 80.37$),
A_{cap} is the surface area of the plates, and
d is the separation between the plates,

the ratio of the plate areas to separation distances would be $5.68 \cdot 10^{10}$ m, $1.79 \cdot 10^{11}$ m, and $1.01 \cdot 10^{11}$ m for the TEST, WINTER, and SUMMER sea states respectively. Although these physical dimensions are quite large, the ratios would be even larger if a dielectric having a smaller relative permittivity were used. Thus, since the coils' inductance value is very low ($L_{coil} = 12.7$ mH) and dissipates little reactive voltage for the relatively small cyclic frequencies expected for ocean surface waves, and due to the fact that an immensely large capacitor would need to be constructed in order to cancel out the small reactive losses incurred by the inductive coils, no nullification of reactive voltage will be considered in this work.

4.3.4 Efficiency

The final property to be considered in this topic is generator efficiency. A linear generators' efficiency is defined by the ratio of output to input power and is relisted as Equation (4.23) below.

$$\eta_{LG} = \frac{P_{out}}{P_{in}} = \frac{P_{out}}{P_{out} + P_{losses}} \ , \tag{4.23}$$

where
η_{LG} is the efficiency of the linear generator,
P_{out} is the power output of the linear generator,
P_{in} is the power input to the linear generator, and
P_{losses} is the power losses due to hysteresis, eddy currents, and resistive losses.

As discussed previously, the hysteresis and eddy current losses are either not applicable or not significant for the specifically modeled linear generator in this work. In fact, the only loss which is considered significant is the copper losses that occur for the linear generator's stator coils. Since the stator circuit represents a series circuit, the current is the same through each resistive element. Thus, the efficiency equation can be simplified to:

$$\eta_{LG} = \frac{P_{out}}{P_{in}} = \frac{i^2 \cdot (R_{LOAD})}{i^2 \cdot (R_{LOAD} + r)} = \frac{R_{LOAD}}{(R_{LOAD} + r)} . \qquad (4.24)$$

A plot of efficiency as a function of load resistance (which is valid for all sea states and wave regimes) is given in Figure 4.16 below. An analysis of this plot reveals that the efficiency of the generator increases with an increase in load resistance. This activity occurs because, as the ratio between the load resistance and coils' resistance increases in magnitude, a greater portion of the generated voltage will be dropped across the load resistance (in accordance with the voltage divider rule). However, as the total resistance increases, the resulting current flow would diminish (as governed by Ohms' law), thereby reducing the magnitude of power transferred from the linear generator to the transmission lines. Therefore, although it would appear best to operate the linear generator under maximum efficiency, it would be advised to operate it under the conditions that result in maximum power transfer.
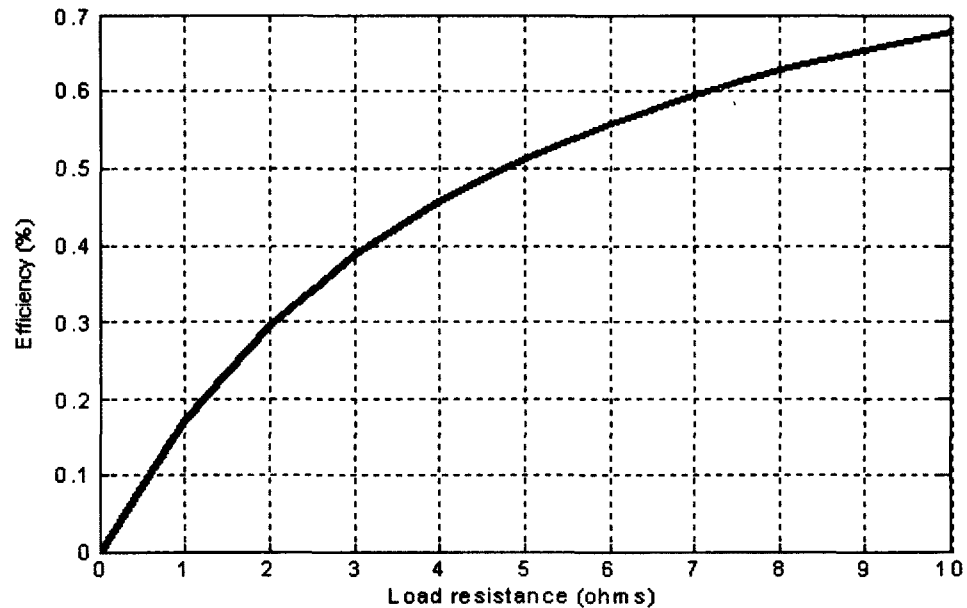
Figure 4.16. Efficiency of the linear generator as a function of load resistance.

4.4   Generated power in heave

4.4.1   Verification and validation of the model

The linear generator model in this work was patterned after the published findings presented by the Oregon State University [21]. In order to validate this model, prediction of the generated voltage will be compared against the published results reported from the University under an identical sea state (H_s = 1.5m and T_s = 3s for the regular wave regime). A valid model only exists when the results of our model compares well to the reported results in both the qualitative behavior and in the magnitude. This would signify accurate validation between the models. In an attempt to accurately reproduce the results as obtained from the Oregon State University, the wave exciting force has been changed from the cosine to the less common sine function for verification purposes.

Since there was no mention of the parameters used for the buoy in the findings published by the Oregon State University group, it is assumed that the rotor's motion for the linear generator travelled in perfect synchronicity with the ocean surface waves (i.e., $|H(\omega)| = 1$, and $\sigma = \phi_{heave} = 0$, where $|H(\omega)|$ is the heave transfer function, σ is the phase angle between the force and the wave, and ϕ is the phase angle between the force and heave motion). Upon incorporating these conditions, the results in Figure 4.17 were obtained. As can be seen in this figure, the results obtained from this simulation (Figure 4.17a) compared favorably with those published from the Oregon State University (Figure 4.17b). Both the behavior and magnitude match, thus confirming the verification and validation for this model under the perfectly synchronous condition; thereby identifying it as a valid model under this condition.
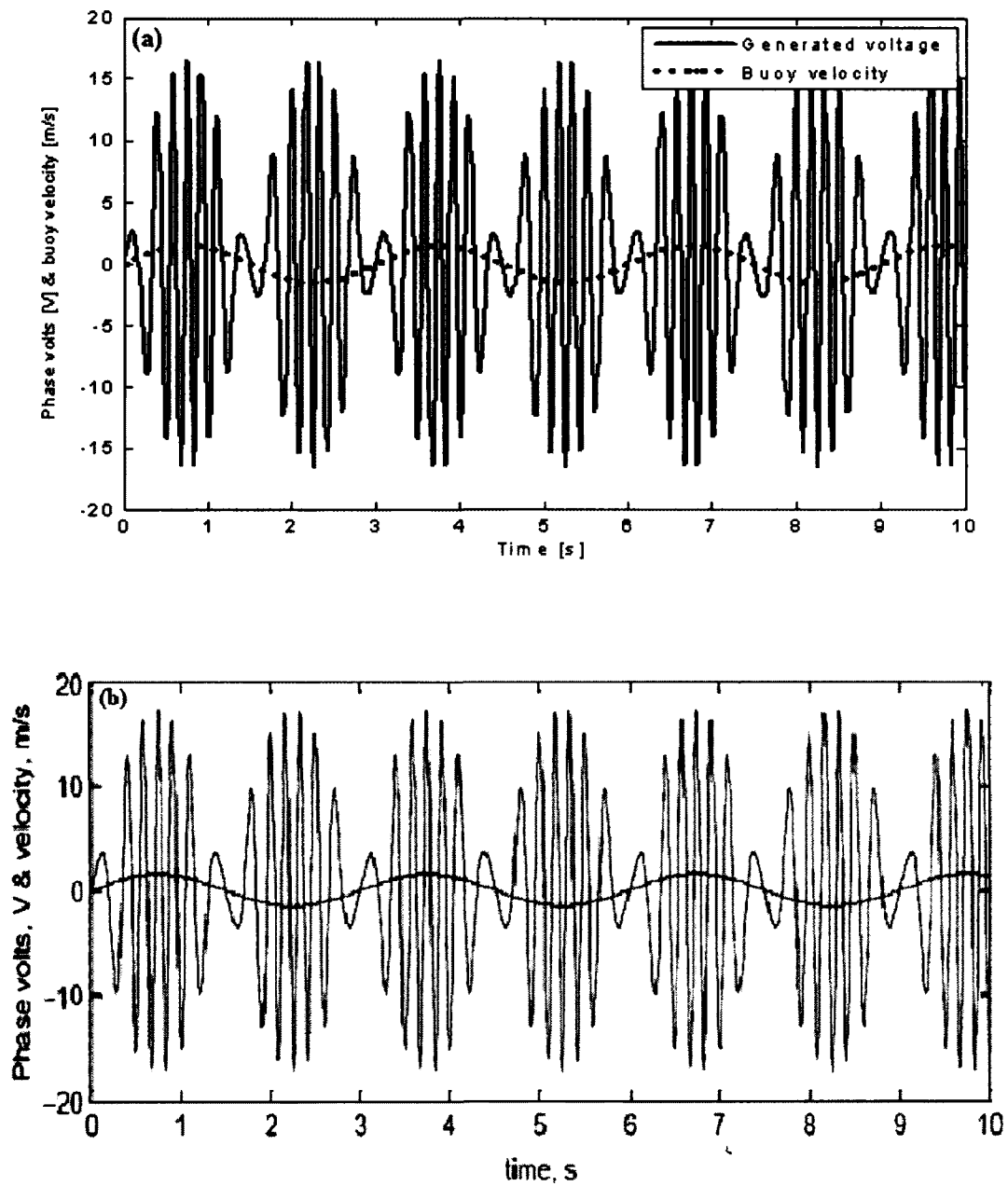
Figure 4.17. Generated voltage and buoy velocity. (a) For the model presented in this work, and (b) Compared to those published by the Oregon State University [21].

The previously described buoy (known as the 'standard or regular buoy') operated favorably for the three selected sea states analyzed in this work, assuming that the buoy followed the motion of the waves. However, proper inclusion of the actual buoy

dynamics shows that this buoy design would not necessarily be the preferred choice for operation in the same sea state as defined by the Oregon State University (H_s = 1.5m, T_s = 3s). Figures 4.18 and 4.19 respectively, illustrate the inefficiency of this buoy in regards to its influence by wave activity and its resulting effect on the generated voltage. This response occurs when the proper motion including the RAO for heave is taken into account.
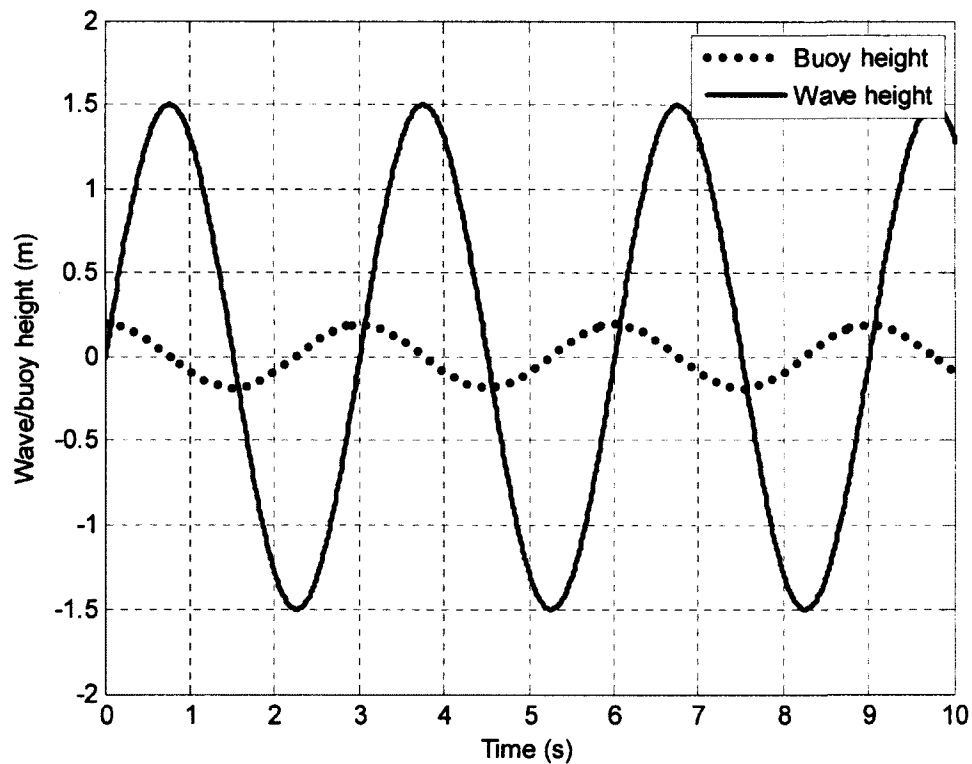
Figure 4.18. Time series for the ocean surface waves and the heave response for the standard buoy operating in the regular wave regime using the sea state parameters defined by the Oregon State University (H_s = 1.5m, T_s = 3s).
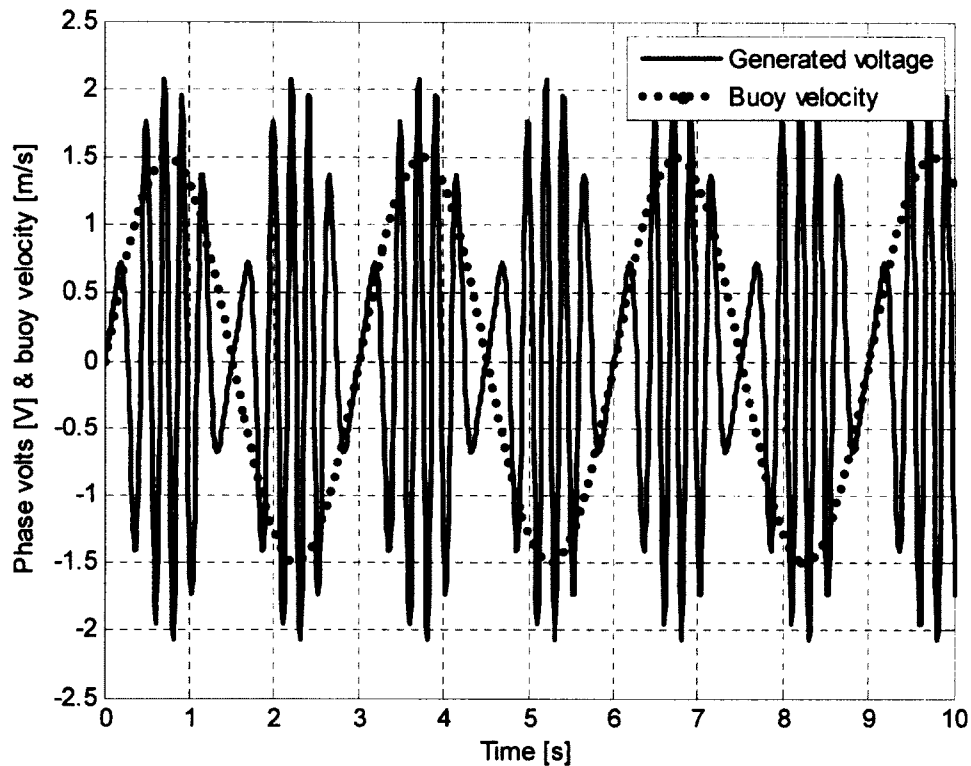
Figure 4.19. Time series for the velocity of the buoy and the resulting generated voltage from a linear generator using the 'standard buoy'.

However, by using an 'ideal buoy' which is 3.5m in diameter, 2.5m in length, and 1.25m in draft, a better response can be attained. Figure 4.20 shows the 'ideal buoy' operating in this particular sea state under less than perfect synchronous conditions (i.e., $|H(\omega)| > 1$, $\sigma \neq 0$, and $\phi_{heave} \neq 0$). Since, the 'ideal buoy' motion follows to near synchronicity with the wave motion, it is logical to assume that the generated voltage would appear similar as well.
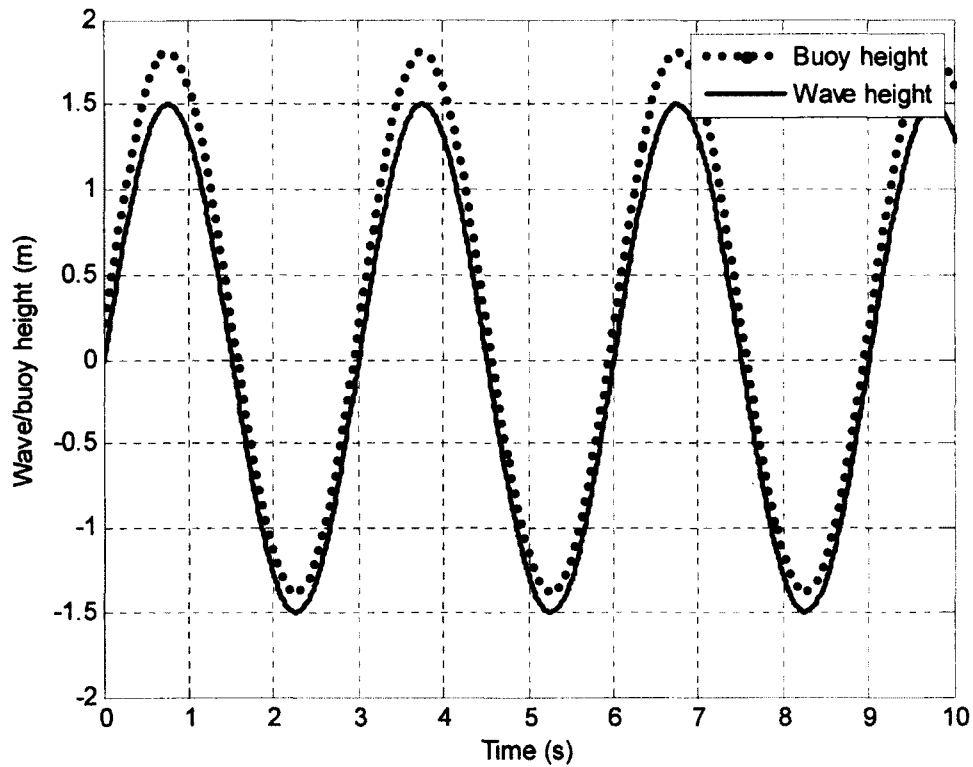
Figure 4.20. Time series for the wave and 'ideal buoy' operating under the identical sea state as provided by the Oregon State University.

Figure 4.21a illustrates the generated voltage for the buoy movement depicted in Figure 4.20 and Figure 4.21b is a re-print of Figure 4.17a for comparison purposes. A comparison of these two plots reveals that they are both similar in appearance and magnitude, but the non-perfect synchronous plot (Figure 4.21a) responds slower to the wave's activity and experiences fewer internal oscillations per period.
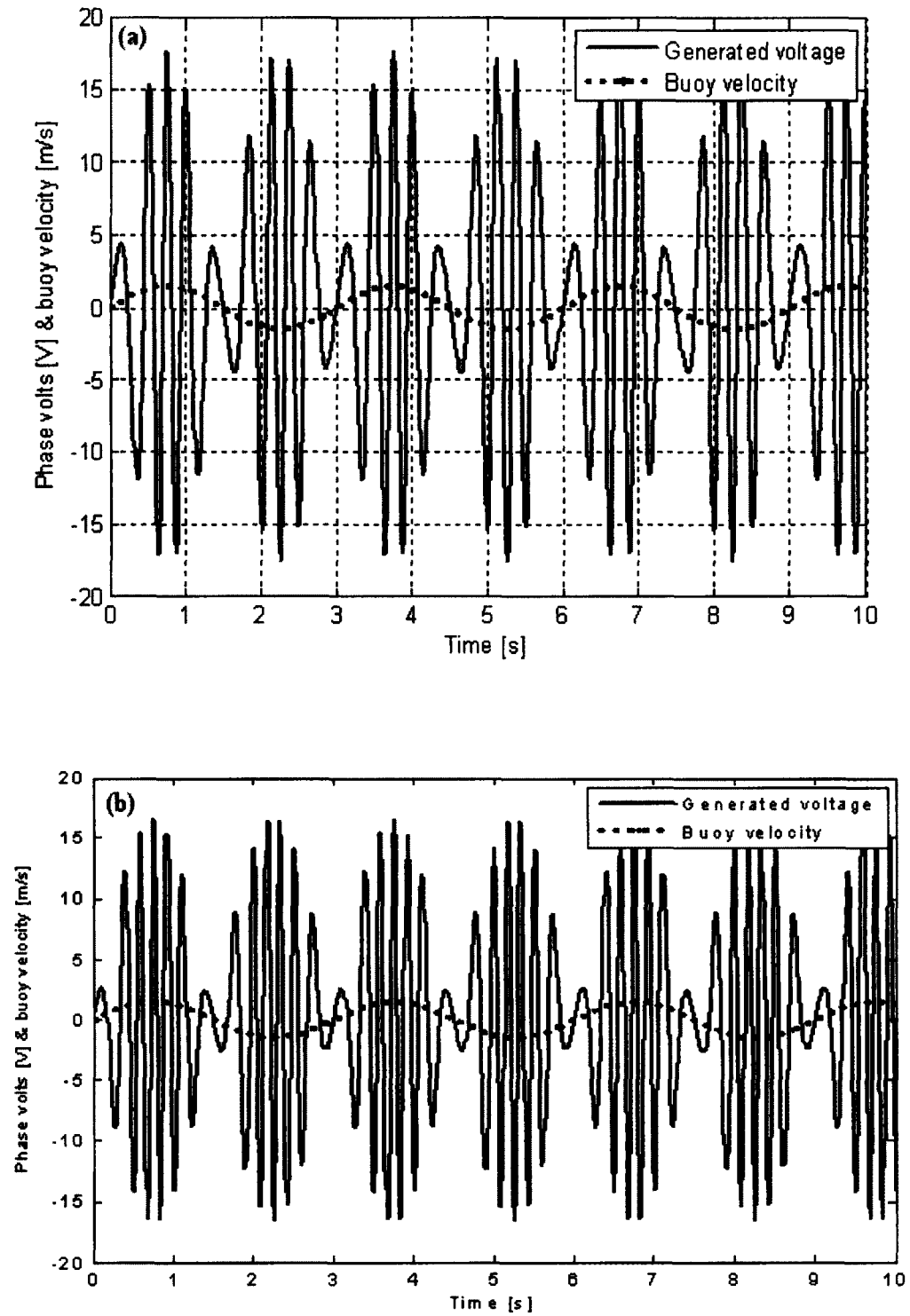
Figure 4.21. Generated voltage and buoy velocity. (a) The non-perfect schronous condition with the waves, and (b) under perfect synchronous conditions.

Finally, since the generated voltage under the 'less-than-perfect synchronous' condition is similar in appearance to the generated voltage under the 'perfect synchronous' condition between the wave and buoy/rotor motion, it is logical to establish both models as valid.

4.4.2 Results for the selected sea states

4.4.2.1 Results for the regular wave regime

Figure 4.22 shows the generated voltage and current, and output voltage and power from a seabed mounted linear generator for a heaving buoy under the regular wave regime for each sea state. Although the waveforms for the WINTER and SUMMER sea states appear compressed for the displayed time, the same oscillatory nature as seen in the TEST sea state persists throughout each of the analyzed sea states. These voltage plots clearly illustrate that the generated voltage is symmetric about both the horizontal and vertical axes, and maintains the same amplitude and shape for each period. This behavior is expected since the surface waves in the regular wave regime maintain a peak amplitude and period. Further inspection of these plots reveals that the period of the generated voltage is equal to half of that of the wave. This condition occurs when the Euler functions for the sine and cosine terms are multiplied together, which produces a product which is equal to half the amplitude and twice the frequency.

In each sea state, the output current correctly approximates 10% of the magnitude of the generated voltage. This condition satisfies Ohms' Law (I = V/R) since the series resistance of the coil and load resistance total 9.75 ohms.

The output voltage for each sea state also correctly approximates 50% of the generated voltage. This condition falls into accordance with the voltage divider rule since the coils and load resistance are nearly identical.

Finally, the output power plots depict the oscillatory nature of the output current and are constantly positive in value, in accordance with the behavior of power dissipation.
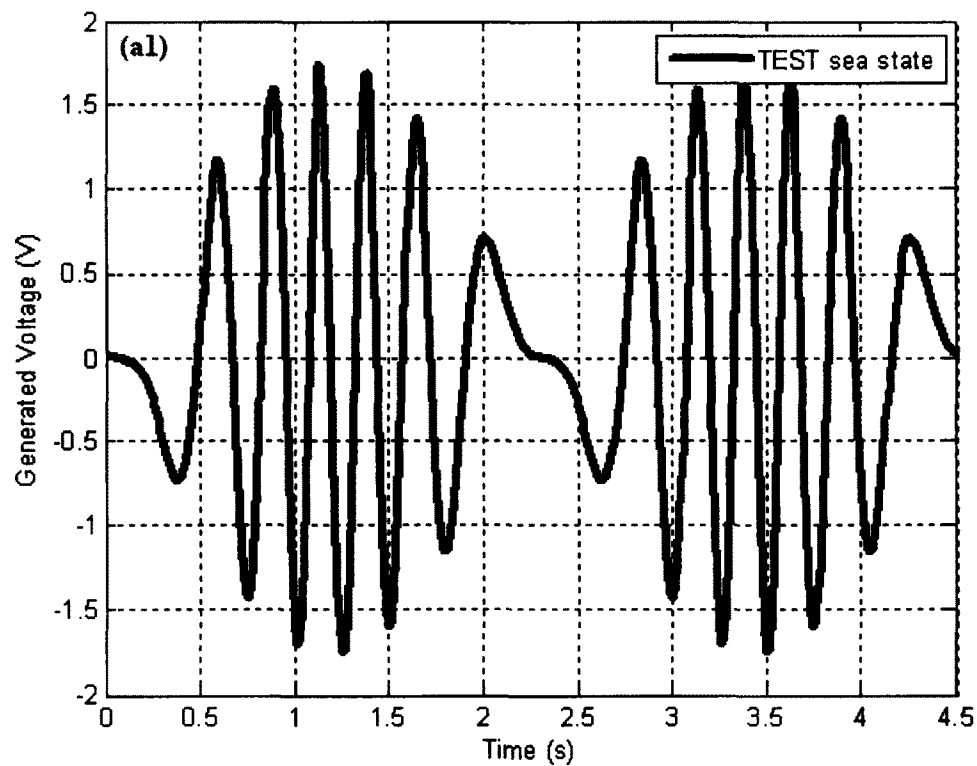
Figure 4.22. Generated properties under the regular wave regime for select sea states. (a) The TEST, (b) WINTER, and (c) SUMMER sea states and their associated values for the generated voltage (1), and current (2), and output voltage (3), and power (4).
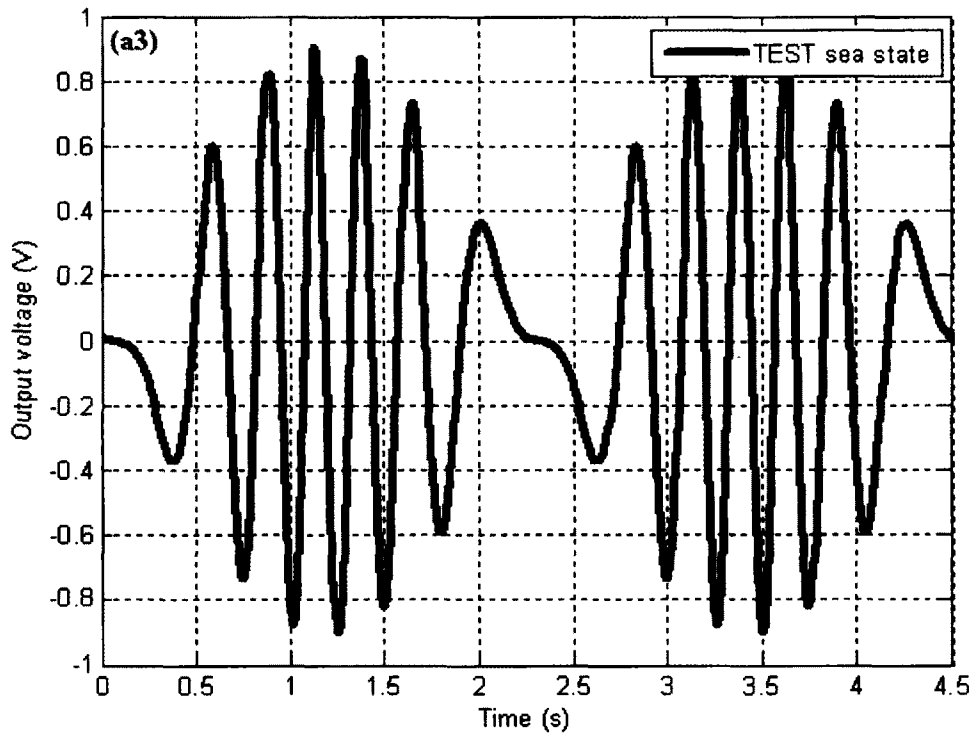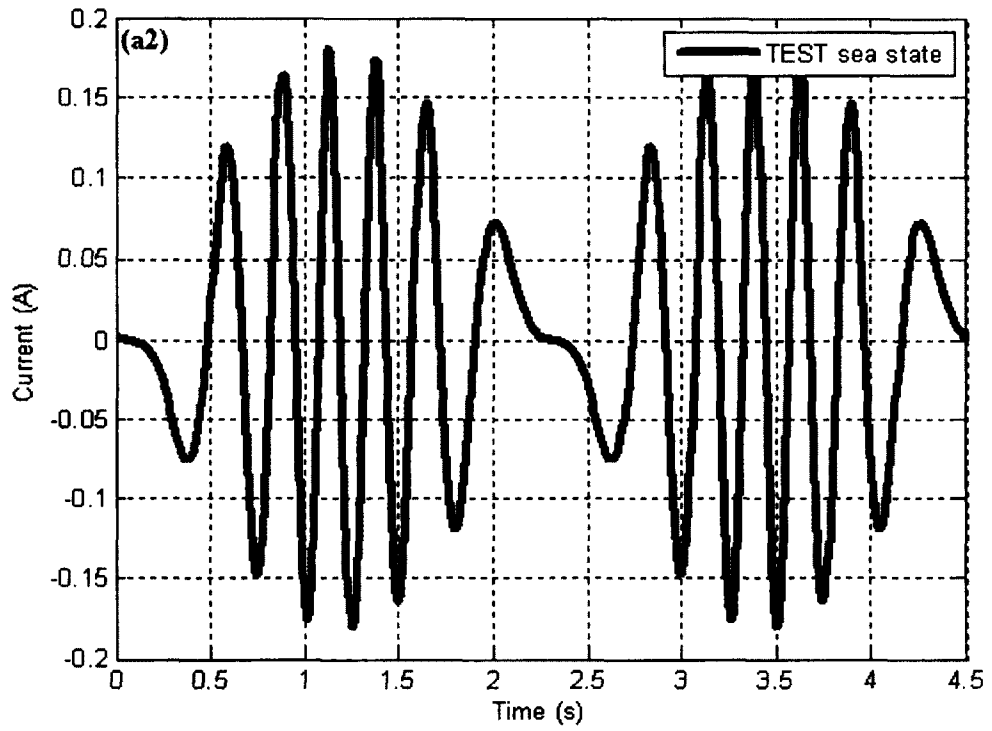
Figure 4.22. Continued.
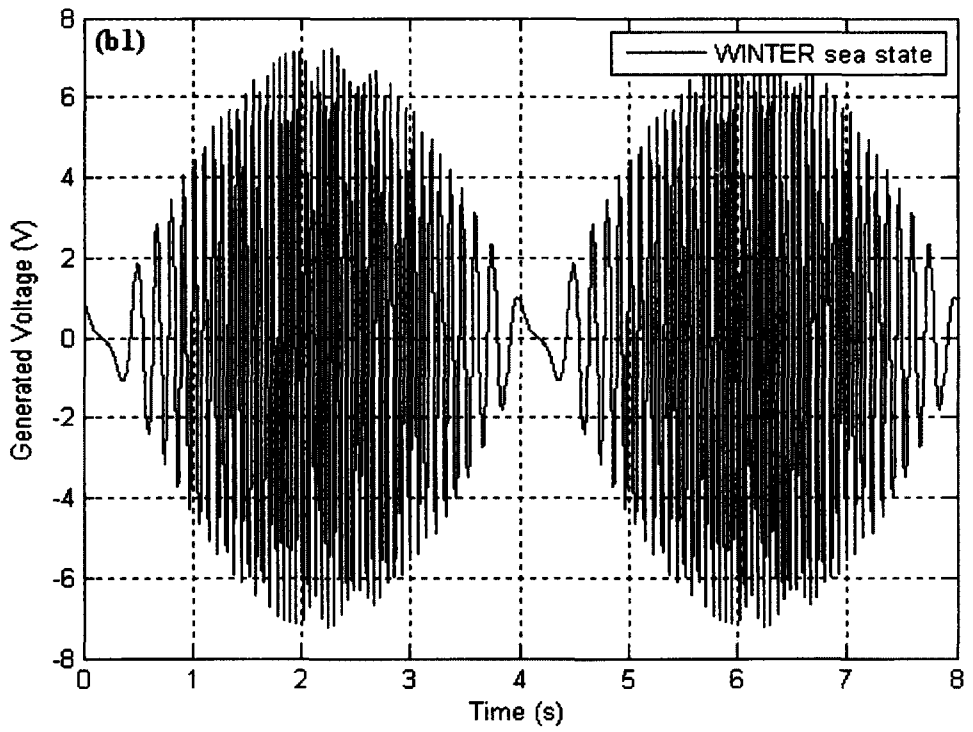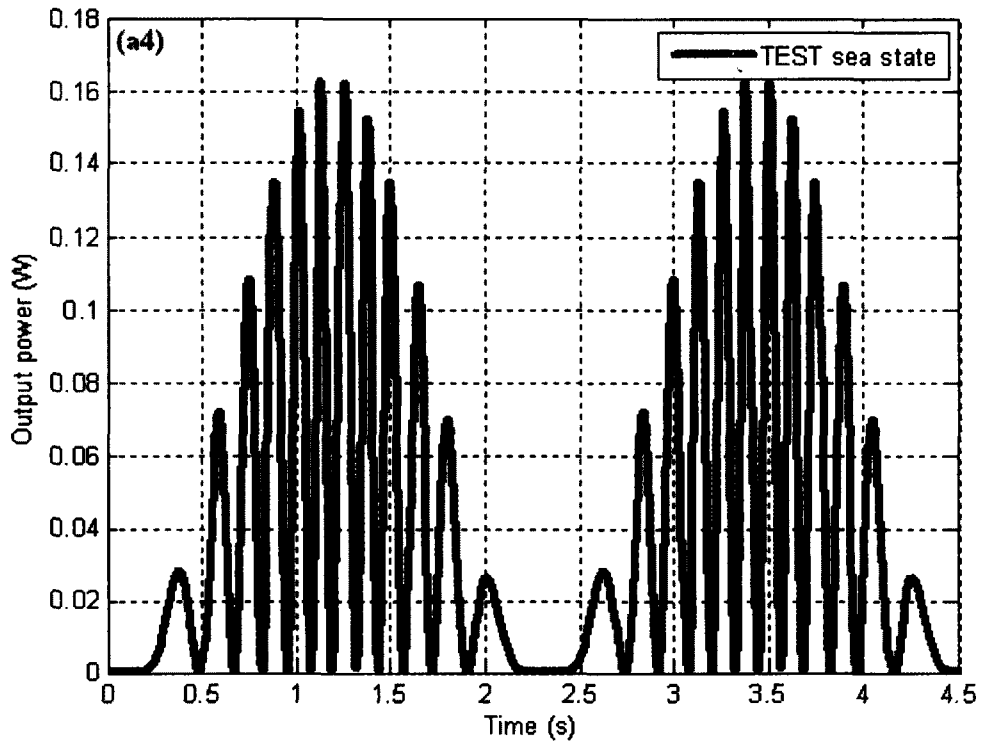
Figure 4.22. Continued.
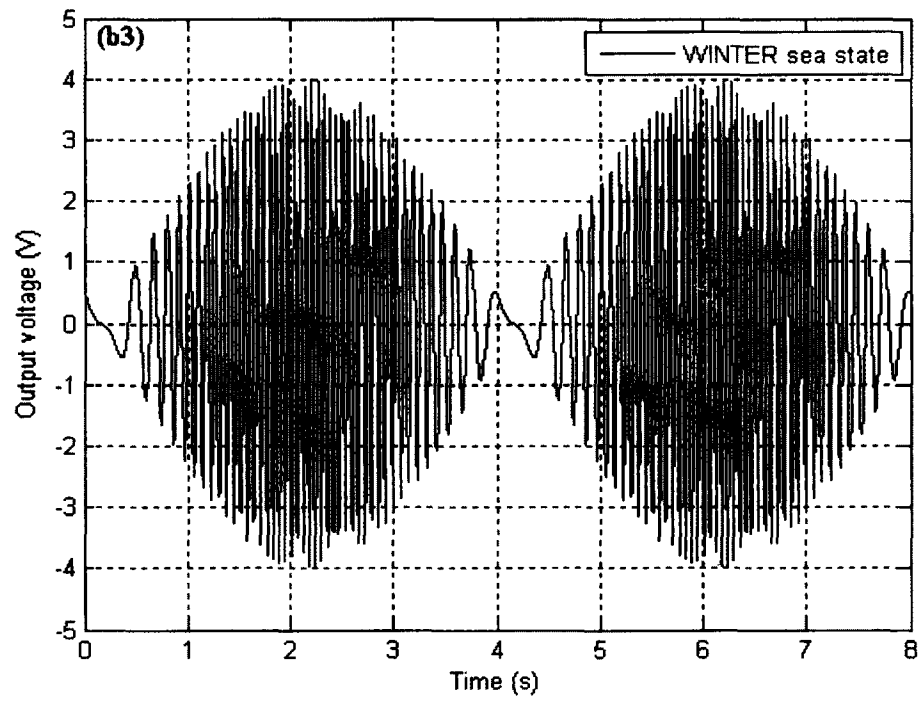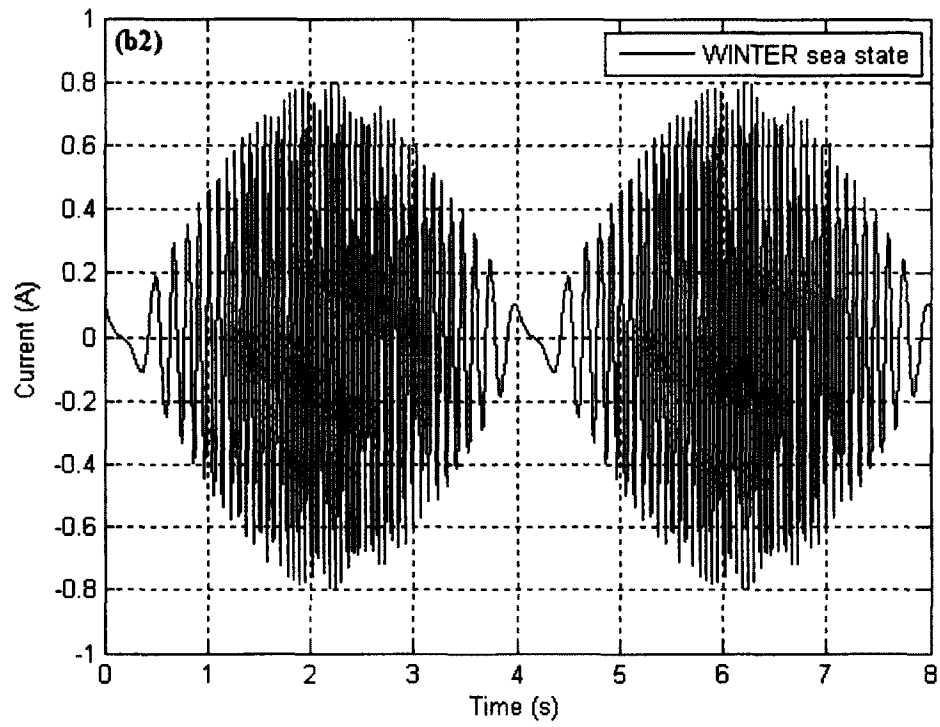
Figure 4.22. Continued.
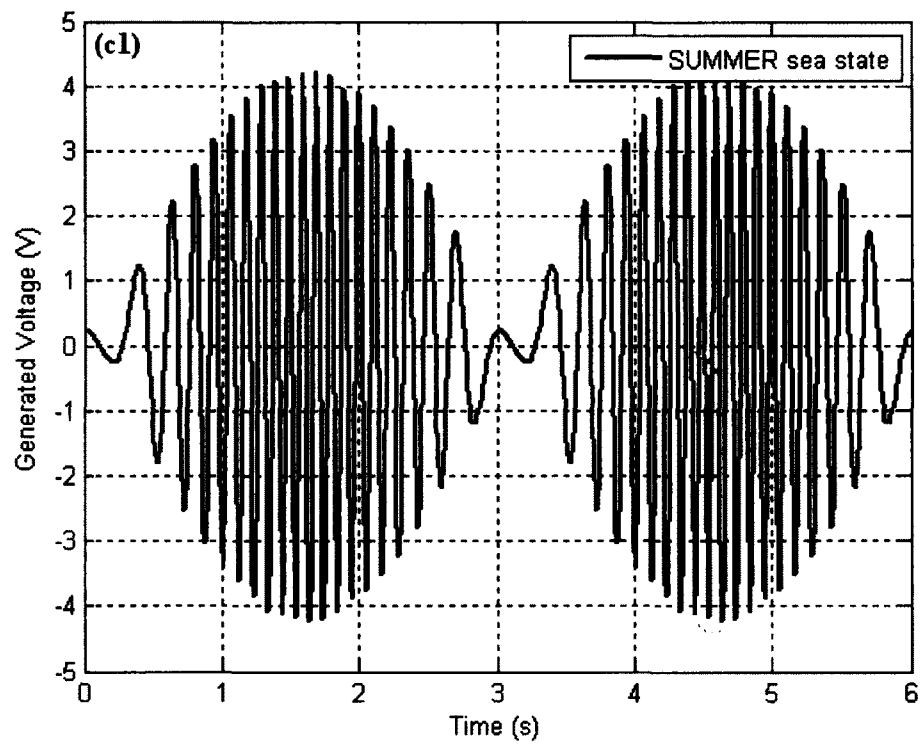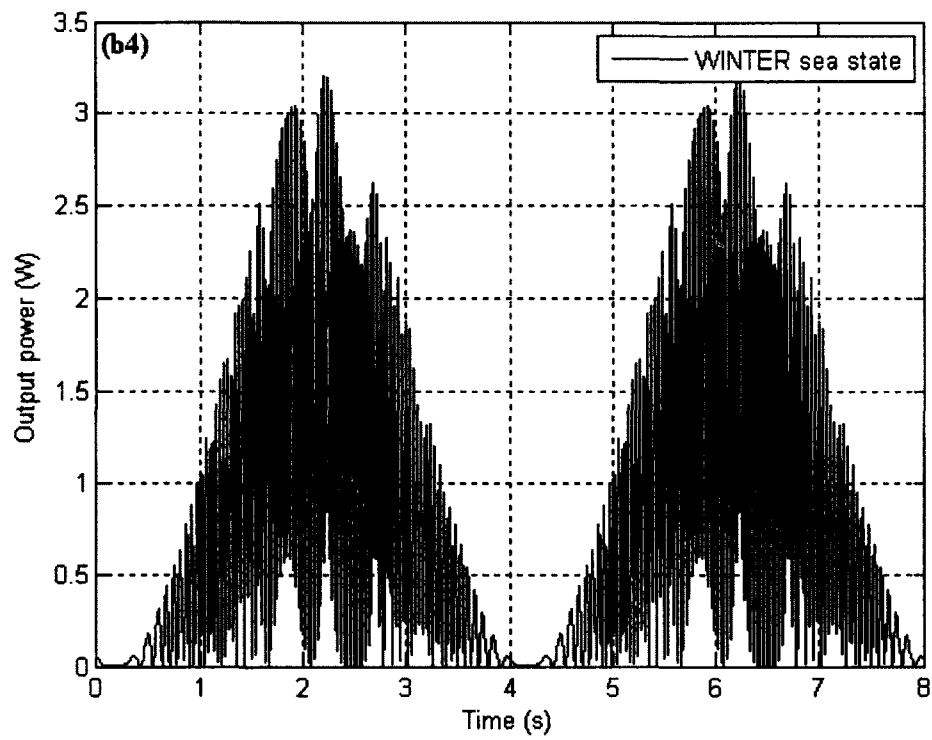
Figure 4.22. Continued.
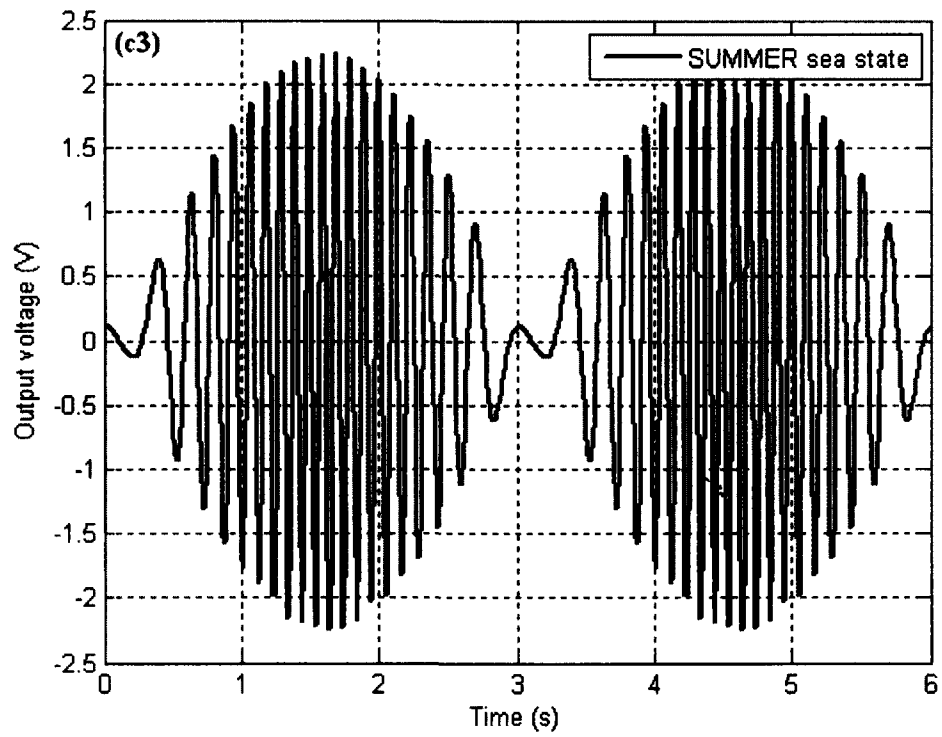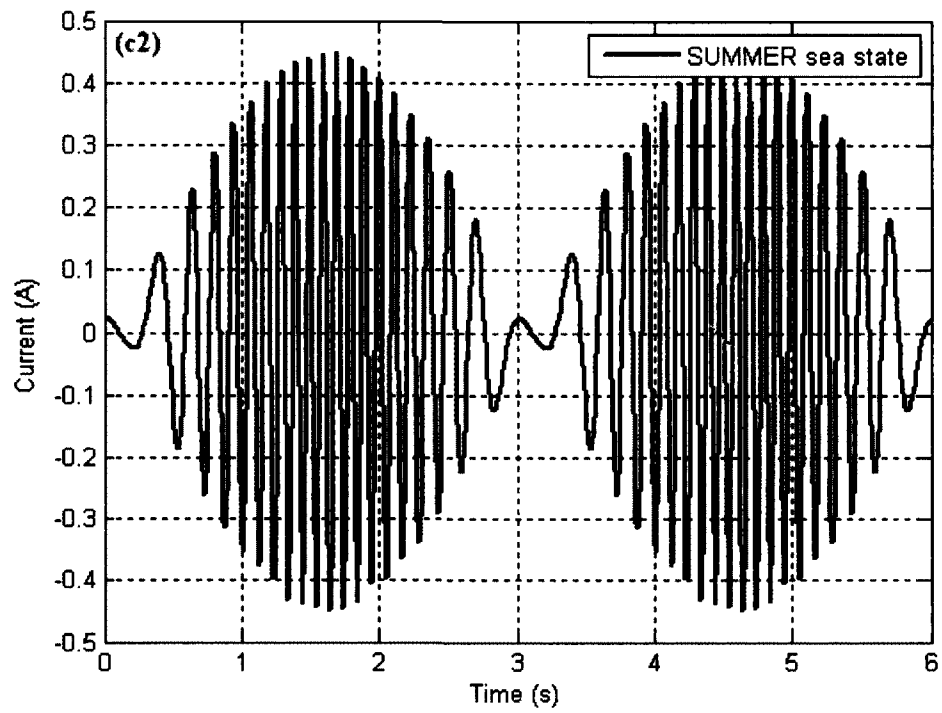
Figure 4.22. Continued.
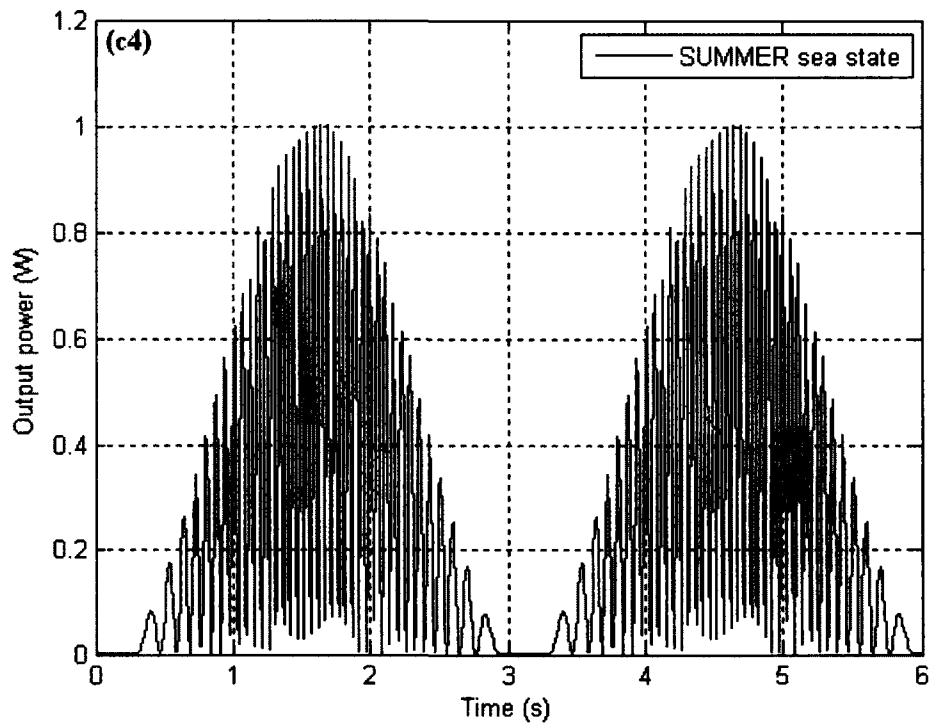
Figure 4.22. Continued.

4.4.2.2 Results for the irregular wave regime

Figure 4.23 shows the same parameters plotted under the irregular wave regime for the selected sea states. In this case, although the generated voltage is symmetrical about the vertical axis, the peak amplitude of the voltage as well as the duration for each period varies between cycles. This behavior makes logical sense because the waves vary in both amplitude and frequency in the irregular wave regime.

Since the output current, voltage, and power are all dependent upon the generated voltage, they will vary proportionally in magnitude and period as well. However, since neither Ohms' Law nor the voltage divider rules are ever violated, the ratios between the circuit parameters will always persist regardless of the wave regime tested by the simulation.
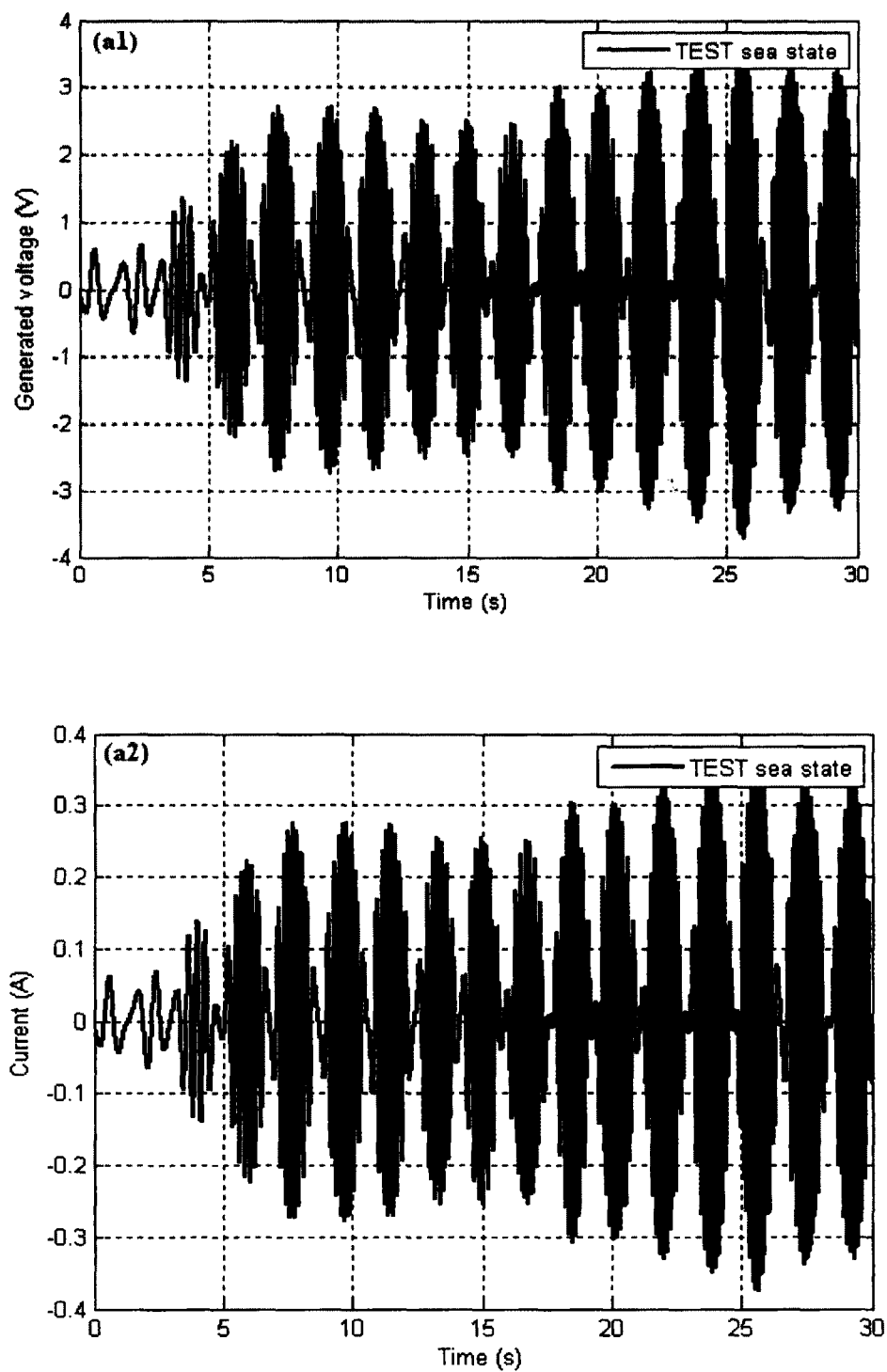
Figure 4.23. Generated properties under the irregular wave regime for select sea states. (a) The TEST, (b) WINTER, and (c) SUMMER sea states and their associated values for the generated voltage (1), and current (2), and output voltage (3), and power (4).
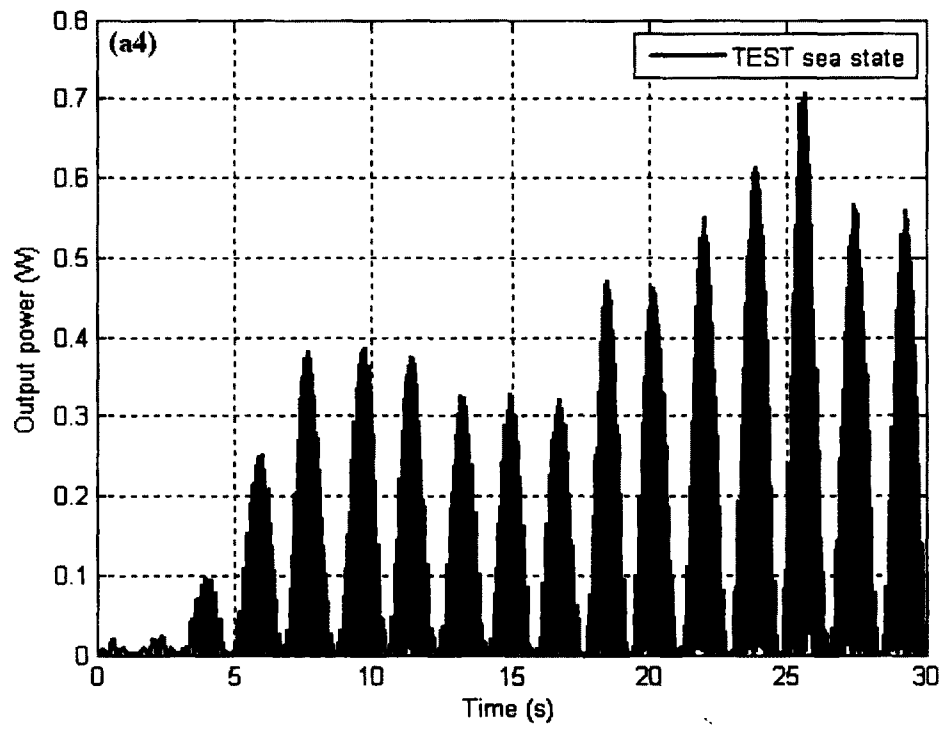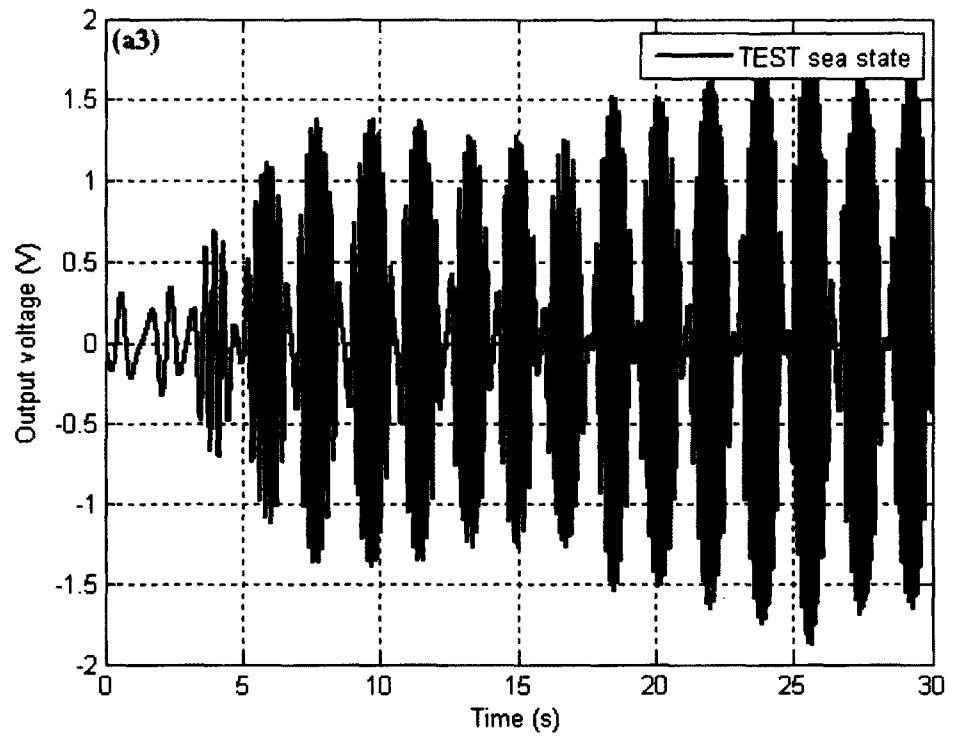
Figure 4.23. Continued.
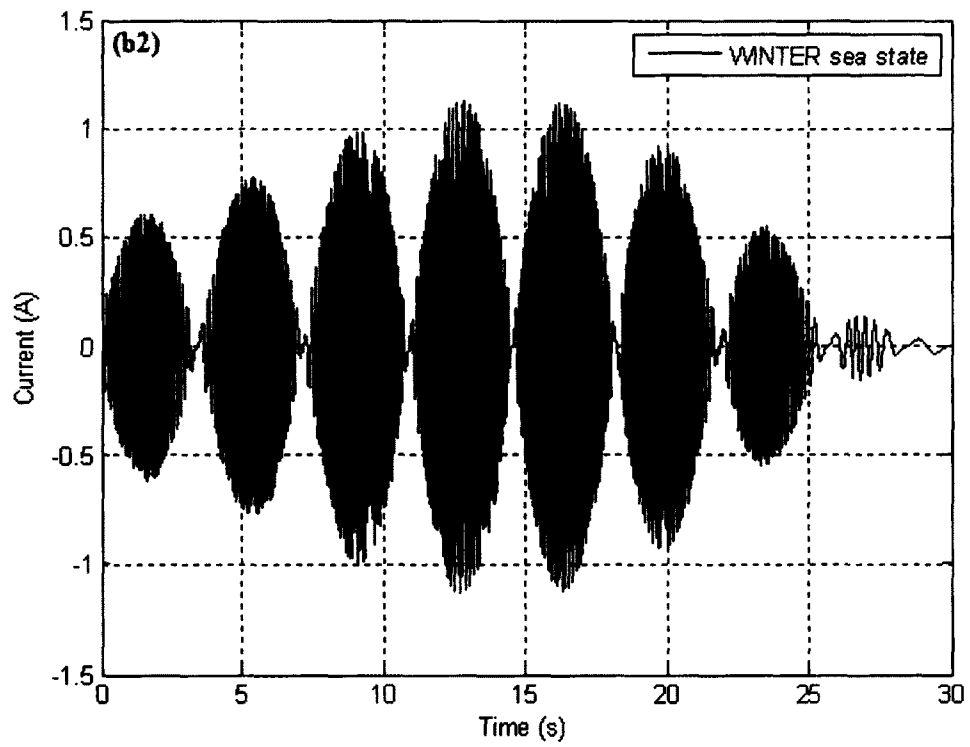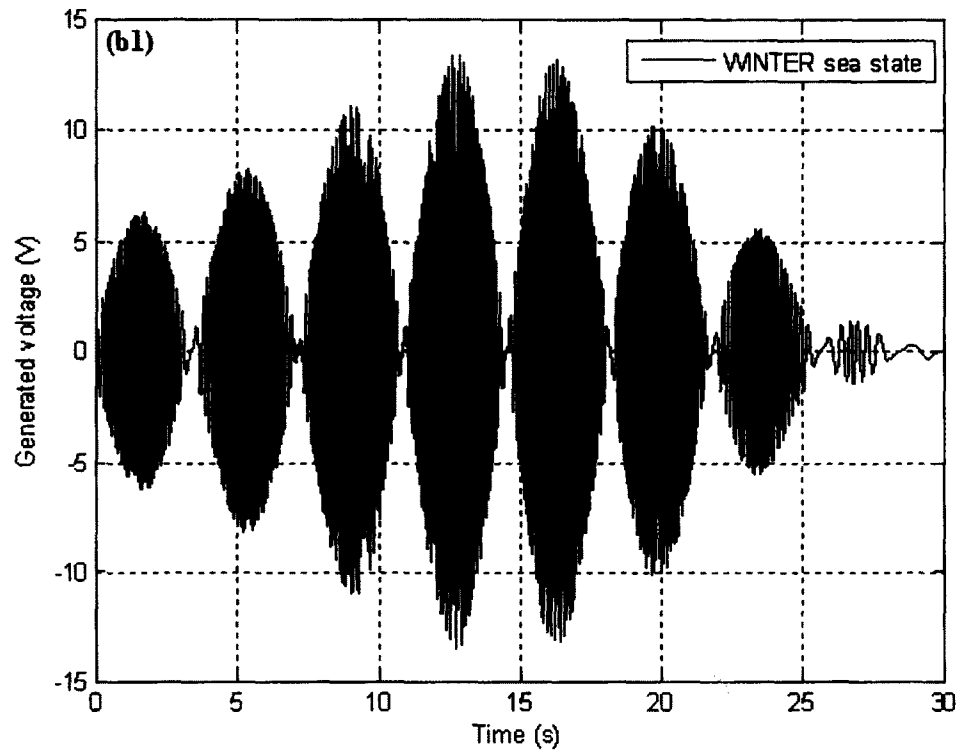
Figure 4.23. Continued.
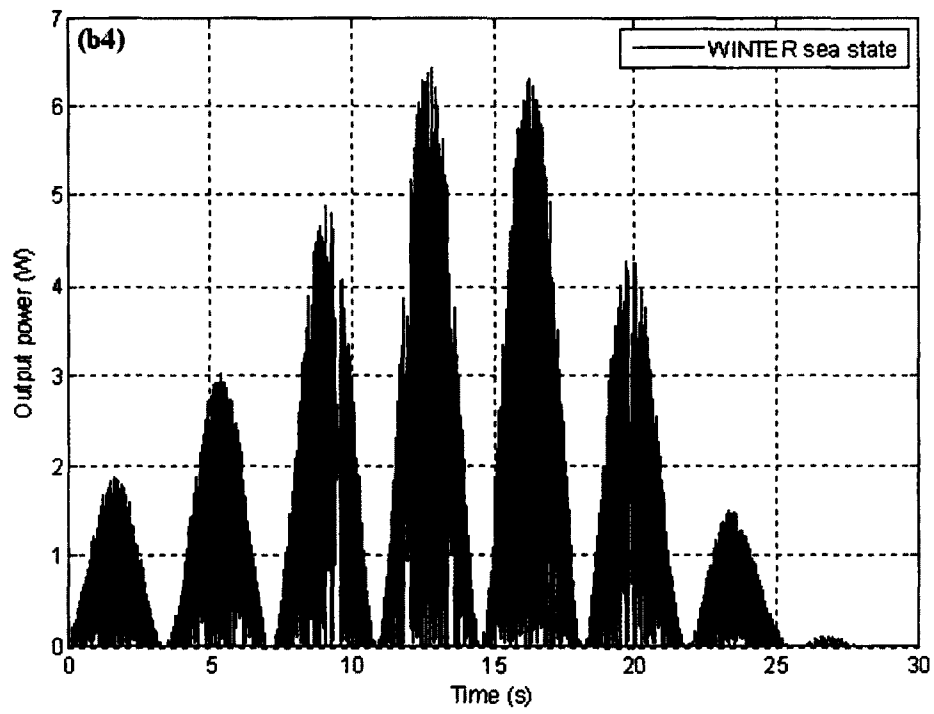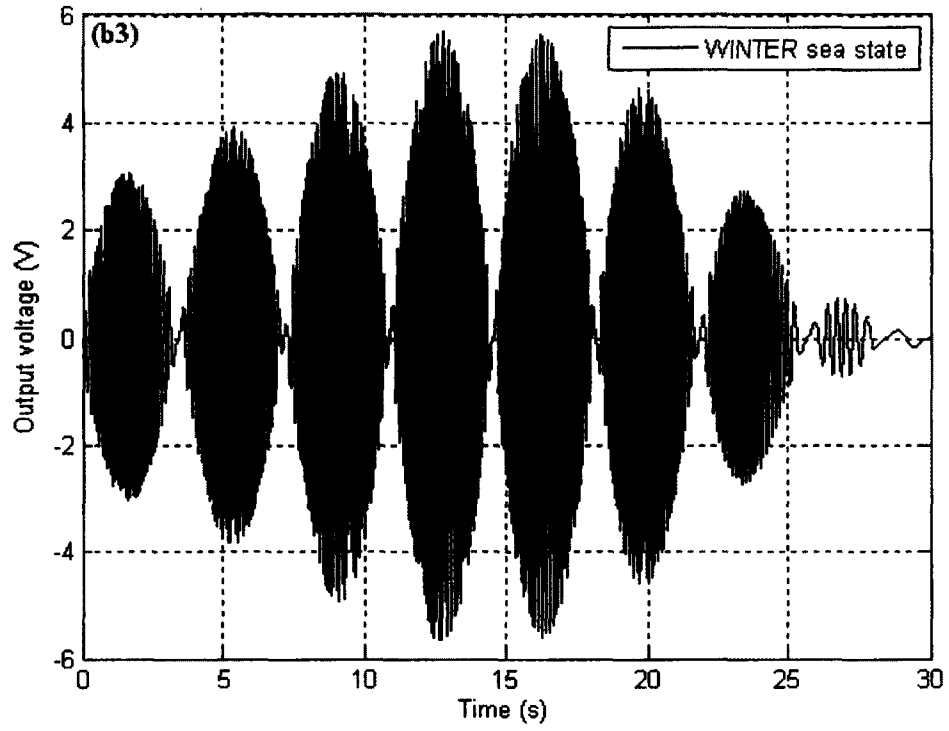
Figure 4.23. Continued.
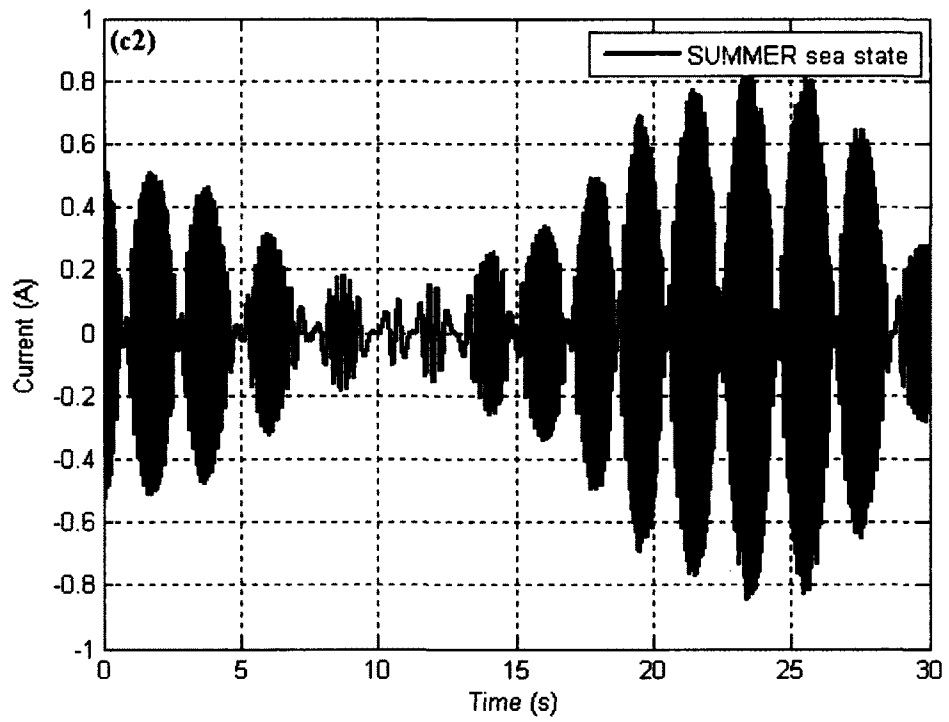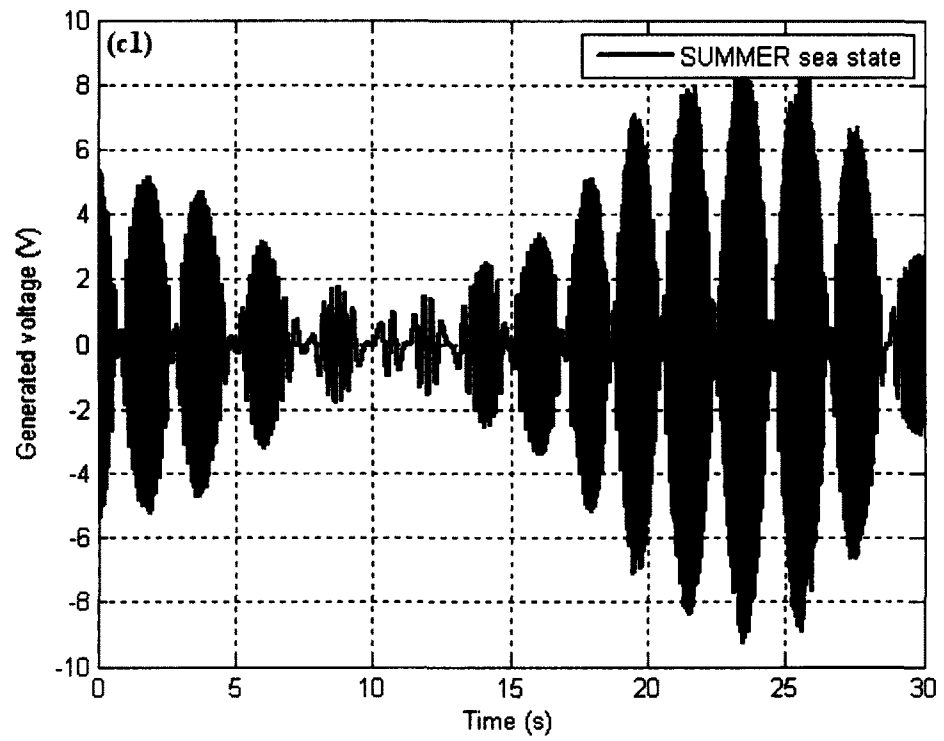
Figure 4.23. Continued.
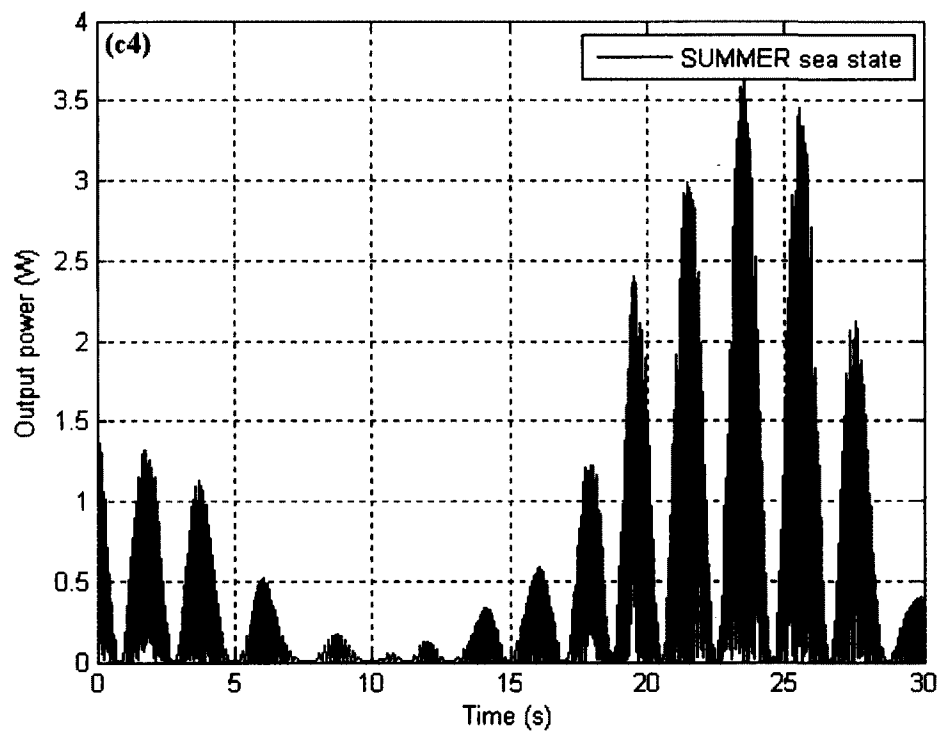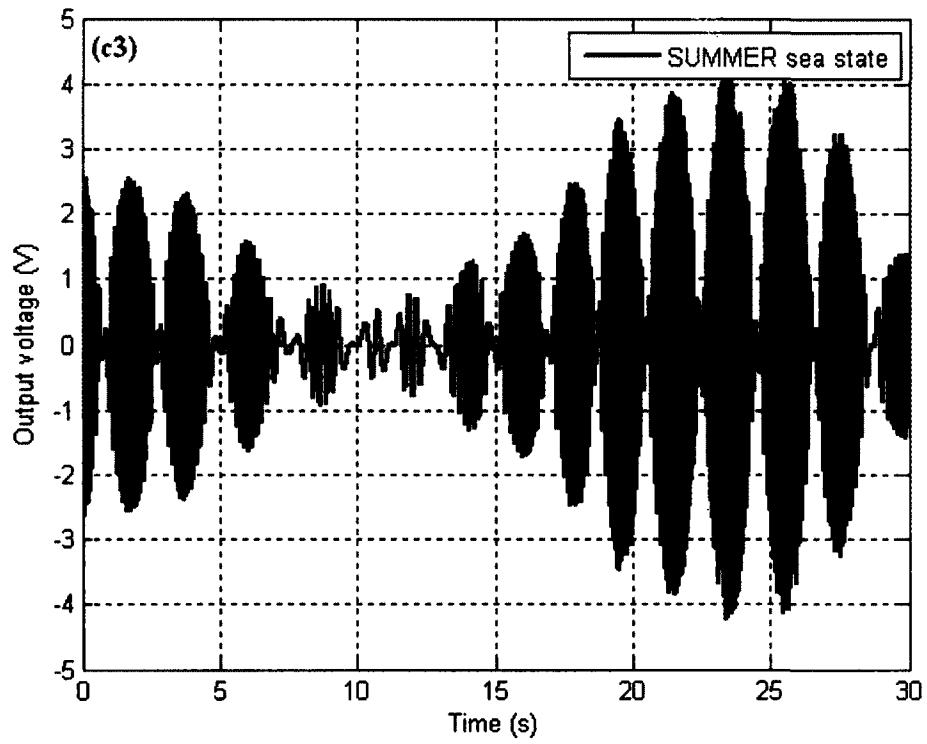
Figure 4.23. Continued.

4.5 The effect of buoy dimensions on its heave response

4.5.1 The heave response for small buoys

The physical dimensions of a vertically floating cylindrical buoy play a significant role on the magnitude of voltage generated from the seabed mounted linear generator. Figure 4.24 shows the Response Amplitude Operator for the SUMMER sea state using various small buoys having a specific diameter (D) and length (L). As can be seen from this figure, the ratio of heave height to wave height starts at one and then attenuates at a rate proportional to the buoy's volume. This behavior occurs specifically for buoys of small size, since the restoring force plays the dominant role in restricting its heave movement. Although, the buoys dimensions play the significant role in the heave to wave height ratio, reducing the spring force can help to improve the heave response at each cyclic wave frequency. Figure 4.25 shows the resulting Response Amplitude Operator for heave using the same buoy dimensions, but under a much reduced restoring spring coefficient (10 Kg/s^2 instead of 40 Kg/s^2).
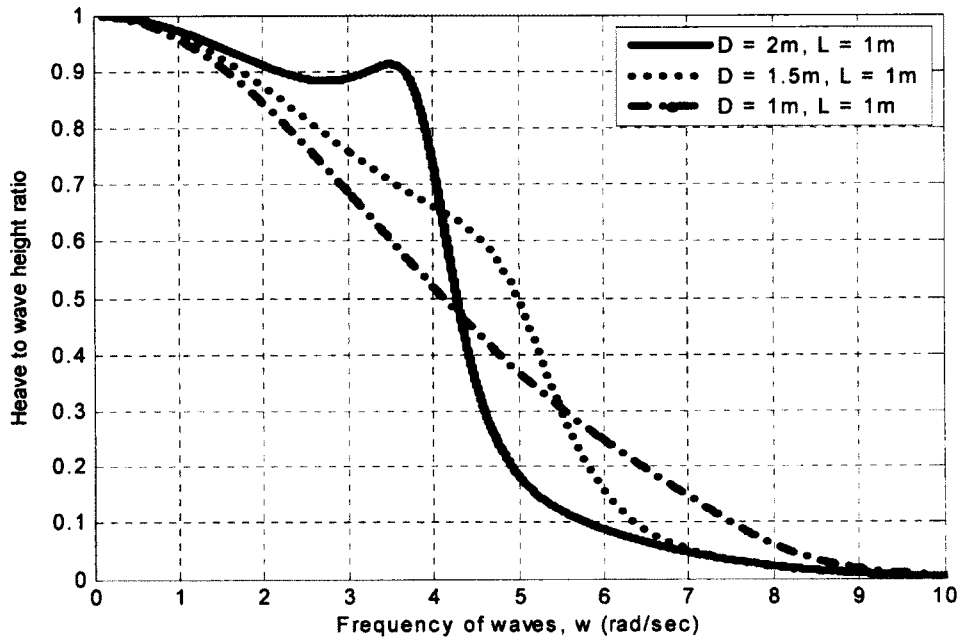
Figure 4.24. The heave response for buoys of exceptionally small size.
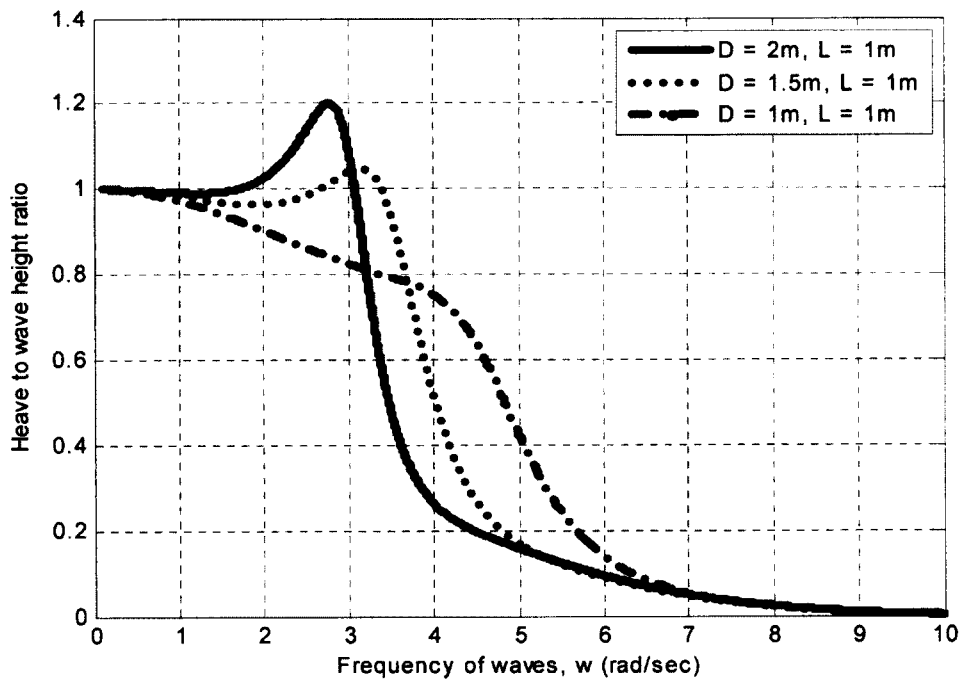
Figure 4.25. The heave response for buoys of exceptionally small size under the influence of a reduced restoring spring force.

4.5.2 The heave response for larger buoys

For larger buoys, however, an improved heave response occurs. Table 4.4 lists the dimensions for four different buoys operating in the SUMMER sea state for the regular wave regime and Figure 4.26 shows their respective Response Amplitude Operators for heave within a specific band of cyclic wave frequencies.

The Response Amplitude Operator, as given in Figure 4.26, clearly shows that as the volume of the buoy increases, the frequency regions are shifted to the left (due to the decrease in the natural frequency for heave of the buoy) and that the heave response for higher cyclic wave frequencies are diminished (see Section 4.2.6.1 for explanation).

Table 4.4. Vertically floating cylindrical buoys of various dimensions for testing under the SUMMER sea state.

Buoy	Diameter [m]	Length [m]	Volume [m^3]	$|H(\omega)|$
1	6	2	57	1.03
2	8	5	251	1.26
3	8	7	352	1.53
4	8	8.33	419	1.86
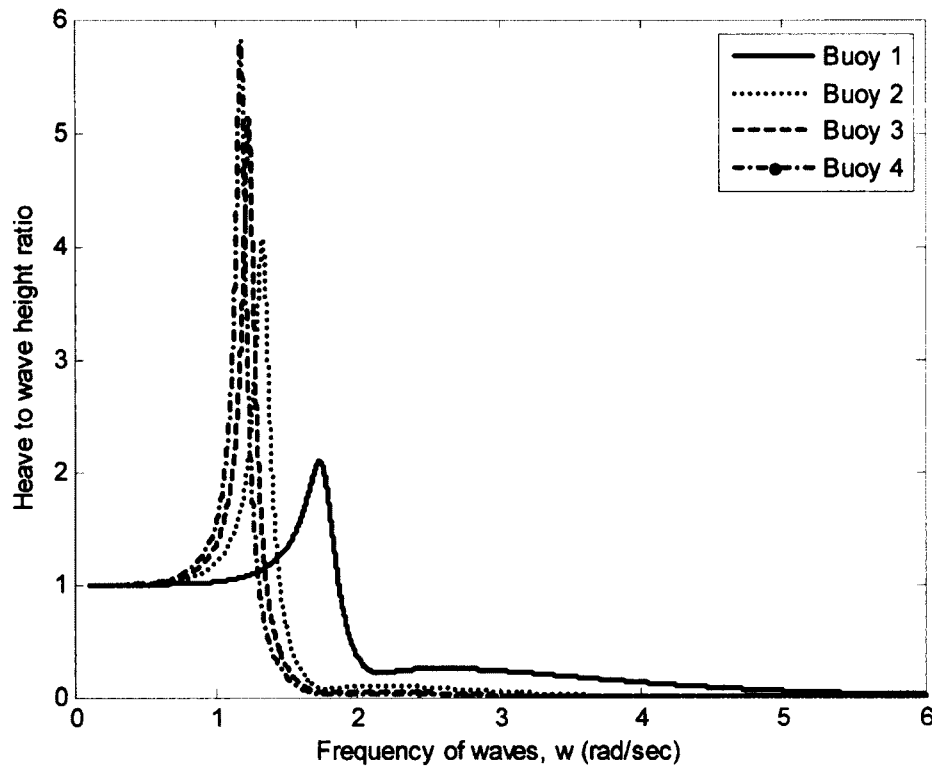
Figure 4.26. Response Amplitude Operator for heave of the cylindrical buoys listed in Table 4.4 operating in the SUMMER sea state.

Figure 4.27 shows the time series for the wave and the height displacements (heave) for each of the buoys listed in Table 4.4. In this figure, the magnitude for heave of each buoy can be derived graphically from the Response Amplitude Operator for heave (Figure 4.26) at a cyclic wave frequency of 1.047 radians/second (The cyclic wave frequency for the significant wave in the SUMMER sea state). These buoys have been specifically chosen to provide heave transfer ratios of 1.03, 1.26, 1.53, and 1.86 under the SUMMER sea state of the regular wave regime for analysis. These ratios are properly matched by the time series for the heave response in Figure 4.27.
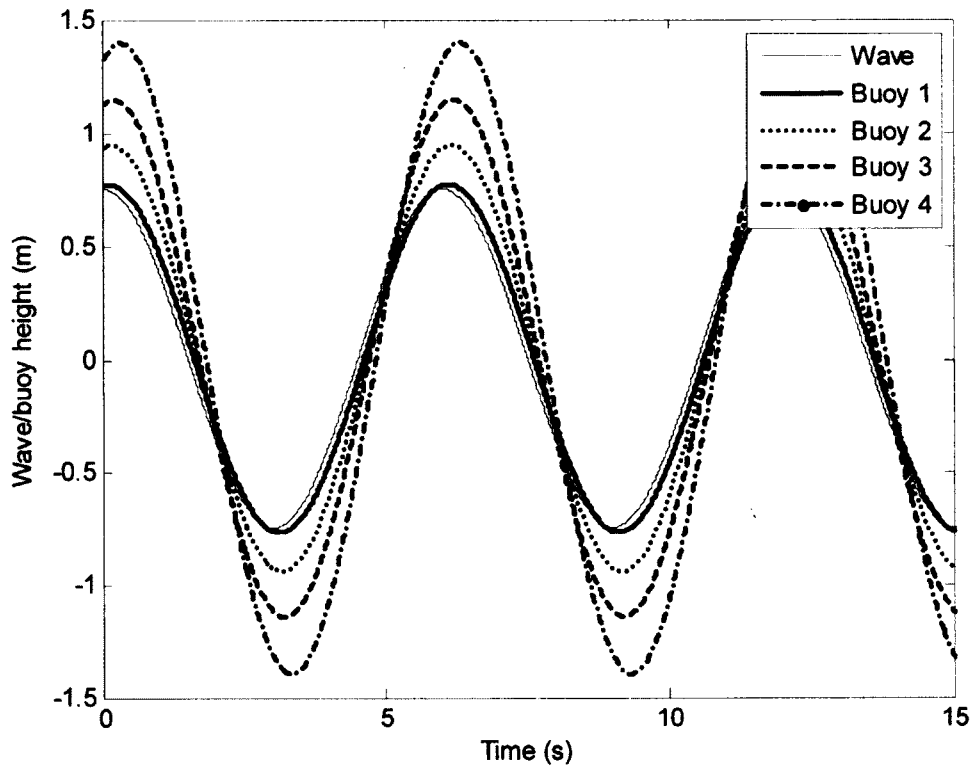
Figure 4.27. Time series for the surface ocean waves and the resulting heave response for the buoys listed in table 4.4 influenced by the regular wave regime for the SUMMER sea state.

The same basic principles apply between the WINTER and SUMMER sea states under the regular wave regime, so the specifics for the alternate sea state will not be discussed again. However, since the ocean parameters are different for the WINTER sea state, the buoy dimensions must be altered to achieve the same heave transfer ratios. Table 4.5 lists the buoy dimensions which are to be simulated under the WINTER sea state.

Table 4.5. Vertically floating cylindrical buoys of various dimensions for testing under the WINTER sea state.

Buoy	Diameter [m]	Length [m]	Volume [m³]	$|H(\omega)|$
1	6	2	57	1.03
2	12	9	1,018	1.26
3	12	12.5	1,414	1.53
4	12	15	1,696	1.86

4.5.3 The generated power for buoys of various sizes

Since the Response Amplitude Operator for heave using small sized buoys is generally much less than unity, the use of these buoys would be considered impractical for electrical energy generation purposes and not considered in this work. Thus, only the power generation potential for the buoys listed in Tables 4.4 and 4.5 will be analyzed.

4.5.3.1 The generated power for various large sized buoys operating in the regular wave regime

Since the Response Amplitude Operator for heave under the regular wave regime is based upon a single cyclic frequency (that of the wave), only one heave transfer function is used to determine the wave height to heave height ratio for the buoy. As the buoy increases in volume (and likewise weight), its frequency response curve is shifted more to the left and the heave transfer function (for a given cyclic wave frequency) more closely approaches the natural frequency for heave of the buoy, causing the heave transfer function to increase in magnitude (as shown by Figure 4.26), which in turn causes the buoy to bounce higher upon the waves (see Figure 4.27). As the buoy bounces increasingly higher upon the waves, the rotor of the linear generator travels up and down

progressively further within the linear generator, causing an increase in flux linkage between the rotor and stator assemblies, thereby generating a larger peak and average power output.

4.5.3.2   The generated power for various large sized buoys operating in the irregular wave regime

The heave response for the buoy influenced by the irregular wave regime is computed as the summation of each product of the amplitude component at each cyclic frequency and the Response Amplitude Operator calculated at the same cyclic frequency. Thus, the heave response of the buoy is composed of the cyclic frequency of every wave in the ocean.

Although an increase in the volume of the buoy generally amplifies its heave response allowing it to magnify the amplitude components near the natural heave frequency of the buoy, it also simultaneously diminishes the effects of the amplitude components at the higher cyclic frequencies. Figure 4.28 shows the natural amplitude components for the SUMMER and WINTER sea states along with the heave response (RAO_{HEAVE} Amplitude component) for buoys of various sizes. This figure clearly shows that as the buoy increases in volume, its peak heave response generally rises in magnitude, but narrows in bandwidth, and the heave transfer function (RAO_{HEAVE}) for the higher cyclic frequencies diminish in magnitude since a heavy buoy does not respond favorably to rapidly moving surface waves. With these higher frequency components removed, the buoy heaves to a lesser degree, thereby reducing the output power of the seabed mounted linear generator.
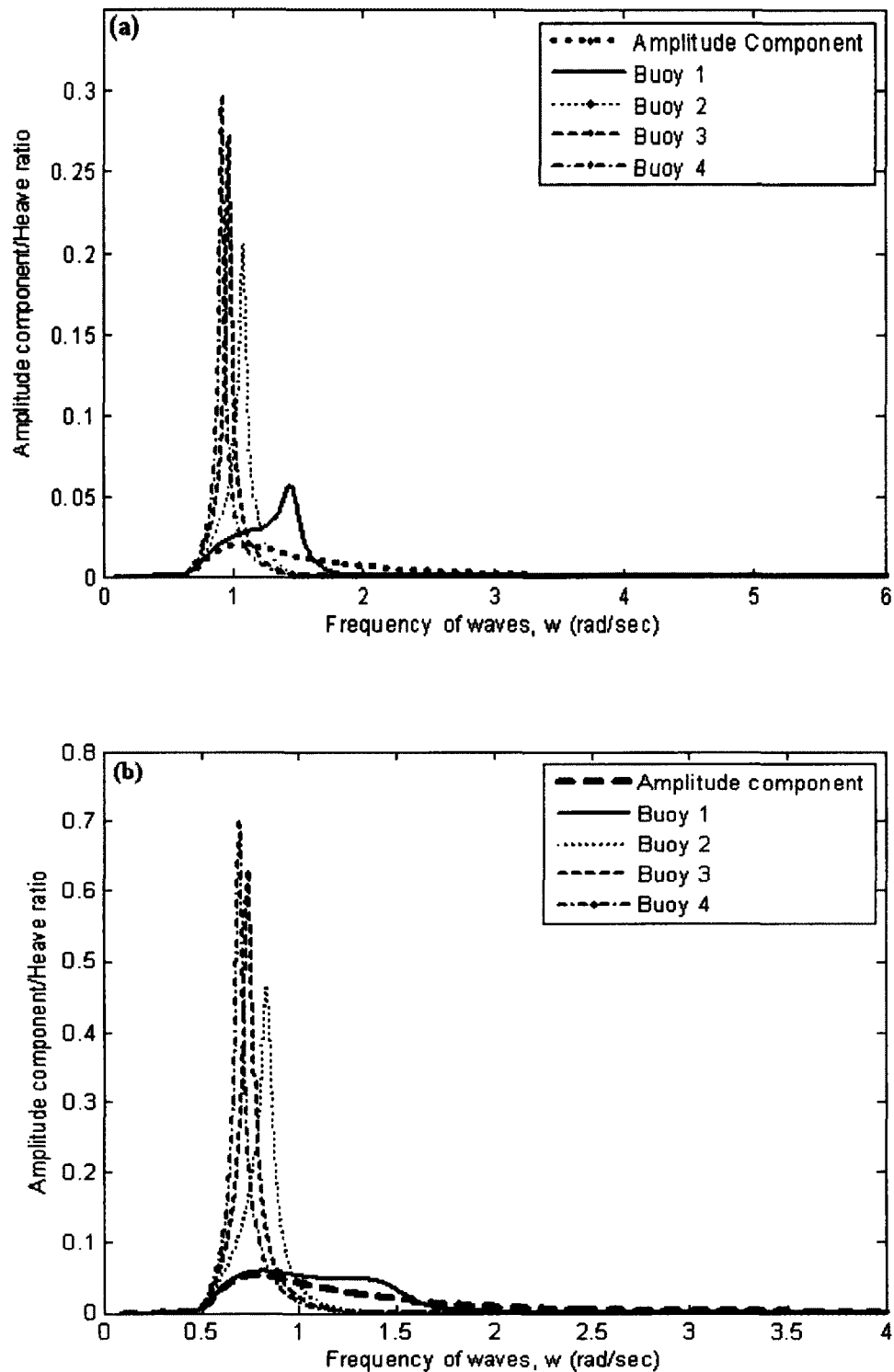
Figure 4.28. The amplitude components and the heave displacement per amplitude
component for buoys of various sizes operating in different sea states. (a) The SUMMER
and (b) WINTER sea states.

For the SUMMER and WINTER sea states (Figure 4.28) the heave ratio for buoys 1 through 4 all increase in magnitude as the buoy raises in volume. This behavior agrees with the intended design, since the buoy sizes were all modeled to provide increasing heave height ratios.

4.5.3.3 Comparison of generated power results

Figure 4.29 plots the average output power of a modeled linear generator operating under a simulated run duration of four hours and influenced by the SUMMER and WINTER sea states of both wave regimes using the buoys listed in Table 4.6 (which is a combined listing of Tables 4.4 and 4.5). Each buoy is identified by its label and plotted on the graph according to its volume on the x-axis, and the corresponding average ouput power by wave regime on the y-axis. Rough estimates for buoys having volumes between the listed buoy sizes were plotted on the graph, but the results have not been verified.

An analysis of Figure 4.29 reveals that when each buoy operates under the regular wave regime in either sea state, it experiences an increase in the average output power, agreeing with the intended design criteria. This response occurs for the regular wave regime because the buoy only responds to a single heave transfer function.
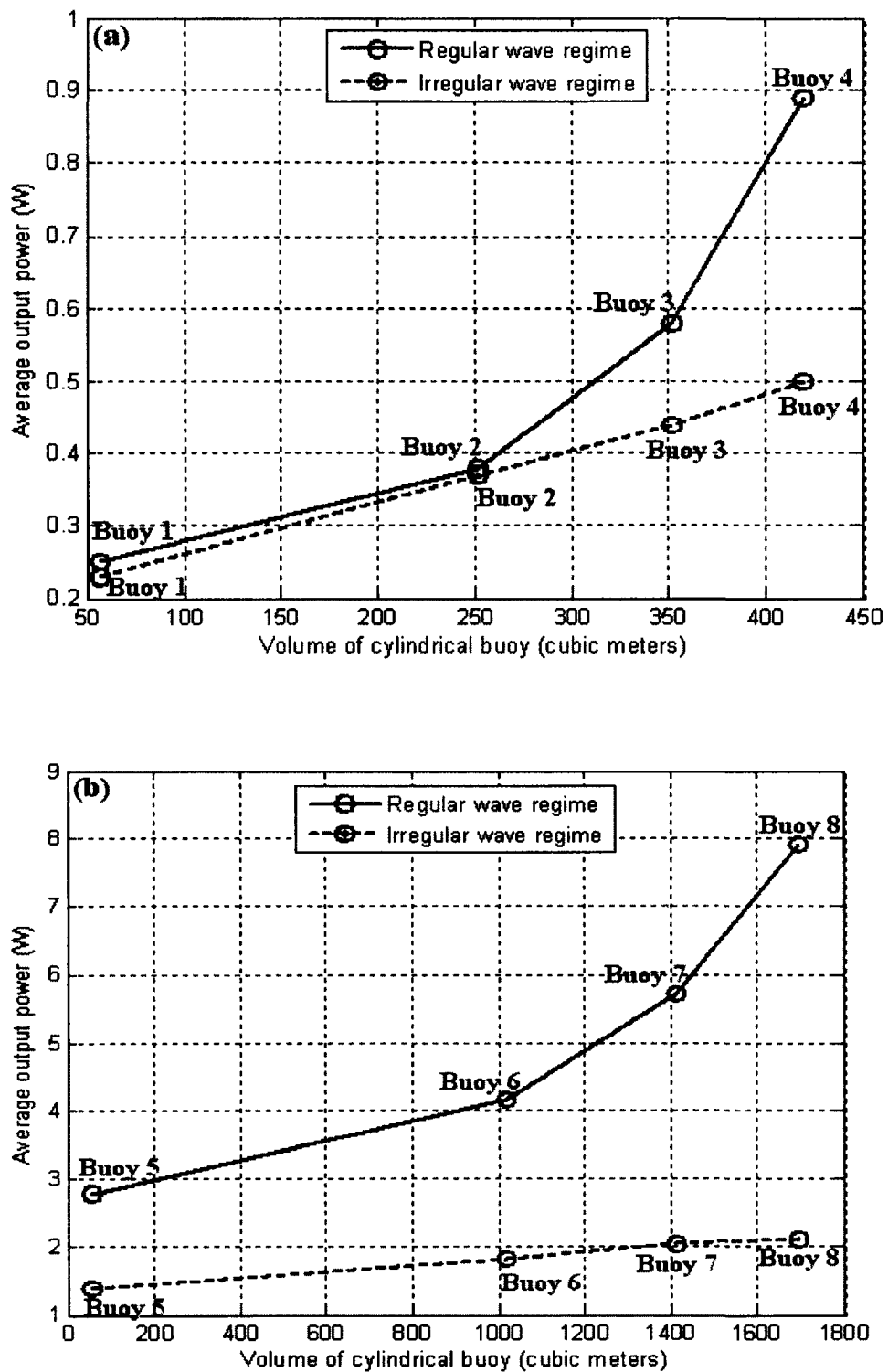
Figure 4.29. Average output power for various buoys operating under the regular and irregular wave regimes for the SUMMER and WINTER sea states. (a) The SUMMER, and (b) WINTER sea states.

Table 4.6. Buoy dimensions by sea state.

Buoy	Sea state	Buoy Size		
		Diameter [m]	Length [m]	Volume [m^3]
1	SUMMER	6	2	57
2		8	5	251
3		8	7	352
4		8	8.33	419
5	WINTER	6	2	57
6		12	9	1,018
7		12	12.5	1,414
8		12	15	1,696

The irregular wave regime, however, is comprised of several amplitude components and cyclic wave frequencies, causing the buoy's heave response to be determined by the combined net effect of each wave's amplitude component, cyclic frequency and its corresponding heave transfer function. Thus, when the average output power increases between the buoys, it is because the amplitude components near resonance are magnified to a greater degree than by which the higher frequency components are suppressed. As the buoy continues to increase in volume, although the amplitude components within the resonance bandwidth are magnified to a greater degree, the bandwidth narrows, causing the higher frequency components to be suppressed and resulting in a diminished increase in the heave response for the buoy as compared to that of the regular wave regime. Since the generated electrical power is proportional to the magnitude of the buoy's heave, the average output power is suppressed as well.

Figure 4.29 clearly identifies buoys 4 and 8 as the ideal choice for generating maximal average output power when influenced by either wave regime of the SUMMER or WINTER sea states, respectfully. Thus, buoys 4 and 8 could be manufactured and

switched as necessary to match the changing ocean conditions in order to theoretically yield the maximum average generated power.

4.6   Improving the efficiency of the linear generator

Thus far, the model was constructed using the same parameters that were found in the available literature, and many were selected from the values suggested by the group at Oregon State University (OSU) [21]. Although the linear generator modeled in this work accurately reflected the same findings as the aforementioned paper, the results are still relatively small to be deemed practical for large scale energy generation purposes. Thus, in order to generate more net electrical power, a large number of buoy-type linear generator WECs would need to be operated in a farm and/or the linear generator(s) must be constructed to provide greater output power.

Operating the buoys in a farm is a common procedure used in virtually all WEC generation facilities. In fact, through the proper alignment of the individual devices, a greater output power can be generated from the array of devices than by the sum of the individual devices acting independently. Although, this is an important issue in the design of a WEC farm, this aspect of the research is beyond the present scope, and could be a topic for a future study.

An additional method to accomplish the objective of generating a larger output power may be by altering the properties of the magnetic circuit. In general, the generated voltage, which is proportional to the output power of a linear generator can be increased (according to Equations 3.33 and Figure 3.6) by performing one or more of the following changes: (a) designing a smaller pole pitch (τ), (b) selecting magnets which have a stronger magnetic field (B), (c) increasing the number of stator coil turns (N), and/or (d)

changing the air-gap distance to achieve a greater peak magnetic flux density (ϕ'). These variables are all set during the design stage of the device and function as constants during the operational stage. Changes in factors (a) and (b) would create an alternate profile for the magnetic flux density within the air-gap region of the linear generator (see Figure 3.6), and is beyond the intended scope of this work. However, factors (c) and (d) can be incorporated into this model rather easily and yield very encouraging results.

Since the generated voltage is directly proportional to the number of stator turns (see Equation (3.33)), the generated voltage can easily be raised by increasing the number of stator coil turns. Figure 4.30 shows the generated voltage over a half period of the SUMMER sea state influenced by the regular wave regime for a stator having 250 turns. This is approximately five times that produced when only 48 turns were assumed, thereby confirming the ratio between stator coil turns and generated voltage. A voltage as high as 20 Volts is predicted for the device.
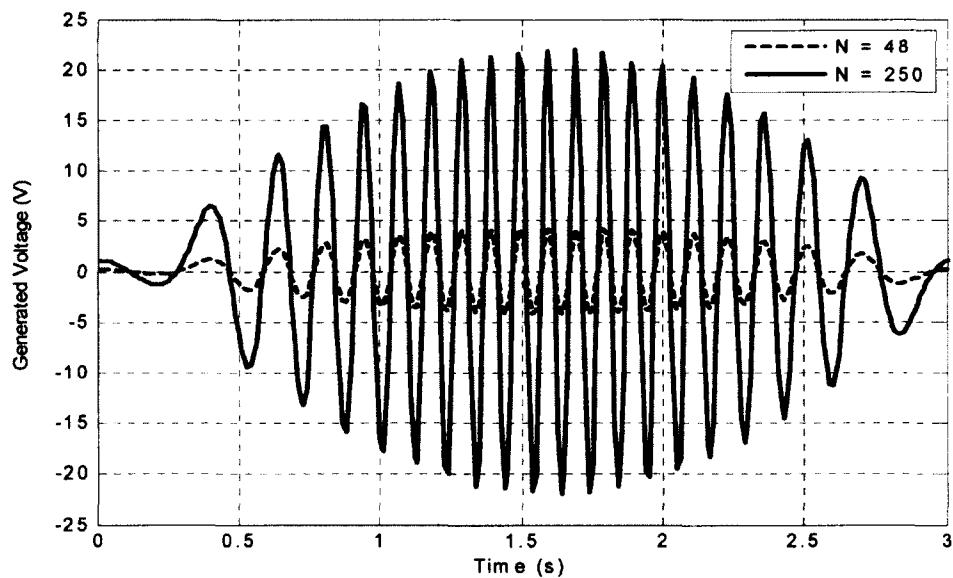
Figure 4.30. Generated voltages as a function of different stator coil turns.

The generated voltage can also be increased by raising the peak magnetic flux to the stator coils. Figure 3.6 shows that the magnetic flux density varies with the air-gap distance. Here we compare the associated magnetic flux density and resulting area of influence (as well as the percent change from the original model) for an air-gap of 10mm relative to a 6mm air-gap. The field would be approximately be 0.85T (representing a 155% change), over an area of 0.0033m^2 (representing 127% of the original value). This air-gap change yields a generated voltage which is approximately twice (= 155% * 127% = 197%) in magnitude. The results are shown in Figure 4.31 for the same sea state conditions as those of Figure 4.30. This new Figure 4.31 reveals that the generated voltage for a stator having 250 turns of coil has effectively doubled up to 40 Volts for an air-gap clearance of 10mm as opposed to a 6mm air-gap. The net result of both alterations together thus raises the generated voltage by a factor of ten from the original design.
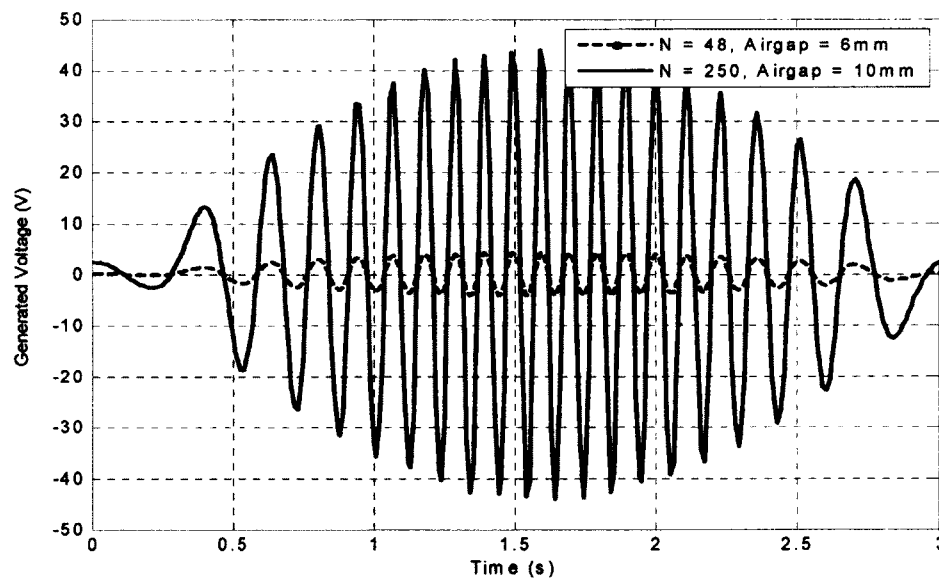
Figure 4.31. Generated voltage as a function of different coil turns and air-gap distances.

A rise in the generated voltage produces an increase in the resulting generated current. As the current rises in magnitude, the diameter of the stator's coil must rise as well to accommodate the increase in current flow, leading to a decrease in the coil's resistance value (see Equation 3.43). This causes an even greater current to be produced for a given generated voltage. Figure 4.32 compares the generated current under the original modeling conditions, with that produced using the new customized parameters. Figure 4.32 clearly shows that since the generated voltage has increased by approximately ten times in magnitude and that the resistance has effectively decreased by 3 times, the resulting generated current has been magnified over 30 times.
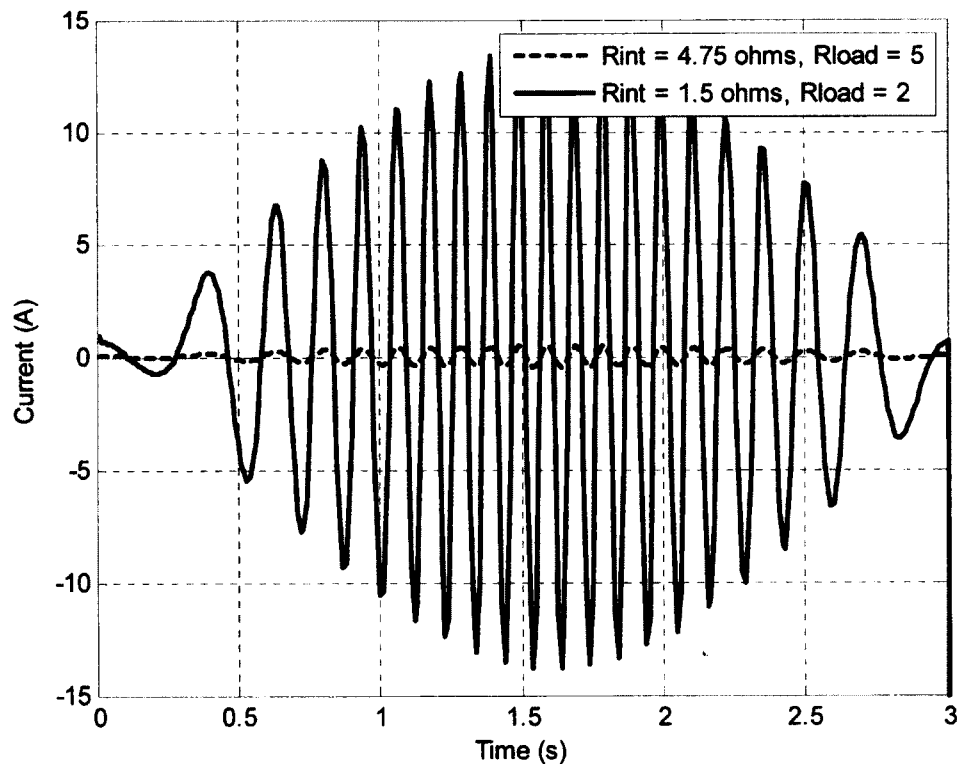
Figure 4.32. Generated current under the original and customized modeling parameters.

In view of the two changes to the output voltage produced and the current throughput, the change in power generated can now be obtained. Since the output power is proportional to the square of the generated current and the load resistance, it is suspected that the output power would be magnified by approximately 360 times (P_{MAX2}/P_{MAX1} = $\{(30 \cdot i(t)^2) \cdot 2\Omega\}/\{i(t)^2 \cdot 5\Omega\}$= 360). Figure 4.33 shows the output power for the linear generator operating under the customized modeling parameters for the same sea state conditions as used throughout this section. The original power output cannot be displayed in Figure 4.33 because its peak magnitude was only 1W, and thus appears insignificant under the new value scales.
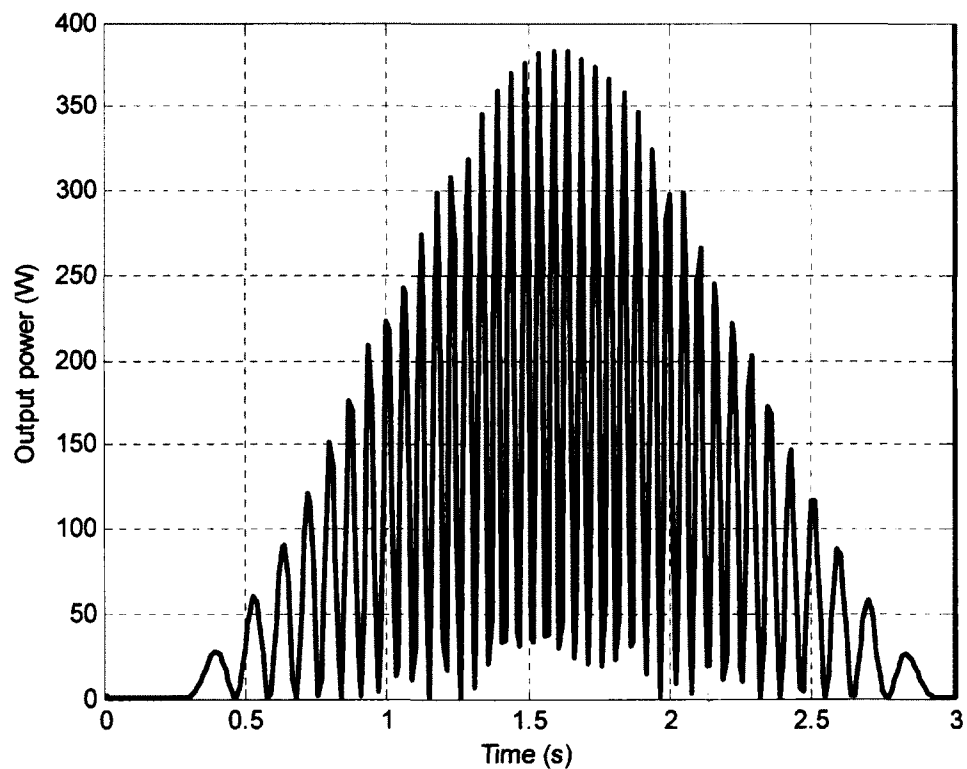
Figure 4.33. Output power for a half period of the SUMMER sea state influenced by the regular wave regime operating under the customized modeling parameters.

The maximum current encountered in the above discussion for the customized linear generator design from each wave regime, sea state, and buoy size, was found to be 40 Amperes. A return to Table 4.2 shows that 11 AWG wire exceeds this maximum current criterion for chassis wiring and is thus a good choice for use as the stator coil. Recalculating the eddy-current power loss (via Equations 3.40 and 3.41) using the parameters of the customized linear generator reveal that the new power loss values are approximately 80 percent less than the original values for both wave regimes, which again justifies this loss as being insignificant.

Figure 4.34 plots the average output power from the newly designed modeled linear generator operating under a simulated run duration of four hours for both the SUMMER and WINTER sea states. The buoys listed in Table 4.6 were used for these calculations. By comparing this figure with that of Figure 4.29, it becomes evident that the shape for each plot is similar in appearance since the plots are proportional to one another. However, there is a difference in their magnitudes. A further analysis of this plot again confirms that buoys 4 and 8 would be the preferred choice for generating maximal output power under both wave regimes for the SUMMER and WINTER sea states, respectfully. Thus, these buoys may be switched when necessary to theoretically provide optimal power throughout the changing seasons.
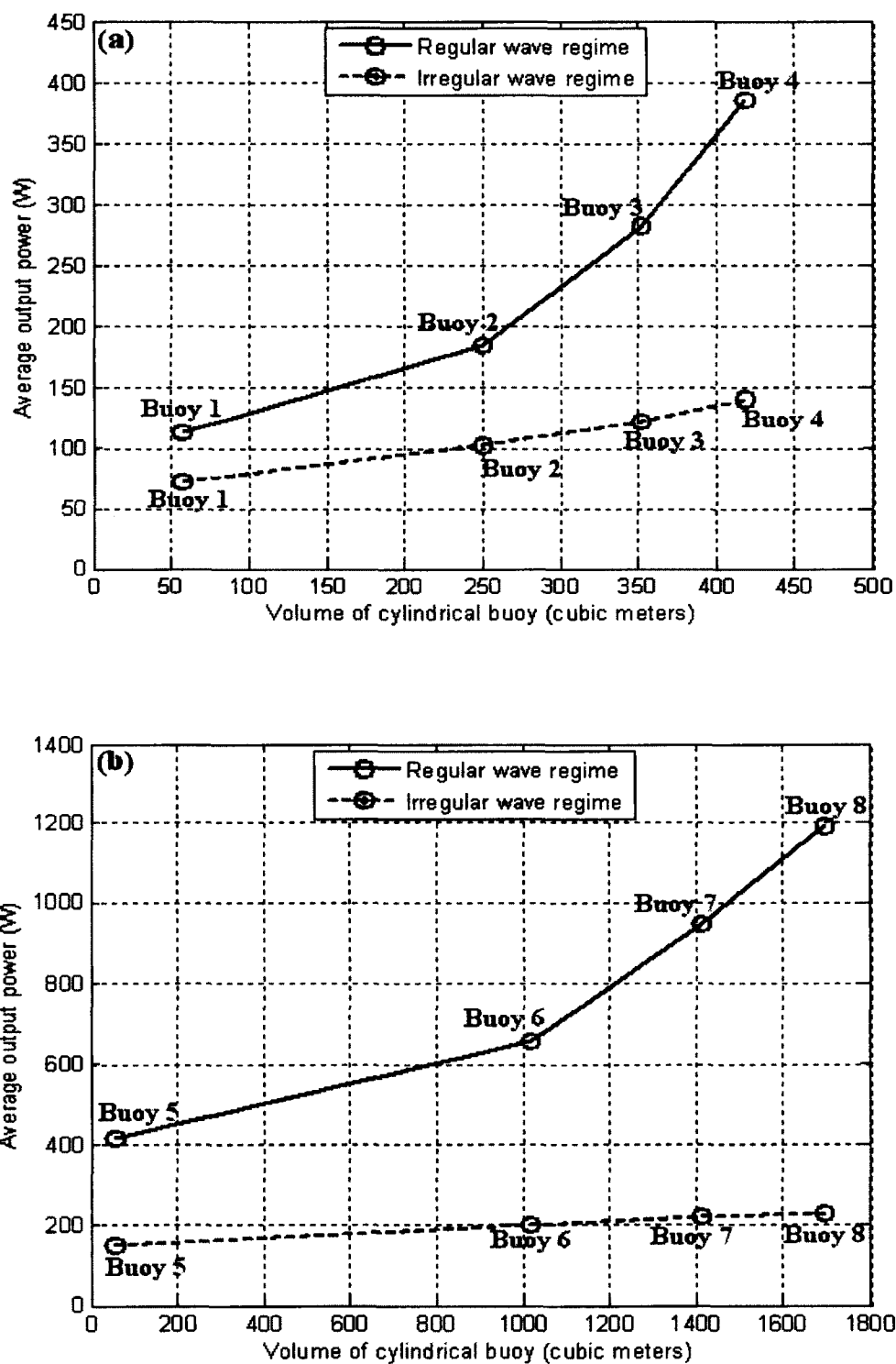
Figure 4.34. Average output power for various buoys operating under the regular and irregular wave regimes for the SUMMER and WINTER sea states of the customized linear generator. (a) The SUMMER, and (b) WINTER sea states.

4.7   Maximizing the generated power through the use of a single buoy

In the previous sections, an analysis was performed on how the buoys can be switched between the changing seasons to yield the maximum generated average output power. This procedure, however, may not prove cost effective to perform since expenses are required to construct the buoys as well as to travel to the site and switch them as necessary when dictated by the changing ocean surface conditions. Thus, in order to produce the greatest average power at the most efficient price, a single buoy (per linear generator) would need to be selected that provides a 'fairly good' power generation throughout the year.

Figure 4.35 shows the average power generated from the customized linear generator which is influenced by the SUMMER and WINTER irregular wave regimes for the buoys listed in Table 4.7 (which is a condensed version of Table 4.6). Since buoy 1 is designed to provide a Response Amplitude Operator for heave close to unity for both sea states, it is grouped with the other three buoys designed to respond optimally in each sea state (i.e. buoys 2, 3, and 4 for the SUMMER sea state, and buoys 5, 6, and 7 for the WINTER sea state) in Figure 4.34. A comparison of Figure 4.34 with Figure 4.35 reveals that the average output power remains unchanged when the buoys operate in their intended sea state conditions (i.e. buoys 1 through 4 of Figure 4.34a correspond with buoys 1 through 4 in Figure 4.35a and buoys 5 through 8 of Figure 4.34b correspond with buoys 1, 5, 6, and 7 in Figure 4.35b).
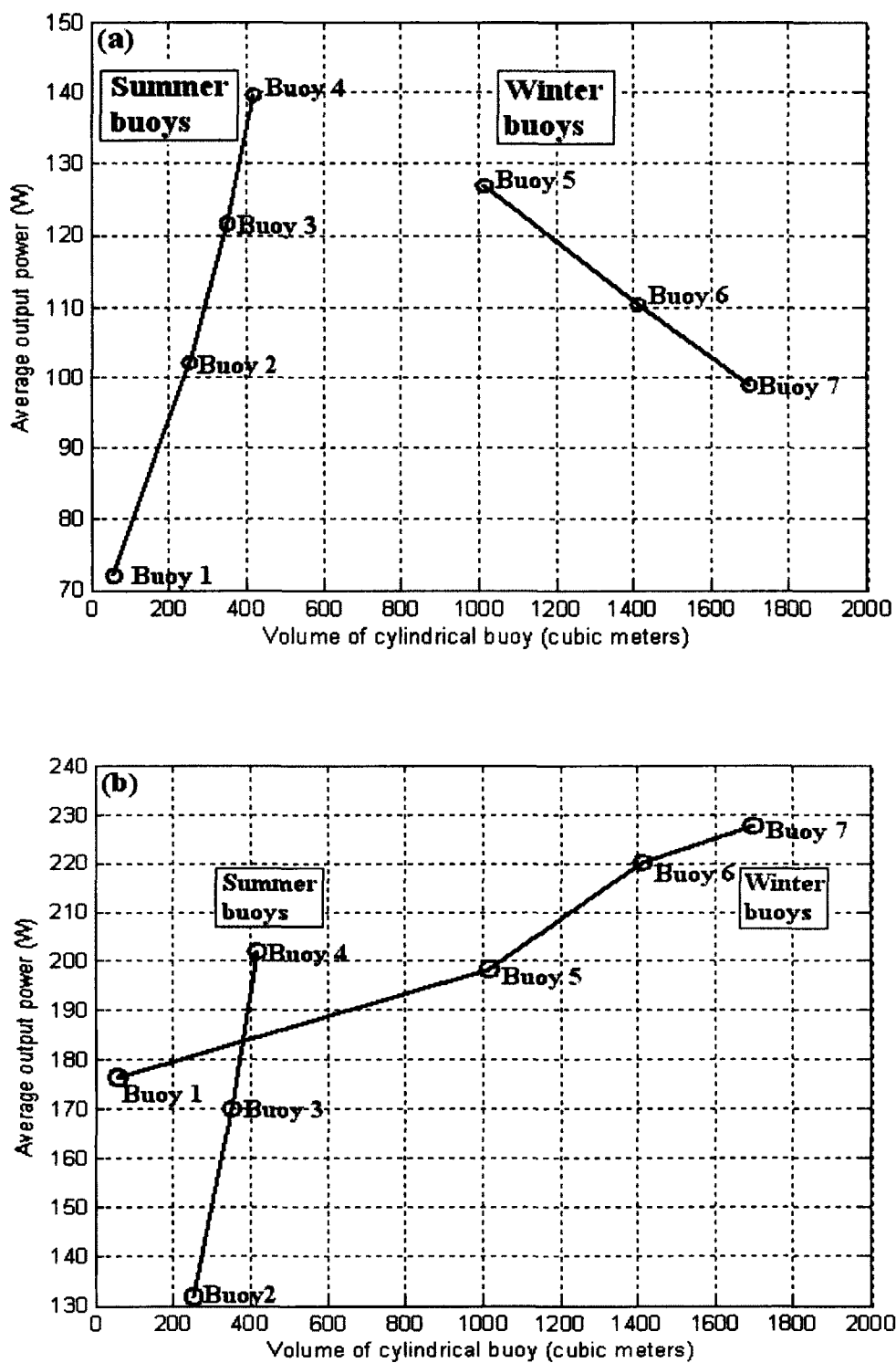
Figure 4.35. Average output power for various buoys operating under the irregular wave regimes for the SUMMER and WINTER sea states of the customized linear generator. (a) The SUMMER, and (b) WINTER sea states.

Table 4.7. Various buoy dimensions.

Buoy	Buoy Size			Sea state intended for operation
	Diameter [m]	Length [m]	Volume [m³]	(RAO for regular wave regime)
1	6	2	57	SUMMER and WINTER (1.03)
2	8	5	251	SUMMER (1.26)
3	8	7	352	SUMMER (1.53)
4	8	8.33	419	SUMMER (1.86)
5	12	9	1,018	WINTER (1.26)
6	12	12.5	1,414	WINTER (1.53)
7	12	15	1,696	WINTER (1.86)

When those buoys designed to operate within a specific sea state are made to function within their intended environment (i.e., summer buoys operating in the SUMMER sea state, and winter buoys in the WINTER sea state), the average output power rises with an increase in the buoys' volume, agreeing with expectations. However, when the buoys are made to function outside of their designed operating environment, a different response can occur. Figure 4.36 plots the Response Amplitude Operator for the buoys operating under their opposite sea state to justify their responses in Figure 4.35.

Figure 4.36a reveals that although the peak ratio increases between buoys 5 through 7, the bandwidth for the cyclic frequencies which are amplified narrows considerably. This action occurs due to the fact that the SUMMER sea state waves do not possess the energy required to create an increasing heave response on the much larger winter buoys, thereby resulting in a loss of average output power as the buoys increase in size.

A much better response, however, occurs for the summer buoys operating in the WINTER sea state. As Figure 4.36b illustrates, the Response Amplitude Operator for the summer buoys all experience a 'fair' response (by having a high peak ratio as well as a

wide bandwidth for the range of cyclic frequencies which are amplified) when influenced by the WINTER sea state. This response agrees with the physical properties of the system since the winter waves (which possess greater energy) will have a greater influence on the heave response on the smaller sized summer buoys. Thus, Figure 4.35b accurately indicates that the average output power rises with an increase in the summer buoys volume.
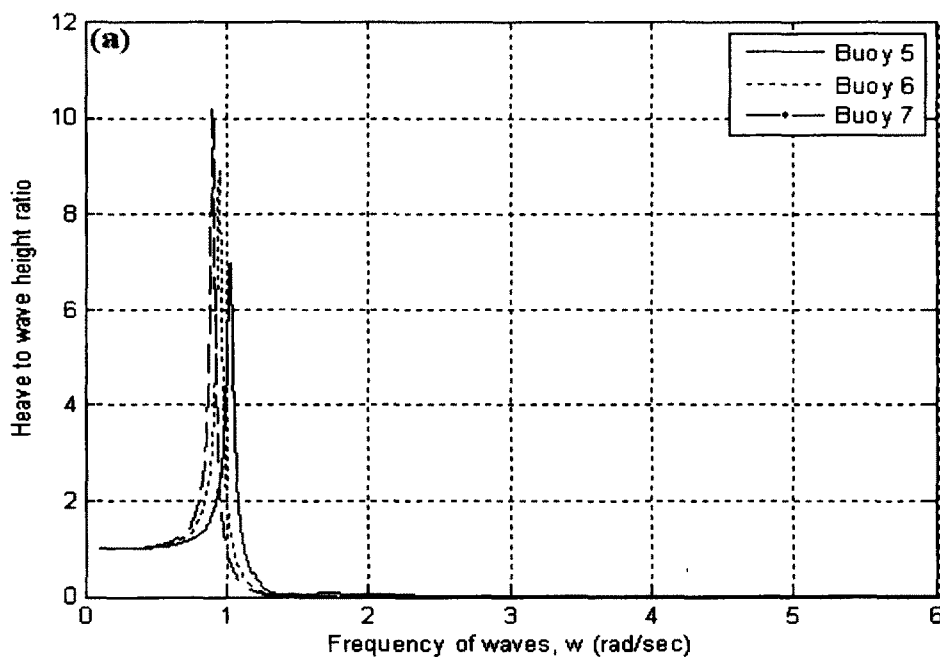
Figure 4.36. The Response Amplitude Operator for buoys operating under the opposite sea state from which they were designed. (a) The winter buoys operating in the SUMMER sea state, and (b) the summer buoys operating in the WINTER sea state.
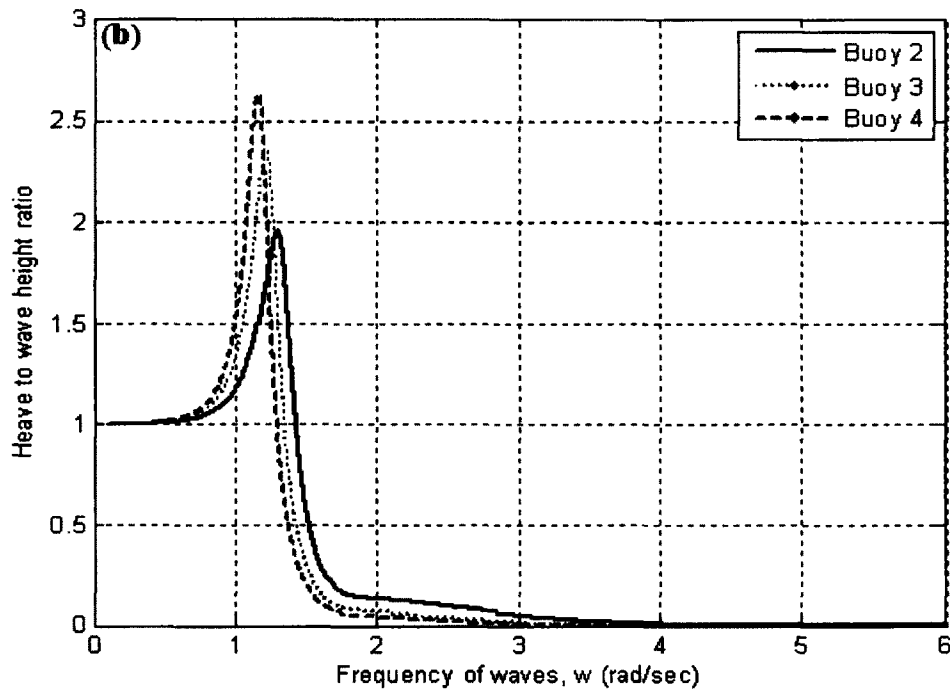
Figure 4.36. Continued.

Upon deriving the average annual output power from the SUMMER and WINTER sea states for each buoy (using the enhanced linear generator model), it is found that buoy 4 yields the highest annual average output power of approximately 170W (see Figure 4.37). Although buoys 5, 6, and 7 offer comparable results for the average annual output power, the decreased yield, as well as the increased costs associated with constructing the larger buoys, further substantiates buoy 4 as the preferred choice.

Although this specific buoy does not generate the maximum average output power per season, it produces the largest average output power annually. Hence, it would thus be the desired choice for use in order to maintain the highest power yield throughout the year.
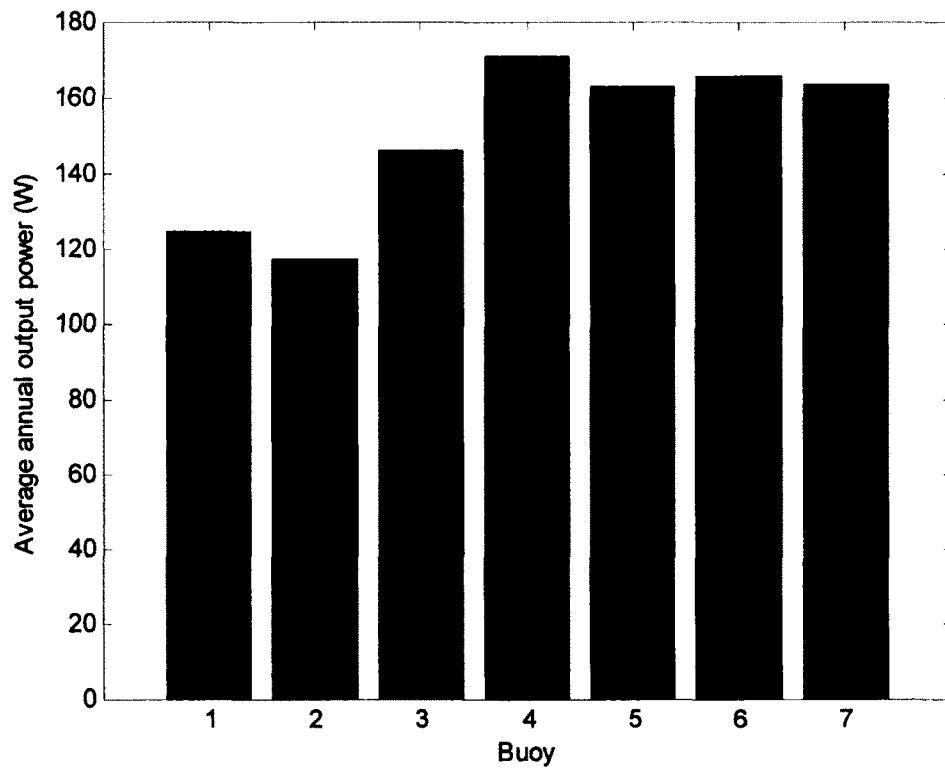
Figure 4.37. Average annual output power per buoy for the enhanced linear generator.

CHAPTER V

SUMMARY AND CONCLUSIONS

5.1 Summary and conclusions

The capability to harness the natural motion of ocean waves to generate electrical energy shows considerable promise. Ocean waves occur naturally, are predictable in occurrence, and are capable of producing a greater energy density than wind and solar power. Additionally, when ocean waves are used to generate electrical power they do not, unlike fossil fuels, pollute the environment nor deplete natural resources. Hence, generation of electrical energy from ocean waves appears to have merit, and should be viewed not as a replacement alternative, but rather as an additional source of energy production.

In order to accurately construct a model which represents the ocean's surface, real measurement data must first be collected. Wave gauges mounted on floating buoys can provide the three essential variables (wind speed, and significant wave height and period) necessary to model the ocean's surface activity within a particular region. This information is readily available for download at the National Buoy Data Center (NBDC) website.

Here, using the significant wave height and period data, the Bretschneider spectrum was used to model the wave's height as a function of time for the same ocean surface region. The Pierson-Moskowitz spectrum was another tool that was also used for re-constructing the wave activity on the ocean's surface. This two-parameter spectrum relies upon the cyclic frequency of the waves and the speed of the wind at a specific

distance (19.5 or 10m) above the ocean's surface. Although the wind speed or significant wave height can be algebraically derived from one another to generate nearly identical wave spectrums and time series (as performed in this work), the Bretschneider spectrum is accepted as the standard by the ITTC (International Towing Tank Conference) and only considered in this work.

The majority of previously published work has assumed perfect synchronous motion between the waves, the buoy's heave response, and the resulting motion of the linear generators' piston, to create electricity. Furthermore, most of the data has been analyzed only under the regular wave regime, and not the more realistic irregular wave regime (where a wave is super-imposed by many regular waves of different heights, periods, and phase angles). This work, however, analyzed the WEC system in much greater detail and introduced a more accurate model. It incorporated the effects of a non-ideal buoy, i.e., one that does not react synchronously with ocean surface waves. In the process, the analysis was aimed at determining the optimal conditions for power generation. Additionally, this work closely inspected the power losses which occur within the linear generator when the floating buoy is influenced under both wave regimes.

The linear generator constructed in this work compared favorably with those from published findings [21] under the conditions for a synchronously and asynchronously coupled wave/buoy/piston interaction. Furthermore, the generated voltage and current, and the output voltage and power for all of the tested sea states and wave regimes agreed with the anticipated results as well as fundamental circuit laws, thereby further validating the mathematical model for this system.

Additional simulations were conducted to explore the possibility of generating greater average output power from a linear generator using a 'non-ideal' buoy. The objective was to design the buoy dimensions to yield an RAO value for heave under the regular wave regime greater than unity. The results of the numerical experiments have shown that although the concept proved successful under the regular wave regime, it failed to produce substantial gains under the irregular wave regime. The less than favorable results under the irregular wave regime were analyzed and could be accounted for in terms of the following argument. Although the amplitude components near the natural frequency for heave of the buoy were magnified as attempted in the design, the higher frequency components were suppressed due to the diminished heave response for waves having faster cyclic frequencies. Since an irregular wave comprises of a superposition of many frequencies, the overall gains could not be sustained throughout the spectrum. This dissertation research did prove, however, that it is theoretically possible to increase the average output power of the linear generator by switching (or selecting) between different buoys depending on the sea conditions.

Simulated modifications to the physical properties of the basic linear generator model were performed in an attempt to create an improved electrical output response. This new model performed much better than the original version, in that it produced greater values for the output voltage, current, and power.

Although it is theoretically possible to exchange the buoys in order to generate a larger average output power from the linear generator during the changing seasons, a buoy-type WEC operates most efficiently financially when a single buoy can be designed to maintain a 'fair' response through the seasonal changes in the ocean's surface

conditions. In this work, it has been found that buoy 4 can be coupled to the linear generator to maintain an adequate average power output throughout the year.

Table 5.1 summarizes the average output power generated from both linear generator models simulated as being coupled to buoy 4 as well as the total number of WEC devices required per sea state of the irregular wave regime to supply 100 percent of the power requirements for an average American home [80] and an isolated community [27]. As is evident from this table, due to the excessive number of devices required to supply the desired power rating, the first linear generator model (Model 1) proves impractical from both the engineering and financial viewpoints. This model was originally constructed merely to compare the results against previously published findings [21] to confirm the validity of the model. The second linear generator model (Model 2), however, shows more promising results. Although, the total number of devices are still considered relatively high, it is suspected that further improvements can be incorporated into the linear generator as well as the overall system to yield a greater average power output, resulting in a fewer number of devices required to produce the same power requirement.

Table 5.1 Number of WEC devices required to supply a specific load requirement by linear generator model type and sea state.

Sea state	Average output power (W)		Number of WECs required to supply for a specific load (Hourly power requirement)			
			Average American home (1 KW)		Isolated community (100 KW)	
	Model 1	Model 2	Model 1	Model 2	Model 1	Model 2
SUMMER	0.50	139.48	2,000	7	200,000	717
WINTER	0.86	202.04	1,163	5	116,279	495

5.2   Future work

This work explored the output power of a simple, buoy-driven, single-phase linear generator operating in the regular and irregular wave regimes under different sea state conditions and buoy sizes. Future work into this subject should be aimed at increasing the output power of the linear generator by incorporating one or more of the following suggestions:

1.   Using different buoys –This work only investigated the response of a single vertically floating cylindrical buoy having a uniform cross-sectional area. Commercially available buoys come in a variety of shapes, sizes and floating orientation and can be operated under different levels of submergence. All of these factors affect the heave response and thus the generated output power of the linear generator. Under these conditions, mutual coupling and distortion of the wave motion from individual buoys would need to be considered. Furthermore, the collective fluid (sea) motion would need to be carefully included.

2.   Expand the model into a 3-phase system – With the inclusion of two additional identically wound sets of stator coils, a three phase system can be constructed where each phase is separated by its neighbor by 120°. The benefits of a 3-phase system allow a voltage to be generated from 3 stator coils instead of only one for a change in position of a single rotor. These individual voltages can then be tapped individually or combined together to form a single phase voltage with a greater output power.

3. Change the properties of the magnetic circuit – The generated voltage, which is proportional to the output power of a linear generator can be further increased (according to Equation 3.33) by altering the parameters of the magnetic circuit. This task may be accomplished by designing the rotor to have a smaller pole pitch (τ) and/or selecting magnets which have a stronger magnetic field (B). These variables are all set during the design stage of the device and function as constants during the operational stage.

4. Multi-buoy farm – In this work, only the reaction of a single buoy's heave response to an exciting wave force and the resulting electrical energy generated has been analyzed. It is possible, however, to generate additional electrical energy by operating a multitude of similar devices within a specific array configuration to create a WEC farm. The overall benefit of the farm is determined by the interaction factor. The interaction factor, q, as it applies to wave energy converter arrays is defined as the ratio of the maximum power which may be absorbed by an array of identical wave energy devices to the maximum power available from the same number of individual members of the array acting independently of their neighbors [81]. Since absorbing more power from the group of WECs would be more advantageous than that which could be absorbed from the sum of its individual members, it would be ideal to maximize the interaction factor. Although this topic is beyond the intended scope of this work, it represents an important issue that should be studied in further research.

5. The effects of a non-ideal attachment rope – The simulations in this work assumed that the rope connecting between the floating buoy and linear generator was constructed of an inelastic and non-deforming material and remained taut throughout its movements. A more realistic model, however, would incorporate non-ideal material properties as well as the effects of slack in the rope.

6. Buoy Interactions – The mutual interactions between buoys that would affect the motion of each device and the linear generator built into them, could also be considered.

5.3 Final conclusions

The world continues to demand greater productivity and lifestyle enrichment through technological advancements. As a result, the growing dependency upon electrical power will continue to escalate dramatically. It has been hypothesized that unless a clean, renewable, and efficient alternate source of energy is found soon, the world will either exhaust its supplies of energy producing materials, or drastically degrade its environment.

The world should continue to research and experiment with creating new technologies and perfecting the techniques for producing 'green energy'. Since no one specific type of energy producing technique is infallible (for example, solar cells cannot function in the dark, windmills can not function in a calm environment, etc.), an optimal strategy might be to incorporate all of these such devices in their most appropriate environments in order to produce electricity without exhausting the Earth's resources and polluting the environment. Even though a particular technique may have a relatively low yield or efficiency, this should not mean that it should be abandoned completely. Even

small and modest savings per year can generate a profound net worldly effect when it is used on a global scale. Additionally, as research within these areas of alternative energy production are investigated, it is quite reasonable to assume that advances will be made to improve a given form of green-energy production.

The generation of electrical energy through the use of a floating buoy and linear generator was evaluated as the focus of this work. This is one of the first efforts in the field of 'Green energy' at Old Dominion University. Although some very useful conclusions and results were obtained, a relatively simple scenario was studied. Further research is required and more advanced models need to be constructed in order to simulate this type of WEC operating both independently, and within a farm, so that a greater power output and efficiency could be attained.

REFERENCES

[1] R. Shaw, "Energy supply and demand," in *Wave Energy a Design Challenge*, West Sussex, England: Market Cross House, 1982, ch. 1, sec. 1.1, pp. 19 - 21.

[2] M. Leijon, O. Danielsson, M. Eriksson, K. Thorburn, H. Bernhoff, J. Isberg, J. Sundberg, I. Ivanova, E. Sjöstedt, O. Ågren, K. Karlsson, and A. Wolfbrandt, "An electrical approach to wave energy conversion," Renewable Eng., vol. 31, pp. 1309-1319, Sep. 2006.

[3] A. Joule and A. Thermie. (2010, Jan. 4). Wave energy ready to contribute to EU's sustainable electricity production [Online]. Available: http://www.docstoc.com/docs/21180093/Wave-energy-ready-to-contribute-to-EUs-sustainable-electricity

[4] Minerals Management Service, "Technology white paper on wave energy potential on the U.S. outer continental shelf," U.S. DOI., Washington, DC., May 2006.

[5] S. Sen, A. Sokolow, R. Simion, D. Sun, R. Doney, M. Nakagawa, J. Agui, Jr., and K. Shenai, "Ocean waves, mechanical impulses and electrical energy: concept of a simple conversion process," presented at the International Conference on Advances in Energy Research (ICAER), Bombay, India, 2007.

[6] J. Falnes, "A review of wave-energy extraction," Marine Struct., vol. 20, no. 4, pp. 185-201, Oct. 2007.

[7] R. Charlier, J. Justus, "State of the art" in *Ocean energies environmental, economic and technological aspects of alternative power sources*, Amsterdam, The Netherlands, Elsevier science pub., 1993, ch. 1, pp. 1-20.

[8] Wikipedia. (2012, March 12). Barrage de la Rance.jpg [Online]. Available: http://upload.wikimedia.org/wikipedia/commons/e/eb/Barrage_de_la_Rance.jpg

[9] B. Ram, "Energy from Offshore Wind," presented at Offshore Technology Conference, Houston, TX, 2006.

[10] Wikipedia. (2011, March 18). Windmills D1-D4 (Thornton Bank) [Online]. Available: http://en.wikipedia.org/wiki/File:Windmills_D1-D4_(Thornton_Bank).jpg

[11] U.S. Department of the Interior. Ocean energy [Online]. Available: http://www.boemre.gov/mmskids/PDFs/OceanEnergyMMS.pdf

[12] T. Lewis, "The wave energy resource," in *Wave Energy*, Gaithersburg, MD: Graham & Trotman Ltd., 1985, ch. 2, sec. 2.1, pp. 3.

[13] T. Brekken, A. Jouanne, and H. Han, "Ocean Wave Energy Overview and Research at Oregon State University," presented at the 2009 IEEE Power Electronics and Machines in Wind Applications (PEMWA) Conference, Lincoln, NE, Aug. 2009.

[14] A.Westwood. (2004, Sep./Oct). Ocean Power: Wave and tidal energy review. reFOCUS[Online]. pp. 1-2. Available: www.re-focus.net.

[15] G. Hagerman and R. Bedard. (2003, Dec. 22). EPRI Wave Energy Conversion (WEC) Project [Online]. Available: http://oceanenergy.epri.com/waveenergy.html.

[16] D. Elwood, "Evaluation of the performance of a taut-moored bual-body direct-drive wave energy converter through numerical modeling and physical testing," M.S. thesis, Ocean Eng., OR State Univ., Corvallis, OR, 2008

[17] D. Evans, "Some theoretical aspects of three dimensional wave energy absorbers," in Proceedings of the first symposium on wave energy utilization, Gothenburg, Sweden, 1979, pp. 77–106.

[18] J. Falnes, "Introduction," in *Ocean waves and oscillating systems: linear interactions including wave energy extraction*, Cambridge, UK: Cambridge Univ. Press, 2002, ch.1. pp. 1-3.

[19] R. Curran and L. Gato, "The energy conversion performance of several types of wells turbine designs", Proc. of the Inst. of Mech. Eng., vol. 211, no. 2, pp. 133-145, Mar. 1997.

[20] Voith Hydro Wavegen Ltd. (2009, June 9). Nearshore OWC [Online]. Available: http://www.wavegen.co.uk/pdf/what_we_offer_nearshore_owc.-voith%2009pdf.pdf

[21] K. Rhinefrank, E. Agamloh, A. Jouanne, A.Wallace, J. Prudell, K. Kimble, J. Aills, E. Schmidt, P. Chan, B. Sweeny, and A. Schacher, "Novel ocean energy permanent magnet linear generator buoy," Renewable Energy, vol. 31, no. 9, pp. 1279-1298, July, 2006.

[22] Pelamis wave power [Online]. Available: http://www.oceanpd.com.

[23] Wikipedia (2012, March 24). Pelamis at EMEC.jpg [Online]. Available: http://en.wikipedia.org/wiki/File:Pelamis_at_EMEC.jpg.

[24] A. Weinstein. Harvesting the Motion of the Ocean [Online]. Available: http://hydropower.inel.gov/hydrokinetic_wave/pdfs/day1/10_heave_wave_devices_1_aw.pdf

[25] A.Wacher and K.Neilsen, "Mathematical and Numerical Modeling of the AquaBuOY Wave Energy Converter," Mathematics-in-Industry Case Studies Journal, Volume 2, pp. 16-33, 2010.

[26] F. Krupp and M. Horn, "Ocean Energy" in *Earth: The Sequel*, New York: W.W. Norton & Comp., Inc., 2008, ch. 6, pp. 115-120.

[27] T. Lewis, "Systems and applications," in *Wave Energy*, Gaithersburg, MD: Graham & Trotman Ltd., 1985, ch. 4, sec 4.5, pp. 17-21.

[28] R. Shaw, "Environmental, social and industrial considerations," in *Wave Energy a Design Challenge*, West Sussex, England: Market Cross House, 1982, ch. 6, pp. 168-171.

[29] OSPAR Commission, "Assessment of the environmental impacts of cables," OSPAR Commission, Lauterbach, Germany, Pub. Num. 437/2009, 2009.

[30] Y. Huang, "Electromagnetic simulations of 135 kV three-phase submarine power cables," Cent. for Marine and Coastal Studies Ltd., Birkenhead, Merseyside, 2005.

[31] S. McArthur and T. Brekken, "Ocean Wave Power Data Generation for Grid Integration Studies," Department of Energy, Rep. no. DE-FG36-08GO18179, Corvallis, Oregon, 2010.

[32] J. Khan, G. Bhuyan, and A. Moshref, "Potential opportunities and differences associated with integration of ocean wave and marine current energy plants in comparison to wind energy," Powertech Labs Inc., Tech. Rep. Doc. no. T0311, Mar. 2009.

[33] ABB. Offshore wind energy: Grid Connections-Markets, concepts, Studies [Online]. Available: http://www.abb.com/

[34] European Commission, "Offshore Wind Energy Ready to Power a Sustainable Europe, Final Report: Concerted Action on Offshore Wind Energy in Europe," Supported by the European Commission, Rep. NNE5-1999-562, 2001.

[35] D. Richardson. Chapter 8: Waves and water dynamics [Online]. Available: faculty.mdc.edu/jbarros/OCEppTT/CH08_Outline.ppt

[36] R. Sorensen. (1997, April 28). Water Wave Celerity [Online]. Available: http://scubageek.com/articles/wwwceler.html

[37] G. Gore, "Scaled modeling and simulation of ocean wave linear generator buoy systems," M.S. thesis, Elec. and Compt. Eng., Oreg. St. Univ., Corvallis, OR, 2006.

[38] I. Ivanova, H. Bernhoff, O. Agren, and M. Leijon, "Simulated generator for wave energy extraction in deep water," Ocean Eng., vol. 32, pp. 1664-1678, Oct. 2005.

[39] R. Charlier and J. Justus, "Waves," in Ocean Energies Environmental, Economic and Technological Aspects of Alternative Power Sources, Amsterdam, The Netherlands: Elsevier sci. pub., 1993, ch. 5, pp. 112-113.

[40] Wikipedia (2011, April 23). Sea State [Online]. Available: http://en.wikipedia.org/wiki/Sea_state

[41] S. Sagiraju and R. Kumar, "Harnessing of Wave Power from Horizontal Flow Dynamics of Shallow Waves," M.S. thesis, Elect. and Inst. Eng., Nat. Inst. Tech., Rourkela, India, 2009.

[42] M. Amundarain, M. Alberdi, A. Garrido, and I. Garrido, "Modeling and Simulation of Wave Energy Generation Plants: Output Power Control", IEEE Trans.on Ind. Elec., vol. 58, no. 1, pp. 105-117, Jan. 2011.

[43] W. Michel, "Sea Spectra Simplified," presented at the Gulf Section of The Society of Naval Architects and Marine Engineers, New York, NY, Jan. 1968.

[44] R. Stewart. (2008, Nov. 19). 16.6 Measurement of Wave [Online]. Available: http://oceanworld.tamu.edu/resources/ocng_textbook/chapter16/chapter16_06.htm

[45] E. Schiele. High Frequency Radar [Online]. Available: http://oceanmotion.org/html/gatheringdata/hfradar.htm

[46] Wikipedia. (2011, Feb. 23). Acoustic Doppler velocimetry [Online]. Available: http://en.wikipedia.org/wiki/Acoustic_Doppler_velocimetry

[47] Wikipedia. (2011, Jun. 23). Laser Doppler velocimetry [Online]. Available: http://en.wikipedia.org/wiki/Laser_Doppler_velocimetry

[48] A.Techet. (2005, Feb. 24). 13.42 Design Principles for Ocean Vehicles [Online]. Available: http://ocw.mit.edu/courses/mechanical-engineering/2-22-design-principles-for-ocean-vehicles-13-42-spring-2005/readings/r8_wavespectra.pdf

[49] Wikipedia. (2011, July 11). Dispersion relation [Online]. Available: http://en.wikipedia.org/wiki/Dispersion_relation

[50] R. Stewart. (2007, July 30). 16.1 Linear Theory of Ocean Surface Waves [Online]. Available: http://oceanworld.tamu.edu/resources/ocng_textbook/chapter16/chapter16_01.htm

[51] R. Stewart. (2006, Nov. 15). 16.4 Ocean-Wave Spectra [Online]. Available: http://oceanworld.tamu.edu/resources/ocng_textbook/chapter16/chapter16_04.htm

[52] A. Techet. (2005, Feb. 1). Lecture: Ocean Waves Spring 2005 [Online]. Available: http://web.mit.edu/13.42/www/handouts/wave_spectra_slides2.pdf

[53] K. Sadeghi. "A numerical simulation for predicting sea waves characteristics and downtime for marine and offshore structures installation operations," Soc. & Appl. Sci., vol. 3, no. 5, pp. 1-2, 2007.

[54] MIT OpenCourseWare. Bretschneider Spectrum Definition [Online]. Available: http://ocw.mit.edu/courses/mechanical-engineering/2-017j-design-of-electromechanical-robotic-systems-fall-2009/assignments/MIT2_017JF09_p04.pdf.

[55] B. Gotthardsson, "Analysis and evaluation of the wavebox wave energy converter," M.S. thesis, Elect. Eng., Uppsala Univ., Uppsala, Sweden, 2011.

[56] National Oceanic and Atmospheric Administration. (2010 Aug. 5). National Data Buoy Center [Online]. Available: http://www.ndbc.noaa.gov.

[57] H. Berteaux, "Oceanographic buoy systems, classes, design, and components," in Buoy Engineering, New York: John Wiley & sons, 1976, Ch. 2, pp. 212-216.

[58] H. Berteaux, "Statics of free floating bodies," in Buoy Engineering, New York: John Wiley & sons, 1976, Ch. 1, pp. 3-4.

[59] Wikipedia. (2011, July 3). Added mass [Online]. Available: http://en.wikipedia.org/wiki/Added_mass.

[60] Wikipedia. (2011, January 27). Restoring force [Online]. Available: http://en.wikipedia.org/wiki/Restoring_force.

[61] Wikipedia. (2011, December 13). Damping [Online]. Available: http://en.wikipedia.org/wiki/Damping

[62] R. Shaw, "Wave energy conversion to mechanical energy," in Wave Energy a Design Challenge, West Sussex, England: Market Cross House, 1982, ch. 3, pp. 83-99.

[63] Wikipedia. (2010, September 13). Response amplitude operator [Online]. Available: http://en.wikipedia.org/wiki/Response_amplitude_operator

[64] J. Camara, "Electromagnetic theory" in Electrical Engineering Reference Manual for the Electrical and Computer PE Exam, 6th ed. Belmont, CA: Prof. Pub., Inc., 2001, ch. 16, pp. 16-22.

[65] O. Danielsson, "Design of a linear generator for wave energy plant," M.S. thesis, Eng., Uppsala school of Eng., Uppsala, Sweden, 2003.

[66] W. Storr (2011, Aug.). Magnetic Hysteresis [Online]. Available:
http://www.electronics-tutorials.ws/electromagnetism/magnetic-hysteresis.html

[67] I. Boldea and S. Nasar, "Linear electric generators," in *Linear Electric Actuators and Generators*, New York: Camb. Univ. Press, 1997, ch. 8, pp. 201-209.

[68] H. Berteaux, "Dynamics of free floating bodies," in *Buoy Engineering*, New York: John Wiley & sons, 1976, Ch. 2, pp. 51 - 66.

[69] H. Chung and S. Chen, "Hydrodynamic mass," Argonne Nat.Lab., Argonne, Ill, Tech. Rep. COHF-840647—9.

[70] J. Palm, "Mooring of a wave power device: simulation of the dynamic response to wave loading," M.S. thesis, Civ. and Env. Eng., Chalmers Univ. Tech., Göteborg, Sweeden, 2010.

[71] A. Santana, D.Andrade and A. Jaén, "Control of hydrodynamic parameters of wave energy point absorbers using linear generators and VSC-based power converters connected to the grid," presented at the International Conference on Renewable Energies and Power Quality, Granada, Spain, 2010.

[72] Wikipedia (2011, Dec. 24). Neodymium magnet [Online].
Available.http://en.wikipedia.org/wiki/Neodymium_magnet

[73] A. VanderMeulen, "Novel Control of a Permanent Magnet Linear Generator for Ocean Wave Energy Applications," M.S. thesis, Elec. Eng., OR St. Univ., Corvallis, OR, 2007.

[74] M. Journée and W. Massie, "Rigid body dynamics," in *Offshore hydrodynamics*, 1st edition, Delft, Netherlands: Delft Univ. Tech., 2001, ch. 6, pp. 6-24.

[75] E. Purcell, "The derivative," in *Calculus with analytic geometry*, New York, NY: Meredith Pub. Co.,1965,ch. 5, sec. 5.1, pp. 113.

[76] Wikipedia, (2011, Dec. 23). Magnetic flux [Online]. Available:
http://en.wikipedia.org/wiki/Magnetic_flux.

[77] Powerstream Technologies. Wire gauge and current limits [Online]. Available:
http://www.powerstream.com/Wire_Size.htm

[78] J. Camara, "AC Circuit Fundamentals" in *Electrical Engineering Reference Manual for the Electrical and Computer PE Exam*, 6th ed. Belmont, CA: Prof. Pub., Inc., 2001, ch. 27, pp. 27-13.

[79] J. Camara, "Electromagnetic Theory" in *Electrical Engineering Reference Manual for the Electrical and Computer PE Exam*, 6th ed. Belmont, CA: Prof. Pub., Inc., 2001, ch. 16, pp. 16-10.

[80] J. Mosher. (2011, Feb. 24). Power consumption of a home [Online]. Available: http://hypertextbook.com/facts/2003/BoiLu.shtml.

[81] Marine Energy Research Group. The hydrodynamic of wave energy converter arrays [Online]. Available: http://www.qub.ac.uk/research-centres/eerc/ResearchThemes/CoastalandHydraulicEngineeringMRE/ResearchPosters/Filetoupload,180509,en.pdf

APPENDIX I

NOMENCLATURE

a	Acceleration of the buoy in the vertical direction, m/s^2
A_S	General constant for the wave spectrum equation, $m^2 \cdot s$
A_{BUOY}	Cross-sectional area defined by the undisturbed water free-surface, m^2
A_{cap}	Surface area for the plates of a capacitor, m^2
A_{coil}	Cross sectional area of the coil, m^2
A_i	Amplitude component at cyclic frequency ω_i, m
A_w	Significant waves' amplitude, m
B_S	General constant for the wave spectrum equation, (No Units)
B	Magnetic flux density of a material or emanating from the rotor, T
C	Celerity of waves, m/s
C_D	Measured drag coefficient for the buoy, (No Units)
C_E	Material constant representing the conductivity of the coils, m/Ω
C_g	Group velocity of the wave, m/s
C_m	Added mass coefficient, (No Units)
C_{OUT}	Neutralizing capacitance value, F
d	Separation distance between the plates of a capacitor, m
$d\text{A}$	Elemental section of area for a buoy, m^2
$d\text{F}$	Elemental force acting upon a buoy, N
$d\text{s}$	Differential distance traveled by the conductor through a magnetic field, m

$d\mathbf{S}$	An infinitesimal vector, whose magnitude is the area of a differential element of S, and whose direction is the surface normal, m^2
D	Draft of the buoy, m
D_f	Damping force coefficient, Kg/s
D_E	Energy extraction damping coefficient, Kg/s
D_F	Frictional damping coefficient, Kg/s
D_R	Radiation damping coefficient, Kg/s
E	Generated voltage from the linear generator, V
$E_{density}$	The total average wave energy per unit surface area, Kg/s^2
E_{WAVE}	The total wave energy in one wavelength per unit crest width, N
f	Periodic frequency of the wave, Hz
f_{hs}	Hydrostatic force coefficient on the buoy, Kg/s^2
$f_{MIN\omega}$	Minimum periodic frequency contributing to eddy current power losses in the irregular wave regime, rad/s
$f_{MAX\omega}$	Maximum periodic frequency contributing to eddy current power losses in the irregular wave regime, rad/s
f_{rotor}	Periodic frequency of the rotor, s^{-1}
f_s	Restoring force coefficient for the spring, Kg/s^2
F	Applied force upon a buoy, N
F_1	Force exerted at the top of a floating buoy, N
F_2	Force exerted at the bottom of a floating buoy, N
F_e	Wave exciting force, N·m
g	Acceleration due to gravity, m/s^2
h	Water depth, m

h_1	Distance that a buoy floats above the water or the depth in which the top surface of the buoy is submerged, m
h_2	Depth that the buoy is submerged in water, m
H	Magnetic field intensity, A/m
H_{BUOY}	Heave transfer function for the buoy in heave, (No Units)
$H_{1/3}$ and H_s	Significant wave-height, m
i	Stator current, A
j	imaginary number, (No Units)
k	Wave number, m^{-1}
k_s	Spring constant, Kg/s^2
l	Length of the conductor in a magnetic field, m
l_{coil}	Length of a stator coil, m
L_{COIL}	Self and mutual inductances for the stator coils, H
Lsubmerged	Depth to which the buoy is submerged, m
m	Mass of the buoy in seawater, Kg
m^*	Added mass of the buoy due to the surrounding seawater, Kg
m_{ax}, m_{ay}, m_{az}	Mass of the displaced seawater along the x,y, and z-axis, respectfully, Kg
m_v	Virtual mass of the buoy, Kg
M	Magnetization of a material, A/m
n	Constant for the group velocity, (No Units)
n	Linear damping coefficient, s^{-1}
N	Number of stator turns in the linear generator, (No Units)
p	Natural frequency for heave of a floating buoy, rad/s

p_1	Pressure exerted at the top of a floating buoy, $Kg\,m^{-1}\,s^{-2}$
p_2	Pressure exerted at the bottom of a floating buoy, $Kg\,m^{-1}\,s^{-2}$
P_c	Power due to copper losses, W
$P_{density}$	Wave power density
P_E	Total eddy current power loss in the stator coils in the regular wave regime, W
$P_{E-IRREGULAR}$	Total eddy current power loss in the stator coils in the irregular wave regime, W
P_{in}	Power input to the linear generator, W
P_{LOAD}	Power delivered to the electrical load, W
P_{losses}	Power losses due to hysteresis, eddy currents, and resistive losses, W
P_{out}	Power output of the linear generator, W
$P_{WAVEFRONT}$	Power per square meter of wave front, W/m^2
r	Stator coils' resistance, Ω
RAO_{HEAVE}	Response Amplitude Operator for the buoy in heave, (No Units)
R_{BUOY}	Radius of the buoy, m
R_{LOAD}	Load resistance, Ω
S	Restoring force coefficient, Kg/s^2
S^+	Wave spectrum, $m^2\,s$
T	Waves' period, s
u	Fluid velocity in the x- direction, m/s
U_w	Wind speed, m/s
U_{10}	Wind speed at a height of 19.5m above the sea surface, m/s
$U_{19.5}$	Wind speed at a height of 19.5m above the sea surface, m/s

v	Velocity of the conductor traveling in the magnetic field, m/s
v_1	Velocity of the heaving buoy, m/s
V	Induced voltage in a conductor, V
(Volume)	Volume of seawater displaced by the immersed buoy, m^3
(Volume of cable)	Geometric volume of the stator coil, m^3
V_{LOAD}	Voltage drop across the load resistance, V
V_p	Phase velocity/speed for the wave, m/s
$V_{rectification\ loss}$	Voltage loss due to reticifation of the output voltage, V
$V_{STATOR\ COILS}$	Voltage loss across the stator coils of the linear generator, V
w	Fluid velocity in the z- direction, m/s
x, y,z	Position for the floating buoy, m
X_{COIL}	Impedance of the stator coils of the linear generator, Ω
X_{LOAD}	Impedance of the load necessary to cancel the impedance of the stator coils of the linear generator, Ω
z	Displacement of the linear generators rotor relative to the stator, m
z^* and z^{**}	Velocity and acceleration for a heaving buoy, respectfully, m/s and m/s^2
Zwave	Waves' peak amplitude, m
α	Constant for A in the Pierson-Moskowitz spectrum, (No Units)
β	Constant for B in the Pierson-Moskowitz spectrum, (No Units)
$\Delta\omega$	Increment between cyclic frequencies used in the simulation, rad/s
δ	Skin depth, m
ε_o	Permittivity of free space, $C^2/N \cdot m^2$
ε_r	Relative permittivity of water, (No Units)

ζ^2	Significant wave-height derived from the integral of the Pierson-Moskowitz spectrum, m
η	Elevation of the water surface, m
η_{LG}	Efficiency of the linear generator, %
θ_i	Phase angle for each amplitude component, rad
λ	Waves' wavelength, m
λ_f	Flux linkage between the rotor and stator coils, V
μ_o	Permeability of a vacuum, V·s/(A·m)
μ_r	Relative permeability of a material, (No Units)
ρ	Seawater density, Kg/m^3
ρ_{water}	Density of the water in which a buoy is submerged, Kg/m^3
σ	Phase angle between the force and the wave, rad
σ_c	Conductivity of the coils' material, Ω^{-1}
σ_s	Skin effect coefficient, (No Units)
τ	Pole pitch of the linear generator, m
ϕ	Magnetic flux, T
ϕ'	Peak magnetic flux, T
ϕ_{heave}	Phase angle between the force and heave motion, rad
φ	Phase difference between the wave and the force, rad.
ω	Cyclic frequency of the wave, rad/s
ω_c	Limiting frequency of the wave influenced by the wind, rad/s
ω_i	An individual cyclic wave frequency in the irregular wave regime, rad/s.

ω_m Modal or peak frequency of any given wave, rad/s

ω_o Significant cyclic wave frequency for the Pierson-Moskowitz spectrum, rad/s

ω_p Peak frequency for the Pierson-Moskowitz spectrum, rad/s

APPENDIX II

APPROVAL FOR IMAGES

Figures 1.2, 1.7, 2.7

I, the copyright holder of this work, release this work into the **public domain**. This applies worldwide.
In some countries this may not be legally possible; if so:
I grant anyone the right to use this work for any purpose, without any conditions, unless such conditions are required by law.
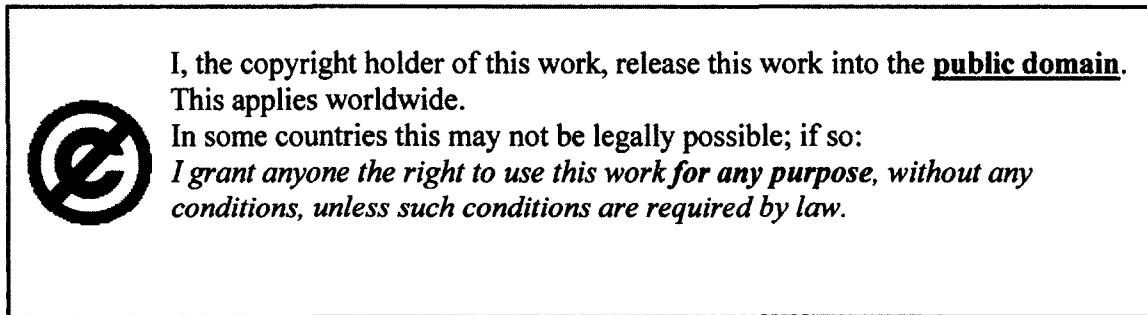
Figure 1.3

This file is licensed under the Creative Commons Attribution-Share Alike 3.0 Unported license.

You are free:

- **to share** – to copy, distribute and transmit the work
- **to remix** – to adapt the work

Under the following conditions:

- **attribution** – You must attribute the work in the manner specified by the author or licensor (but not in any way that suggests that they endorse you or your use of the work).
- **share alike** – If you alter, transform, or build upon this work, you may distribute the resulting work only under the same or similar license to this one.

Figures 1.6, 3.3, 3.5, 3.6, 3.7, 4.13, and 4.17

Hello, I am a Ph.D. student at Old Dominion University in Norfolk, Va.
> As part of my dissertation, I would like to insert the 'following figures from your paper into my manuscript: Figures 1, 4, 5, 6, 7, and 10) from Novel ocean energy permanent magnet linear generator buoy

Yes, I give approval via this email.

-Dr. von Jouanne

Dr. Annette von Jouanne, Ph.D., P.E.
Professor, Power Electronics/Energy Systems
Electrical Engineering & Computer Science
Oregon State University
3027 Kelley Engineering Center
Corvallis, OR 97331-5501

Tel: (541) 737-0831
Fax: (541) 737-1300
Email: avj@eecs.orst.edu
http://eecs.oregonstate.edu/research/members/vonjouanne
http://www.eecs.oregonstate.edu/wesrf

> In order to do this, I need a written confirmation letter to add to the appendix of my manuscript. I would also like to publish this manuscript to the public. If this is acceptable, please contact me as to your specifications (and limitations) and send or e-mail me an acceptance or rejection letter. Thank you Mike Stelzer

Figure 1.8

You are welcome to refer to the Figure 5.6 on capital cost breakdown as part of your thesis, as long as you make appropriate citation to the following report:

Khan, Bhuyan & Moshref (2009). Potential ....Wind Energy, a report prepared by Powertech Labs for the IEA OES-IA

Also, please note the original sources of this figure/info (as identified in the above report) are from ABB , Offshore wind energy ... and the EC Final report - that you should mention - references 11 and 46 of the above Powertech report available at www.

Iea-oceans.org

All the best

Gouri S. Bhuyan, Ph. D., P.Eng., FASME, FCAE
Principal Advisor for Alternative Energy
...

Powertech Labs Inc.
12388-88th Avenue, Surrey
British Columbia, Canada, V3W 7R7

T: 604 590 7407
F: 604 590 6656

Email: gouri.bhuyan@powertechlabs.com
Web: www.powertechlabs.com

-----Original Message-----
From: Susan Hancock
Sent: Thursday, March 22, 2012 10:24 AM
To: Gouri Bhuyan
Subject: FW: Inquiry Form Response

Helio Gouri,

Would this be an inquiry for you?

Susan

-----Original Message-----
Sent: Thursday, March 22, 2012 10:19 AM
To: Reception Powertech
Cc: Susan Hancock
Subject: Inquiry Form Response

Received: March 22, 2012 at 09:19 AM

First Name: Michael
Last Name: Stelzer
Company: Old Dominion University

Topic: Other
Message: Hello, I am a Ph.D. student at Old Dominion University in Norfolk, Va. As part of my dissertation, I would like to insert the 'Figure 5.6: Capital cost breakdown of onshore and offshore wind farm' picture into my manuscript from

Potential opportunities and differences associated with integration of ocean wave and marine current energy plants in comparison to wind energy In order to do this, I need a written confirmation letter to add to the appendix of my manuscript.

I would also like to publish this manuscript to the public.

If this is acceptable, please contact me as to your specifications (and limitations) and send or e-mail me an acceptance or rejection letter.

Thank you
Mike Stelzer

Heard About Us: Advertising
Referring URL: http://www.powertechlabs.com/contact-us/

Figures 2.5, 2.9, 2.10

Mike,
You may use figures 167, 16.8, and 16.11 from my book Introduction to Physical Oceanography in your PhD thesis at Old Dominion and in any publication based on your thesis.
Bob Stewart

Robert Stewart
Retired Professor of Oceanography
Texas A&M University
College Station, Texas 77843-3146 USA

On Mar 21, 2012, at 5:06 PM, michael stelzer wrote:

Hello, I am a Ph.D. student at Old Dominion University in Norfolk, Va. As part of my dissertation, I would like to insert the 'Figure 16.11' picture into my manuscript (on http://oceanworld.tamu.edu/resources/ocng_textbook/chapter16/chapter16_06.htm) and figures 16.7 and 16.8 on http://oceanworld.tamu.edu/resources/ocng_textbook/chapter16/chapter16_04.htm. In order to do this, I need a written confirmation letter to add to the appendix of my manuscript.

I would also like to publish this manuscript to the public.

If this is acceptable, please contact me as to your specifications (and limitations) and send or e-mail me an acceptance or rejection letter.

Thank you
Mike Stelzer

Figure 2.6

Hi Mike, yes you have permission to use.

Good luck and regards-

 Christina Iarossi

SonTek Marketing Communications

9940 Summers Ridge Road

San Diego, CA 91921

O: +1.858.546.8327

ciarossi@sontek.com

www.sontek.com

SonTek

a xylem brand

 From: michael stelzer
Sent: Sunday, March 25, 2012 9:27 PM
To: General
Subject: Copyright request

 Hello, I am a Ph.D. student and my dissertation is generating power from ocean waves, I would like your permission to publish the following picture (should it be copyrighted) into my manuscript which is hoped to be inserted into my dissertation as well as a title for public release,

Thank you,

Mike Stelzer
Figure 2.12

Dear Mike,
Thank you for your recent correspondence about MIT OpenCourseWare (OCW).

The underlying premise and purpose of OCW is to make course materials used in MIT courses freely and openly available to others for non-commercial educational purposes. Through OCW, MIT grants the right to anyone to use the materials, either as is, or in a modified form. There is no restriction on how a user can modify the materials. Under our Creative Commons license, materials may be edited, translated, combined with someone else's materials, reformatted, or changed in any other way.

However, there are three requirements that an OCW user must meet to use the materials:

. Non-commercial: Use of OCW materials is open to all except for profit-making entities who charge a fee for access to educational materials.

. Attribution: Any and all use or reuse of the material, including use of derivative works (new materials that incorporate or draw on the original materials), must be attributed to MIT and, if a faculty member's name is associated with the material, to that person as well.

. Share alike (aka "copyleft"): Any publication or distribution of original or derivative works, including production of electronic or printed class materials or placement of materials on a Web site, must offer the works freely and openly to others under the same terms that OCW first made the works available to the user.

Please refer to the MIT OpenCourseWare Terms of Use at http://ocw.mit.edu/terms for our specific licensing terms and conditions.

Sincerely,
The MIT OpenCourseWare Team

You wrote:
>I have found your information at the following to be very helpful:
>
>http://ocw.mit.edu/courses/mechanical-engineering/2-017j-design-of-electrom echanical-robotic-systems-fall-2009/assignments/MIT2_017JF09_p04.pdf
>
>I would like to include the table and plots in my dissertation, In order to

do this, I would need a written acceptance letter.
>
>I would also like to publish this dissertation for public use, please advise if the acceptance/rejection covers that as well.
>
>Thank you,
>Mike Stelzer

Figures 2.15 & 2.16

Hi Mike,

We'd be happy for you to use them in your dissertation.
Best regards,
Erika

Erika Fitzpatrick

Media Relations

Woods Hole Oceanographic Institution

MS#5

Woods Hole, MA 02543

Phone: 508.289.3281   Fax: 508.457.2182

Office Hours: M-F 8:30am to 12:30pm

Please consider the environment before printing this email.

Visit WHOI online at:

Web site – http://www.whoi.edu/

Twitter - http://twitter.com/WHOIMedia

YouTube - http://www.youtube.com/user/WoodsHoleOceanInst

Facebook - http://www.facebook.com/pages/Woods-Hole-MA/Woods-Hole-Oceanographic-Institution-WHOI/56661991371

Figure 2.23

Hello Mike,

Firstly, thank you for you email and for asking in avance to use one of my images as part of your dissertation. Most people would have just copied them regardless.

As you have kindly asked, I would have no objection to you using the BH curve image as part of your work free of charge.

However, I must ask that you reference my work and site www.electronics-tutorials.ws accordingly.

Also please note that the graphical image shows normalised curves to get the idea across and does not represent any particular quality of material.

Good luck with your course.

Kind regards.
Wayne Storr
webmaster@electronics-tutorials.ws

-----Original Message-----
Sent: Wednesday, March 21, 2012 11:37 PM
To: webmaster@electronics-tutorials.ws
Subject: Copyright request
Hello, I am a Ph.D. student at Old Dominion University in Norfolk, Va. As part of my dissertation, I would like to insert the 'Magnetization or B-H Curve' picture into my manuscript (http://www.electronics-tutorials.ws/electromagnetism/magnetic-hysteresis.html). In order to do this, I need a written confirmation letter to add to the appendix of my manuscript.

I would also like to publish this manuscript to the public.

If this is acceptable, please contact me as to your specifications (and limitations) and send or e-mail me an acceptance or rejection letter.

Thank you
Mike Stelzer

CURRICULUM VITA

For
Michael Stelzer

DEGREES:

Master of Science, Electrical Engineering   August 2001
Bachelor of Science, Electrical Engineering Technology   October 1990

SCIENTIFIC AND PROFESSIONAL SOCIETIES MEMBERSHIP:

Cambridge Who's Who
Electronics Technician Association

HONORS AND AWARDS

Professional of the Year, Cambridge Who's Who, 2010
Certified Professional Project Manager, Management Science Institute, 2008
Master of Science, Electrical Engineering, Old Dominion University, 2001
General Radiotelephone Operator's License with Radar Endorsement, FCC, 1999
Senior Certified Electronic Technician, Electronics Technician Association, 1998
Electronic Mechanic Journeyman, U.S. Department of Labor, 1998
Naval Nuclear Power Training Course, U.S. Navy, 1993
Honors Society, DeVry Institute of Technology, 1990

Published Titles

Mathematical strategies to winning casino poker
Mental mathematics: an introduction to solving everyday math problems in your head
Learn a language your own way
SPICE based heat transport model for non-intrusive thermal diagnostic applications